Chapter Three. Scaling and accommodation of the jaw adductor muscles in the Canidae.

3.1 Introduction

The work presented in this chapter is modified from a paper published in the Anatomical Record in 2016 (Penrose *et al*., 2016). I would like to thank Dr Nathan Jeffery for advice on experimental design, for offering suggestions for manuscript improvement and for the critical revision of this chapter. I would also like to thank Professor Graham Kemp for his help in the concept development and critical revision of this chapter.

Interspecific differences of carnivoran skull shape are dependent on numerous factors, most notably phylogeny, dietary function and allometry with the relative importance of each depending on the group of species under investigation. Here, I attempt to resolve the relative importance of allometry and diet in determining cranial morphology among one particularly widespread and varied carnivoran family, the canids. I aim to account for phylogeny and determine how labile the musculoskeletal morphology of the wild canid head is by combining advances in imaging with conventional dissection and more advanced computational methods such as geometric morphometrics. In contrast to many previous studies (Christiansen and Adolfssen, 2005; Wroe and Milne, 2007; Figueirido *et al*., 2011; Damasceno *et al*., 2013) I directly quantify the masticatory muscles as well as the bony morphology.

Radinsky (Radinsky, 1981) was amongst the first to document that carnivoran skull shape is linked to negative allometric scaling of the brain among related species but did not consider, in detail, questions concerning the potential knock-on effects for the masticatory apparatus. In particular, are the areas for muscle origin on the skull compromised with the relative reduction of brain size and of the surrounding neurocranium, and does this influence the size of the muscle mass that can be accommodated? In addition, is this further compounded by the positive allometric scaling of the masticatory muscles needed to maintain the same level of biomechanical function? Emerson and Bramble (Emerson and Bramble, 1993) state that large species can exert relatively less muscle force than small species and are required to

move relatively and absolutely heavier jaws. This implies that with increases of body size, species either lose function or must have relatively larger muscles that in turn require a commensurate increase in the bony areas for their attachments. Numerous studies of Carnivora have also linked skull form with dietary function (Sacco and Van Valkenburgh, 2004; Meachen-Samuels and Van Valkenburgh, 2009; Tseng and Wang, 2010; Sicuro and Oliveira, 2011; Tseng *et al.*, 2011). Slater and Van Valkenburgh (Slater and Van Valkenburgh, 2008; Slater and Van Valkenburgh, 2009) have shown that big cats have lengthened their jaw to facilitate a relatively wider gape than small cats. This suggests that big cats are not simply 'scaled up' small cats but make different functional demands of their jaws. This morphological difference coincides with a difference in their diet and hunting strategies; whereas small cats take prey smaller than themselves, big cats require a relatively wider gape to subdue prey which may be larger than them (Slater and Van Valkenburgh, 2009).

Here I look collectively at the scaling of brain size and of masticatory muscle size as well as at trophic niche as determinants of canid skull morphology. Canids were selected for the present study because they are diverse in body mass, geographical location and dietary group specialization, and their phylogeny is relatively well documented (Gittleman, 1985; Wayne *et al*., 1989; MacDonald and Sillero-Zubiri, 2004; Sillero-Zubiri *et al*., 2004; Finarelli, 2007; MacDonald, 2009; Wang and Tedford, 2010). All 36 species (Nowak, 2005) of extant canids, the Canidae, belong to the subfamily Caninae and are thought to have evolved from a common ancestor that originated in North America around 8-12million years ago (Wang and Tedford, 2010). Modern species are arranged in four main phylogenetic clades, the fox-like *Vulpes* clade, the wolf-like canis clade, the South American clade and the grey fox-like Urocyon clade (Lindblad-Toh *et al*., 2005). Both convergent and divergent patterns of morphological adaptation are found within and amongst these clades. For instance, the South American foxes, although phenotypically very similar to members of the *Vulpes* fox clade, are more closely genetically related to the wolf-like canids (Wayne *et al*., 1997; Perini

et al., 2010; Nyakatura *et al.,* 2012). Conversely, morphologies amongst closely related species such as the South American *Speothos venaticus* and *Chrysocyon brachyurus* are very distinct and highlight a great potential for phenotypic plasticity. Three trophic groups exist which allow for correlations of head morphology with hunting behaviour and functional dietary requirements; these are the small prey specialists, the generalists and the large prey specialists. These dietary specialisms are not dictated by phylogenetic clade: the fox-like group consists both of generalists and small prey specialists, the South American group of generalists and small and large prey specialists and the wolf-like group of generalists and large prey specialists. Both of the urocyon clade members are generalists (Slater *et al*., 2009). For more details on canid diet see Chapter One, part 1.4.

3.2 Aims of the study

Scaling of masticatory muscle masses, as opposed to bony proxies, is not widely described in many species of mammal but previous studies have established that there is no common rule regarding the relative size of the jaw adductors within clades. Primates demonstrate isometric scaling regardless of diet or phylogeny (Cachel, 1984; Perry and Wall, 2008). Herrel *et al*. (2008) describe the mass of the temporalis muscles of a wide range of bats, including frugivorous, insectivorous and sanguivorous species, scaling with negative allometry. Macropodoideal marsupials show a range of scaling patterns in all jaw adductors, according to dietary preference (Warburton, 2009). Similarly, the relative masseter muscle mass in ruminants has been shown to differ amongst species with different feeding categories independent of body mass or phylogeny (Clauss *et al*., 2008). Within the carnivoran order Hartstone-Rose *et al.* (2010) established that the masticatory muscle masses scale with isometry that tends towards positive allometry. Here I aim to describe the jaw adductor muscles of several species of canid and establish whether they scale isometrically against body mass, or more closely follow other patterns that reflect dietary function or phylogeny.

Specifically, I will consider how temporalis, masseter and the pterygoids contribute to the entire jaw adductor mass, their mass compared to body mass and to endocranial volume, and their specific and relative areas of attachment to the skull. I also evaluate the hypothesis that species with a high bite force and large body mass, such as the hypercarnivores (Wroe *et al*., 2005; Christiansen and Wroe, 2007), have absolutely and relatively larger muscles, and I speculate that the morphology of the masticatory musculature of hypercarnivorous canid species differs from those of generalists and small prey specialists and deviates significantly from simple predictive patterns of size scaling. Hypercarnivorous species apprehend, kill and dismember large prey such as bison, zebra and wildebeest, and may be expected to have more robust skulls and greater muscle masses to tackle such biomechanically demanding tasks as slicing through tough skin, and stripping soft tissue from large bones. Conversely, small prey specialists and generalist species tackle prey with small body masses and commensurately smaller bones, thinner skin and slighter muscles, and may be expected to have less powerful muscles driving jaw adduction. As the jaw adductor muscles arise solely from the cranium and cover much of its external surface, I also consider how they are accommodated on the skull and, through shape analysis, explore whether the diversity of head shape among canids is influenced by constraints and concomitant compensatory adjustments for housing the masticatory muscles. Previous studies have been able to categorise canids according to diet based on overall skull shape (Radinsky, 1981; Van Valkenburgh, 2007) or upper jaw morphology (Slater *et al*., 2009), with the hypercarnivorous species tending toward a broad stocky skull and shortened snout, and the small prey specialists being more gracile with a long rostrum and narrow jaws. Here I regard the bony skeleton of the head to be made of three modules – the cranial part, the rostral part and the mandible, and consider if all of the modules aid in determining diet or if some are instead allied with muscle accommodation.

3.3 Materials and Methods

3.3.1 Specimens, imaging and skull reconstruction.

Specimens from 8 of the 13 genera that make up the Canidae family were obtained from either euthanased zoo stock or vermin control (Table 3.1). There were 19 individuals from 12 species with representatives from the three major clades and the three trophic groups. Body mass values were based on the average published values for each species and are stated in Table 3.1. (MacDonald and Sillero-Zubiri, 2004; Nowak, 2005). The data set is not inclusive of all canid species; however, it covers a broad range of head shapes, body sizes and phylogenetic groups, and it includes all four of the hypercarnivorous species (Van Valkenburgh, 2007). For the purposes of this study species were identified as being from one of the three trophic groups as described by Slater et al. (Slater *et al*., 2009) (Table 3.1). Further details of the specimens used are given in Chapter Two, Table 2.2. Specimens were either chilled fresh or frozen and then defrosted, but no fixative agent was used on any specimen. All heads were dissected at near occlusal bite, that is, with minimal gape (Figure 3.1A), and the jaw adductor muscles, that is temporalis, masseter and the pterygoids were identified and removed. Photographs of the key structures are given in Figure 3.1. Further details of dissection techniques and gross muscle anatomy and are found in Chapter Two, part 2.4.2.

All specimens were digitally imaged using computer tomography (CT). CT methodology is discussed in Chapter Two, part 2.3.1, and details of CT settings, pixel resolution and slice spacing used during imaging are given in Chapter Two, part 2.3.3.

Pre-processing of CT data was done with ImageJ v1.45s (Schneider *et al*., 2012).

The CT scans were used to create virtual three-dimensional reconstructions of the skeletal components of each head using Avizo 8.1 software (FEI Systems, Oregon, USA). For this chapter of the thesis there was no requirement to identify multiple different materials within each skull, and so the CT scans were partitioned into either high density bony and dental materials (coloured orange in the figures), or low-density soft tissue structures and air

(coloured dark grey) (Figure 3.3B). Partitioning was done using a thresholding algorithm to distinguish and isolate greyscale tones representative of skeletal material in the CT data. This created a 3D surface of each skull, which was used to identify morphological landmarks for use in further analyses (this chapter, part 3.3.2.1).

All 19 specimens were used for the dissections to determine cranial volume and muscle masses, and in the initial landmarking and geometric morphometric analyses. Following preliminary analysis based on spatial positioning with the principal component scatterplot for whole skull shape, mean shape individuals were selected to represent species with more than one sample. Subsequent GMM and PC analyses focused only on these 12 representative individuals.

Table 3.1. Details of specimens, mean muscle masses, muscle attachment surface areas, endocranial volumes and endocranial surface areas.

	n/sex	Phylogenetic group	Dietary specialism	Mean body mass (g) from literature [1,2]	Temporalis mass (g)	Masseter mass (g)	Pterygoid mass (g)	Total jaw adductor mass (g)	Temporalis surface area (mm^2)	Masseter surface area (mm^2)	Pterygoid surface area (mm^2)	Total jaw adductor surface area (mm^2)	Endocranial volume (mm^3)	Endocranial volume surface area (mm^2)
Alopex lagopus	1M	Fox-like	Small prey specialist	5200	43.8	14.9	4.47	63.1	2298	486	329	3113	45290	9360
Canis lupus	1F,2M	Wolf-like	Hypercarnivore	36500	179.5	84.5	25.7	289.7	5593	2069	1397	9059	143367	18575
Canis mesomelas	1M	Wolf-like	Small prey specialist	9700	46.6	20.2	6.7	73.5	2822	682	479	3983	67830	11042
Chrysocyon brachyurus	1F	South American	Small prey specialist	25000	106.1	61.5	13.2	180.8	5428	1443	937	7808	111800	14988
Cuon alpinus	1F	Wolf-like	Hypercarnivore	13500	81.6	40.6	10.4	132.6	4383	1197	776	6356	108200	16365
Lycaon pictus	1F,2M	Wolf-like	Hypercarnivore	26500	141.7	84.4	19.4	245.5	5853	1611	1311	8775	149500	19877
Nyctereutes procyonoides	1M	Fox-like	Generalist	6500	19.9	10.6	3.2	33.7	2237	632	276	3145	30120	7905
Otocyon megalotis	1M	Fox-like	Generalist	4200	13.5	6.6	2.3	22.4	1140	406	248	1794	30490	7159
Speothos venaticus	1F	South American	Hypercarnivore	6500	42.7	24.6	5.1	72.4	2864	694	438	3996	51720	9341
Vulpes corsac	3M, 1unknown	Fox-like	Small prey specialist	2850	14.7	6.4	2.3	23.4	1520	381	275	2176	31910	6677
Vulpes vulpes	1M	Fox-like	Small prey specialist	8500	48	19.3	5.7	73	2739	725	498	3962	52430	10060
Vulpes zerda	1F	Fox-like	Generalist	1150	5.6	2.4	0.9	8.9	927	203	117	1247	19560	5100

1. Nowak, 2005 (Nowak, 2005), 2. MacDonald and Sillero-Zubiri, 2004 (MacDonald and Sillero-Zubiri, 2004).

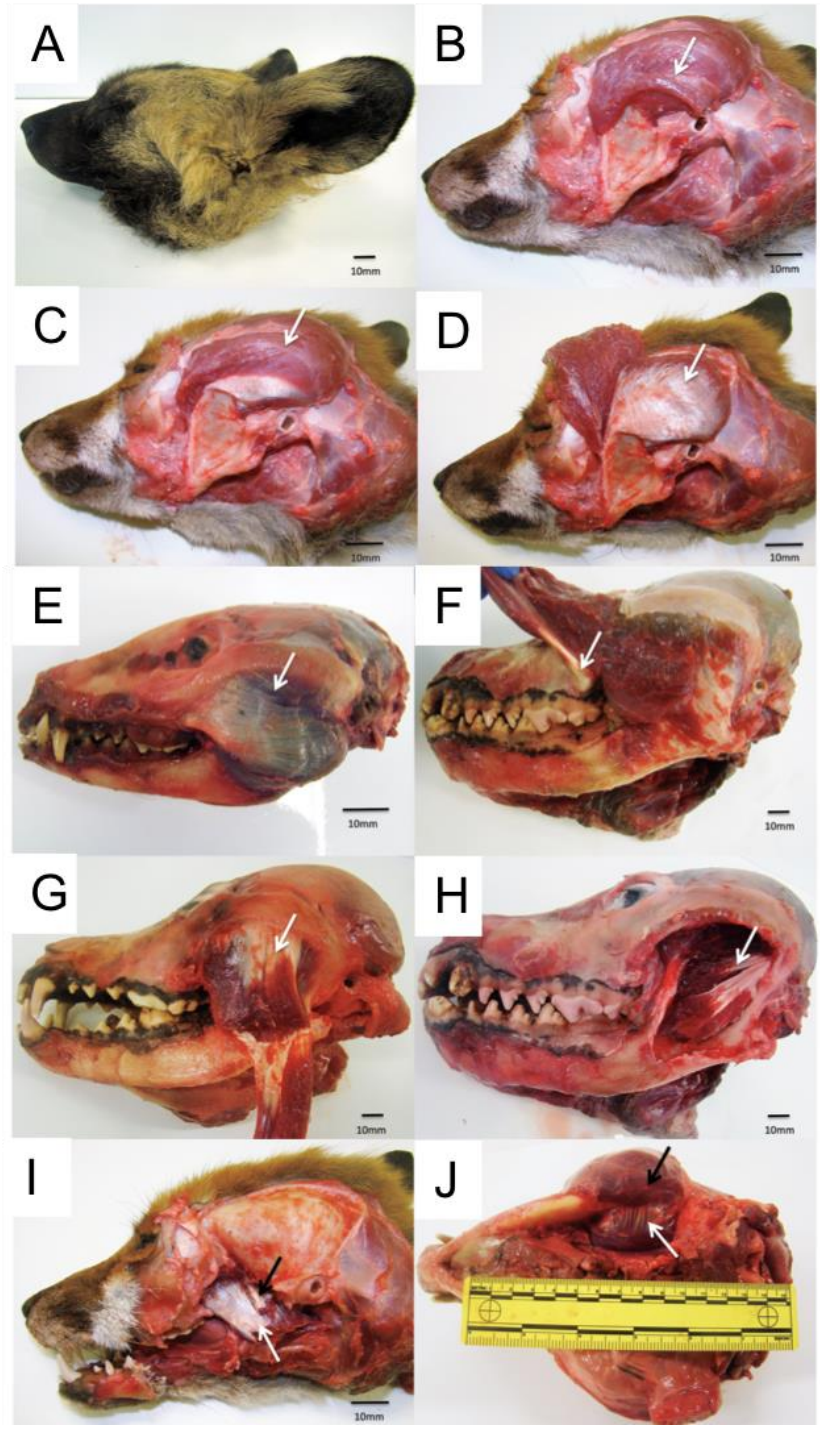

Figure 3.1 A) *Lycaon pictus*, intact head, B) *Vulpes vulpes,* suprazygomatic temporalis (white arrow), C) *Vulpes vulpes,* superficial temporalis (white arrow), D) *Vulpes vulpes,* deep temporalis (white arrow), E) *Nyctereutes procyonoides*, superficial masseter (white arrow), F) *Lycaon pictus,* tendon of origin of superficial masseter (white arrow), G) *Canis lupus*, deep masseter (white arrow), H) *Lycaon pictus*, zygomaticomandibularis (white arrow), I) *Vulpes vulpes*, Medial pterygoid (white arrow) and lateral pterygoid (black arrow), J) *Canis lupus*, superficial masseter (black arrow) and pterygoids (white arrow).

3.3.2 Form, Shape and Morphometric Analysis

Form analysis considers the shape, size, location and orientation of an object, whilst shape analysis considers shape alone. Morphometrics, the quantitative analysis of form or shape, is key in a wide range of biological studies. For example, morphometric analyses in ontogenetic studies describe normal growth within a species lifespan (Herring, 2005; Segura and Prevosti, 2012; Tarnawski *et al.*, 2015), whilst pathological studies identify abnormal changes within an individual (Soibelzon *et al.*, 2014; Milella *et al.*, 2015). Fossil evidence may be explored to quantify morphological changes over an evolutionary timescale (Wroe and Milne, 2007; Christiansen, 2008; Figueirido *et al.*, 2010; Tanner *et al.*, 2010; Klingenberg and Marugán-Lobón, 2013). In this chapter I use form analysis to quantify allometric differences between species, and geometric morphometric shape analysis to identify species level differences in cranial morphology.

Traditional morphometric analyses use linear measurements (i.e. lines drawn between landmarks), or ratios or angles relating to linear measurements, to produce tables of data for statistical analysis. Although aspects of the form are measured, the geometry of the object is not retained in the analyses. This results in numerical descriptions of shape differences which are difficult to interpret and visualize (O'Higgins, 2000; Cooke and Terhune, 2015). An alternative approach, geometric morphometrics (GMM), was pioneered by researchers including Bookstein, Rholf, Marcus and Corti, Dryden and Mardia, in the late 1980s and early 1990s (Bookstein, 1986; Rohlf and Marcus, 1993; Marcus and Corti, 1996; Dryden and Mardia, 1998). This approach defines shape using landmarks within a Cartesian coordinate space, rather than measured distances, and allows for retention of shape detail throughout analyses, and visualization of shape differences. An additional advantage is that rather than treating each linear record as an independent measure, GMM allows for the categorisation of the entire shape. This enables further analyses to identify entire shape covariation with other variables, for example, categories of diet or body mass (O'Higgins, 2000; Cooke and

Terhune, 2015; Klingenberg, 2016). Geometric morphometric analysis requires several steps, the first of which is to capture the geometry of the specimens under investigation. In this chapter I used 3D landmarks to record the bony morphology of each head.

3.3.2.1 Landmarking.

The most intuitive, although until the advent of modern computational ability, the most technically difficult, way to quantify form and shape is by recording landmark co-ordinates. Landmarks are discrete points at a specified locus that are homologous between specimens, and can be identified using two or three-dimensional data (O'Higgins, 2000; Zelditch *et al.*, 2012; Adams *et al.* 2013; Cooke and Terhune, 2015). Three-dimensional landmarks are recorded as a series of X, Y, Z coordinates within a Cartesian space. Landmarks need to be selected to ensure that their final configuration suitably describes an object or specific area of interest within an object, and that individual landmarks are homologous between similar objects. Selection of specific landmarks was based on three criteria after Webster and Sheets (Webster and Sheets, 2010): that they must have same relative position i.e. are homologous between samples, that they must offer an adequate summary of morphology, and that they must be reliably digitisable. Following Bookstein (Bookstein, 1997), landmarks are identified and categorised as one of three types: Type I landmarks are defined locally and are evidenced by unambiguous features such as the intersection of three points. They are strongly homologous between specimens and provide the most confidence. Type II landmarks offer some clear local boundary such at the tip of a tooth or an area of minimal curvature but are not as well bounded as type I landmarks. Type III landmarks are constructed geometrically and may be relational to other landmarks e.g. the midpoint between two landmarks, or the furthest caudal distance from one. Type III landmarks typically lack at least one co-ordinate and offer the least degree of confidence. Landmark classification is also therefore hierarchical, with Type I being optimal, and Type III least optimal. The difficulty

with limiting sampling to only Type I landmarks is that they can be low in number for a given structure and not cover the form adequately or may fail to describe the region of interest. For this reason, landmarks of Type II and III are also widely used (Bookstein, 1997; O'Higgins, 2000; Barbeito-Andrés *et al.*, 2012; Zelditch *et al.*, 2012). Semi-landmarks are used to describe curved forms where no true landmarks are identifiable. Their distribution along a concave or convex surface is often determined by an algorithm. Some authors describe this type of landmark as a Type III (Cooke and Terhune, 2015; Echarri and Prevosti, 2015). The use of Type II, Type III and semi-landmarks is prevalent in many skull studies throughout the literature (Monteiro and Nogueira, 2010; Barbeito-Andrés *et al.*, 2012; Prevosti *et al.*, 2012; Echarri and Prevosti, 2015; Terhune *et al.*, 2015; Fabre *et al.*, 2017).

In this chapter a series of 71 anatomical landmarks per specimen, representing the entire skull and mandible, were selected (Figure 3.2 and Table 3.2). Axial, coronal and sagittal CT slices (Figure 3.3A) plus computer generated isosurfaces of the skulls (Figure 3.3B), were viewed using Avizo software (FEI Systems, Oregon, USA) and used to locate and place each landmark. Landmarks were recorded using Cartesian (X,Y,Z) coordinates to place them within virtual three-dimensional Euclidean space. They consisted of Type I, Type II and Type III landmarks (Table 3.2). The nasion, despite being a Type I landmark, was difficult to identify with certainty in the more aged specimens due to the closure of the nasal and frontal bone sutures. In these instances, the position of the landmark was estimated with reference to other local features. For the GMM analyses tooth point landmarks were avoided due to a some age-related wear being evident within the sample set.

Bony landmarks that were common to both the CT and MR datasets were co-registered using Avizo software to combine both imaging modalities into one series (Chapter Two part 2.3.5). This enabled visualisation of muscles and other soft tissue structures relative to the reconstructed skull (Figure 2.4). The aim was to determine if muscle placement on the skull, relative to bony landmarks such as the TMJ, was quantifiable, and if so could it distinguish

between trophic or phylogenetic groups. To do this, a further series of 74 landmarks were placed on the surfaces of the jaw adductor muscles (Appendix 3).

3.3.2.2 Modularity

The head is the most complex region of mammalian anatomy, both morphologically and functionally. It houses the major component of the central nervous system, the brain, plus the special sensory organs associated with vision, olfaction, taste, hearing and balance. It also houses the start of both the gastrointestinal and respiratory tracts. To separate out one form or function and consider it in isolation is impossible, and to attempt to do so would be misleading. The functional interrelatedness of the phenotypic traits of the head are demonstrated in many examples, where one structure may fulfil multiple functional roles. For instance, the bones making up the calvarium, must house and protect the brain and the vestibulocochlear organs on their internal surfaces, and accommodate the muscles of mastication and swallowing, and house and protect the eyes on their external surface. The bones of the caudal rostrum must accommodate premolar and molar teeth, withstand stress and strain forces during biting, act as a respiratory filtration system by way of their internal turbinate bones, house olfactory receptors and accommodate muscles of the face and soft palate. Evolution clearly demonstrates that morphologies change over time and between species, and this raises many questions about the integration of biological traits. The ability to change one trait without changing another, depends in how linked, or integrated, the traits are. If a trait were not linked to any other trait it could be independently adjusted either through developmental (ontological), generational or evolutionary time scales. However, if it is related (either genetically, developmentally or functionally) to any other trait, all linked structures must either be constrained, or all change together (co-vary) (Bolker, 2000; Frankino *et al.*, 2007; Mitteroecker and Bookstein, 2008). The integration of traits may determine the extent to which species are adaptable and ultimately influence their

evolutionary pathways (Emerson and Hastings, 1998; Bolker, 2000). Sets of related traits are often referred to as modules, and whilst being integrated amongst themselves, are relatively independent from other modules (Cheverud, 1996; Goswami, 2006a, 2006b; Klingenberg, 2008; Klingenberg and Marugán-Lobón, 2013). In her study on mammalian skull (Goswami, 2006a), Goswami identified six discrete modules that make up the eutherian skull (anterior oronasal, molar, zygomatico-pterygoid, orbital, cranial vault and basicranium), but also noted that levels of integration were not equal across all species. For example, the primate cranial vaults were significantly less integrated than those of the carnivorans. This supported the hypothesis that primates expanded their cranial vaults to accommodate large brains, whereas carnivorans were more constrained (Goswami, 2006a).

Other work on canid head modularity has identified the skull component as having two modules (Drake and Klingenberg, 2010), and those that include the mandible (Curth *et al.,* 2017) have also considered this to be a discrete module. Following this, the 71 landmarks identified in this thesis were accordingly subdivided into three subsets to represent the three modules of the bony skeleton. These are the cranial component, that is most closely associated with housing the brain and the origin of the masticatory muscles, the rostral component that is most closely associated with the nasal cavity and upper dental arcade, and the mandibular component associated with housing the lower dental arcade and the insertion of the masticatory muscles (Table 3.2). The landmarks and their modular subsets were used in geometric morphometric analyses to explore shape variation (this chapter), and measurements and ratios from landmarks were also used in regression analyses in Chapter Four.

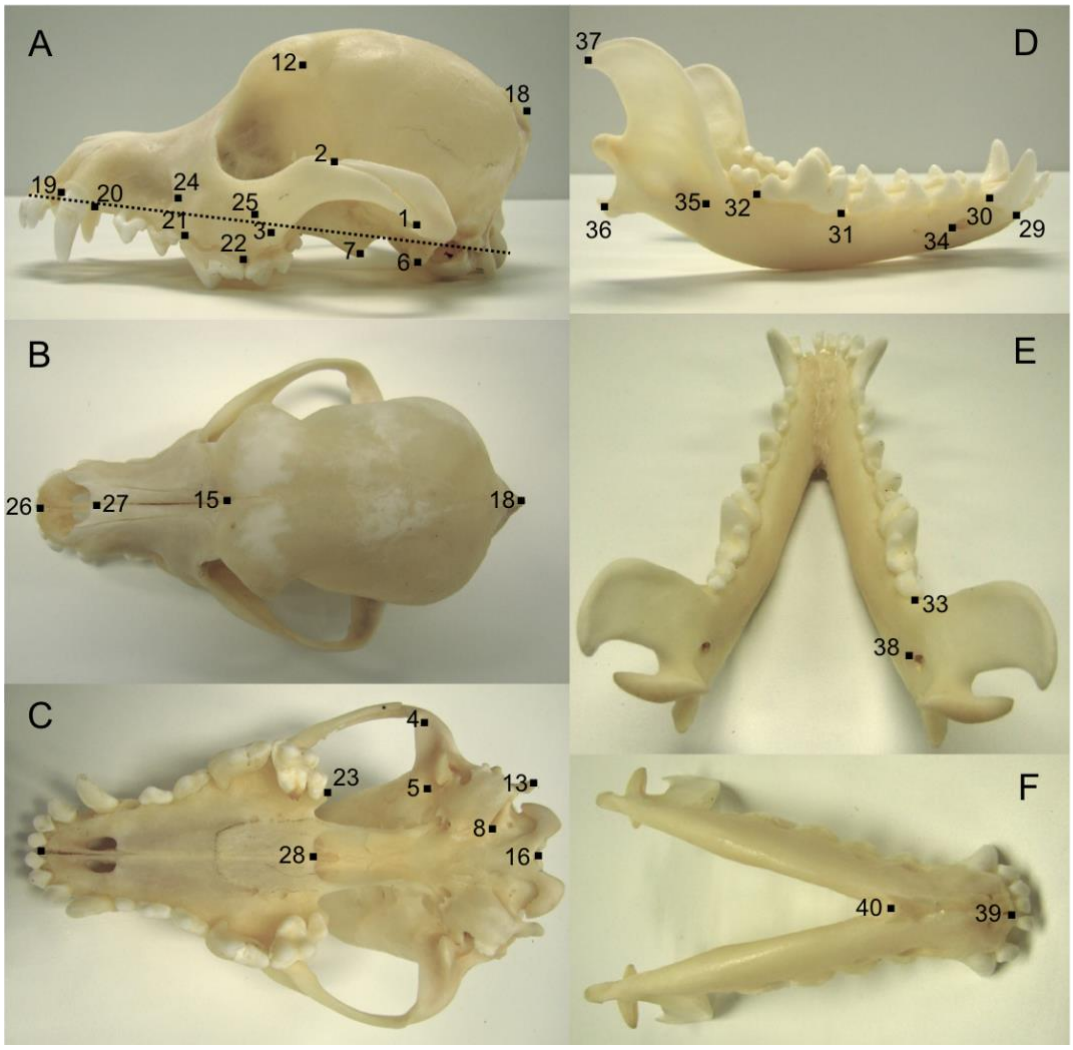

Figure 3.2. Domestic dog skull. Lateral(A), dorsal (B) and ventral (C) aspects of the skull illustrating position of the cranial and rostral component landmarks. Landmarks 9, 10, 11, 14 and 17 are not visible. Lateral (D), caudodorsal (E) and cranioventral (F) aspects of the mandible illustrating the mandibular component landmarks.

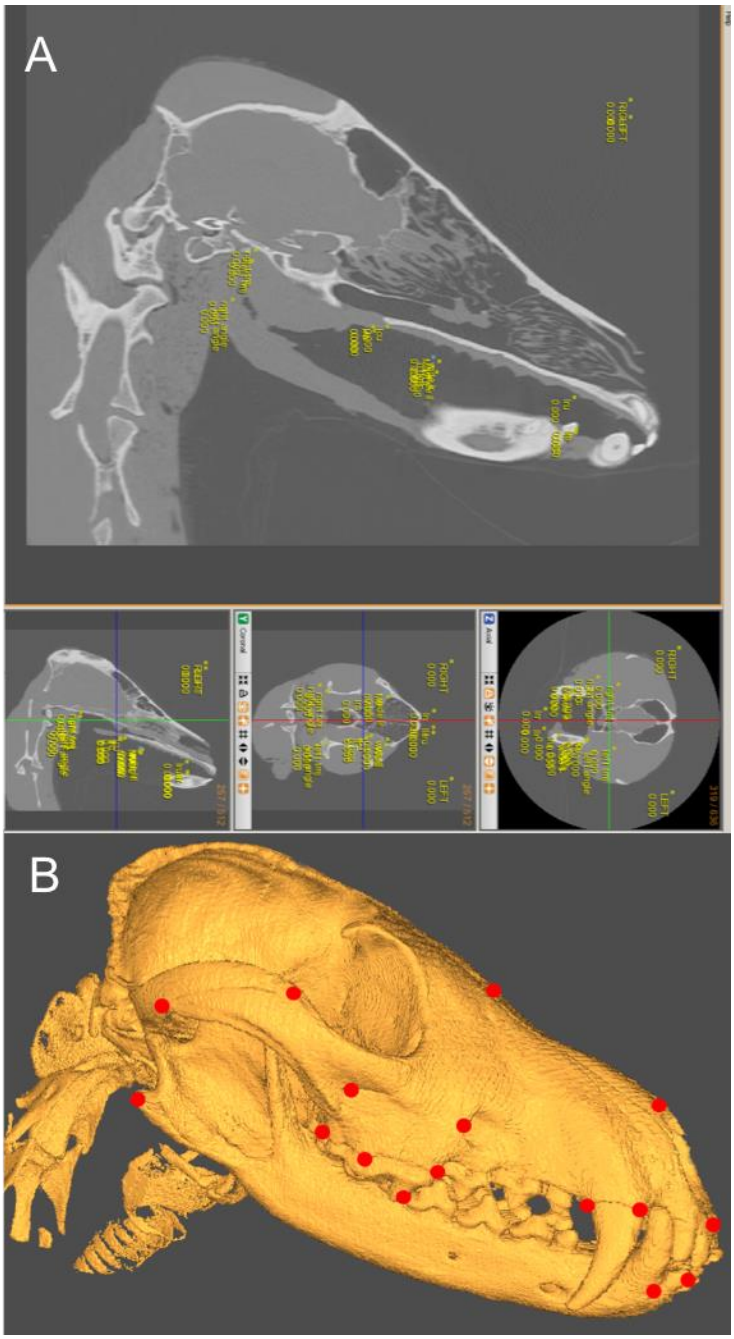

Figure 3.3 A, Coronal slices of *Chrysocyon barchyurus* CT scans used to identify landmarks B, isosurface of *Vulpes vulpes* skull used to place landmarks (red circles).

Table 3.2 List of skull component landmarks and their landmark types

CRANIAL COMPONENT			ROSTRAL COMPONENT			MANDIBULAR COMPONENT		
LANDMARK		TYPE	LANDMARK		TYPE	LANDMARK		TYPE
1	Caudal zygomatic temporal junction	I	19	Rostral alveolus of upper canine	II	29	Rostral alveolus of lower canine	II
2	Rostral zygomatic temporal junction	I	20	Caudal alveolus of upper canine	II	30	Caudal alveolus of lower canine	II
3	Lower rostral zygomatic ridge	I	21	Rostral alveolus of upper carnassial	II	31	Rostral alveolus of lower carnassial	II
4	Lateral articular mandibular condyle	II	22	Caudal alveolus of upper carnassial	II	32	Caudal alveolus of lower carnassial	II
5	Medial articular mandibular condyle	II	23	Caudal upper tooth row	II	33	Caudal lower tooth row	II
6	Ventral retroglenoid process	II	24	Lateral point of infraorbital foramen	II	34	Lateral point of rostral mental foramen	II
7	Pterygoid process	II	25	Zygomatic maxillary junction	I	35	Rostroventral masseteric fossa on mandible	III
8	Tympano-occipital fissure, medial point	II	**26**	**Interincisive (Prosthion)**	II	36	Angular process on mandible	III
9	Rostral pterygoid ridge	II	**27**	**Rostral internasal**	I	37	Caudal coronoid process	III
10	Caudal pterygoid ridge	II	**15**	**Nasion**	I	38	Medial point of inferior alveolar foramen	II
11	mid pterygoid ridge	III	**28**	**Caudal hard palate**	II	**39**	**Rostral mandibular symphysis**	II
12	Zygomatic process of frontal bone	II				**40**	**Caudal mandibular symphysis**	II
13	Caudal ventral jugular process	II						
14	Cochlear apex	I						
15	**Nasion**	I						
16	**Basion**	II						
17	**Dorsal foramen magnum**	II						
18	**Inion**	III						

Landmarks in bold type are midline and unpaired. All other landmarks are bilaterally paired.

3.3.2.3 Geometric morphometric analysis

After landmark acquisition the next stage in GMM is to align all specimen landmark configurations to a common position and orientation. Due to the mathematical complexity required to perform this and the further analyses of GMM, computational software is required. For this I used MorphoJ (Klingenberg, 2011) as it is widely utilised in many similar studies (Drake and Klingenberg, 2010; Palmqvist *et al.*, 2011; Curtis and Van Valkenburgh, 2014; Echarri and Prevosti, 2015; Figueirido *et al.*, 2015; Martín-Serra *et al.*, 2016; Curth *et al*., 2017), and is freely available to download. Superimposition was performed using the Generalised Procrustes Analysis (GPA) method. GPA uses the first shape within the dataset to estimate an initial mean shape. Subsequent shapes are aligned as closely as possible to the mean shape. The estimate of the mean shape is then recalculated. Iterations of this process are repeated until the mean shape does not change significantly. Other methods include two-point registration, sliding baseline registration and resistant fit registration. These are based on alternative methods of establishing the configuration of landmarks to which all others are referenced to describe shape differences (Webster and Sheets, 2010). Although GPA has some disadvantages (the process of translation, rotation and scaling reduces the numbers of degrees of freedom, making outputs unsuitable for standard statistical analyses, and the orientation of axes may not be respected during realignments) (Webster and Sheets, 2010), it is considered statistically robust and has been used by many previous authors (Gröning *et al.*, 2011; Walmsley *et al.*, 2012; A-C Fabre *et al.*, 2017; Meloro *et al.*, 2017; Nanova *et al.*, 2017). Next, a common centroid size is determined. Centroid size is a measure of size. To do this the centroid location for each individual specimen is identified as the mean of the co-ordinates for all X, Y, Z landmarks. Centroid size is then determined for each individual by calculating the square root of the sum of the squared distances of all the landmarks from the centroid. All specimens are then scaled to the common centroid size to remove size variability. All that remains is shape data, with minimal distances

between the homologous landmarks of each specimen. From this a Procrustes distance can be calculated. The Procrustes distance is the square root of the sum of the squared distance between homologous landmarks and is a measure of shape difference (Zelditch *et al.* 2012; Cooke and Terhune, 2015; Klingenberg, 2016). A consensus (mean) landmark configuration is computed and individual landmarks are visualisable relative to the consensus figuration (Figure 3.4). Procrustes co-ordinates or residuals are produced for each individual which represent deviations from the consensus configuration (Mitteroecker and Gunz, 2009).

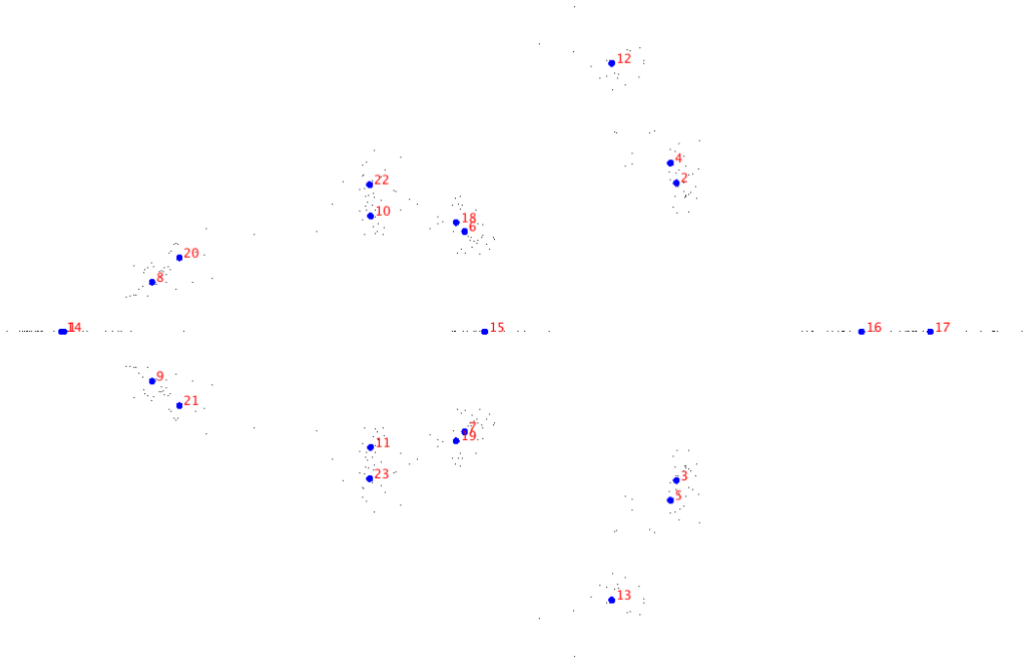

Figure 3.4 MorphoJ mapping of CT derived bony landmarks. Each large blue dot represents the mean Procrustes landmark, and are numbered in red. The smaller blue dots are representative of the individual samples within the dataset.

The Procrustes coordinates of each individual are represented by a single data point within a shape space. Shape space is a multidimensional non-Euclidean (curved manifold) space that allows for the isotropic distribution of individual specimens. In GMM, Kendall's shape space is used as it represents all possible shapes for a given number of dimensions (2D or 3D)

and a given number of landmarks (O'Higgins, 2000; Mitteroecker and Gunz, 2009; Klingenberg, 2016). The number of dimensions of the shape space for 3D landmarks is determined by the equation *3k-7,* where *k* represents the number of landmarks. Only the simplest shape space, that for 2D triangles is easy to visualise; it corresponds to the surface of a globe, more complex shapes fit into more complex shape spaces. Every potential shape has a specific space within the shape space. If landmarks are distributed isotropically between objects, the objects are isotropically distributed within the shape space (O'Higgins, 2000). The next step is the ordination of the dataset. In essence, this summarises the complex multidimensional dataset into a low dimensional space where similar shapes (in this instance similar head shapes) group together. Ordination allows shape differences to be visualised and quantified. The most frequently used ordination method, and the one used in this study, is principal component analysis (PCA) in the tangent plane to the shape space. The tangent plane to the curved Non-Euclidean shape space is used as this allows the data points to be represented in a Euclidean shape space for easier statistical analyses. Landmarks with the greatest variation between individuals had the greatest influence on the principal component (PC) scores and describe the most morphologically diverse regions of the skull. PC scores are illustrated using eigenvalue plots (Figure 3.5), and scatterplots place species in terms of morphological similarity to one another (Figures 3.12 and 3.13). Species with similar morphologies cluster together on the scatterplot. Phylogenetic trees can be mapped onto this data to visualise how individuals, species or genera are dispersed throughout the space (Figures 3.12 and 3.13).

In this thesis, GMM analysis was used to identify and quantify patterns of morphological variation across species and between dietary niche groups. To ensure that all species had equal weighting in the analysis, one representative individual was chosen for each species. These individuals were identified from a preliminary morphometric analysis as the specimen closest to the mean shape for that species. The three-dimensional co-ordinates for all sets

of landmarks were imported into MorphoJ 1.45s and paired across the midline (Klingenberg and Gidaszewski, 2010). Generalised least squares full Procrustes fit was performed on all sets of data, which were then aligned by their principal axes. The asymmetric component of the shape change was briefly reviewed as it can highlight errors as well as asymmetries and the symmetric component was then further explored with a covariance matrix and principal components analyses to ascertain interspecific shape changes (Klingenberg and Gidaszewski, 2010). Landmark sets representing the entire head and the individual component modules were analysed. Scatterplots of the principal component (PC) scores were produced to visualize the distribution of datum points within the shape space, and wireframe models were created using key landmarks to visualize the range of shape deformation between the extremes. Scree plots of eigenvalues were produced and the broken stick method was used to assess which PCs to explore. Broken stick analysis assumes that if the total variance, that is the sum of all eigenvalues, is divided randomly amongst the various components then the expected distribution follows that of the expected values of a stick randomly broken into the same number of decreasingly sized sections. Eigenvalues that exceed the expected values are likely to be more significant that those that do not (Frontier, 1976; King & Jackson, 1999; Mhamdi & Devaux, 1994; Ordination & Goodall, 1984; Sakamoto, Lloyd, & Benton, 2010; Society, 2019).

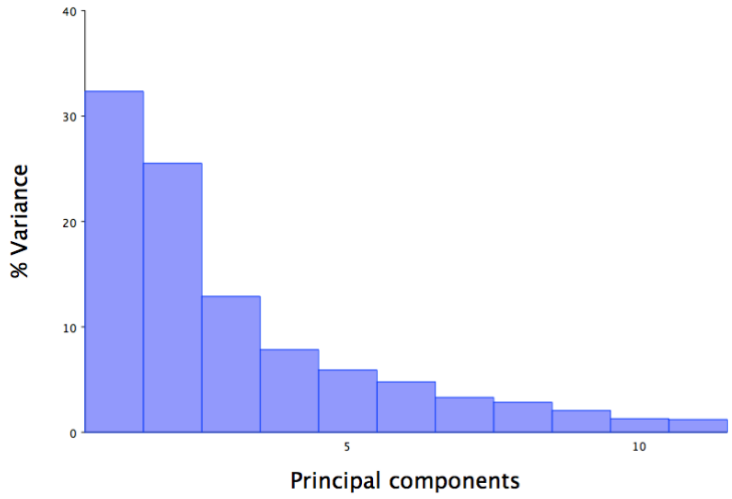

Figure 3.5 Eigenvalue scale showing the proportion of variance within the dataset for each principal component.

3.3.3 Calculating muscle origin surface areas, endocranial volumes and endocranial volume surface areas.

The bony boundaries of each jaw adductor muscle origin were established using the combined CT/MR scans (Chapter Two, part 2.3.5), dissection photographs (Chapter Two, part 2.4.2) and literature on domestic canids (Getty, 1975; Liebich *et al.*, 2009; Evans and De Lahunta, 2013) as guides. The surface of each virtual 3D skull model was visualised by using the surface generation module in Avizo 8.1 (FEI Systems, Oregon, USA), and then simplified into many small triangles using the surface view module. Muscle origins where then demarcated on each skull and their surface area calculated using the area calculation tool (Figure 3.6).

Brain size is an important variable to consider when studying head shape and size. Comparative measurements can identify allometric trends and identify constraints on overall head size or head shape. In this chapter endocranial volume (EV), the space within the cranial cavity, was used as a proxy for brain volume. EV was calculated from CT images using the semi-automatic segmentation 3D Active Contours function built into ITKsnap v2.4 software (Yushkevich *et al.*, 2006). This allowed a contiguous region of similar density voxels in an

individual slice to be identified and filled with an identifying coloured label. All slices are then reconstructed to make a volume. Manual editing of selected regions was performed to correct any anomalies, for example in the region of the cribriform plate where the bone was very thin. The cranial cavity appeared as a defined space and was labelled red (Figure 3.7A). The reconstructed volume represented the space within the cranial cavity, the endocranial volume (Figure 3.7B). This is the first time this data has been reported for CT derived data for such a large number of closely related canid species. Previous canid studies have used external skull measurements (Finarelli, 2006; Damasceno *et al.*, 2013), or by filling the cranial cavity with glass beads to measure EV (Gittleman, 1986) (Table 3.3). To validate the CT derived values, Shapiro-Wilk statistical tests were used to determine if the data was normally distributed and further appropriate statistical tests used to compare CT derived values with the given values from previous authors.

One advantage of using the virtual modelling method to determine endocranial volume was that a virtual model of the brain was constructed (Figure 3.7B). This in turn allowed the endocranial volume surface area (EVSA) to be determined. The model module in 3D Slicer v4.3 (Fedorov *et al.*, 2012) was used to calculate EVSA values. These were then used as a proxy for the internal surface area of the cranium. The internal surface area of the cranium and external attachment surface areas of the neurocranium could then be considered as two separate variables.

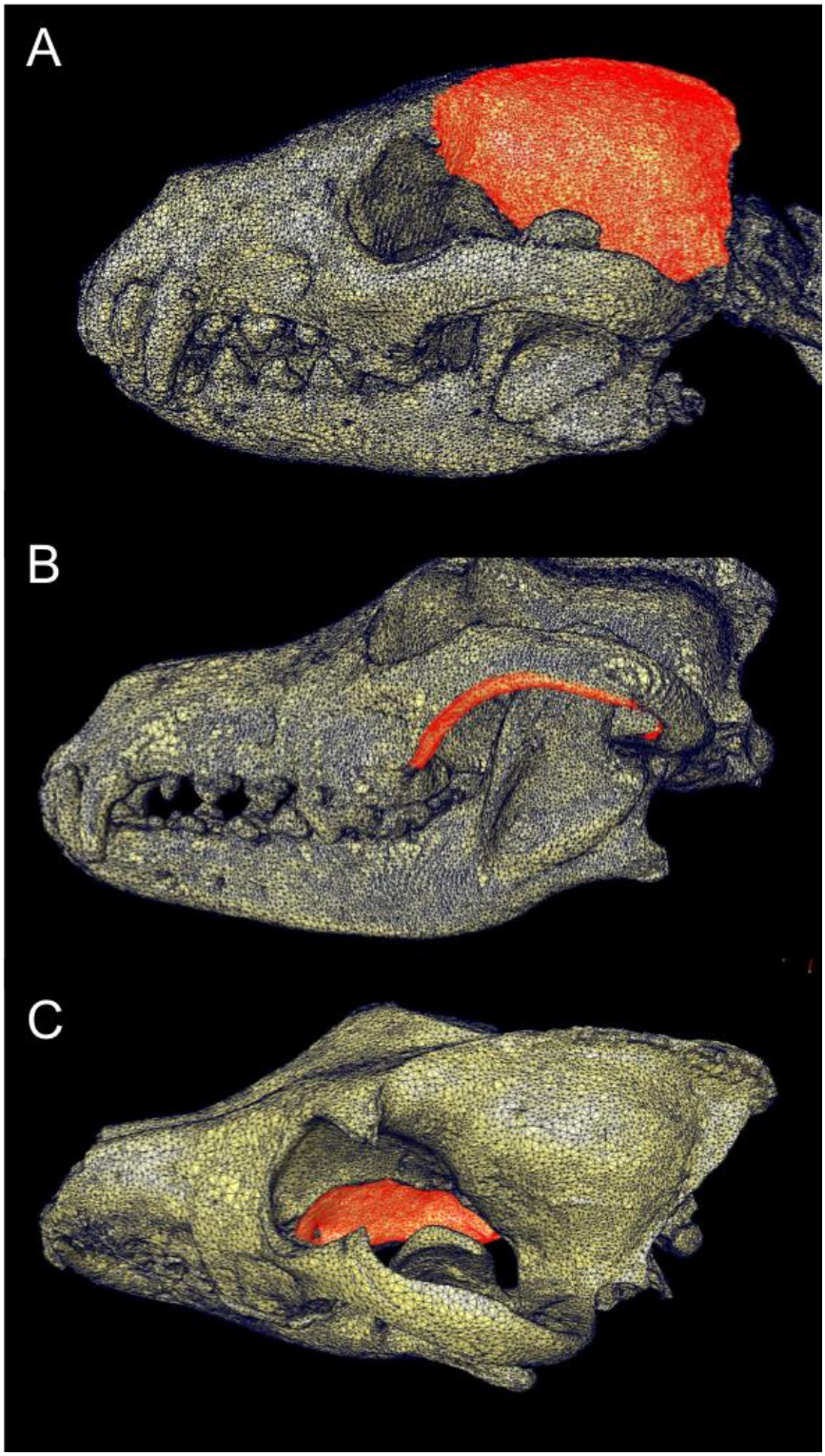

Figure 3.6 CT reconstructions illustrating the surface area attachment site for A temporalis, *Speothos venaticus*, B masseter, *Canis lupus* and C, the pterygoids, *Canis lupus*.

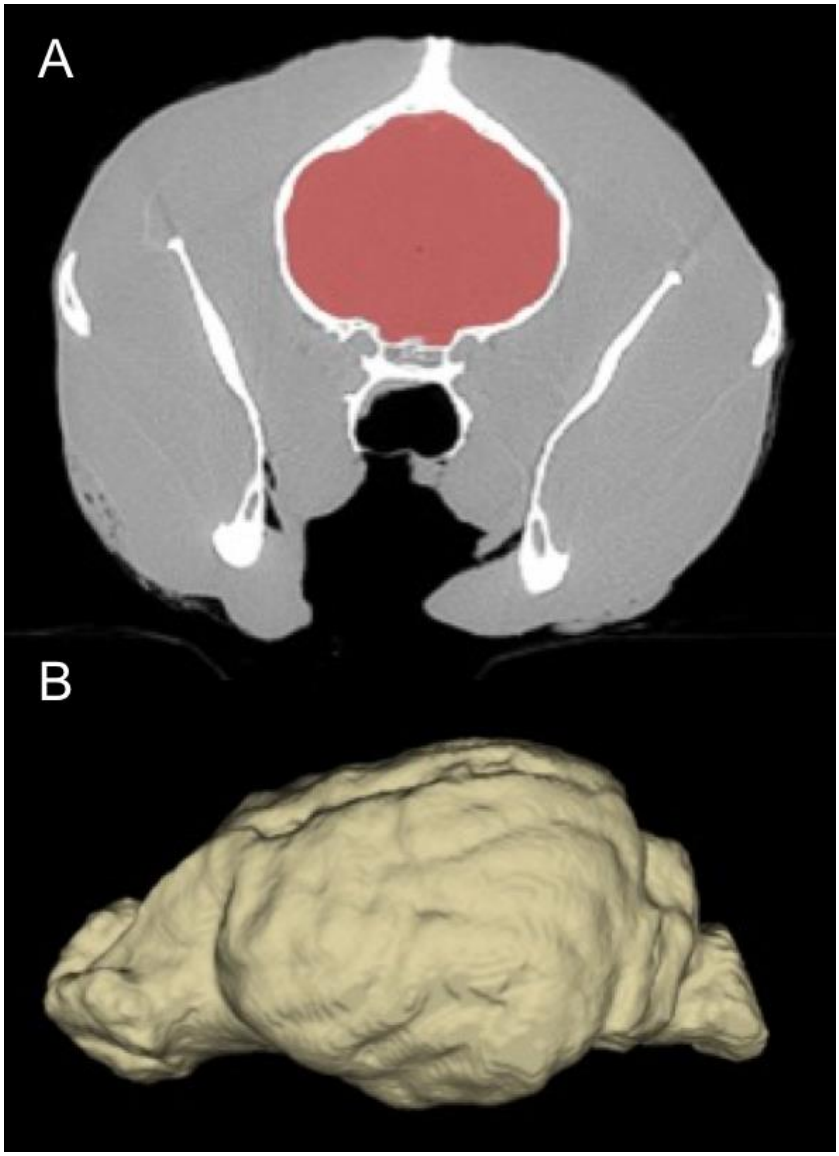

Figure 3.7 A. Individual axial CT slice of *Vulpes corsac* with endocranial cavity highlighted in red. B. Virtual 3D endocast of *Chrysocyon brachyurus.*

3.3.4 Phylogenetic Analyses.

Comparative studies of morphological differences are used to imply functional adaptations of traits. This considers that certain species have evolved particular traits in order to carry out specific functions. However, the shared phylogenetic history of related species means that traits are not statistically independent (Felsenstein, 1985; Maddison and Maddison, 1989; Harvey and Pagel, 1991; Garland *et al.*, 1999; Garland, 2005; Ricklefs *et al.*, 2016) Traits may occur in closely related species due to inheritance from common ancestors, rather than functional adaptation. In their 1991 work Harvey and Pagel (Harvey and Pagel, 1991) describe three key processes to account for why phylogenetically related species are similar. Firstly, phylogenetic niche conservatism, where vacant ecological niches become occupied by species that occupy similar environments and are phenotypically similar. Secondly, phylogenetic time lag describes traits persisting after speciation, even if they are to become obsolete, and thirdly the similarity of closely related species adaptive responses due to genetic or environmental constraints (Harvey and Pagel, 1991). Therefore, when comparing closely related species an independent estimate of their phylogenetic relatedness may give insight into the evolution of traits. Figure 3.8 illustrates how the more realistic phylogenetic trees that take into account hierarchy and non-independence can cause statistical problems. Phylogenetic independent contrast (PIC) analyses are a statistical method used to compare traits that takes into account the interrelatedness of species. In brief, PIC transforms original species data using algorithms, into independent and equally distributed contrasts, that consider the length and divisions of the branches (Garland, 2005; Freeman and Herron, 2014). From this point, standard statistical tests for correlation and regression may then be performed.

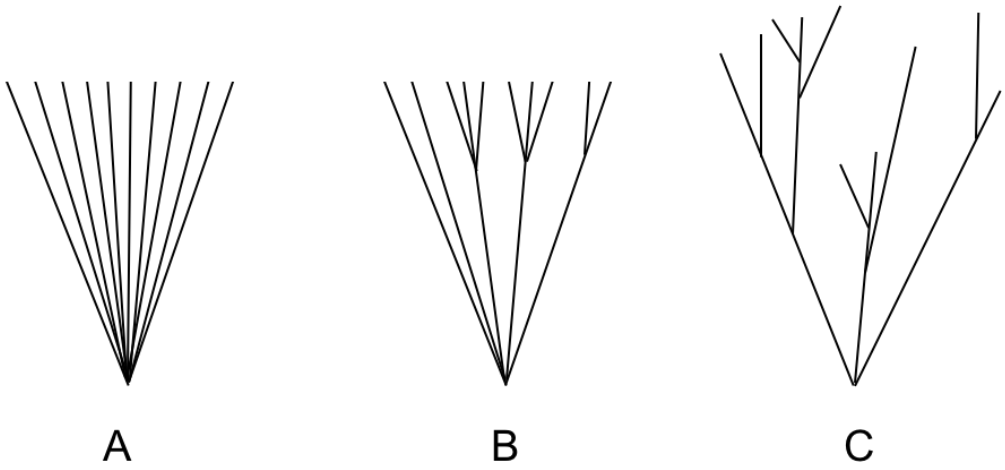

Figure 3.8 Phylogenetic tree structures after Garland (Garland, 2005). A indicates the star structure that assumes an unrealistic statistical independence and equal distribution. B is derived from a taxonomic tree that assume species are in unrelated 'mini-star' formation. C estimates real phylogenies that include hierarchical relationships and non-contemporaneous branch ends to indicate extinct species. This illustrates the non-independence of species.

As with any test, the reliability of the results reflects the quality of the input data. For such a closely related group as the extant canids establishing a clear phylogenetic tree is troublesome, and many different versions are available (Chapter One, part 1.2.5). In this study we used the canid tree published by Nyakatura (Nyakatura *et al.*, 2012) as this was an open source resource and could be trimmed to accommodate only the species within this study, and has been extensively used by previous studies (Conith *et al.*, 2018; Harano and Kutsukake, 2018; Machado *et al.*, 2018; Mazel et al., 2017; Rizzuto *et al.*, 2018; Veron *et al.*, 2017; Wu *et al.*, 2018). For further details of the tree used in PICs see Chapter One, part 1.2.5. The pruned tree is given in Appendix Four. A Brownian motion model of evolution was assumed, where rates of character change follow a normal distribution across the phylogeny. The canid phylogenetic tree was mapped onto the scatterplots of the shape variation performed in the GMM analyses (this chapter). Diagnostic tests were performed using the PDAP:Pdtree module v 1.16 in Mesquite v. 3.01 (Midford *et al.*, 2006; Maddison and Maddison, 2016). Eleven variables representing species means were analysed (Table 3.4). I determined the absolute values of the standardized phylogenetic independent contrasts

(PIC) for each character versus their standard deviations. A *P*-value of ≤ 0.05 would be regarded as significant and would indicate phylogenetic influence (with values greater than 0.05 indicating negligible phylogenetic signal). The reduced major axes regressions were also repeated using the PICs and the slopes compared against those for the standard data.

3.3.5 Statistics

Differences between endocranial volume studies, the dietary groups regarding the percentage contribution of each muscle to the overall jaw adductor mass and the percentage contribution of each muscle division to the total muscle mass were identified using statistical tests. Initially a Shapiro-Wilk test was performed for each variable to determine if the dataset was normally distributed. Kruskal-Wallis tests were used to compare variance between groups as not all datasets were evenly distributed and the sample size was small. Dunn's post hoc test were used to assess differences between groups. To evaluate body size scaling trends log transformed values of muscle mass, muscle attachment surface area, endocranial volume, endocranial volume surface area, geometric mean and zygomatic arch width were regressed against body mass using the non-parametric Reduced Major Axes (RMA). RMA regression was used as there is measurement error in both variables. However, it is worth noting that whilst the non-parametric RMA is the most appropriate method for these particular bivariate comparisons, the findings do not differ significantly from those calculated with ordinary least squares regression. Evaluations of isometry were made on the basis of the RMA slope 95% confidence intervals and *t*-tests against predicted slope values. As temporalis is the largest of the jaw adductors, with the largest surface area attachment, I chose it to be the main focus of the accommodation part of this study. Shapiro Wilk tests were also used to test for normal distribution of the significant differences between skull shapes (principal component values) and dietary groups, and Kruskal-Wallis tests used for comparing data between groups. The pruned phylogenetic tree (Nyakatura *et al*., 2012)

was then mapped against the principal component datum points to indicate the overall influence of phylogeny on shape variation and permutation tests were performed on the null hypothesis of no phylogenetic signal (Klingenberg and Gidaszewski, 2010). Multivariate regression of the Procrustes coordinates against the body mass, where the shape landmark datasets were the dependent variables, tested for allometric signal, that is, the percentage of shape change that could be predicted by the change in body mass. Similarly, multivariate regression of the Procrustes co-ordinates of the shape landmark datasets on both temporalis mass and endocranial volume identified the percentage of shape change that was related to the change in temporalis mass and endocranial volume. The statistical significance of the regression analyses was tested with permutation tests against the null hypothesis of independence, and *P*-values reported. Reduced major axes regressions, Kruskal -Wallis, post-hoc analyses and *t*-tests were computed in PAST (Hammer *et al*., 2001). Mapping the phylogeny onto shape, and the multivariate regression of shape on body mass, temporalis mass and endocranial volume were computed in MorphoJ (Klingenberg, 2011). A significance level of 0.05 was used in all statistical tests.

3.4 Results.

3.4.1 Muscle morphology

The masses (g) of the individual jaw adductor muscles and their subdivisions are presented in Table 3.1. Temporalis contributed between 57.4 and 69.3% to the total muscle mass (mean 62.1%), masseter contributed between 23.6% and 35.1% (mean 29.8%), and the pterygoids contributed between 6.7 and 10.5% (mean 8.2%). Next, individual muscles were considered. Temporalis was made up of three distinct divisions; suprazygomatic, superficial and deep temporalis. All species exhibited a well-defined suprazygomatic portion of temporalis (Figure 3.1B). This was consistently the smallest subdivision of temporalis, contributing 3.5 – 9.2 % (mean 6.5%) of the overall temporal mass. Origin was by way of a short wide tendon arising

from the temporal bone just dorsal to the external auditory meatus, and insertion was on the rostral aspect of the vertical ramus of the mandible. The remaining bulk of temporalis arises from the calvarium and divides into discrete superficial and deep parts. In the smallest species, *Vulpes zerda*, *Vulpes corsac* and *Otocyon megalotis*, the origin of temporalis was lateral to midline. In all other species left and right temporalis met at midline, and in the larger species were associated with a pronounced sagittal crest (Figures 2.17 and 3.6). Both the superficial and deep parts of temporalis insert onto the coronoid process and medial vertical ramus of the mandible (Figures 3.1C and 3.1D). The superficial part of temporalis contributes between 39.7 and 59.5% (mean 46.5%) of the overall temporalis mass and the deep between 33.2 and 54.8% (mean 47.0%). The masseter is highly complex with more than the previously noted superficial, deep, and zygomaticomandibularis layers. The superficial division was well defined and contributes between 38.3 and 56.8% (mean 47.6%) to the overall masseteric mass. The origin is chiefly from the most ventral part of the zygomatic arch, but there is also a strong tendinous component originating dorsal to the upper molars (Figures 3.1E and 3.1F). The caudal part of the superficial masseter extends beyond the caudal angle of the mandible to insert partly on the medial aspect of the mandible, and partly on the superficial aspect of the medial pterygoid (Figure 3.1J). The deep masseter (Figure 3.1G) originates from the medioventral aspect of the zygomatic arch. It is less clearly defined than the superficial division with many fibres arising or inserting onto aponeuroses within the muscle rather than directly to the bone of the mandible or zygomatic arch. It contributes between 12.2 and 36.4% (mean 24.1%) of the masseteric mass. Zygomaticomandibularis (3.1H) originates from the caudal medial zygomatic arch and contributes between 16.7 and 44.0% (mean 28.3%) of the overall masseteric mass. Both of the pterygoid muscles were considered together as one muscle, the pterygoids, as the medial pterygoid was considerably more extensive than the lateral pterygoid (Figure 3.1I). The (combined) pterygoids contributed between 7.0 and 10.5 % of the total jaw adductor mass (mean 8.2%). The

fascicles originate from the pterygoid plate of the skull and insert on the medial mandible. Temporalis arises from an extensive area of the lateral calvarium, in particular from the parietal, temporal, frontal and occipital bones (Figure 3.6A). The masseter arises from the ventral and medial borders of the zygomatic arch, which itself is made up from the zygomatic and temporal bones (Figure 3.6B), and the pterygoids arises from the sphenoid, pterygoid and palatine bones (Figure 3.6C). Temporalis originates from a mean of 69.0% of the total jaw adductor attachment surface area, the masseter 18.6% and the pterygoids 12.0%.

3.4.2 Surface area, endocranial volume and endocranial volume surface area.

Muscle attachment surface areas, endocranial volume surface area and endocranial volumes from this study and studies by Damasceno (Damasceno *et al*., 2013) and Gittleman (Gittleman, 1986) are reported in Table 3.3. Despite the comparative data from the earlier studies coming from different individual specimens, all three methods gave similar results. A Shapiro Wilk test determined that the data was not normally distributed and in the subsequent Kruskal-Wallis test, the *H* statistic was 0.4405 and the *p*-value was 0.80232. The result was not significant, implying that endocranial volumes determined from CT reconstructions were statistically indistinguishable than those determined by skull measurements or glass beads. This finding supports the use of any of these three methods to reliably determine endocranial volume.

Table 3.3 Muscle attachment surface area (SA), endocranial volume, and endocranial volume surface area.

	Temporalis SA mm^2	Masseter SA mm^2	Pterygoid SA mm^2	Endocranial volume SA mm^2	Endocranial volume mm^3	Endocranial volume mm^3 (Damascen a)	Endocranial volume mm^3 (Gittleman)
Alopex lagopus	2298	486	329	9360	45300	40000	35500
Canis lupus	5593	2069	1397	18575	143400	159200	131600
Canis mesomelas	2822	682	479	11042	67800	58000	56800
Chrysocyon brachyurus	5428	1443	937	14988	111800	120800	120300
Cuon alpinus	4383	1197	776	16365	108200	110800	94600
Lycaon pictus	5853	1611	1311	19877	149500	146900	129000
Nyctereutes procyonoides	2237	632	276	7905	30100	28200	28500
Otocyon megalotis	1140	406	248	7159	30500	32200	26800
Speothos venaticus	2864	694	438	9341	51700	65400	40500
Vulpes corsac	1520	381	275	6677	31900	x	x
Vulpes vulpes	2739	725	498	10060	52400	52700	43400
Vulpes zerda	927	203	117	5100	19600	20600	17300

*Comparative values from Damasceno (Damasceno *et al*., 2013) and Gittleman (Gittleman, 1986).

3.4.3 Metric analysis

Results for the dietary group Shapiro-Wilk tests determined that they all had normal distribution and the subsequent Kruskal-Wallis tests revealed that there were no statistically significant differences between the dietary groups both for percentage contribution of each muscle to the overall jaw adductor mass, and percentage contribution of each muscle division to the total muscle mass (Table 3.6). Probability *P*-values for the phylogenetic independent contrasts, comparing absolute values of the standardized phylogenetic independent contrasts versus their standard deviations ranged from 0.054 to 0.39. This suggests that phylogeny has a negligible effect. The RMA regressions on the pairs of variables that were generated with PICs showed no significant differences to those generated from the standard data, with similar slope and confidence intervals in all cases (Table 3.4). Phylogenetic influence on these variables and regressions is therefore considered minimal and subsequent allometric analyses focused on the raw metric data.

Reduced major axis regressions of variables scaling against body mass are reported in Table 3.4. Scaling of total muscle mass was not significantly different to isometry and no trophic group appeared to deviate from this general scaling trend (Figure 3.9). All three individual jaw adductor muscles scale close to isometry. Therefore species with a greater body mass have, in general, the same proportion of masticatory muscles to body mass as smaller species. Some regressions for muscle attachment surface area measurements may appear to be indicative of deviations from isometry (e.g. pterygoids and total muscle mass) but the confidence intervals encompass isometry in all cases and were not significantly different from isometry. Scaling of endocranial volume to body mass shows significant negative allometry (Figure 3.10) with results showing a slope of 0.68 from an expected isometric slope of 1 and a *t*-test *P*-value of 0.0007. That is, as species size increases the brain size increases to a lesser degree, and the brain takes up a lower proportion of overall body mass in large species of canids than in small ones. This was also reflected in the scaling of EVSA to body mass, which has a slope of 0.43 from an expected slope of 0.66 (*t*-test *P*-value 0.0001). The zygomatic arch width scales isometrically to body mass.

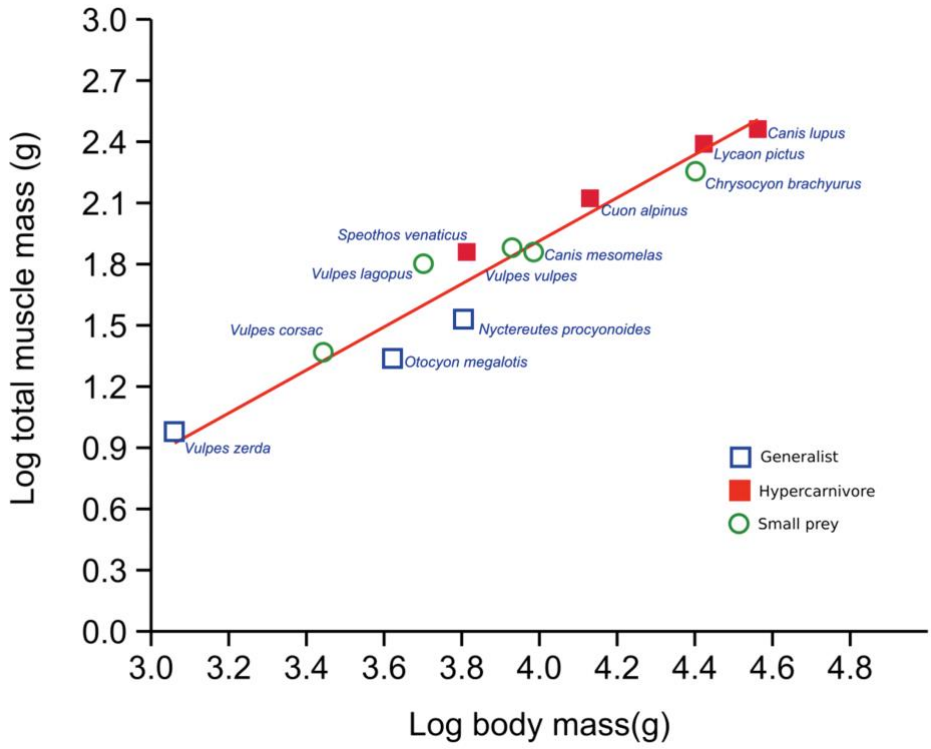

Figure 3.9 Reduced Major Axis regression, log body mass vs log total jaw adductor muscle mass. Dietary groups are highlighted.

Table 3.4. Reduced Major Axes regressions of variables scaled against body mass.

		Standard RMA				PIC RMA	
Variable vs Log Body Mass (g)	Expected slope for isometry	RMA slope	95% conf. int. slope	R^2	*t*-test	Slope	95% conf. int. slope
Log total adductor mass vs Log BM	1	1.05	0.89,1.17	0.94	ns	1.03	0.92, 1.18
Log endocranial volume vs Log BM	1	0.68	0.46, 0.77	0.90	***	0.60	0.47, 0.77
Log total surface area vs Log BM	0.67	0.64	0.49,0.70	0.95	ns	0.59	0.50,0.67
Log temporalis SA vs Log BM	0.67	0.64	0.49,0.70	0.95	ns	0.56	0.46, 0.67
Log masseter SA vs Log BM	0.67	0.68	0.60, 0.72	0.98	ns	0.64	0.56, 0.70
Log pterygoids SA vs Log BM	0.67	0.74	0.61, 0.82	0.93	ns	0.72	0.65, 0.83
Log temporalis mass vs Log BM	1	1.05	0.87,1.16	0.93	ns	1.05	0.93,1.20
Log masseter mass vs Log BM	1	1.1	0.94,1.20	0.95	ns	1.04	0.90,1.19
Log pterygoid mass vs Log BM	1	0.97	0.84, 1.06	0.97	ns	0.89	0.77,1.05
Log zygomatic arch width vs Log BM	0.33	0.32	0.27, 0.35	0.97	ns	0.31	0.26,0.36
Log EVSA vs Log BM	0.67	0.43	0.31, 0.50	0.92	***	0.40	0.32, 0.51

ns, not significant; *, $p<0.05$; **, $p<0.01$; ***, $p<0.001$.

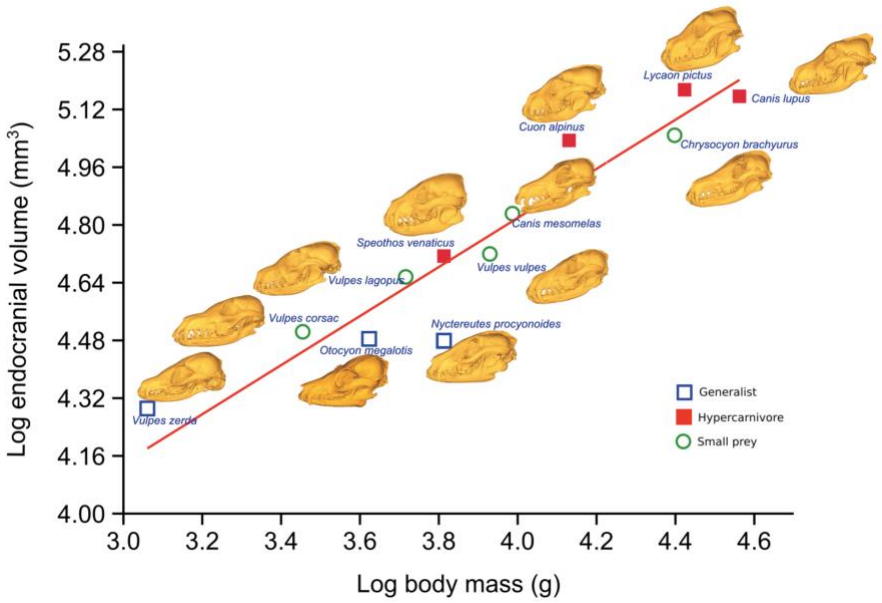

Figure 3.10 Reduced Major Axis regression, log body mass vs log endocranial volume. Dietary groups are highlighted and reconstructed skulls from CT scans illustrate variation in head shape.

3.4.4 Form analyses of the bony morphology

In the whole skull landmark data set, the first 4 PCs make up 78.5% of the variance. PCs 1 and 2 were above the predicted broken stick value and are described here in detail and shown in Figure 3.12. Scree plots and broken stick analyses are shown in Figure 3.11. PC1 constituted 32.3% of shape variance. At the negative extreme of the axis (-0.11, represented by wireframe S3) the rostral landmarks move caudolaterally, resulting in an overall shape change of a shorter broader snout and mandible. The landmarks associated with the zygomatic arches and caudal mandible move laterally, representing a relative broadening of the skull, and the dorsal landmarks of the inion and dorsal skull move dorsally - a shape change associated with a larger sagittal crest. Landmarks relating to the ventral aspect of the skull move ventrally resulting in an overall deepening of the cranium. At the other extent of the axis (0.07, represented by wireframe S4), the snout and mandible become longer and more gracile and the cranium appears dorsoventrally flattened. The PC1 axis clearly differentiated the data into dietary groups. The species occupying the lower end of the range (-0.12 to – 0.01) were exclusively hypercarnivorous, the generalists occupied the middle zone

and (0 to 0.03) and the small prey specialists the higher end of the range (0.015 to 0.07) with some overlap of the generalist species at their lower values. The Kruskal-Wallis test for the whole skull PC1 scores shows significant difference between the dietary groups, H = 7.88; *p*= 0.02. Dunn's post hoc tests showed that the hypercarnivores were significantly different to small prey (*P*-value 0.006). Of particular note are *Speothos venaticus*, a small hypercarnivorous canid that lies with the other three hypercarnivores at the low value extreme of this axis despite weighing only 6.5 kg, and its close relative, *Chrysocyon brachyurus*, a 22.5kg specimen, that lies with the *Vulpes* group at the other extreme of the axis. PC2 makes up 25.5% of variance. At one extreme (-0.06, represented by wireframe S2) the cranium appears relatively shorter and more domed and the dorsal border of the mandible is straighter. At the other extreme, (0.11, represented by wireframe S1) the cranial component appears dorsally flattened and elongated and the dorsal border of the mandible is curved. The Kruskal-Wallis test for the whole skull PC2 scores shows significant difference between the dietary groups, H = 6.26; *p*= 0.04). Dunn's post hoc tests showed that the hypercarnivores were significantly different to the generalists (*P*-value 0.02) and that the generalists were significantly different to the small prey specialists *(P*-value 0.03).

In the cranial subset (32 landmarks) the first 4 PCs make up 76.8% of the variation: PCs 1, 2 and 3 were above the predicted broken stick value and PCS 1 and 2 are described here in detail and shown in Figure 3.13. Scree plots and broken stick analyses are shown in Figure 3.11. PC1 constituted 33.1% of the shape variance. At the negative extreme of the axis (-0. 11, represented by wireframe C3), caudal landmarks move rostrally and dorsal landmarks move dorsally resulting in a relatively shorter deeper skull. Lateral landmarks moving laterally achieve relative widening of the zygomatic arch. At the positive extreme of the axis (0.09, represented by wireframe C4), the cranium lengthened whilst the zygomatic arches became relatively narrower. All dorsal landmarks shifted ventrally, resulting in a flatter skull. The relatively ventral position of the inion indicates a small or absent sagittal crest. The PC1 axis

showed some differentiation of the data into dietary groups. At the negative end of the axis were 3 of the hypercarnivores and at the other, the generalists. The small prey specialists occupied the middle space with some overlap with the hypercarnivores. *Speothos venaticus*, the fourth hypercarnivore appeared between the small prey specialists and generalists. The Kruskal-Wallis test for the cranial PC1 scores shows significant difference between the dietary groups H = 7.096; *p*= 0.02). Dunn's pairwise post hoc tests showed that the hypercarnivores were significantly different to the generalists (*P*-value 0.008). PC2 made up 19.6% of the shape variance. At the negative extreme of the axis (-0. 06, represented by wireframe C2), the zygomatic landmarks move dorsally and the dorsal landmarks move ventrally. At the positive end of the axis (0.11 represented by wireframe C1) the zygomatic landmarks move ventrally and the dorsal landmarks move dorsally. However, only one specimen, *Speothos venaticus*, lay towards the extreme end of the positive axis, all other specimens were closely grouped between -0.06 and 0.03. PC2 showed no appreciable grouping of species into dietary specialisms and Kruskal-Wallis tests showed no significant differences between the dietary groups.

When the pruned phylogenetic tree was mapped onto the PC scores it showed that the whole skull, rostral and mandibular component analyses contained phylogenetic signal, with *P*-values from 0.009 to 0.014, whereas the cranial subset demonstrated no statistically significant phylogenetic signal (Table 3.5). This indicates that the rostral and mandibular components of the skull are strongly linked to phylogeny, whereas the form of the cranial component changes in response to other constraints. The overall phylogenetic maps (Figures 3.12 and 3.13) show some long terminal branches, compared to shorter internal branches, indicating that some closely related species have diverged considerably within the shape space demonstrating substantial differences in related morphologies. In tests for allometric signal, regression of the cranial component shape on body mass showed the greatest percentage (16.5%) of shape variance of any of the landmark sets, and was the only landmark

dataset with a statistically significant permutation *P*-value (Table 3.5). The cranial component thus demonstrates evidence against the null hypothesis of complete independence, suggesting that shape change is related to size change. The multivariate regression analyses of shape on temporalis mass shows that the highest percentage change was found in the cranial shape dataset and was statistically significant. Similarly, the highest percentage shape change linked to endocranial volume was also the cranial dataset, and was also statistically significant. This demonstrates that change in temporalis mass and endocranial volume are linked with change to cranial shape (Table 3.5). Figure 3.16 compares the cranial wireframe shapes of two distantly related species with the cranial wireframe shape representative of the low PC1 score. The low PC1score wireframe indicates a short deep skull with increased space medial to the zygomatic arches for housing the temporalis muscles. Although *Canis lupus* and *Chrysocyon brachyurus* are from different clades and exhibit distinct dietary preferences and hunting strategies both have large body masses and relatively small endocranial volumes. The wireframes indicate that in both species cranial shape is very similar, both to each other and to the PC1 wireframe. The remaining three shape datasets shapes showed lower percentage changes and had no statistical significance, indicating that overall head shape, rostral shape and mandibular shape changes are independent of temporalis mass or endocranial volume change.

Table 3.5 Summary statistics for form analyses.

	Phylogenetic signal	Allometric signal		Effect of temporalis mass on cranial shape		Effect of endocranial volume on cranial shape	
Form	*P*-value (<0.05 indicates phylogenetic signal)	% Shape change	Permutation test *P*- value	% Shape change	Permutation test *P*- value	% Shape change	Permutation test *P*- value
Whole skull	**0.009**	11.0	0.26	14.7	0.11	16.3	0.053
Cranial component	0.053	16.5	**0.04**	19.1	**0.01**	22.4	**0.002**
Rostral component	**0.012**	11.9	0.24	14.6	0.15	16.2	0.11
Mandibular component	**0.014**	9.1	0.39	12.9	0.19	15.1	0.118

Significant values are shown in bold.

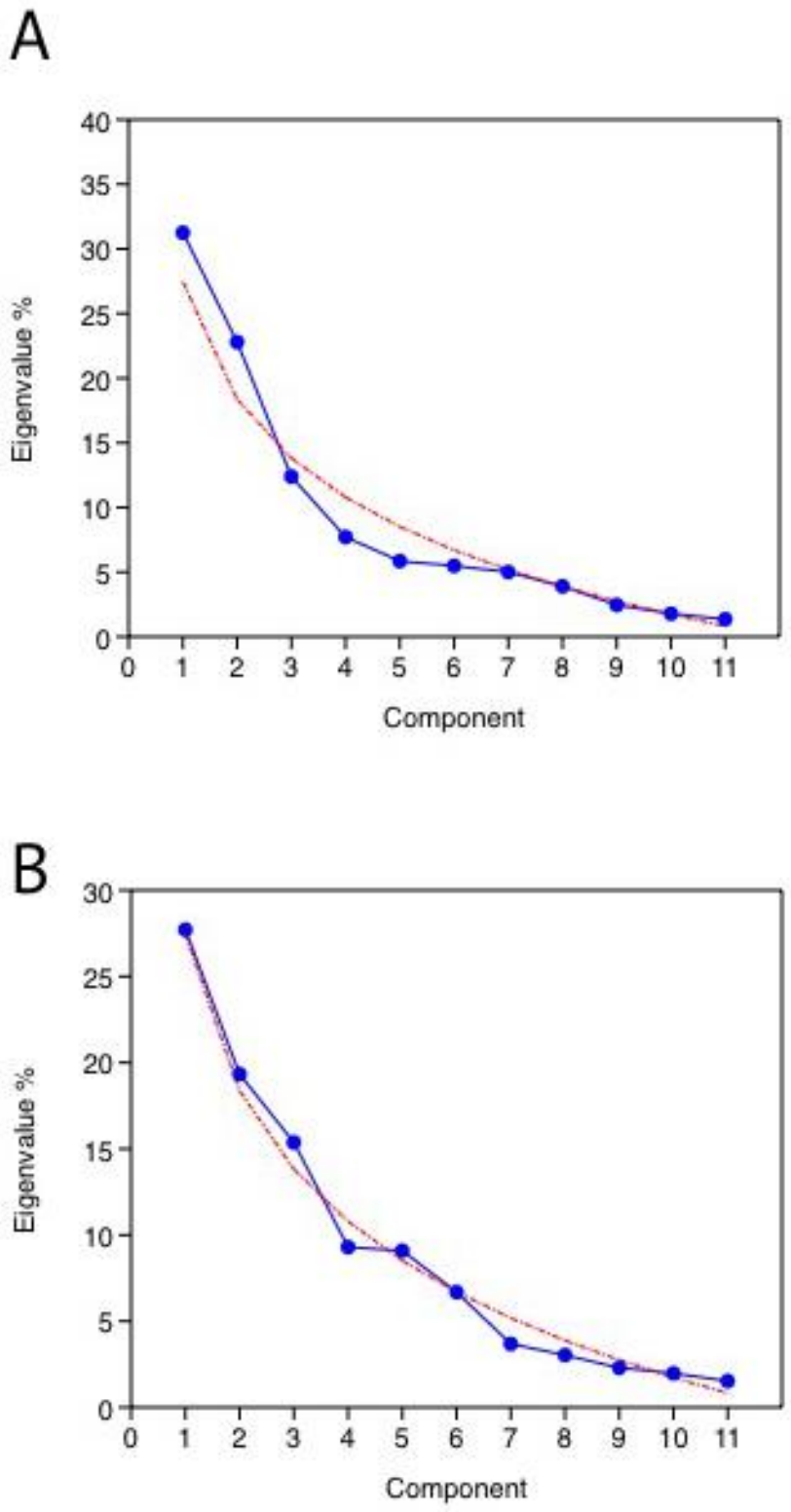

Figure 3.11. Scree plots of the PC eigenvalues for A, the whole skull and B, the cranial components of the skull. The blue line represents the reported eigenvalues, and the red line the predicted broken stick values.

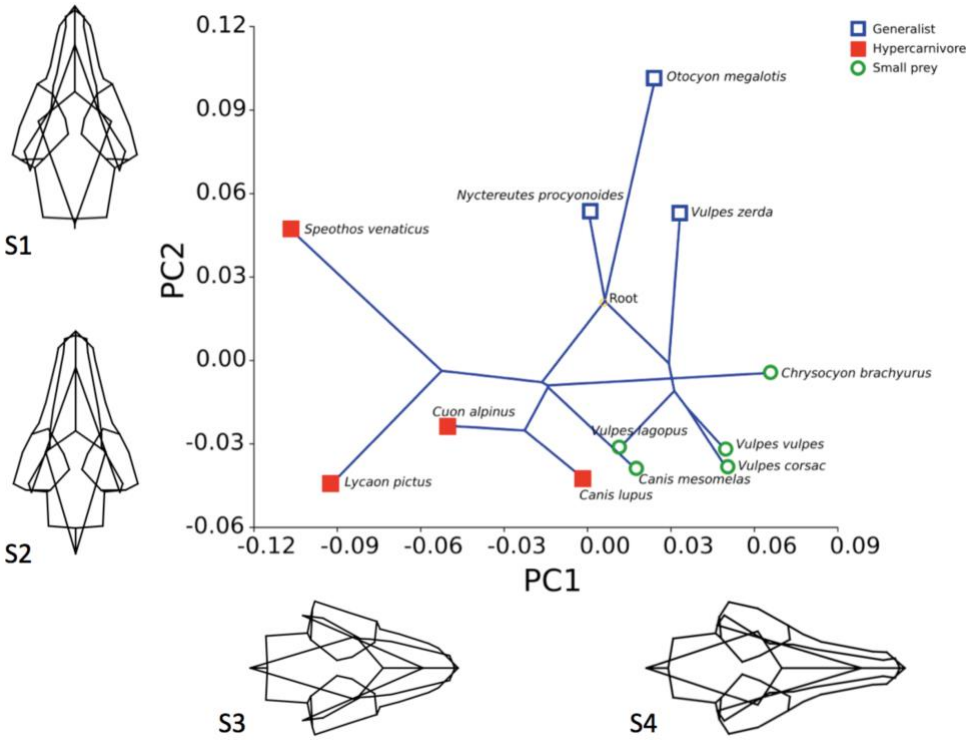

Figure 3.12 Whole skull principal component scores PC1 vs PC2. Dietary groups and the mapped phylogenetic tree is shown within the plot and wireframes representing skull shape changes are aligned along the relevant axes.

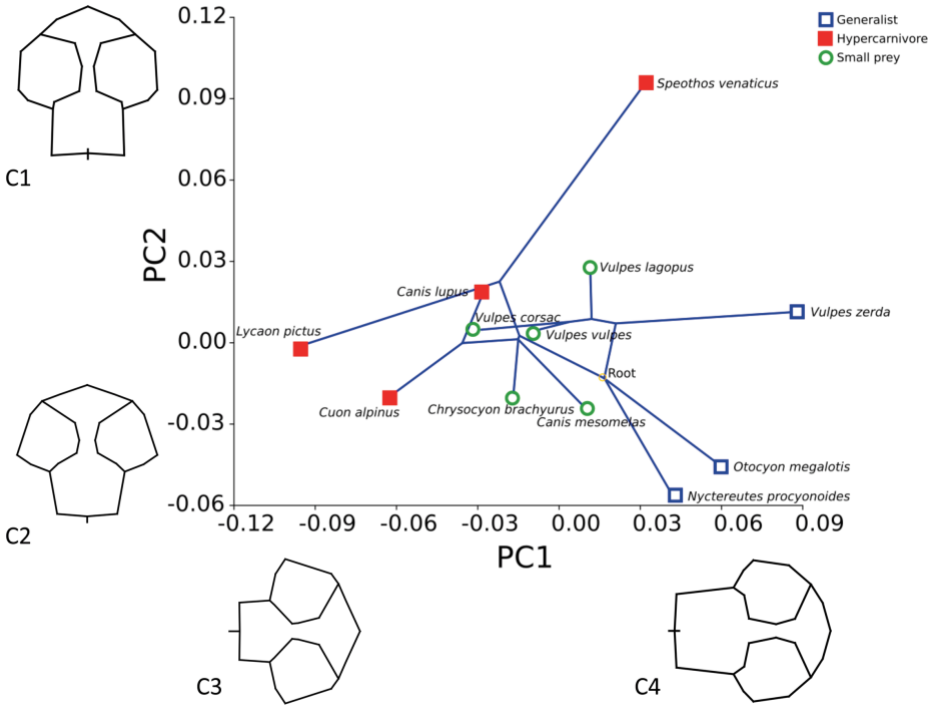

Figure 3.13 Cranial principal component scores PC1 vs PC2. Dietary groups and the mapped phylogenetic tree is shown within the plot and wireframes representing skull shape changes are aligned along the relevant axes.

Table 3.6 Kruskal-Wallis test results for the differences between the dietary groups both for percentage contribution of each muscle to the overall jaw adductor mass, and percentage contribution of each muscle division to the total muscle mass.

	H	*P*-value
Temporalis as a % of total jaw adductor mass	4.18	0.12
Masseter as a % of total jaw adductor mass	3.54	0.17
Pterygoids as a % of total jaw adductor mass	0.63	0.73
Suprazygomatic temporalis as % of total temporalis mass	0.24	0.88
Superficial temporalis as % of total temporalis mass	2.68	0.26
Deep temporalis as % of total temporalis mass	2.95	0.28
Superficial masseter as a % of total masseter mass	4.41	0.11
Deep masseter as a % of total masseter mass	3.50	0.17
Zygomaticomandibularis as a % of total masseter mass	5.11	0.08

3.4.5 Form analyses of the muscle morphology

It was challenging to find consistently homologous points, and consequent geometric morphometric shape analysis did not distinguish between dietary groups (Figure 3.13). This workflow was not considered in any further analyses.

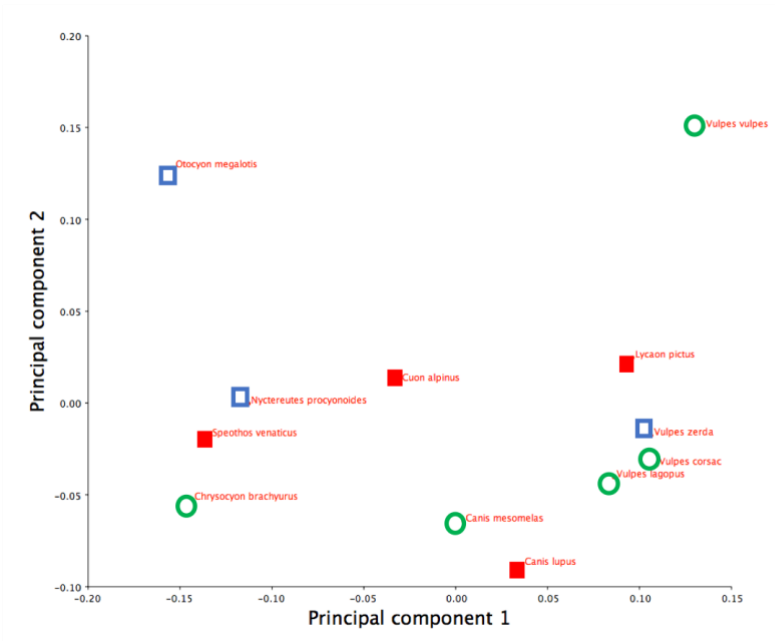

Figure 3.14 Scatterplot of PCA analyses from geometric morphometric muscle shape analysis. Dietary groups are identified: hypercarnivores, filled red squares, small prey specialists, green circles, generalists, open blue squares.

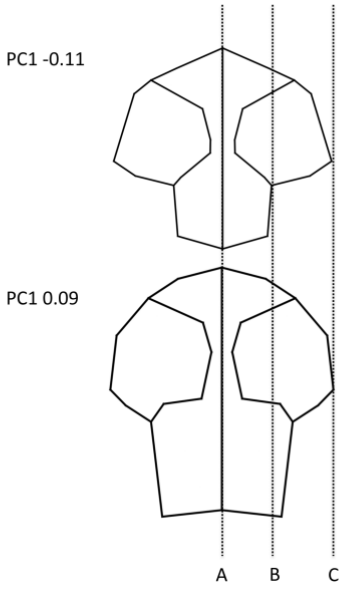

Figure 3.15 Dorsoventral view wireframes taken PC1 of the cranial component analysis. Both diagrams have been scaled to have equal zygomatic width as this scales isometrically. Line ‘A’ represents the midline and line ‘C’ the lateral extent of the zygomatic arch. Line ‘B’ represents the lateral extent of the cranium in the species with low PC1 scores.

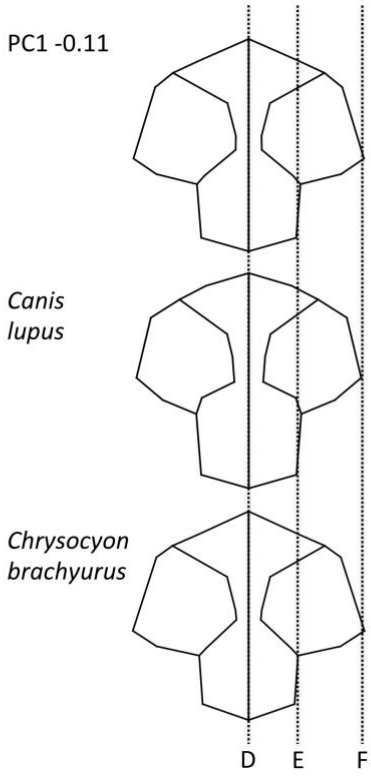

Figure 3.16 Dorsoventral view of cranial wireframes comparing the -0.11 principal component analysis with that of *Canis lupus* and *Chrysocyon brachyurus*. Line 'D' represents the midline, and line 'F' the lateral extent of the zygomatic arch. Line 'E' represents the lateral extent of the cranium.

3.5 Discussion

The results show that the morphology of the jaw adductor muscles is remarkably conserved across canid species. The form of each muscle and its subdivisions were surprisingly similar in all cases given the diverse dietary niches, different body sizes and phylogeny (Table 3.1). I also found that the jaw adductor mass as a whole, and all three of the jaw adductor muscles individually, scale isometrically (Table 3.4). Although I reported a couple of differences of muscle subdivision scaling between the different dietary groups, none were statistically significant and morphological variance was minimal and much less than I expected – that is, hypercarnivorous species, which might be expected to have a have relatively larger muscles to generate greater bite force, have the same ratio of muscle masses to body mass as those with assumed weaker bites, the generalists and small prey hunters (Table 3.1). All individuals were consistent with the scaling pattern and there were no correlations relating to phylogeny or dietary groups (Figure 3.9). Skull shape variation is therefore not attributable to housing differently scaled muscle masses for specialist dietary or different phylogenetic groupings. Whilst our sample sizes per species were relatively modest and were not sex matched, there were large scale interspecific differences and evidence from previous studies (see methods) suggests that there is minimal sexual dimorphism.

Our endocranial volume scaling results are in accordance with previous studies (Jerison, 1955; Gould, 1966; Bauchot, 1978) that describe interspecific scaling at a rate of two thirds relative to body mass (Table 3.4). This presents the problem of accommodating isometrically scaling muscle masses onto negatively scaling neurocrania. I considered the cranium to have two discrete surface areas: an internal one which reflects the accommodation needs of the brain and which was calculated as the surface area of the endocast (EVSA), and an external one, which was calculated as the area of origin for temporalis (I acknowledged that this only accounts for part of the external surface of the cranium). The EVSA scales to body mass with marked negative allometry, whilst the scaling of temporalis surface area to body mass is not

significantly different to isometry. The disparity between the demands of the internal and external surfaces of the neurocrania was further evidenced by the very small canids displaying a sagittal gap at dorsal midline where there is no muscle attachment, demonstrating that in these species the external surface of the cranium more closely reflects its internal surface area which is driven by brain accommodation. The sagittal gap was only seen in species below 5kg, that is, *Vulpes zerda*, *Vulpes corsac* and *Otocyon megalotis* (Figure 2.17). From 5-10 kg the contralateral temporalis muscles met at midline as temporalis utilised all of the available external surface area, with little or no sagittal crest present. Above 10 kg a pronounced sagittal crest was seen which increased the surface area available for temporalis (Figure 3.6). The exception to this was the 6.5kg *Nyctereutes procyonoides* that also had a well-developed sagittal crest. However, this was also the species with the smallest endocranial volume relative to body mass, as evidenced by the greatest negative distance from the regression line for endocranial volume against body mass (Figure 3.9). By contrast, the *Nyctereutes* temporalis surface area scales at a similar rate to other species and so the sagittal crest demonstrably increases the external surface area commensurate with temporalis requirements. These findings suggest that the exterior surface area of the calvarium does not simply reflect the interior but is driven by the necessity to accommodate the temporalis and probably the other muscles too. The other major morphological adaptation to increase the space on the skull for housing the temporalis is the isometrically scaling zygomatic arches (Figure 3.15). Other authors (Radinsky, 1981; Emerson and Bramble, 1993) have speculated that if the arch width remains relatively constant but the endocranial volume decreases, the space medial to the arches increases and could be used to accommodate a larger temporalis. This chapter shows that this 'increased accommodation' principle is correct but that in canids, the space is utilised to house an isometrically, rather than positively, scaling temporalis (Table 3.4). Interestingly, primates have also been shown to have isometrically scaling masticatory muscles (Cachel, 1984) as

well as negatively scaling endocrania (Rilling, 2006) and large species of primate exhibit similar morphological features as large species of canid, such as sagittal crests (Ankel-Simons, 2007) and relatively wide zygomatic arches (Frost *et al*., 2003). This might suggest that the problem of muscle accommodation is more universal than indicated here, although it is important not to extrapolate findings too far as the two groups have, for instance, distinct dietary behaviours.

Principal component analysis of the whole skull form differentiated the species into the three broad dietary groups and in the multivariate regression analyses demonstrated phylogenetic signal but no allometric signal. Total skull shape aligned broad stocky head shapes with hypercarnivourous hunters, and narrow slender head shapes with the small prey specialist. The generalists lay in the middle ground. This is in agreement with previous studies (Wroe and Milne, 2007; Goswami *et al.*, 2011). However, when I removed all of the rostral and mandibular components and focused only on the cranial component, there was no significant phylogenetic signal, dietary specialism grouping was less marked and a significant allometric signal indicated that shape change was allied to size change. More specifically, cranial shape changes correlate with body mass and temporalis mass and endocranial changes indicating that shape changes of shorter, dorsoventrally enlarged calvaria, increased sagittal crests and widened temporal spaces correspond with the decreasing endocranial volume to temporalis ratio that is seen as body mass increases. This directly links shape change in the cranium with accommodation of temporalis and suggests that the rostral and mandibular components are chiefly concerned with dietary specialism, whilst the cranial component is more strongly associated with muscle accommodation. In the whole skull analysis (Figure 3.12), *Chrysocyon brachyurus,* for example, is closely aligned with the *Vulpes* group at the furthest distance from the hypercarnivore species. All species at the positive end of the axis exhibit the long narrow jaws of the small prey hunter, and in the case of *Chrysocyon brachyurus*, the crossing tree branches also demonstrate convergent evolution (Gidaszewski

et al., 2009). However, when I focused on the cranial component (Figure 3.13) *Chrysocyon* shape is more closely aligned with the hypercarnivores, due to the large sagittal crest and wide medial zygomatic space that accommodates the temporalis. It is presumed that some elements of cranial shape change will not directly associate themselves with muscle accommodation but may be linked with considerations other than scaling. Such factors may include generating biomechanical advantage to facilitate certain bite behaviors such as fast jaw snapping or increasing bite force. Similarly, other biomechanical functions of the skull such as withstanding stress or dissipating bite forces have not been considered in this study. These factors warrant further consideration in order to understand how canids have applied similar muscle proportions in the generation of different bite forces and speeds to occupy remarkably distinct dietary niches.

3.6 Summary

There are two main factors that align with shape change in the canid skull: features that are scaled relative to body mass (whether isometrically or allometrically), and features that change independently of body mass. These findings show that the jaw adductor muscles scale isometrically to body mass, even though they are functionally aligned to independently changing features such as jaw length or bite force, both of which are allied to dietary specialisms (Christiansen and Wroe, 2007; Van Valkenburgh, 2007; Figueirido *et al*., 2011; Damasceno *et al.*, 2013). These results suggest that much of the cranial shape change is correlated with accommodating temporalis. These findings may help inform work on interpreting the feeding habits of extinct species (e.g. Wroe *et al*., 2005; Meloro *et al*., 2015). It should be noted, however, that our findings do not preclude the cranial shape changes also being biomechanically advantageous to the different trophic groups. In future work, I hope to consider how the architectural details of the jaw adductor muscles such as fascicle orientation, fascicle length and angles of pennation, may affect muscle force capability, and

how the spatial relationships between muscle centroid size and key skull features such as the temporomandibular joint and carnassial or canine teeth, impact on bite force capabilities.

Chapter Four. Functional morphology of the jaw adductor muscles in the Canidae.

4.1 Introduction

The work presented in this chapter is modified from a paper submitted to the Journal of Anatomy in 2018. I would like to thank Dr Nathan Jeffery for advice on concept development, experimental design, offering suggestions for manuscript improvement and for the critical revision of this chapter. Dr Philip Cox performed the phylogenetic comparative methods. I would also like to thank Professor Graham Kemp for his help in the concept development and critical revision of this chapter.

That anatomical form can broadly distinguish between species is a central tenet of comparative biology, reflecting intercorrelated differences of body mass, behaviour and environmental conditions as well as of phylogenetic inheritance. However, the matching of specific phenotypes, or parts thereof, to particular biomechanical functions is more nuanced and requires more sophisticated analyses beyond that of form alone. Here I explore the role of differences in cranial anatomy in the biomechanics of feeding performance among a closely related, but otherwise remarkably varied, subfamily, the Caninae.

The 36 extant canid species range in body mass from less than one kilogram (*Vulpes zerda*) to in excess of 80kg (*Canis lupus*). The largest reported species of Caninae is often described as *Canis dirus*, but recent work estimates it to be in the region of the size of *Canis lupus* (Anyonge, 2006). Caninae are found on all land masses except for Antarctica (Wozencraft, 1993; Macdonald and Sillero-Zubiri, 2004; Sillero-Zubiri *et al*., 2004; Nowak, 2005; MacDonald, 2009). As is to be expected in such a globally successful clade, they inhabit a wide variety of environments, from arid desert to tropical jungles, and fulfil many roles from apex predator to scavenger. Although all canids are easily recognisable as such, there are clearly many morphological differences that allow species to be distinguished, and anatomical specialisations exist, often in the context of dietary and hunting behaviours. Although all canids belong to the order Carnivora, many have adapted to include a wider

variety of foodstuffs into their diet, such as fruit, shellfish and invertebrates. Distinct hunting strategies are linked to particular diets, and consequently canids are often categorised by trophic groupings. For this study, I follow the categorization of Slater *et al*. (Slater *et al*., 2009). Four species (*Canis lupus, Cuon alpinus, Lycaon pictus* and *Speothos venaticus*) are considered hypercarnivorous, that is, they mainly take mammalian prey larger than their own body mass, and preferentially hunt in co-operative packs (Ewer, 1973; Van Valkenburgh and Koepfli, 1993; Mech and Boitani, 2003). Killing is by way of ventral abdominal evisceration, with many individuals involved in the kill. Thus, their hunting strategy is to exhaust and then overpower their quarry after a long chase. The remaining canid species can be categorised as small prey specialists or generalists/omnivores. The small prey specialists take prey smaller than themselves, usually small mammals, and are lone stealth hunters. Killing tends to be by vigorous shaking to snap the vertebral column and sever the spinal cord. The generalist/omnivores also hunt by stealth but their diet includes a greater quantity of invertebrates which, although often fast moving, are more easily overwhelmed (Ewer, 1973; Sillero-Zubiri *et al*., 2004; MacDonald, 2009). I refer to this group as generalists for the remainder of this work. All canid species are opportunists and will consume carrion, and both the small prey hunters and generalist canids are also known to eat varying quantities of plant material. Many previous studies have demonstrated the link between these trophic groups and the bony morphologies of the skull: hypercarnivorous species have short broad snouts, domed skulls and robust mandibles whilst the head shapes of non-hypercarnivorous canids are more gracile with somewhat flattened skulls and long slender muzzles (Van Valkenburgh and Koepfli,1993; Wroe and Milne, 2007; Slater *et al*., 2009; Goswami *et al*., 2011; Meloro *et al*., 2015).

The form of the rostral part of the skull is strongly influenced by the requirements of the dental apparatus. Unlike some other families of carnivorans, most notably felids and ursids, the cursorial specialisation of the canid distal limb means that the forelimbs are not directly

used in prey apprehension, and consequently the dentition is used for prey capture, submission, killing and subsequent food processing. The 'model' canid dental formula is I3/3 C1/1 P4/4 M2/3, but two hypercarnivorous species, *Cuon alpinus* and *Speothos venaticus*, have a reduced number of post carnassial teeth, and one generalist species, *Otocyon megalotis* has an increased number of molars. The carnassial teeth of hypercarnivorous species exhibit enlarged cutting surfaces, whilst the generalists have a more bunodont form (Ewer, 1973; Sillero-Zubiri *et al*., 2004; Van Valkenburgh, 2007; MacDonald, 2009). It is not only the shape of the teeth that determines their function, but also their position within the jaw (Greaves, 2012). Those at the rostral end have less force driving them than those lying toward the temporomandibular joint (TMJ), which acts as the fulcrum in a third-class lever system. As the molars lie at the most caudal end of the dental arcade, reducing either their size or number has the effect of bringing both the canine and carnassial teeth closer to the TMJ, which in turn increases the force of the piercing and slicing apparatus respectively. However, there is a trade-off between bite force and gape: teeth nearer to the TMJ have more power driving them, but can only achieve a narrow gape between the upper and lower counterparts. Excessive reduction of the post carnassial dentition would therefore restrict the functionality of the jaw. Lengthening the tooth row has the effect of positioning the teeth that catch prey, the canines, further from the TMJ. As in the third-class lever model, this lessens the force that can be generated at the canine bite point, but increases both the maximum gape and the speed with which the canines can come together, an advantage in catching fast moving prey. Two of the generalist species, *Otocyon megalotis* and *Nyctereutes procyonoides,* also exhibit a pronounced ventral process on the caudal part of the mandible (Chapter Two, Figure 2.15), a feature that has been attributed to an enlarged attachment area for the jaw opening digastricus muscle (Ewer, 1973; Fujiwara and Suwa, 1991; Tedford *et al*., 1995; Reynolds, 2012; Asahara and Takai, 2017).

The correlation of jaw shape with feeding and hunting behavior has led previous authors to hypothesize that dietary adaptations have a significant influence on jaw morphology, and that, in carnivorans in particular, hypercarnivorous jaws are built for strength, whereas those of the small prey hunters and generalists are built for speed (Van Valkenburgh and Koepfli, 1993; Andersson, 2005; Slater *et al*., 2009; Figueirido *et al*., 2011; Prevosti *et al.,* 2012: Meloro *et al*., 2015). The precise function of the different morphologies is less well explored. Do the robust jaws of the hypercarnivores produce relatively greater bite forces than the slender jaws of the small prey hunters? Alternatively, perhaps the robust skulls of the hypercarnivores are engineered to withstand potentially violent encounters with their large prey, or to dissipate great forces generated whilst chewing on tough materials. Understanding the distinction between absolute and relative bite forces is key to understanding behavioral and morphological adaptations. Absolute forces indicate the predicted values of bite force in a species at a given bite point, and as species size increase, absolute bite forces tend to increase, that is, larger species have greater bite forces. Relative bite forces, however, allow for a comparison against an identifiable metric such as body mass, to identify if all species scale the same, or if larger species have relatively as well as absolutely greater or weaker bites forces. Identifying differences or similarities in scaling patterns between taxa or dietary groups may give insight into adaptations in form.

Shape differences in the caudal part of the skull are not as easy to align with diet. Previous analyses revealed that the differences in form of the cranial part of the skull are associated with changes in body mass, and specifically, that shape change is related to housing the jaw adductor muscles on the cranium (Chapter Three). Body mass related shape change is associated with the disparity in scaling between the jaw adductor muscles, which scale isometrically, and brain volume, which scales with negative allometry (Radinsky, 1981; Chapter Three). This does not however, preclude the possibility that there may be additional functions to the cranial shape differences as well as simply increasing surface area. The siting

of the jaw adductor muscles on the skull, and the position of their origins and insertions may also influence bite performance. Differences in cranial and mandibular shapes may alter the relative arrangement of muscles on the skull with respect to key functional components such as the carnassial teeth, TMJ or coronoid process of the mandible, and thus may impact function.

The jaw adductor muscles are fundamental in producing forces that close the mandible and many previous studies have estimated their physiological cross-sectional areas and force production capabilities using dry skull techniques (Wroe *et al*., 2005; Slater *et al.,* 2009; Tseng and Wang, 2010; Damasceno *et al*., 2013; Forbes-Harper *et al*., 2017). However, Taylor and Vinyard's work on primate jaw architecture (Taylor and Vinyard, 2013) established that studies using dry skull craniometric measurements to estimate muscle force production capabilities may greatly under or overestimate physiological cross-sectional areas, and that ideally, muscle architectural data should be incorporated into studies that estimate jaw muscle forces. In addition, the internal architecture of a muscle can greatly influence its functionality (Gans, 1982; Anapol and Barry, 1996; Huq *et al*., 2015; Terhune *et al*., 2015). For example, muscles with parallel fibres allow for maximum excursions and high contractile velocities, whilst muscles with internal tendons or a pennate arrangement of fibres, maximize force production capability (Taylor and Vinyard, 2013). Therefore, estimations of cross sectional areas or even directly recorded muscle masses, are broad approximations of force production and may not directly translate into a pro-rata amount of force, with inequalities between mass and force contributions accounted for by the internal architecture and composition of the muscles.

The aim of the work in this chapter is to explore the form and function of the jaw adductor muscles, and to determine if differences in skull shape influence bite performance.

Specifically, I test two hypotheses:

1. That there are significant relative, as well as absolute, differences of muscle force and bite force that reflect canid dietary niches.

This predicts for example, that hypercarnivorous species can generate larger muscle and bite forces than small prey specialists and generalists, and that these differences persist after body size scaling. Previous studies (Christiansen and Wroe, 2007; Damasceno *et al*., 2013) have posited and evaluated variations of this hypothesis on the basis of dry skull calculations methods. Here I use *ex vivo* entire heads from twelve species of Caninae, covering a range of body masses, phylogenetic and trophic groups. Individual muscles were explored to test earlier theories pertaining to the calculation of muscle force, and their contributions to the total jaw adductor muscle force. To compare methodologies, I also calculated muscle forces based on the dry skull data. I used the specimen specific muscle force and computer tomography (CT) data to build finite element (FE) models to predict bite forces and determine if they scale with isometry. To reflect a range of functional conditions, models were made at two different bite points, and two different gapes.

2. That the efficacy of muscle force production, and its conversion into bite force, is indicative of different dietary niches.

This predicts, for example, that the hypercarnivorous species are more effective at generating force than any other dietary groups. Here I test the hypothesis using three key measures of performance. These are: *mechanical efficiency*, a measure of input muscle forces versus bite forces generated (Dumont *et al*., 2011; Cox *et al*., 2012); *mechanical advantage,* considered here in terms of the angle between lines of action of temporalis, the largest jaw adductor, and the occlusal plane as well as in terms of lever arm ratios (Fearnhead

et al., 1955; Reduker, 1983); and *cranial deformation*, reflecting the amount of energy expended in deforming the skull during bite force production and typically approximated on the basis of finite element simulations of strain energy density (Dumont *et al*., 2009).

4.2 Materials and methods

4.2.1 Specimens, imaging and landmarking.

Specimens from 8 of the 13 genera that make up the Canidae family were obtained from either euthanased zoo stock or vermin control (Table 4.1). There were 19 individuals from 12 species with representatives from the three major clades and the three trophic groups. The data set is not inclusive of all canid species, however, it covers a broad range of head shapes, body sizes and phylogenetic groups, and it includes all four of the hypercarnivorous species (Van Valkenburgh, 2007). Diversity of scale covers two orders of magnitude in the Canidae and interspecific differences are greater than intraspecific ones. For the purposes of this study species were identified as being from one of the three trophic groups as described by Slater et al. (Slater *et al*., 2009) (Table 4.1). Further details of the specimens used are given in Chapter Two, part 2.2.3. Specimens were either chilled fresh or frozen and then defrosted, but no fixative agent was used on any specimen. All specimens, with the exception of *Vulpes vulpes* 7 (this chapter part 4.2.2), were dissected at near occlusal bite, that is, with minimal gape. The jaw adductor muscles, that is temporalis, masseter and the pterygoids were dissected for each species. Further details of dissection techniques and gross muscle anatomy and are found in Chapter Two, part 2.4.2.

All but one specimen (*Vulpes vulpes* 7) were digitally imaged using computer tomography (CT). CT methodology is discussed in Chapter Two, part 2.3.1, and details of settings and spacing used to image the specimens in this chapter are given in Chapter Two, part 2.3.3.

Vulpes vulpes 7 was imaged using Magnetic Resonance (MR), to determine the configuration of the jaw adductor muscles at wide gape (this chapter, part 4.2.2). MR methodology is

discussed in Chapter Two, part 2.3.2, and details of settings and spacing used for this specimen are given in Chapter Two, part 2.3.3.

Some of the landmarks identified in Chapter Three, part 3.3.2.1, were used to identify and measure metrics of the skull. The prosthion to the caudal hard palate is a measure of hard palate length, and the prosthion to the lateral points of both mandibular fossae as a measure of rostrum length. These measurements were used in regression analyses (this chapter part 4.2.8). Tooth point landmarks for the upper canines and upper carnassial teeth were also identified and used in the mechanical advantage analyses (this chapter, part 4.2.6). Further details regarding selection and recording of landmarks is found in Chapter Three, part 3.3.2.1.

Table 4.1 Details of specimens used in this study including body mass, jaw adductor muscle masses and forces as calculated by the RPCSA and dry skull methods.

	Sex	Phylogenetic group	Dietary specialism	Mean body mass (g) from literature [1,2]	Temporalis mass (g)	Mean temporalis fascicle Length (cm)	Masseter mass (g)	Mean masseter fascicle length (cm)	Pterygoid mass (g)	Mean pterygoid fascicle length (cm)	Total jaw adductor mass (g)	Temporalis force (N) from RPCSA	Masseter force (N) from RPCSA	Pterygoid force (N)	Temporalis force (N) from dry skull	Masseter force (N) from dry skull
Alopex lagopus	M	Fox-like	Small prey specialist	5200	43.8	2.4	14.9	1.5	4.47	1.9	63.1	530	251	82	336	298
Canis lupus	2M,1F	Wolf-like	Hypercarnivore	36500	179.5	4.3	84.5	2.7	25.7	2.5	289.7	1328	935	441	1432	823
Canis mesomelas	M	Wolf-like	Small prey specialist	9700	46.6	2.6	20.2	2.0	6.7	1.8	73.5	603	361	130	403	358
Chrysocyon brachyurus	F	South American	Small prey specialist	25000	106.1	4.5	61.5	2.7	13.2	2.1	180.8	852	770	220	900	775
Cuon alpinus	F	Wolf-like	Hypercarnivore	13500	81.6	4.2	40.6	2.8	10.4	2.4	132.6	753	508	151	777	523
Lycaon pictus	2M, 1F	Wolf-like	Hypercarnivore	26500	141.7	5.1	84.4	3.0	19.4	2.6	245.5	880	836	225	950	680
Nyctereutes procyonoides	M	Fox-like	Generalist	6500	19.9	1.8	10.6	1.4	3.2	1.2	33.7	360	262	95	341	212
Otocyon megalotis	M	Fox-like	Generalist	4200	13.5	1.9	6.6	1.0	2.2	0.8	22.4	252	227	99	231	212
Speothos venaticus	F	South American	Hypercarnivore	6500	42.7	2.7	24.6	1.9	5.1	1.9	72.4	559	442	94	370	289
Vulpes corsac	3M, 1F, 1 unknown	Fox-like	Small prey specialist	2850	14.7	2.0	6.4	1.4	2.3	1.3	23.4	309	171	61	205	194
Vulpes vulpes	M	Fox-like	Small prey specialist	8500	48	3.0	19.3	2.4	5.7	2.0	73	487	262	101	438	318
Vulpes zerda	F	Fox-like	Generalist	1150	5.6	1.4	2.4	0.8	0.9	1.2	8.9	127	96	26	97	85

1. Nowak, 2005(Nowak, 2005).

2. Macdonald and Sillero-Zubiri 2004. (MacDonald and Sillero-Zubiri, 2004)

4.2.2. Gape angle at wide gape

One specimen, *Vulpes vulpes* 7, was used to determine the angle to be applied to the wide gape models in all species. This specimen was secured at wide gape and imaged using MR to visualise the internal skeletal and soft tissue structures (Figure 4.1A). The specimen was consequently dissected at wide gape to confirm the angle of the mandible relative to the rostrum, and to confirm the identity and configuration of the jaw adductor muscles (Figure 4.1B). Gape angle was measured from the caudal margin of the upper canine alveolus at the gumline, to the caudal extent of the mandibular fossa of the temporal bone, and to the caudal margin of the lower canine alveolus at the level of the gumline. This last reference point was chosen in preference to a more rostral point to minimize the amount of time spent partitioning the mandible during the Finite Element modelling (Figure 4.1C). Wide gape angles measured in the specimen were very similar in both the MR images and dissection methods, at 84° and 81° respectively. These observations were used to inform the building of the FE models (this chapter part 4.2.4.2).

Figure 4.1 Specimen Vulpes vulpes 7, MR image(A), dissection(B) and FE model(C) showing the position of the mandible at wide gape.

4.2.3 Reconstruction of muscle function

4.2.3.1 Review

The majority of carnivoran head studies consider only the skeletal components of the head, often including the teeth, and sometimes endocasts (Damasceno *et al.*, 2013). In studies that

focus on categorizing species by observing and quantifying diagnostic skeletal features, (Prevosti and Rincón, 2007; Meloro *et al.*, 2008; Tseng, 2011; Slater, 2015; Lucenti and Rook, 2016; Drake *et al.*, 2017) bony morphologies suffice. This type of study is often used to identify fossil evidence, where distinctive but often small, differences in shape, for example on tooth cusps or inner ear bones, allow palaeontologists to classify specimens and infer taxonomic and phylogenetic relationships. In studies that consider biomechanical function as well as form, the musculature driving the bony components must also be considered. In cases where the muscles are absent, their morphologies can be at least partly inferred by using bony correlates and landmarks. In this chapter masticatory muscle performance is explored by determining the force generated by the jaw adductor muscles and the output forces at specific bite points along the dental arcade. The size of muscles, the extent and position of their origins and insertions, their internal architecture and angles of insertion all contribute towards their functional ability. Although work by previous authors has also quantified either or both muscle input forces and bite output force outputs, the methodology differs between studies. The most frequently used methods to determine muscle force and their advantages and disadvantages are discussed here.

Live data gathering through use of bite plate force transducers

Previous studies have measured bite force in live (anaesthetised or conscious) animals. This requires stimulating the animal to bite onto a force transducer which records force values. Although theoretically simple this method is difficult to perform due to practical, financial and ethical considerations, and is hard to replicate and validate. In small animals such as lizards, the experimental procedures are easier due to the size of the animals involved and their ease of handling and housing, and these studies are more numerous in the literature (McBrayer and White, 2002; Verwaijen *et al.*, 2002; Herrel and O'Reilly, 2006; Lappin *et al.*, 2006; Gröning *et al.*, 2013). Mammalian studies, with their concomitant technical difficulties,

are much less common, although they have been reported in bats (Dumont and Herrel, 2003), primates (Dechow and Carlson, 1983) opossums (Thompson, 2003) and pigs (Ström and Holm, 1992; Bousdras *et al.*, 2006). Only a few studies consider carnivorans (Dessem and Druzinsky, 1992; Lindner *et al.*, 1995; Binder and Van Valkenburgh, 2000; Ellis *et al.*, 2008). One major disadvantage of recording transducer recorded bite values is that it is not possible to determine how close to maximal force the animal is biting. Even in anaesthetised animals Ellis *et al.* (2008) found that electrically stimulated bite forces varied greatly, some of which was attributed to the difficulty in reliably and consistently placing the electrodes used to stimulate muscle contraction. Values from their study in anaesthetised domestic dogs with a body mass range of 5-40kg, ranged from 147 - 926N in canine biting, and 574 to 3417N in carnassial biting. These figures are greater than those reported by Lindner *et al.* (1995) who, in domestic dogs ranging from 7 to 55kg, reported a range of bite forces from 13 to 1394 N, with a mean of 256N, although the bite position on the tooth row was not reported. I am unaware of any work published on transducer derived bite force values in wild canids.

The dry skull method

Arguably the easiest samples to access in any great variety or number, are dry skulls. Most natural history museums have carnivoran skull collections and these are widely used in comparative morphological research. In the early 1990s Thomason (1991) devised a method of calculating jaw adductor muscle forces by taking 2D photographs of a skull. As well as being simple and cost effective, this method is clearly advantageous when working with incomplete or fossil material, and this method has been adopted by many researchers (Wroe *et al*., 2005; Christiansen and Adolfssen, 2005; Christiansen and Wroe, 2007; Wroe *et al.*, 2007; Damasceno *et al.*, 2013; Forbes-Harper *et al.*, 2017). Muscle attachment areas or spaces between bony landmarks are used to calculate muscle cross sectional areas, which

are then multiplied by a value for mammalian isometric muscle force to determine consequent force production capabilities. For example, the region between the frontal and parietal bones of the skull, and the medial aspect of the zygomatic arch is photographed from a caudo-dorsal direction and the resultant image used to calculate the cross-sectional area of the temporalis muscle. This area value is multiplied by a mammalian muscle force value, to determine the temporalis muscle force. The same method, using different bony landmarks, is used to calculate the masseter muscle force. The inclusion of the pterygoid muscles is varied: Slater *et al.* (2009) and Damasceno *et al.* (2013) report it as part of the pterygoids. Other studies considered it to form a functional group alongside the masseter as the pterygoid-masseteric complex (Christiansen and Adolfssen, 2005; Christiansen and Wroe, 2007; Tseng and Wang, 2010). In some studies the pterygoids are not included (Tanner *et al.*, 2010), or in others not explicitly stated whether they were included or not (Wroe and Milne, 2007). The nominal inclusion, or not, of the pterygoids when using this method is a moot point. The area highlighted in this method whether labelled 'masseter' or 'medial masseter-pterygoid complex' or 'pterygoids' actually covers the area occupied by the masseter and both the medial and lateral pterygoid, and they are, by default, included in the calculation.

The dry skull method has four main disadvantages. Firstly, as the cross-sectional area measurement is taken at one fixed point it does not take into account how the extent of the muscle origin or insertion may vary between species. This may affect the total muscle mass, as more extensive muscles may be larger than less extensive muscles. For example, the temporalis in *Canis lupus* originates from midline, whereas on *Vulpes corsac* it originates parasagittally (Figure 2.17). Secondly, the muscle cross sectional area boundaries include other structures, such as the vertical ramus of the mandible and some of the contents of the periorbita of the eye. There also appears to be a sizable area of overlap between the temporalis cross section and the pterygoid-masseter cross section, in effect counting the

area of overlap twice. Thirdly, the angle at which the photograph is taken can vary and have an effect on the perceived cross-sectional area. A photograph taken at a more oblique view to the bony landmarks may overestimate the cross-sectional area when compared to a photograph that is taken from a more perpendicular angle. The complexity of skull morphology means that it is difficult to be consistent between specimens when aligning photographic angles. Lastly, the dry skull method cannot take into account the internal architecture of the muscle. Internal architecture describes the features of the muscle such as fascicle length, presence of internal tendons and angles of fascicle pennation, and can have a marked input on muscle force production (Eng *et al.*, 2009; Taylor *et al.*, 2018).

Physiological cross-sectional area (PCSA) method

In contrast to the dry skull method, physiological cross-sectional area (PCSA) calculations take into account the internal architecture of the muscle to describe some of the complexity of its structure function relationships (Close, 1972; Spector *et al.*, 1980; Gans, 1982; Sacks and Roy, 1982; Gans and Gaunt, 1991). This method requires access to the muscle itself, to quantify mass and fascicle length. This data has traditionally been obtained via manual dissection, although this is by nature destructive. Some authors are cautious of this technique as it may damage muscle fascicles and lead to erroneous measurements (Hartstone-Rose *et al.*, 2018), although this can be somewhat mitigated by using careful dissection techniques, or with the use of chemical dissection methods (Hartstone-Rose *et al*., 2012; Clair and Reback, 2018). Chemical dissection methods have the advantage of measuring individual fascicles more accurately but disallow for the measuring of pennation angles as the integrity of the muscle is destroyed (Herrel *et al.*, 2008). More recent work uses high resolution microCT scans to reconstruct and measure muscle architecture and has the advantages of gathering large amounts of data and is non-destructive (Kupczik *et al.*, 2015; Cox, 2017; Dickinson *et al*., 2018; Santana, 2018). However, these techniques are

difficult to replicate consistently in large specimens and are very time consuming. For this study manual dissection techniques were used to establish muscle architecture. Muscles were carefully removed from the cadavers and internal tendon pennation angles and fascicle lengths recorded. The formula to calculate PCSA is

$$PCSA = \frac{mass}{fascicle\ length\ x\ muscle\ density}$$

It can be seen that PCSA and fascicle length are inversely proportional. In two muscles of a given mass, a configuration of many short fascicles would produce a greater force that if the same muscle were to be arranged with fewer but longer parallel fibres. As discussed in Chapter One part 1.3.2.3, internal tendons within a muscle allow for the packing of many short fascicles and give an advantage for muscle force. A muscle with parallel fibres would advantage excursion and speed. The PCSA formula, whilst taking into account fascicle length, does not take into account the energy lost due to the direction of fascicle pull being orthogonal to the internal tendon, rather than in the same orientation as the long axis of the muscle. Thus, a refinement of the PCSA formula, the reduced physiological cross-sectional area (RPCSA) was proposed by Anapol and Barry (Anapol and Barry, 1996) adapted from earlier work by Weber (Weber, 1851) Haxton (Haxton, 1944) and Schumacher (Schumacher, 1961).

The formula to calculate RPCSA is:

$$RPCSA = \frac{mass\ \times\ cosine\ of\ pennation\ angle}{fascicle\ length\ \times\ muscle\ density}$$

where the cosine of the pennation angle reduces the output value accordingly. The greater the angle the more energy is lost. However, this method is criticised by some authors as

they consider that the *ex situ* muscle vector, does not replicate the *in-situ* muscle vector as the muscle itself is pulling at an angle relative to the adduction vector of the jaw. They also point out that pennation angles can change dramatically throughout the mass of the muscle (Perry *et al.*, 2011; Hartstone-Rose *et al.*, 2018). These authors propose using the unreduced PCSA method without pennation correction. I use the RPCSA method as it goes some way to describing the three dimensionality of the muscle architecture and is widely used within the literature (Taylor *et al.*, 2006, 2015, 2018; Anapol *et al.*, 2008; Williams *et al.*, 2008; Dickinson *et al.*, 2018).

4.2.3.2 Method for calculating RPCSA and force of muscle

Muscle mass was determined using Redwag WPS600/C/2 digital scales, accurate to 0.001g. The specific muscle density value used was 1.056 gcm^{-3} based on cat soleus muscle (Murphy and Beardsley, 1974). To verify this parameter, individual volumes of the jaw adductor muscle subdivisions were predicted in two specimens, *Vulpes vulpes* 1 and *Vulpes zerda*, by dividing mass by 1.056 gcm^{-3}. The volume for each muscle subdivision was then measured directly with a microvolumeter, using a method adapted by Vickerton after Douglass and Wcislo (Douglass and Wcislo, 2010; Vickerton *et al.*, 2013). The two values were compared using *t*-tests.

Digital photographs were analysed using the angle and measurement tools in ImageJ (Schneider *et al.*, 2012). To account for the variety of pennation angles I sampled each muscle subdivision up to 20 times depending on its overall size and used the mean value of these measurements. The pterygoids have no internal tendon and hence have parallel fascicles, and no pennation angles to take into account. Fascicle length was measured at 5-20 locations, depending on the size of the muscle (Figures 4.2A and B). Mean values are reported in Table 4.1 and were used for calculations. It was noted that many of the muscle layers exhibited a great variety of pennation angles and, even more markedly, fascicle lengths. It is

therefore acknowledged that the complex architecture of the masticatory muscles is difficult to capture using simple equations; however, it was felt that the RPCSA method reflects the effect of the diversity of the muscle architecture. Muscle force was then calculated by multiplying RPCSA by an intrinsic muscle strength value of 37 Ncm^{-2} (Weijs and Hillen, 1985; Koolstra *et al*., 1988; Christiansen and Adolfssen, 2005; Christiansen and Wroe, 2007).

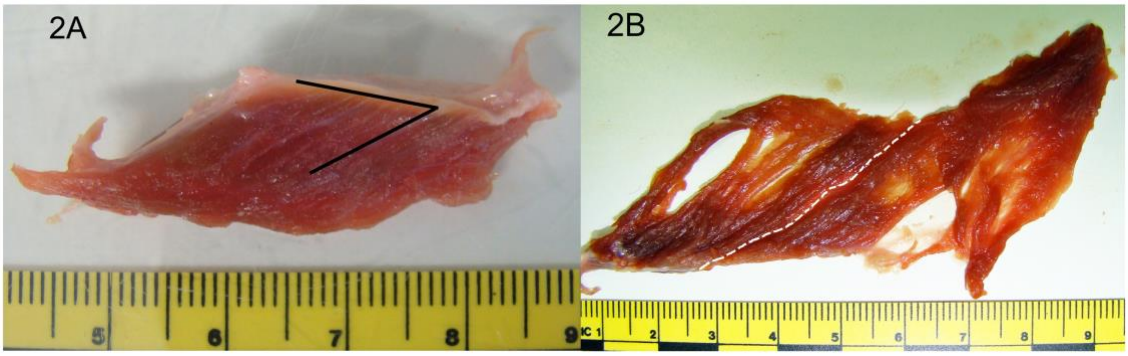

Figure 4.2. Muscles of *Canis lupus*. (A) Deep temporalis showing angle of pennation. (B) Pterygoid muscle showing fascicle length measurement.

As many previous bite force studies have used Thomason's (Thomason, 1991) dry skull method to calculate cross sectional areas and muscle forces, I also used this method as a comparison to the RPCSA method (Christiansen and Adolfssen, 2005, Christiansen and Wroe, 2007; Damasceno *et al.,* 2013). Authors cited here have calculated predicted bite force at canine and/or carnassial bite points, but all at occlusal bite angle only, which I follow for this part of the study. This method uses 2D images to calculate cross-sectional areas of the jaw adductor muscles, identifying them as belonging to one of two functional groups: the temporalis or the masseter/pterygoid mass. For this I used screenshots of the CT head reconstructions. Whilst some authors do not distinguish between the medial and lateral pterygoid muscles (Slater *et al*., 2009; Tseng and Wang, 2010), others nominally only include the medial pterygoid (Christiansen and Adolfssen, 2005; Christiansen and Wroe, 2007; Damasceno, *et al*., 2013; Forbes-Harper *et al.*, 2017). However, as the dry skull method includes the cross-sectional area occupied by the very small lateral pterygoids, I feel it is

acceptable to include them in our calculations for this part of the study. The muscle cross-sectional areas are then multiplied by the estimated isometric force for muscle. Although other authors have sometimes used different values, I use 37 Ncm^{-2} for consistency and comparability with the RPCSA method.

Potential differences between calculation method results were explored using *t*-tests, and regression analyses. The regression analyses plotted muscle force against body mass for both of the data sets to determine if the muscles scaled with allometry and if the method of determining muscle force made significant differences to the result.

4.2.4 Computer Modelling.

4.2.4.1. Review

Bite force is the force output at a particular tooth and reflects the power with which an animal can subdue, kill or dismember prey. Being able to hypothesise either actual values or relative values between species allows for interspecific comparisons and inference with behavioural correlates. The simplest method to calculate bite force at a specific tooth position is to consider the mandible as a third-class lever. In this model, the input force (the attachments of the jaw adductor muscles) inserts between the fulcrum (the temporomandibular joint) and the output force (the tooth). Using simply geometric principles, static 2D lever models can predict the values of bite force. Due to its simplicity and cost effectiveness this method has long been popular with researchers (Greaves, 1982, 1983, 2000; Thomason, 1991; Satoh and Iwaku, 2006, 2009; Ellis *et al* 2009; Davis *et al.*, 2010; Druzinsky, 2010; Santana, 2016) although some argue that it often appears to underestimate bite forces especially when compared to *in-vivo* models (Christiansen and Wroe, 2007; Ellis *et al.*, 2008; Davis *et al.*, 2010). In their 2009 work Ellis *et al* predicted bite forces from the dry skulls of different sized/shaped domestic dog breeds. They used three different models: two lever models and one regression based model that considered measurements of cranial

variables to predict bite force. Findings revealed that regression models were not good indicators of bite force in breeds with extreme skull shape modifications, such as brachycephalic animals, where some negative values were predicted. Both of the lever models used, based on models from Kiltie (Kiltie, 1984) and Thomason (Thomason, 1991), appeared to be more sensitive to differences in skull shape and hence predicting more realistic bite forces. Even the more realistic lever models however, fail to capture the complexities of the biological structures that they represent (Röhrle and Pullan, 2007). For more biologically accurate simulations, computer generated models are superior. Computer modelling has several advantages. Experiments are repeatable without the ethical considerations of *in vivo* specimens, they are not timebound by the viability of *ex vivo* specimens, and models can be extensively modified to reflect real or hypothetical conditions. However, it is inevitable that virtual models do not replicate the true condition of *in vivo*, or even *ex vivo* specimens. Due to the huge complexity of biological samples all models are simplifications, and all methods have some shortfalls and compromises. Techniques such as multibody dynamics (MDA) and finite element analysis (FEA) have been extensively developed and become accessible to biological research in recent years, and address specific questions. MDA uses rigid but dynamic models to predict muscle force, bite force and joint force in moving models. It is often used as a precursor to FEA analyses, when muscle data is lacking (Curtis *et al.*, 2008; Moazen *et al.*, 2008, 2009; Dutel *et al.*, 2017). FEA on the other hand, models the object under consideration, in this instance the skull, to be made up of many smaller geometries, which are subject to external forces. The resultant output not only determines bite force but is also able to describe the behaviour of the skull under loading conditions. This chapter focused on FEA as the earlier PCSA work goes some way to informing the muscle geometry, and the key area of interest was the performance of the skull during biting.

Finite element analysis

Although the principle of finite element analysis, that many small mathematically solvable problems contribute to an overall output, has existed since the early 1900s (Richardson, 1911; Courant, 1943; Turner, 1956), it is only with powerful modern computers that this has been an accessible tool for biologists. FEA is based on the theory that simple geometries of known material properties behave in certain predictable ways when exposed to external loading stimuli. Large structures can be broken down into a number of small discrete geometric elements, which are interconnected at certain points, called nodes. During loading, nodal displacements are calculated for each element and the aggregate outcomes used to calculate structural deformation, strain and stress for the entire form (Richmond *et al.*, 2005; Rayfield, 2007; Cox *et al.*, 2011). This technique, whilst formulated initially to solve engineering problems for man-made structures, can also be applied to biological specimens. The building of FE models requires several steps: as FEA is a computer modelling technique, the first step in solving a problem is to gain a digital representation of the structure under investigation, in this case the skull and mandible of each of the canid species in this study. As with all models, accurate information is needed to create a realistically meaningful output, and judgements must be made on what structures to include, how much detail to add and which sources of information are used during construction. For this work the skull morphology was captured using computer tomography (CT) scans (Figures 4.4 A, B). CT image data allows for all aspects of the specimen to be visualised, not just the external surfaces as seen in photographic or surface scanning techniques. The voxels within the CT data are partitioned into the different biological materials such as cortical bone, trabecular bone, teeth and sutures (Figure 4.4 B). The next step is to assemble the CT data into a virtual 3D volumetric model of the skull (Rayfield, 2007). The third stage, discretisation, is to break the models down into many smaller elements (Figure 4.4 C). Each element represents a discrete volume within the model and is a predefined geometric shape, in this case a

tetrahedron. Tetrahedra are commonly used in biological FEA as their form can more accurately describe the complexities and curves of biological specimens, than the block or brick elements commonly used in structural engineering work (Ulrich *et al.*, 1998; Ramos and Simões, 2006; Burkhart *et al.* 2013). A tetrahedra is shaped like a triangular pyramid and has four sides and four nodes (Figure 4.3). The node is the point where three sides of the element meet, i.e. at the vertices. Together the elements and nodes form an interconnected mesh describing the form of the skull. The number of elements from which a mesh is composed is that which provides the most accurate solution with the smallest number of elements (Burkhart *et al.*, 2013). Meshes with a great number of elements may better reflect biology but may take too long to compute and generate a working model. Those with too few may be too coarse to accurately reflect the true geometry of the form. Ideally the correct number of elements should be determined by validation and sensitivity studies that compare outcomes of experimentally derived data to that from FE data (Kupczik *et al.*, 2007; Gröning *et al.*, 2009; Bright and Gröning, 2011; Burkhart *et al.*, 2013). Both the accuracy and solvability of the model depend upon the quality of the mesh (Knupp, 2007). An ideal mesh exhibits several characteristics: firstly, that the aspect ratio of each element is considered. The aspect ratio divides the longest element edge by the minimum altitude of the tetrahedra (Figure 4.3), the ideal element having an aspect ratio of one. Previous authors report that any elements with aspect ratios above 10 are to be treated with circumspection (Burkhart *et al.*2013). Secondly, the dihedral angles within each element are considered and should be above 10 to produce an accurate mesh (Maas *et al.*, 2012). Lastly, the Jacobean matrix value from each element should also be considered when assessing mesh quality. This is a measure of volume distortion from an ideally shaped element. Inverted elements report as negative Jacobeans and further analysis is aborted (Knupp, 2001; Burkhart *et al.*, 2013).

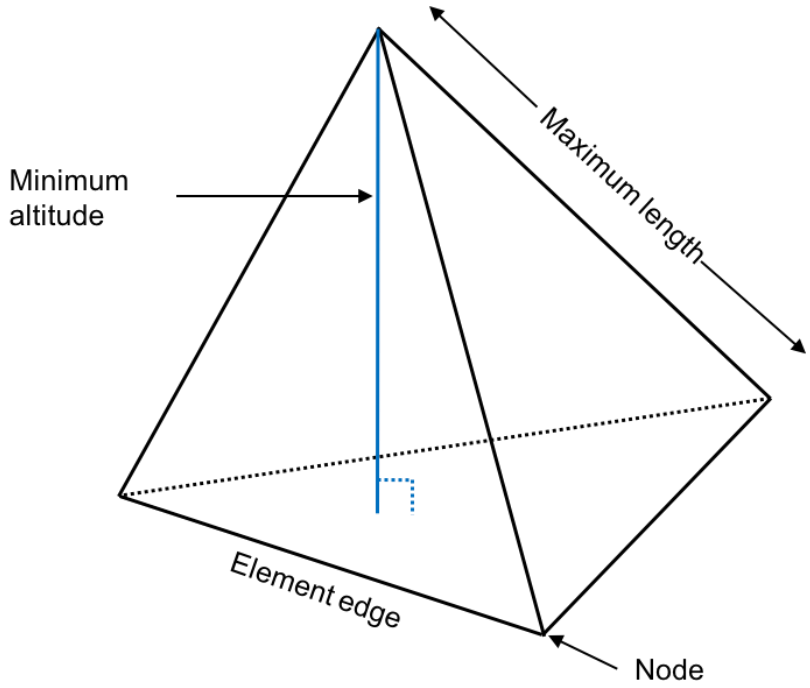

Figure 4.3. After Burkhart (2013). Diagram showing the components of a tetrahedral element used in finite analysis studies.

The completed mesh is uploaded to FEA software. The individually partitioned regions representing the different tissues are attributed with different material properties (Figure 4.4 D, E). The properties describe the elasticity of each material using Young's modulus and Poisson ratio values. Elastic deformation is the non-permanent deformation of a structure under load. The structure will return to the original form when the load is removed (Martin *et al*., 2004). Young's modulus, also called elastic modulus, determines the extent to which a material deforms under load. A high value Young's modulus equates to a stiff material. The Poisson ratio is the ratio of the change in width to the change in length as a result of directional strain. It describes how a material stretched in one direction tends to become thinner in the transverse direction. Similarly, if a material is compressed in one direction it tends to expand in the transverse direction. In unconstrained objects it functions within the numerical boundaries of -1 to 0.5, and as it is a ratio, is unitless. Incompressible materials have a Poisson ratio of 0.5, as their bulk is forced laterally under compression. Completely

compressible materials have a Poisson ratio of 0. Negative values occur in material that expand in transverse section when loaded longitudinally (Maas *et al.*, 2014).

Each model must next be loaded with its boundary conditions. These attempt to describe the forces and constraints that would occur during function in the living organism. Forces are the magnitude and direction of individual muscle forces, whilst boundary constraints limit directional movement of the model and allow only certain actions to occur.

The final consideration when building the FE model is the siting of constraints. Without any constraints, the model would not solve as it would be unable to resist the applied forces, and so move continuously within the virtual space. Deciding how to constrain a model in a meaningful way relies on an accurate understanding of the real life biological condition. For instance, allowing only rotational movements around the TMJ, rather than translational movements reflects the condition found within canids, and this was the condition adopted here. Future work could also consider looking at constraints from the neck muscles, as these are shown to play a role in food acquisition and processing in many large carnivores (Radinsky, 1981; Van Valkenburgh, 1996; Wroe *et al.*, 2005; Wroe, 2010).

When all boundary conditions are set the analysis is then solved using a quasi-static non-linear implicit method with ten time steps. Quasi static means the inertial terms are ignored, and that there are negligible effects of inertia (Maas *et al.*, 2014). Non-linear refers to the non-linearity of the stress strain curves of the materials constituting the model. Most biological materials exhibit non-linear behaviour under stress, that is they have some degree of elastoplasticity. Non-linear analysis is applied to a model where the matrix exhibits non-constant stiffness under loading. Implicit FE calculations ensure that energy equilibrium is met after each time step, and subsequent calculations are based on the most recent iteration (Maas *et al.*, 2012, 2014). The implicit method is computationally costly but more accurate. This method is used where the end result is important and has no element of time dependency. FEA uses partial differential equations to calculate individual nodal

displacements, which describe structural stress and strain for each node (Richmond *et al.*, 2005; Rayfield, 2007). The composite calculation of all nodal displacement is used to calculate stress and strain distribution throughout the model. Outputs of the analyses are displayed graphically as a time stepped volumetric skull models with scaled colours representing different stress or strain values (Figure 4.4 F).

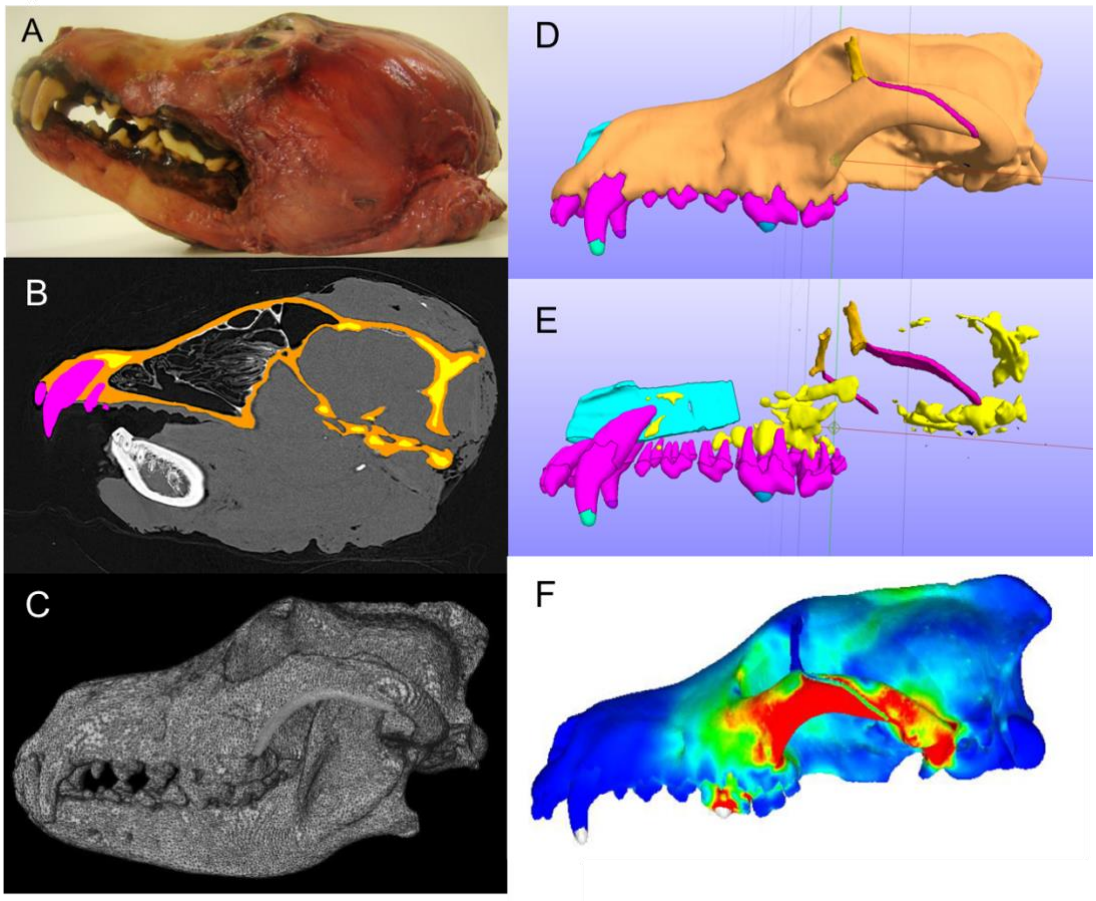

Figure 4.4 Finite element analysis workflow, A, *Canis lupus* specimen, B, segmented sagittal CT slice, C, discretised, D, constrained and loaded model, E, as D but with cortical bone removed to show internal materials and F, the finite element output model with colour map indicating regions of differing stress.

4.2.4.2 Finite element analysis method.

For the FE work in this chapter, more complex models were required than those used to place landmarks in Chapter Three. A CT scan from each species was imported into Avizo Lite 9.0.1 (FEI Systems, Oregon, USA) for material segmentation. In species with more than one

specimen, a representative individual was chosen based on earlier shape analysis (Chapter Three part 3.3.2.3). Each model consisted of two main structures, the skull, and a separate region representing the caudal part of the left mandible. The inclusion of the caudal mandibular region allowed me to ascertain the correct insertion points of the jaw adductor muscles, which enabled me to model the muscle vectors with greater accuracy. There was no necessity to model the right mandible as findings from the left mandible were reflected mathematically to model muscle vectors on the right. To reduce the computational burden the mandibular structure does not form part of the final model subjected to FEA simulations. The next stage was to partition the visible structures of the CT scan into distinct materials. Partitioning was achieved via manual and semi-automated segmentation of the CT scans. Segmentation assigns voxels to a specified material which are then stored as separate object called label fields. Automatic segmentation selects voxels to be assigned to a material based on their greyscale value. This method, whilst simple for the user, results in many errors as similar grayscale values may be common to more than one material and boundaries between materials or structures may not be clearly defined. Semi-automated segmentation relies on initial thresholding but also uses subsequent algorithms for filling or expanding or smoothing selections (Mazonakis and Damilakis, 2016). Again, this system is not infallible and creating biologically accurate models usually requires a high degree of manual segmentation and iterative refinement. Manual segmentation requires the user to select and assign materials using paintbrush and lasso tools on a slice-by-slice basis (Figure 4.5). Although giving a greater degree of accuracy than automated techniques, manual segmentation is very time consuming. It also relies to some degree on prior knowledge of biological form and the resolution of the CT scans to make meaningful decisions as to which voxels to assign to which materials. For this work, manual and automatic segmentation methods were used to identify six different materials (cortical bone, trabecular bone, teeth, nasal septum, orbital ligaments and zygomatic sutures). It is important to note that models are intended to simulate rather

than replicate the biomechanics of the skull. The true biological condition is far too complex to capture and recreate, and compromises in the fidelity of the reproduction must be made. For example, in this study only the more significant regions of trabecular bone were assigned, the teeth were treated as a single material and the periodontal ligament (PDL) was not segmented but included as part of each tooth. Previous workers have discussed the importance of including the PDL in FEA mandible models. Although some authors argue that it plays an important role in the dispersal of strain throughout the entire mandible (Gröning *et al.*, 2011), others conclude that it only has an effect in the alveolar region adjacent to each tooth root. All authors concur that visualising and modelling such a thin structure as the PDL, even when using microCT scan data is very challenging. The original image resolution and modality, whether CT or MR, determines if the PDL is visualisable in the scan data, and when constructing the FE model the PDL may need to be falsely enlarged to be incorporated into a viable model. In addition, data on key values for the canid PDL (i.e. material properties and thickness) is very scarce or unsubstantiated in the literature (Qian *et al.,* 2001). Published values for the material property parameters for the PDL in other mammalian species e.g. rats, humans, pigs and macaques, appear to differ widely, even within the same species (Kawarizadeh *et al.*, 2003). I am unaware of any published work using PDL in carnivoran FEA models. Other simplifications include the omission of any cranial sutures except for the zygomaticotemporal suture. Previous authors have found that models of mammalian skulls without cranial sutures appear to give valid results in three-dimensional skull models, and many earlier studies have not included cranial sutures in FE models (McHenry *et al.*, 2007; Bright and Rayfield, 2011a; Cox *et al.*, 2011; Curtis *et al.*, 2011; Dumont *et al.*, 2011). Wang *et al.* found that although macaque skulls with sutures exhibited higher total strain energy values than in the models with no sutures, the overall strain patterns and bite force values were relatively unaffected by the inclusion or omission of sutures (Wang *et al.*, 2010). In a later study Wang *et al* speculated that the sutures are weak points on the skull that are

protected from undue stress or strain due to skull morphology, and that their inclusion plays only a limited role in modulating global skull stress and strain (Wang *et al.*, 2012). The zygomaticotemporal suture was included in the models in this chapter as it remains unfused throughout life in canids (Evans and De Lahunta, 2013; Thrall and Robertson, 2015), and is in a region pertinent to this study, i.e. the attachment of the masseter muscle on the zygomatic arch, and has been found to increase model fidelity in other studies (Kupczik *et al.*, 2007).

Other elective reduction in form complexity also occurs at the segmentation stage. For example, the architecturally intricate turbinate bones of the nasal cavity and the cochlear of the inner ear structures were deliberately omitted. This is due to their high level of complexity which would likely be computationally burdensome, and their assumed lack of impact on masticatory models. Smoothing algorithms were also utilised to reduce skull complexity and thus the computational workload.

The segmented models were converted to three dimensional meshes using Avizo software. Models consisted of between 994,992 and 2,483,659 tetrahedral elements. The difference in tetrahedral numbers is accounted for by the differences between the original specimen sizes and scan resolutions. Convergence testing is important in FEA studies to determine if models contain a sufficient number of elements to solve in a timely yet realistic manner (Bright and Rayfield, 2011b). In convergence tests using the *Vulpes vulpes* model, simplified iterations, with no zygomatic sutures or orbital ligaments, would solve using models of around 300,000 elements. However, when fine structures were introduced, element numbers were increased to account for the greater morphological complexity and improve acuity. Several automated tests within the software inspect the mesh for viability. These include checking the aspect ratio, dihedral angle and Jacobean matrix value of each element. All models in this work fell within the acceptable measures in all such tests.

In contrast with some earlier bite force studies (McHenry *et al*., 2006; Slater *et al*., 2009; Attard *et al*., 2011), I did not scale the FE models to identical volumes or load with identical

loads as I had empirically derived values for muscle forces. This approach allowed me to take into account both size and shape differences, with a view to producing more representational functional models. Meshes were scaled with reference to the original CT resolutions and re-orientated such that the hard palate, a relatively flat structure in canids, was broadly parallel to the axial plane Y, rostral and caudal landmarks aligned along the sagittal plane Z, and medial and lateral structures along coronal plane X.

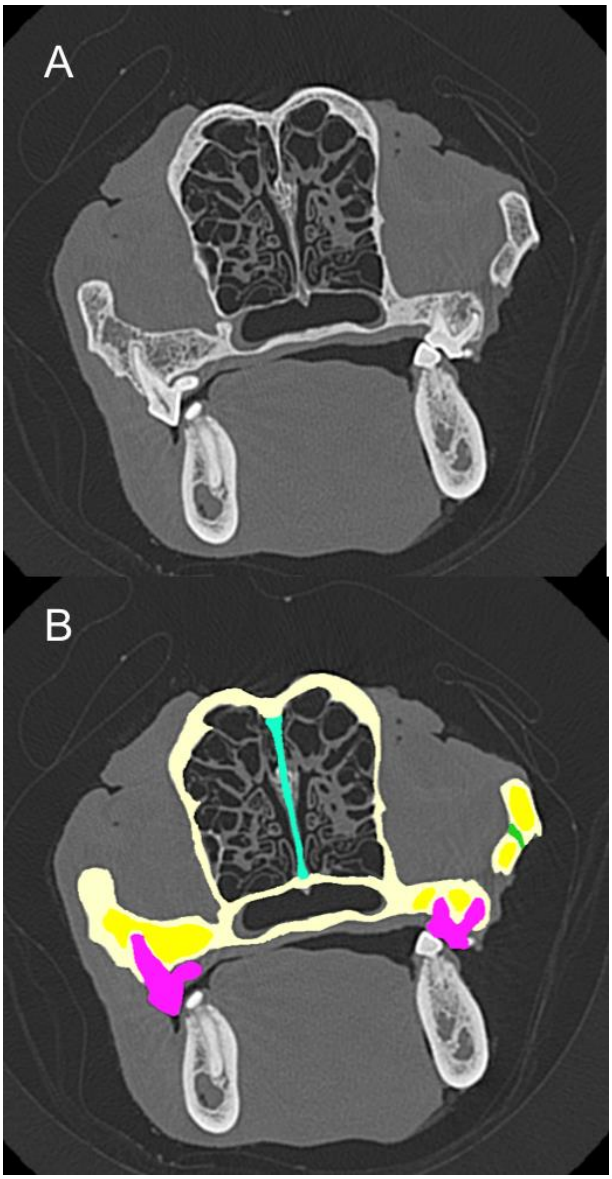

Figure 4.5 A, axial CT slice of Lycaon pictus, and B the same CT slice illustrating manual segmentation into separate materials.

Material properties

The computational meshes were imported into FEBio PreView V1.18.2 (Maas *et al*. 2012), FEBio was used as it is a free downloadable software package that has been widely used in similar studies (Lida *et al.*, 2015; Begonia *et al.*, 2017; Kim *et al.*, 2017; Coogan *et al.*, 2018; Peterson and Müller, 2018). The individual label field volumes were then assigned different material properties. For this chapter, the bony components of the skull were modelled as isotropic elastic materials although, in reality this is unlikely to be the case. Nevertheless, in finite element validation and sensitivity studies where mammalian bone has been modelled as an isotropic material and compared to experimentally derived output values, results are similar from both experimental conditions (Kupczik *et al.*, 2007; Bright and Rayfield, 2011a). In addition, as no further evidence of complexity of the true condition is currently available it was considered unachievable to model the true anisotropic state. I did not account for the diploë, or trabecular bone layer, in the calvarial bones as the resolution of the CT scan was too coarse. I did however model trabecular bone in areas where it was grossly evident on the CT scans, namely in the zygomatic arch, caudal cranium, rostral maxilla and incisive bones. Reported material properties of bone are highly varied with influencing factors including species, site of bone, fresh, dried or embalmed preparation of specimens, experimental methods and age of cadaver. Recorded values of the Young's modulus of human calvarial bones range from 1.2 to 22 GPa (Peterson and Dechow 2003; Motherway *et al*. 2009; Auperrin *et al*. 2014; Boruah *et al*. 2016; Falland-Cheung *et al*. 2017). Studies using fresh or fresh-frozen specimens, that is, not dried or embalmed, reported lower values (Motherway *et al*. 2009; Auperrin *et al*. 2014; Falland-Cheung *et a*l. 2017). As our laboratory experiments used fresh-frozen material I used a relatively low Young's modulus of 7 GPa for cortical cranial bone. This is consistent with values reported by Motherway *et al*. and Auperrin *et al*. for human cranial bone (Motherway *et al*., 2009; Auperrin *et al*., 2014). Reported values for the Young's modulus of trabecular bone are similarly varied, ranging from 35 MPa to 25 GPa

(Ashman and Jae Young Rho, 1988; Ryan and Williams, 1989; Choi *et al.,* 1990; Van Rietbergen *et al*., 1995; Rho *et al*., 1997; Zysset *et al*., 1999). As all authors report that trabecular bone is less stiff than that of the surrounding cortical bone I used a value of 6 GPa for trabecular bone. The only cranial suture that was modelled was the temporozygomatic suture, the oblique ventrocaudally running suture between the temporal process of the zygomatic bone and the zygomatic process of the temporal bone. In all the CT scans and dissected specimens, the temporozygomatic suture could be easily perceived as a simple, rather than interdigitated, dark line, and completely separated the zygomatic and temporal bones. Reported values for Young's modulus for cranial sutures are very variable and range from 1.16 MPa to 7.7 GPa (Margulies and Thibault, 2000; Radhakrishnan and Mao, 2004; Kupczik *et al*., 2007). For the temporozygomatic sutures I used a value of 354 MPa and they were modelled as a neo-Hookian to reflect the hyperelastic nature of the material (Mohamed *et al*., 2010, Weed *et al*., 2010). Teeth were modelled as an isotropic elastic material with a Young's modulus of 30 GPa. This figure was based on a compromise between the Young's modulus of enamel as reported up to 60 GPa and the Young's modulus of dentine from 13.2 GPa to 25 GPa (Rayfield *et al*., 2001; Ausiello *et al*., 2002; Kinney *et al*., 2003; Attard *et al*., 2011). Nasal septum was modelled as isotropic elastic with a value of 9 MPa as reported material properties for nasal septum range from 0.8-168 MPa (Grellmann *et al*., 2006; Al Dayeh and Herring, 2014; Leary *et al*., 2015; Correro-Shahgaldian *et al*., 2016). The postorbital ligaments were modelled as isotropic elastic material with a Young's modulus of 100 MPa. These ligaments were included because work by Herring *et al*. (Herring *et al.,* 2011) has suggested some involvement with muscle force distribution, in particular, resisting deformation of the zygomatic arches by contraction of the masseter during biting. This is further explored in Chapter Five. I am unaware of any published data regarding the material properties of canine postorbital ligament and therefore I based my values on those derived from human spinal and lower limb ligaments that ranged from 1.5 to 284 MPa (Butler *et al*.,

1992; Kumaresan *et al*., 1997; Maurel *et al*., 1997; Cheung *et al*., 2005). A summary table of material properties in given (Table 4.2). A Poisson's ratio of 0.3 was used for all materials.

Table 4.2. Material properties of material used in finite element models.

Material	Young's Modulus	Poisson ratio	References
Cortical bone	7 GPa	0.3	Motherway *et al*. Auperrin *et al*
Trabecular bone	6Gpa	0.3	Ashman and Jae Young Rho, 1988; Ryan and Williams, 1989; Choi *et al.,* 1990; Van Rietbergen *et al*., 1995; Rho *et al*., 1997; Zysset *et al*., 1999
Teeth	30GPa	0.3	Rayfield *et al*., 2001; Ausiello *et al*., 2002; Kinney *et al*., 2003; Attard *et al*., 2011
Nasal septum	9Mpa	0.3	Grellmann *et al*., 2006; Al Dayeh and Herring, 2014; Leary *et al*., 2015; Correro-Shahgaldian *et al*., 2016
Zygomatic suture	354 MPa	0.3	Mohamed *et al*., 2010, Weed *et al*., 2010
Post orbital ligament	100Mpa	0.3	Butler *et al*., 1992; Kumaresan *et al*., 1997; Maurel *et al*., 1997; Cheung *et al*., 2005

GPa - Gigapascal, MPa - Megapascal.

Finite element constraints

All models were constrained at the temporomandibular joint (TMJ) in all but rotational movements around the X axis. This reflects the limited movement of carnivoran mandibles during biting where there is minimal translational or rostro-caudal movement, due to the congruent nature of the of the condyles and the pronounced retroarticular processes (Evans and Delahunta, 2013; Singh *et al*., 2018). Bilateral canine and carnassial biting were simulated by fully constraining either the tips of both upper canine teeth or the paracones of both upper carnassial teeth. The tips of the teeth were chosen as they act as a constraint during biting, i.e. the mass of the food stuff initially prevents closure of the jaw, and forces incurred are transmitted to the skull. In addition, they were easily identifiable and replicable across

all specimens. The canine teeth are chiefly utilised during initial capture, restraint and killing of prey, whilst the carnassial teeth are used during butchering of carcasses and intraoral food processing. Both bilateral and unilateral biting are commonly seen at the canine bite point in carnivorans (Van Valkenburgh and Slater, 2009; Slater *et al.*, 2010; Oldfield *et al.*, 2012). Carnassial biting is less well documented. Observation of wild canids show that they use their carnassial teeth unilaterally to remove flesh from carcasses, but appear to use bilateral carnassial biting for intraoral food processing (Van Valkenburgh, 1996). Weijs (1994) conducted an analysis of existing electromyogram (EMG) chewing data in mammals. He concluded that the jaw adductor muscles on each side of the head potentially function in three separable groups: 1. symmetrical vertical closers (deep masseter), 2. Triplet I - balancing side superficial masseter and medial pterygoid plus the working side posterior temporalis, 3. Triplet II - working side superficial masseter and medial pterygoid and balancing side posterior temporalis. He observed that in carnivorans, although the vertically orientated group was the first to contract at the beginning of jaw closing, this was rapidly followed by both sets of triplets contracting simultaneously. That is, the masticatory pattern for carnivorans appears to be that all muscle contract nearly simultaneously to produce a purely jaw closing action. This finding was supported by Davis (2014) in her work on ferrets, and Dessem's (1989) work on domestic dogs. This condition is thought to reflect a reduction in complexity that has evolved from the primitive mammalian condition of unilateral occlusion (Weijs, 1994; Langenbach and van Eijden, 2001; Vinyard *et al.*, 2011). During unilateral biting, although all jaw adductors muscles contract nearly simultaneously, the left and right-side muscles do not do so to the same magnitude. Muscles on the working side contract to a greater extent and consequently produce more force than those on the contralateral balancing side (Dessem, 1989; Davis, 2014). Two reasons for this have been proposed: firstly that balancing side jaw activity is reduced to limit forces acting upon the temporomandibular joint (Dessem, 1989; Clausen *et al.*, 2008), or that the unfused

mandibular symphysis prohibits force transmission from the balancing side to the working side and thus energy is not wasted in contracting unused muscle forces. As this study was concerned with looking at the functional constraints of the skull, it was considered acceptable to look at the limits of normal bite behaviour. Therefore, all bites were modelled as bilateral, and all of the muscles are modelled to be contracting maximally during jaw adduction. This condition is also described by other authors (Wroe *et al.*, 2007; Clausen *et al.*, 2008; Slater *et al.*, 2009; Tseng and Wang, 2010).

Finite element loading

Muscle forces acting upon the skull were simulated by selecting nodes on the skull to represent the origin attachment sites of individual muscles from each individual species. The number of nodes representing temporalis ranged from 3351 to 7630, the number of nodes for the masseter ranged from 290 to 752, and the number of nodes representing the pterygoids ranged from 510 to 1140. In the case of the temporalis and masseter each muscle origin region was subdivided into smaller regions to more accurately describe the complexities of the direction of the muscle vectors of such large muscles and to minimize the number of vectors whose line of action would run through the interior of the cranium. The origin of the temporalis muscle was subdivided into six regions, the masseter into three regions and the pterygoid muscle was modelled as one region (Figure 4.6). As discussed earlier (Chapter Two, part 2.4.5) the pterygoids were considered as one muscle. This follows from previous authors works (Slater *et al*., 2009; Tseng and Wang, 2010). The magnitude of the muscle forces were calculated from the RPCSA findings (this chapter, Table 4.1). The total force is divided by the number of nodes within the muscle attachment area, and each individual node was loaded accordingly. To calculate the direction of the muscle vectors, origin and insertion points for each muscle subsection were identified. One node from each muscle origin region on the left side of the skull was selected as the representative start

node, and one node from each muscle insertion site on the left caudal mandible was selected as the representative end node. To enable this all models initially included a section of the left caudal mandible to enable identification of the end nodes that represented the muscle insertion points. Mandible sections were subsequently removed when running the FE calculations to reduce the computational burden. The locations of the start and end nodes were informed by the dissection work. In the case of the temporalis muscle, as the insertion site was so extensive, two insertion sites were chosen, one at the dorsal part of the coronoid process, and one on the medial aspect of the vertical ramus of the mandible. The two dorsalmost subdivisions of temporalis inserted onto the dorsal attachment site and the remaining four more ventral subdivisions inserted onto the ventral attachment site. Again, this aided in more accurately describing the vectors for each muscle or part muscle and minimized vectors running within the cranium. The vectors calculated on the left side were reflected to create right side sets of muscle vectors. Two gape positions were modelled based on occlusion and maximum gape. The position of the mandible at maximum gape for all species was determined with reference to the dissection of the cadaveric head and MR studies of *Vulpes vulpes* 7 (this chapter part 4.2.2 and Figure 4.1). To simulate the wide gape position in the FE models for each species, the caudal mandibles were rotated to a similar position with a gape angle of approximately 80°. The representative end nodes for each of the muscles were re-identified on the rotated mandible and their new co-ordinates used to recalculate the force vectors acting upon the skull.

All models were solved using FEBio Preview v1.18.2 (Maas *et al*., 2012) using a quasi-static, non-linear implicit method. Solved models were explored and analysed with FEBio Postview v1.9.1. Derived outputs were rigid force at the specific bite points, which were a measure of bite force, and strain energy density (SED), a measure of skull shape efficiency. To measure absolute values and the distribution of SED across the skull, seven midline sampling sites were identified by common landmarks on each of the FE models after Tseng and Wang (Tseng

and Wang, 2010) (Figure 4.6C). Midline landmarks were chosen as they were easily replicable across species and were less subject to noise created by the constraints of the models at the TMJ and bite points. At each sampling site ten nodes were randomly chosen and their mean value recorded. The same nodes were sampled in all four loading conditions (closed canine bite, wide canine bite, closed carnassial bite, wide carnassial bite).

To compare shape only, outputs were scaled to the volume of one specimen, *Canis lupus*, after Dumont (Dumont *et al*., 2009) using the equation:

$$U_{B'} = \left(\frac{V_B}{V_A}\right)^{1/3} \left(\frac{F_A}{F_B}\right)^2 U_B$$

Where A is the model to which B is scaled, and B' is the newly created model. U is SE, V is volume and F is force. *C.lupus* was chosen because it is the largest canid species and so allowed me to consider any size-related performance limitations in the other species.

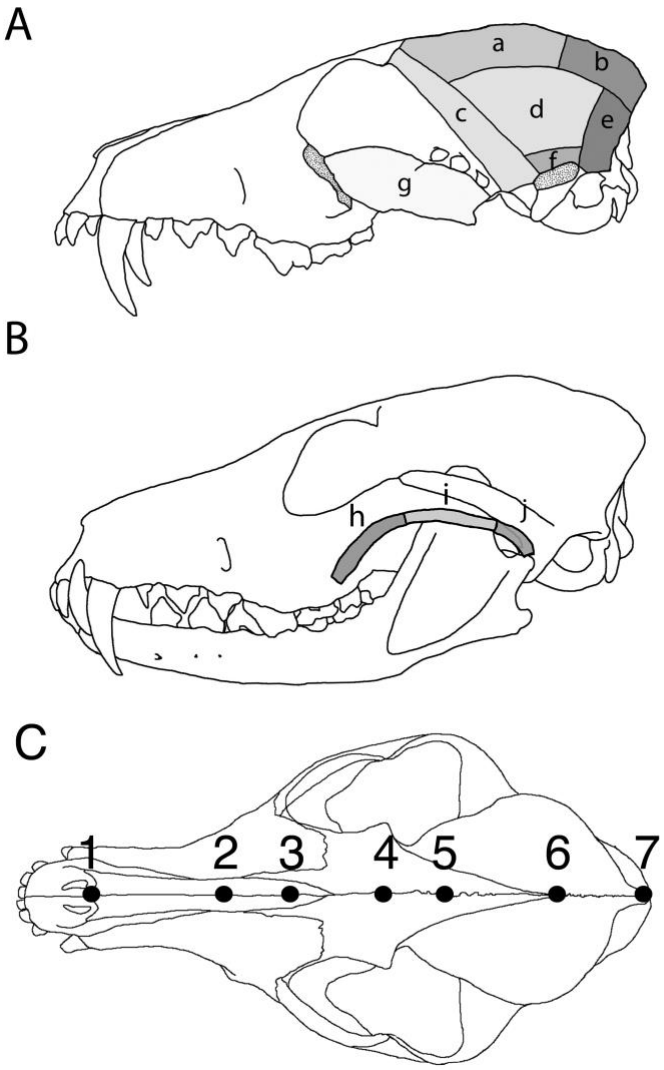

Figure 4.6 *Vulpes vulpes* skull diagram, lateral aspect. (A) zygomatic arch removed to illustrate areas of temporalis and pterygoid muscle attachment. a and b - superficial temporalis, c, d and e - deep temporalis, f- suprazygomatic temporalis, g - pterygoid. (B) with zygomatic arch to show the three regions of masseteric origin, h- rostral, I - middle and j - caudal. (C) Dorsal aspect, numbers 1-7 indicate the seven midline sampling points used in the SED analyses.

4.2.5. Mechanical efficiency

The mechanical efficiency of biting can be calculated to give an indication of the influence of skull shape on performance (Dumont *et al.,* 2011). Mechanical efficiency is derived by dividing the value of the calculated predicted bite force by the total muscle force, that is, force output divided by force input. I calculated the mechanical efficiency of all species for

canine and carnassial bite, at dental occlusion and wide gape. Differences between dietary groups were identified using statistical tests. Initially a Shapiro-Wilk test was performed for each variable to determine if the dataset was normally distributed. Kruskal-Wallis tests were used to compare variance between groups as not all datasets were evenly distributed and the sample size was small. Dunn's post hoc test were used to assess differences between groups.

4.2.6. Mechanical advantage

A further measure of the effect of form on biomechanical function is the mechanical advantage (MA) of a muscle. I determined the MA of the temporalis and masseter muscles at both the canine and carnassial bite points. The pterygoid muscles were not included in this part of the study due to their small size. Following other authors (Radinsky, 1981; Reduker, 1983; Sacco and Van Valkenburgh, 2004; Anyonge and Baker, 2006; Tanner *et al*., 2010; Segura and Prevosti, 2012) I calculated MA as a ratio of the length of the muscle in-lever divided by the length of the bite point out-lever. The in-lever is a line connecting the point of muscle insertion on the mandible to fulcrum, in this case the mandibular condyle. In this simplified model, the muscle insertion point for the temporalis was the coronoid process of the mandible, and for the masseter it was the angular process of the mandible. The out-levers connect the fulcrum to the bite points, that is, the tip of the lower canine and the tip of lower first molar. Longer in-levers and/or shorter out-levers increase MA and hence, increase bite force. Higher MA values are negatively correlated with transmission of velocity, and species with short jaws experience a trade-off favouring jaw closing strength over jaw closing speed (Wainwright and Richard, 1995; Preuschoft and Witzel, 2005). Measurements were made using landmarks identified on the reconstructed CT scans, and using the measurement tool in Avizo. Differences between dietary groups were identified using statistical tests. Initially a Shapiro-Wilk test was performed for each variable to determine if

the dataset was normally distributed. Kruskal-Wallis tests were used to compare variance between groups as not all datasets were evenly distributed and the sample size was small. Dunn's post hoc test were used to assess differences between groups.

4.2.7 Temporalis muscle angles relative to the occlusal plane

To determine whether the muscle architecture was topographically related to the bony morphology to increase jaw closing strength or speed, I considered how the muscle line of action related to the occlusal plane. Previous work on bats (Reduker, 1983) and shrews (Fearnhead *et al*., 1955) has described how the angle of the line of action of the temporalis influences bite force and speed of jaw closure. They conclude that species with more vertically orientated temporalis lines of action are able to close their jaws with greater force by pulling the coronoid process of the mandible dorsally, whilst species with a more horizontal line of temporalis action are able to close their jaws more quickly by pulling the coronoid process caudally. The line of action of a muscle can be calculated by drawing a line from the muscle insertion point to its origin (Jensen and Davy, 1975). The resultant line can then be measured against another, constant line, and the angle between them determined. This allows comparison between specific muscles or muscle layers, as well as between individual specimens or species. To determine the muscle lines of action using the FE models, I disregarded the parasagittal coordinates (Z), and used the X and Y coordinates to draw lines in the dorsoventral and rostrocaudal planes. To illustrate the line of action of the individual muscle layers that make up temporalis I amalgamated the dorsal and ventral crest areas to represent superficial temporalis, the rostral, lateral and caudal areas to represent the deep temporalis, with the remaining ventral area representing the suprazygomatic temporalis (Figure 4.6). Muscle origin points were identified as the average node co-ordinates for each muscle layer attachment area, and the single insertion nodes remained the same as for the FEA bite models. The line representing the occlusal plane was drawn from the lateral aspect

of the alveolus of the upper canine, to the ventral aspect of the retroarticular process of the temporal bone, as these were identifiable in all models. Kruskal-Wallis- tests were used to determine any differences in muscle line of action angles between the dietary groups. Dunn's post hoc test were used to assess differences between groups.

4.2.8 Statistical analysis

Differences between the dietary groups regarding muscle fascicle length, percentage contribution towards total muscle force, mechanical efficiency, mechanical advantage, temporalis lines of action, and SED values were tested using Kruskal-Wallis tests and Dunn's post hoc tests. Potential differences between muscle volumes determined by microvolumeter and those from calculations from muscle mass were compared using *t*-tests. The two methods of muscle force calculation results were also compared using *t*-tests to see if the values were significantly different between the two groups. Rank correlation and reduced major axes (RMA) regression analyses was used to determine if log transformed RPCSA and dry skull calculated muscle force values scaled against log transformed body mass to indicate isometry or allometry, and if the different calculation methods resulted in different scaling conclusions. I also used rank correlation and RMA regression analyses to test the scaling relationships of the following variables: body mass, muscle mass, muscle force, bite force, rostrum length and palate length. Rank correlation and RMA regression were used as the relationships are likely to be monotonic and symmetric. Evaluations of isometry were made based on the RMA slope, 95% confidence intervals and *P*-values from *t*-tests against predicted slope values. Rank correlation, reduced major axes regressions, Kruskall-Wallis, *t*-tests and post hoc analyses were computed in PAST (Hammer *et al*., 2001).

To determine if there were phylogenetic influences amongst the datasets, that is, were related species more likely to resemble each other, we calculated the *K* statistic (Blomberg et al. 2003) for all variables using the phytools package in R (Revell, 2012). All Kruskal-Wallis

were re-run as phylogenetically adjusted ANOVAs and the RMA regression slopes were rerun as phylogenetic generalised least squares (PGLS) regressions. Significant results are reported alongside the raw data analyses. A significance level of ≤ 0.05 was used in all statistical tests.

4.3 Results.

4.3.1 Muscle density

Predicted and measured muscle volumes are reported in Table 4.3. No significant differences were found between the volume predicted from mass and that recorded by the microvolumeter. This indicates that the published density value of 1.056 gcm^{-3} (Murphy and Beardsley 1974) was a reliable estimate for use in the RPCSA calculations.

Table 4.3 Jaw adductor muscle masses predicted volumes and volumes from two species.

Species	Muscle	Mass (g)	Predicted volume (cm^3)*	Volume from microvolumeter
Vulpes vulpes	Suprazygomatic temporalis	2.84	2.69	2.60
	Superficial temporalis	21.80	20.64	20.10
	Deep temporalis	23.06	21.84	22.00
	Superficial masseter	9.40	8.90	9.00
	Deep masseter	5.32	5.04	4.70
	zygomaticomandibularis	4.56	4.32	4.30
	pterygoids	5.75	5.45	5.30
Vulpes zerda	Suprazygomatic temporalis	0.22	0.21	0.20
	Superficial temporalis	2.81	2.66	2.50
	Deep temporalis	2.57	2.43	2.40
	Superficial masseter	1.28	1.21	1.20
	Deep masseter	0.73	0.69	0.70
	zygomaticomandibularis	0.39	0.37	0.40
	pterygoids	0.90	0.85	0.84

* With reference to Murphy and Beardsley 1973.

4.3.2 Dissection, muscle mass, fascicle length and muscle force.

Details of the muscle dissections can be found in Chapter Two. Of particular note is the insertion of both the deep and superficial masseter to the caudal ventral mandible. In most

canid species both muscles insert on and near the angular process, but in two of the generalist species, *Otocyon megalotis* and *Nyctereutes procyonoides*, they also insert on the preangular process. This pronounced process is only found in a small number of canids. The dissection illustrates that the preangular process acts to change the orientation and length of the masseter fascicles (Figure 4.7). The masses and fascicle lengths of the individual muscles are presented in Table 4.1. Although there was some variation between species of the percentage contribution of each muscle to the overall mass, no statistically significant differences were found between the trophic groups. Regression analyses revealed that temporalis fascicle lengths were statistically significant longer in the larger species, but do not scale significantly different from isometry for the masseter or pterygoid fascicles. Results are reported in table 4.4. Kruskal-Wallis tests revealed that the fascicle lengths between dietary groups were statistically different for all three jaw adductor muscles; temporalis (H=7.477, p = 0.02) masseter(H= 7.342, p = 0.02) and pterygoids (H= 8.178, p = 0.01). Post Hoc Dunn's tests revealed that in all cases the generalists were significantly different to the hypercarnivores; temporalis p = 0.006, masseter p = 0.006, pterygoid p = 0.004.

The individual muscle percentage contributions towards total muscle force showed no statistical difference between trophic groups. The temporalis contributed between 44 and 61% to the total force, the masseter between 29 and 43%, and the pterygoids between 8.6 and 17%. The percentage contribution of the individual muscle masses to the total mass is not mirrored by their contribution towards the total muscle force (Figure 4.8). The temporalis muscle contributed a mean value of 62% of the muscle mass, however it only contributed a mean value of 52% of the force. The masseter on the other hand, contributes a mean value 30% of the muscle mass, but a mean value of 36% of the force, and the pterygoids contribute a mean value of 9% of the mass, but a mean value of 12 % of the total force. The inconsistency between mass contribution and force contribution is accounted for by the architecture of the muscles. When considering the physiological cross-sectional area, a long fascicle length

reduces the force production capability of the muscle. As the angles of pennation are small in the temporalis and masseter, typically less than 30° they had only a small effect on the final value, as the cosine value remains close to one. In all the species in this study the area of origin of the temporalis is very extensive, covering the lateral aspect of the cranium, and many of its fascicles were much longer than those of the masseter or pterygoids.

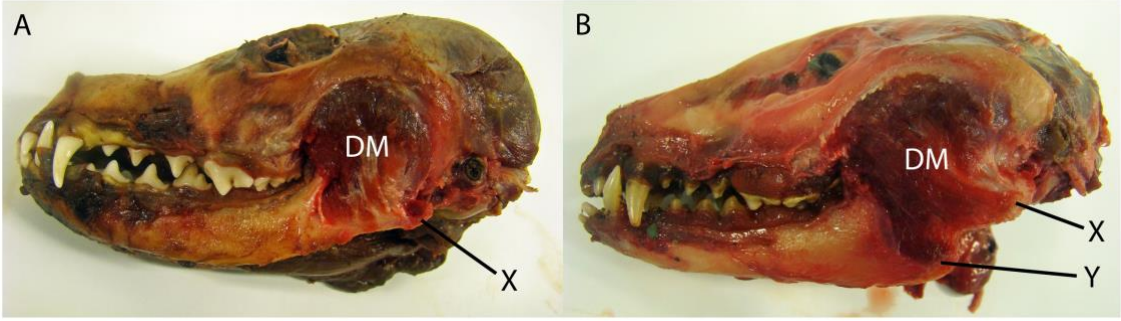

Figure 4.7 (A) *Alopex lagopus* and (B) *Nyctereutes procyonoides*. In both species, the dissection shows the deep masseter muscle 'DM'. Insertion point 'X' is the angular process, insertion point 'Y' is the preangular process seen only in a small number of canid species.

Muscle forces predicted from both the RPCSA and dry skull methods are presented in Table 4.1. Although *t*-tests did not reveal any statistically significant differences between the two methods for our dataset, it was noticeable that in all species over 25kg the predicted temporalis force was higher in the dry skull method, and that in all species below 14kg predicted values were lower using dry skull method. Regression results from the empirically derived muscle data revealed no significant evidence for either positive or negative allometry of muscle force production capability, with slopes that are close to isometry for both the individual jaw adductor muscles and the muscle mass as a whole, when scaled against body mass (Table 4.4). Regression results for the dry skull derived data showed that the masseter force did not scale significantly differently to isometry, but that the temporalis force scaled with positive allometry against body mass, with a slope of 0.76 and was statistically significantly different from an expected isometric slope of 0.67 (P = 0.03, CI 0.69-0.81). A comparison of the two slopes is shown in Figure 4.9 and in Table 4.4. The effect of using the

dry skull method was clearly demonstrated and illustrates the influence of muscle geometry when calculating muscle force.

One muscle force, the masseter, had significant phylogenetic signal (K = 1.04, P = 0.03), and the percentage contributions to overall muscle mass of both temporalis and masseter also revealed phylogenetic signal (temporalis K = 0.98, P = 0.05. masseter = 1.22, P = 0.01.).

Table 4.4 Reduced major axes regression analyses of jaw adductor muscle variables.

	Spearman's rank correlation R	Expected slope for isometry	RMA reported slope	95% confidence intervals	R^2	*P*-value from *t* test
Log Temporalis fascicle length vs BM	0.89	0.33	0.42	0.25,0.49	0.86	0.048
Log Masseter fascicle length vs BM	0.92	0.33	0.43	0.26, 0.53	0.83	0.053
Log Pterygoid fascicle length vs BM	0.86	0.33	0.36	0.13, 0.50	0.56	0.22
Log total muscle force vs log BM	0.94	0.67	0.66	0.61, 0.73	0.96	0.73
Log temporalis muscle force vs log BM	0.95	0.67	0.64	0.53,0.79	0.95	0.63
Log masseter muscle force vs log BM	0.97	0.67	0.69	0.61, 0.73	0.94	0.72
Log pterygoid muscle force vs log BM	0.96	0.67	0.72	0.63, 0.88	0.95	0.36
Log canine occlusal bite force vs log BM	0.97	0.67	0.78	0.63,1.01	0.89	0.21
Log carnassial occlusal bite force vs log BM	0.94	0.67	0.74	0.60,0.94	0.89	0.37
Log canine wide gape bite force vs log BM	0.91	0.67	0.75	0.55, 0.93	0.83	0.43
Log carnassial wide gape bite force vs log BM	0.83	0.67	0.72	0.53,0.86	0.84	0.60
Log palate length vs BM	0.97	0.33	0.30	0.24,0.33	0.93	0.24
Log rostrum length vs BM	0.98	0.33	0.29	0.24, 0.32	0.96	0.06
Log total muscle mass vs log total muscle force	0.96	0.67	0.62	0.57,0.71	0.97	0.17
Log temporalis mass vs log temporalis force	0.95	0.67	0.61	0.55,0.72	0.97	0.11
Log masseter mass vs log masseter force	0.99	0.67	0.62	0.55,0.68	0.96	0.22
Log pterygoid mass vs log pterygoid force	0.90	0.67	0.73	0.63,0.94	0.9	0.43
Log total muscle mass vs log canine occlusal bite force	0.98	0.67	0.74	0.57,0.94	0.95	0.37
Log temporalis mass vs log canine occlusal bite force	0.95	0.67	0.75	0.61,1.05	0.94	0.33
Log masseter mass vs log canine occlusal bite force	0.99	0.67	0.71	0.57,0.93	0.9	0.59
Log pterygoid mass vs log canine occlusal bite force	0.98	0.67	0.79	0.63,1.04	0.9	0.18
Log total muscle mass vs log carnassial occlusal bite force	0.96	0.67	0.70	0.59,0.89	0.93	0.61
Log temporalis mass vs log carnassial occlusal bite force	0.93	0.67	0.71	0.60,0.89	0.93	0.51
Log masseter mass vs log carnassial occlusal bite force	0.98	0.67	0.67	0.55,0.86	0.92	1
Log pterygoid mass vs log carnassial occlusal bite force	0.96	0.67	0.76	0.61,0.96	0.93	0.20
Log total muscle mass vs log canine wide gape bite force	0.93	0.67	0.7	0.56,0.89	0.9	0.68

Log temporalis mass vs log canine wide gape bite force	0.91	0.67	0.71	0.59,0.89	0.9	0.59
Log masseter mass vs log canine wide gape bite force	0.98	0.67	0.67	0.52, 0.84	0.9	1
Log pterygoid mass vs log canine wide gape bite force	0.94	0.67	0.76	0.58,0.96	0.87	0.32
Log total muscle mass vs log carnassial wide gape bite force	0.85	0.67	0.68	0.57,0.79	0.88	0.68
Log temporalis mass vs log carnassial wide gape bite force	0.82	0.67	0.69	0.59,0.80	0.87	0.74
Log masseter mass vs log carnassial wide gape bite force	0.91	0.67	0.65	0.56,0.76	0.88	0.73
Log pterygoid mass vs log carnassial wide gape bite force	0.85	0.67	0.73	0.57,0.88	0.82	0.44
Log total muscle force vs log canine occlusal bite force	0.98	1	1.19	1.0, 1.49	0.94	0.07
Log temporalis force vs log canine occlusal bite force	0.98	1	1.22	1.05,1.56	0.92	0.07
Log masseter force vs log canine occlusal bite force	0.97	1	1.14	0.86,1.50	0.89	0.26
Log pterygoid force vs log canine occlusal bite force	0.91	1	1.09	0.80,1.41	0.88	0.46
Log total muscle force vs log carnassial occlusal bite force	0.99	1	1.13	0.98,1.36	0.96	0.09
Log temporalis force vs log carnassial occlusal bite force	0.98	1	1.16	1.04,1.40	0.96	0.05
Log masseter force vs log carnassial occlusal bite force	0.97	1	1.08	0.86, 1.38	0.9	0.48
Log pterygoid force vs log carnassial occlusal bite force	0.87	1	1.04	0.75,1.31	0.88	0.73
Log total muscle force vs log canine wide gape bite force	0.99	1	1.14	0.89,1.36	0.92	0.19
Log temporalis force vs log canine wide gape bite force	0.97	1	1.17	0.87,1.41	0.9	0.14
Log masseter force vs log canine wide gape bite force	0.95	1	1.08	0.79,1.36	0.89	0.50
Log pterygoid force vs log canine wide gape bite force	0.86	1	1.04	0.61,1.34	0.8	0.79
Log total muscle force vs log carnassial wide gape bite force	0.92	1	1.10	0.86,1.23	0.94	0.27
Log temporalis force vs log carnassial wide gape bite force	0.89	1	1.13	0.84,1.24	0.95	0.15
Log masseter force vs log carnassial wide gape bite force	0.88	1	1.05	0.80,1.28	0.90	0.65
Log pterygoid force vs log carnassial wide gape bite force	0.76	1	1	0.55,1.23	0.79	1
Log total dry skull muscle force vs log body mass	0.98	0.67	0.72	0.66, 0.77	0.98	0.15
Log dry skull temporalis force vs log body mass	0.99	0.67	0.76	0.69. 0.81	0.98	0.03
Log dry skull masseter force vs log body mass	0.96	0.67	0.67	0.59, 0.75	0.96	1

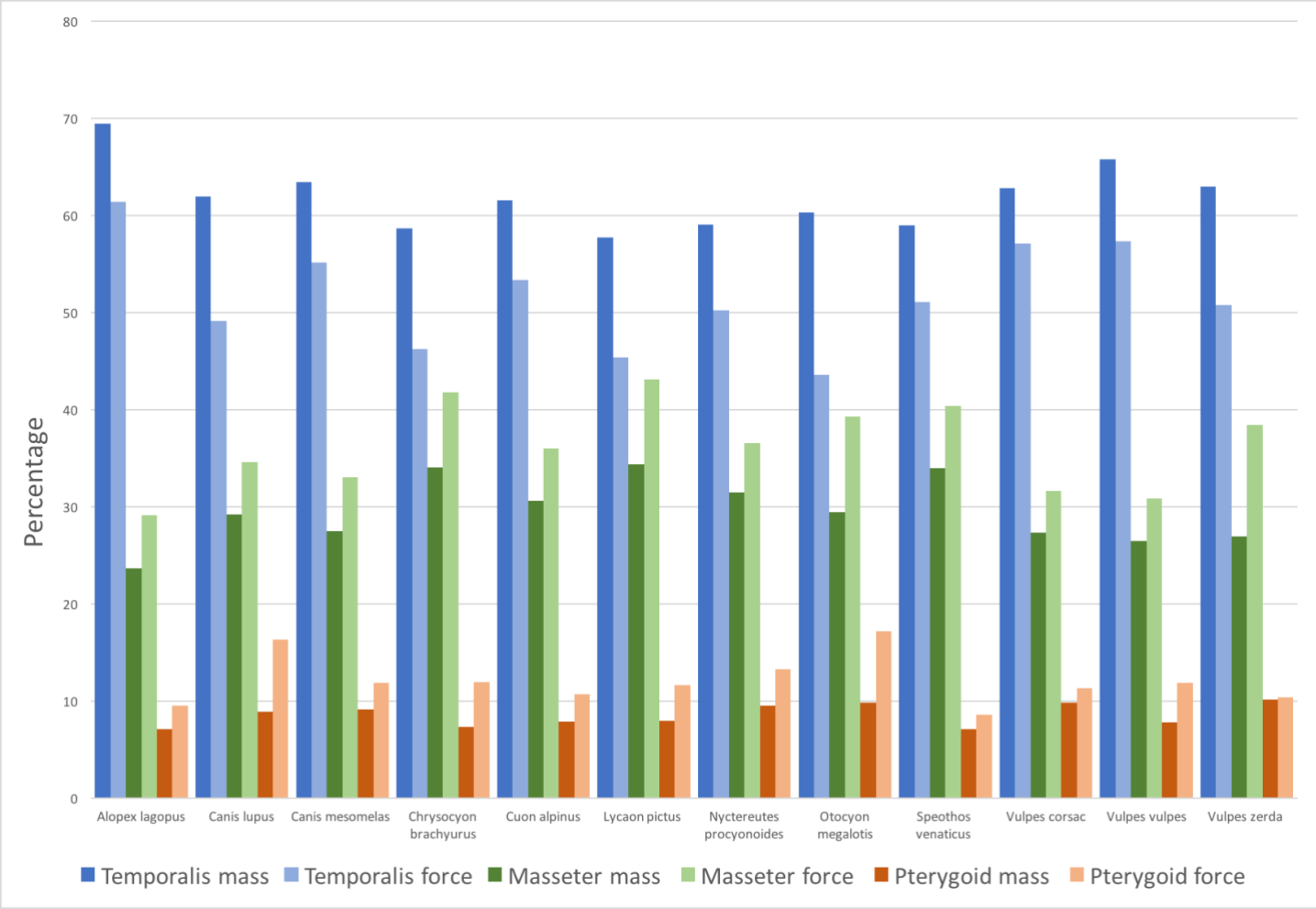

Figure 4.8 Percentage contributions of individual muscles toward total muscle mass and total muscle force in all species.

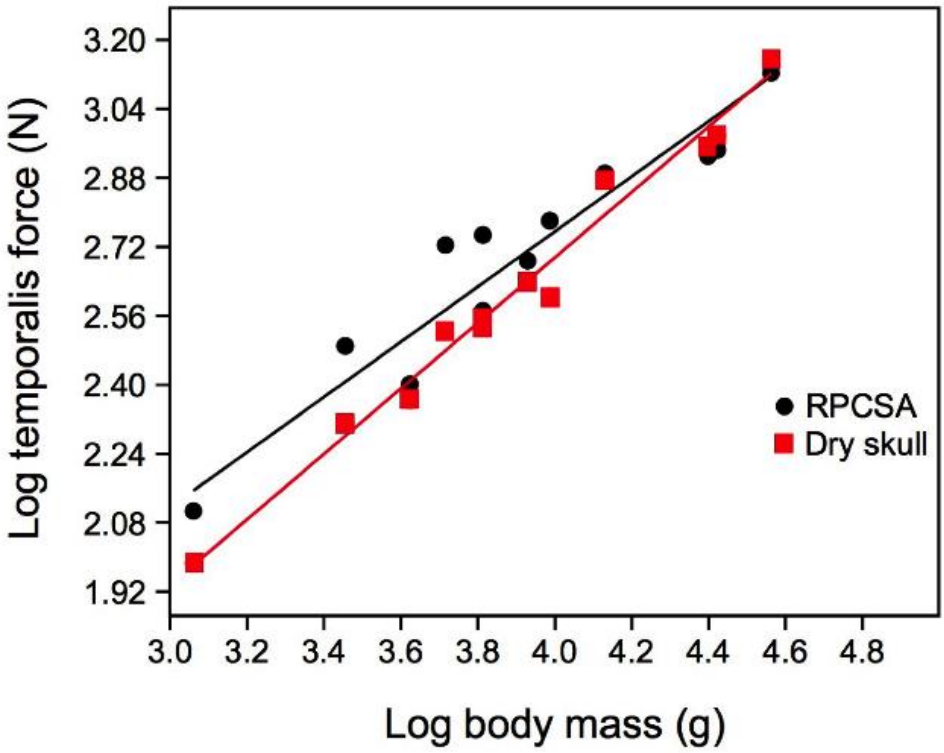

Figure 4.9 Comparison of temporalis force as predicted by reduced physiological cross-sectional area and dry skull methods.

4.3.3 Bite forces

Predicted bite forces from the FEA models in all four loading conditions (canine and carnassial bite, occlusion and wide gape) are reported in Table 4.5. Canine bites are weaker than carnassial bites and wide gape bites are weaker than those at occlusion. All bite force conditions revealed significant phylogenetic signal: canine occlusal bite (K = 1.04, P = 0.03), carnassial occlusal bite (K = 1.04, P = 0.03), canine wide gape (K = 1.58, P = 0.00), and carnassial wide bite (K = 1.40, P = 0.01).

Table 4.5 Predicted bite force and mechanical efficiency in all loading conditions.

Species	Canine bite				Carnassial bite			
	Occlusion		Wide gape		Occlusion		Wide gape	
	BF (N)	ME	BF (N)	ME	BF (N)	ME	BF (N)	ME
Alopex lagopus	158	0.18	124	0.14	261	0.30	201	0.23
Canis lupus	508	0.19	295	0.11	715	0.26	495	0.18
Canis mesomelas	234	0.21	165	0.15	319	0.29	234	0.21
Chrysocyon brachyurus	246	0.13	225	0.12	384	0.21	355	0.19
Cuon alpinus	297	0.22	220	0.16	434	0.31	342	0.25
Lycaon pictus	384	0.20	223	0.11	534	0.27	345	0.18
Nyctereutes procyonoides	131	0.19	63	0.09	186	0.26	99	0.14
Otocyon megalotis	124	0.21	82	0.14	159	0.28	108	0.19
Speothos venaticus	222	0.20	192	0.18	319	0.29	301	0.28
Vulpes corsac	76	0.14	54	0.10	123	0.23	93	0.17
Vulpes vulpes	160	0.19	107	0.13	248	0.29	172	0.20
Vulpes zerda	27	0.11	24	0.10	45	0.18	44	0.18

BF, bite force, ME, mechanical efficiency.

4.3.4 Scaling

Spearman's rank correlation showed a statistically significant association between all pairs of variables tested (Table 4.4). No distinct allometric trends were revealed in comparisons of muscle force production capability against body mass, both the individual jaw adductor muscles and the muscle mass as a whole. In all cases the confidence intervals were distributed around the expected slope for isometry (0.67) and *t*-tests generated *P*-values considerably greater than 0.05. A similar pattern was revealed for bite force, though the intervals and slope for all bite forces were skewed above 0.67, which may be indicative of weak positive allometry (slope values ranged from 0.72 to 0.78). Comparisons of muscle force against muscle mass were also indistinguishable from isometry. However, the upper

limits of the confidence intervals were weighted towards negative allometry in the case of temporalis and masseter, and towards positive allometry in the case of the pterygoids. When canine and carnassial occlusal bite forces were regressed against muscle forces I found that although only temporalis force vs carnassial occlusal bite had a significant *P*-value, all of the confidence intervals and slope values for total muscle force and temporalis force were skewed above the expected slope value for isometry (1) with values ranging from 1.13 to 1.22. This may be indicative of weak positive allometry. Slopes from other comparisons also imply allometry, but were not sufficiently resolved to prove conclusive (Table 4.4). *t*-tests of residual values between the dietary groups revealed no distinctions between any dietary group. The phylogenetically adjusted slopes (PGLS), showed little difference from the raw data slopes (see Supplementary Material Table 1), with no PGLS regression values falling outside of the raw data confidence intervals.

4.3.5 Mechanical efficiency

Mechanical efficiency in all four conditions is reported in Table 4.5. Calculations found that in all species biting is most efficient toward the caudal end of the dental arcade, that is, nearer to the TMJ, and is less efficient at wide gapes. Therefore, the most efficient bite is the carnassial bite at occlusion with an average efficiency of 0.27 and the least efficient bite is the wide gape canine bite, with an average efficiency of 0.13. Kruskal-Wallis tests revealed no statistically significant differences between trophic groups in mechanical efficiency at either of the bite points or gape angles.

4.3.6. Finite element strain energy density models.

Scatter plots of the values from the seven sample points at all four loading conditions are shown in Figure 4.10. It was notable that in all species the SED values were much higher in both of the canine bite models than either of the carnassial bite models. For example, in the largest specimen, *Canis lupus,* the greatest SED values were 3108 mJ at canine wide bite and 282 mJ at carnassial closed bite, and in the smallest specimen, *Vulpes zerda,* the highest SED was 637 mJ in the canine wide bite and 86 mJ in carnassial wide bite. During canine biting, the area of highest midline stress was at sample point 2, the level of the caudal rostrum. There was more variation in which sample site exhibited the highest SED value at carnassial bite. In most cases it was sample site 5, the bregma, but in some species, it was more rostral, at sampling sites 2, 3 or 4 (Figures 4.10C and 4.10D). No midline sample site value in any of the four bite conditions exhibited absolute SED values above 4500 mJ. To detect any differences between the SED values between the different dietary niches I conducted Kruskal-Wallis tests at sample site 2, the area often exhibiting the highest levels of SED. Kruskal-Wallis tests revealed no statistically significant differences between trophic groups in any loading condition. When scaled to be the equivalent volume of *Canis lupus* several of the smaller species had canine bite midline SE values above 10,000 mJ, with *Otocyon megalotis* exceeding 20,000 mJ and *Vulpes zerda* exceeding 30,000mJ. To detect any differences between the scaled SED values between the different dietary niches I conducted Kruskal-Wallis tests at sample site 2. The scaled SED value Kruskal-Wallis test results showed that there were differences between the dietary groups in all of the loading conditions:

Canine occlusal biting ($H = 6.785$, $p = 0.03$), post hoc Dunn's analysis revealed that the generalists were significantly different from the hypercarnivores ($p = 0.01$).

Canine wide biting ($H = 8.215$, $p = 0.02$), post hoc Dunn's analysis revealed that the generalists were significantly different from the hypercarnivores ($p = 0.006$) and that the small prey hunters were also significantly different from the hypercarnivores ($p = 0.03$).

Carnassial occlusal biting (H = 6.368, p = 0.04), post hoc Dunn's analysis revealed that the generalists were significantly different from both the small prey specialists (p= 0.004) and hypercarnivores (p= 0,002).

Carnassial wide biting (H = 6.676, p = 0.004), post hoc Dunn's analysis revealed that the generalists were significantly different from both the small prey specialists (p = 0.02) and the hypercarnivores (p = 0.01).

In all cases the scaled SED values of the generalists were greater than those of the other groups. For illustration, raw and scaled values from sample site 2, are reported in Table 4.6 and illustrated in Figure 4.11.

Colour maps were generated to allow for wider visual analysis of SED distribution in the skulls. The four loading conditions are shown in *Canis lupus*, for illustration (Figure 4.12), but similar patterns were noted in all species. In all models the zygomatic arch experiences high SED, particularly along the ventral aspect. In canine biting, the caudal rostrum both dorsally (made up of the caudal parts of nasal and maxilla bones) and ventrally (made up of the caudal parts of the palatine and maxilla bones) also exhibits high SED. This is more marked at wide gape when the areas of high SED on the dorsal rostrum are contiguous with the areas of high SED on the ventral rostrum and zygomatic arches. The ventral orbital region, made up of the zygomatic, lacrimal, maxilla and palatine bones, exhibits high SED at both canine and carnassial wide gape bites. SED in the cranial region of the skull alters from having a dorsal and rostral focus across the frontal bones at occlusal bite, to having a ventral and lateral focus on the parietal and temporal region at wide gape.

Table 4.6 Raw and scaled SED values from sample site 2.

species	Sample site 2															
	Canine occlusion mJ				Canine wide mJ				Carnassial occlusion mJ				Carnassial wide mJ			
	original	Scaled to *C. lupus*	*C.lupus*	% of *C. lupus* SED	original	Scaled to *C. lupus*	*C.lupus*	% of *C. lupus* SED	original	Scaled to *C.lupus*	*C.lupus*	% of *C. lupus* SED	original	Scaled to *C.lupus*	*C.lupus*	% of *C. lupus* SED
Alopex lagopus	704	4448	2763	161	656	4145	3108	133	23	145	92	158	18	114	282	40
Canis mesomelas	4391	18414	2763	666	2976	12480	3108	402	158	663	92	720	137	575	282	204
Chrysocyon brachyurus	1323	2693	2763	97	2141	4357	3108	140	104	212	92	230	338	790	282	280
Cuon alpinus	1129	3467	2763	125	1340	4115	3108	132	114	350	92	380	47	144	282	51
Lycaon pictus	1130	1887	2763	68	1396	2331	3108	75	73	122	92	132	279	466	282	165
Nyctereutes procyonoides	907	7407	2763	268	727	5937	3108	191	81	661	92	719	86	702	282	249
Otocyon megalotis	1647	18645	2763	675	1894	21442	3108	690	128	1449	92	1575	313	3543	282	1257
Speothos venaticus	545	2326	2763	84	808	3449	3108	111	12	51	92	56	20	85	282	30
Vulpes corsac	778	10192	2763	369	780	10218	3108	329	20	262	92	285	99	1297	282	460
Vulpes vulpes	1299	8602	2763	311	1226	8118	3108	261	17	113	92	122	75	497	282	176
Vulpes zerda	464	23559	2763	853	637	32343	3108	1041	36	1828	92	1987	86	4367	282	1548

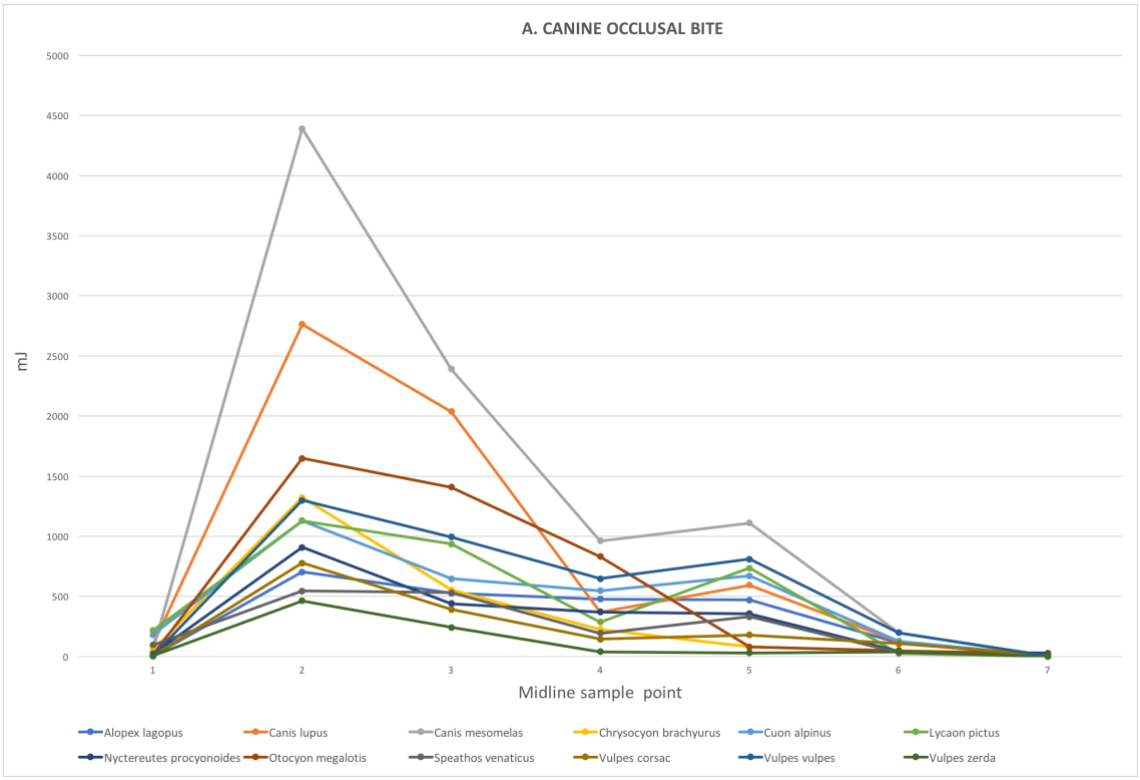

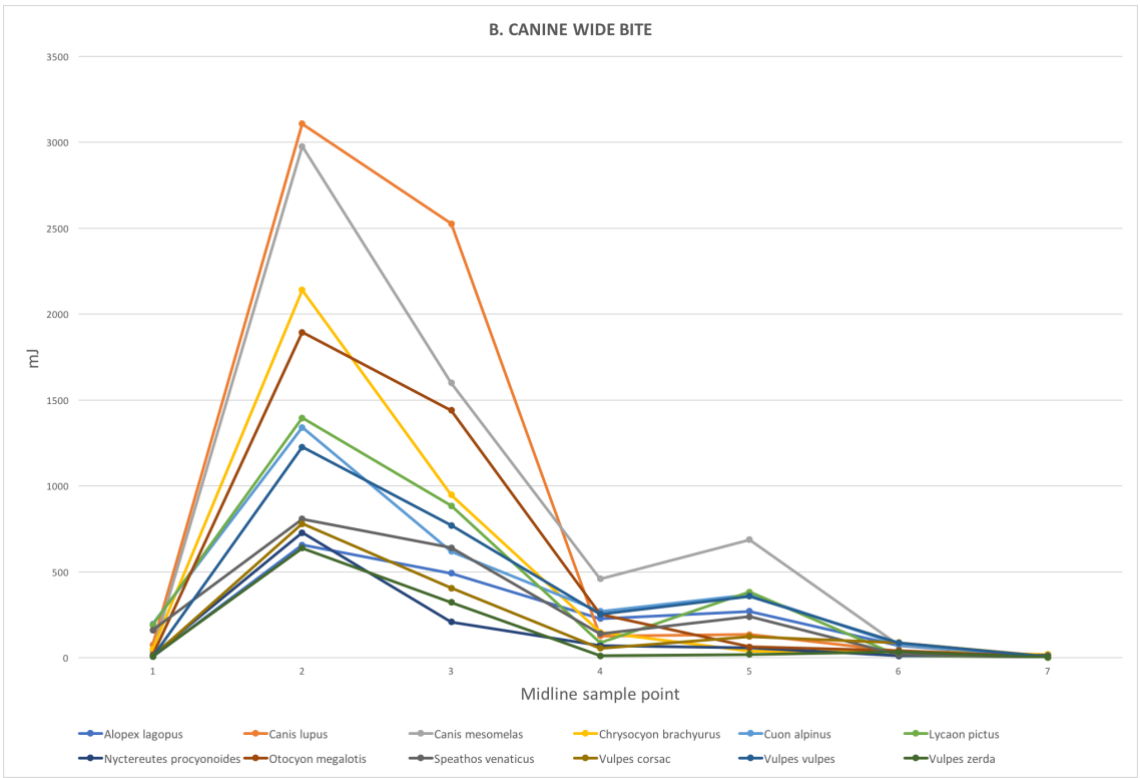

Figure 4.10 A and B Canine bite, mean SED nodal values from seven midline sampling sites, all species.

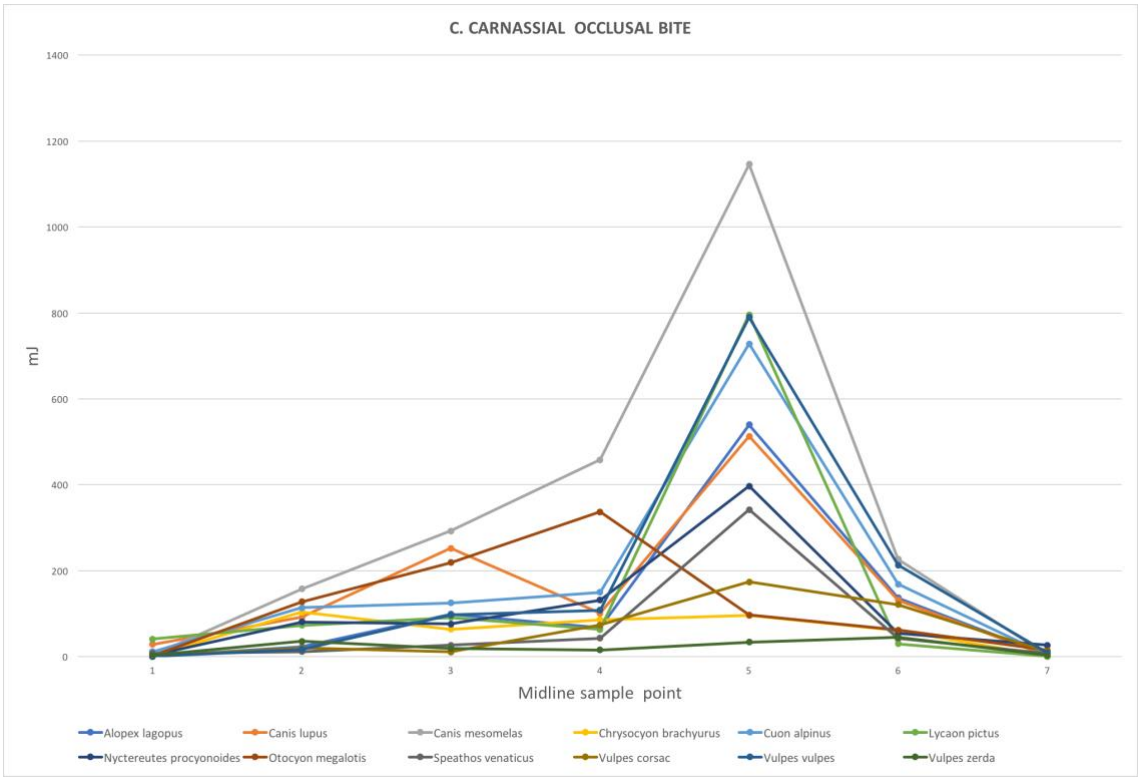

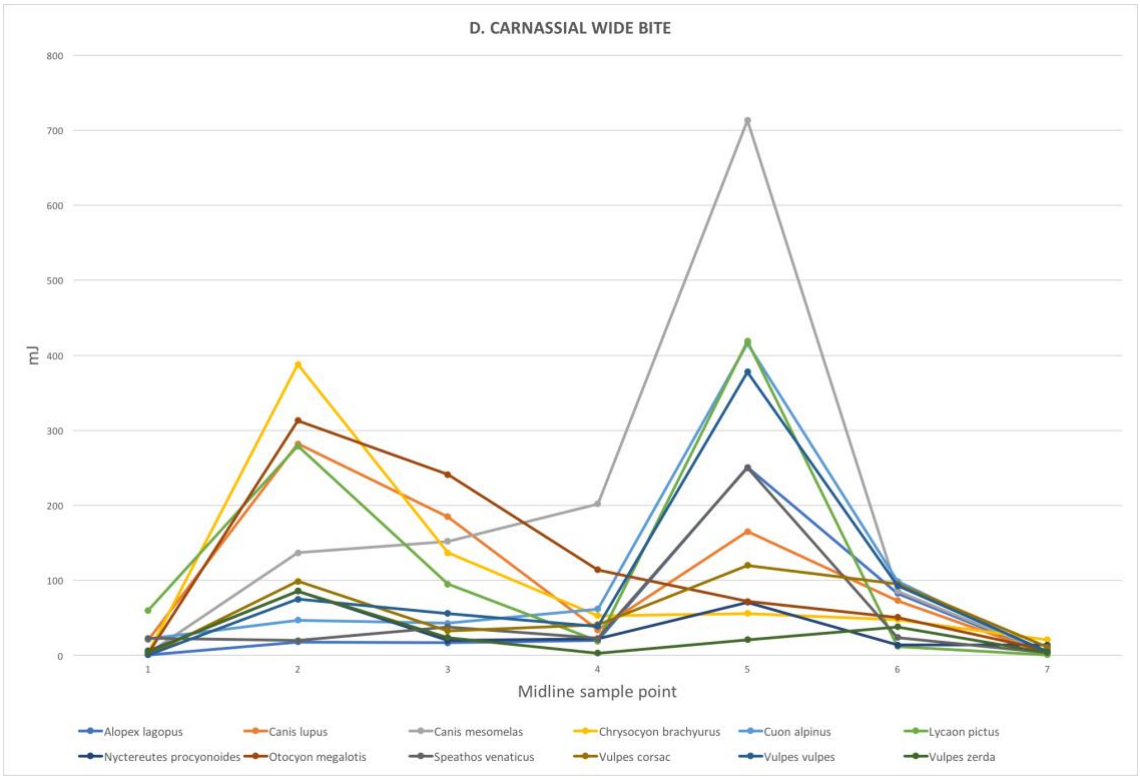

Figure 4.10 C and D Carnassial bite, mean SED nodal values from seven midline sampling sites, all species.

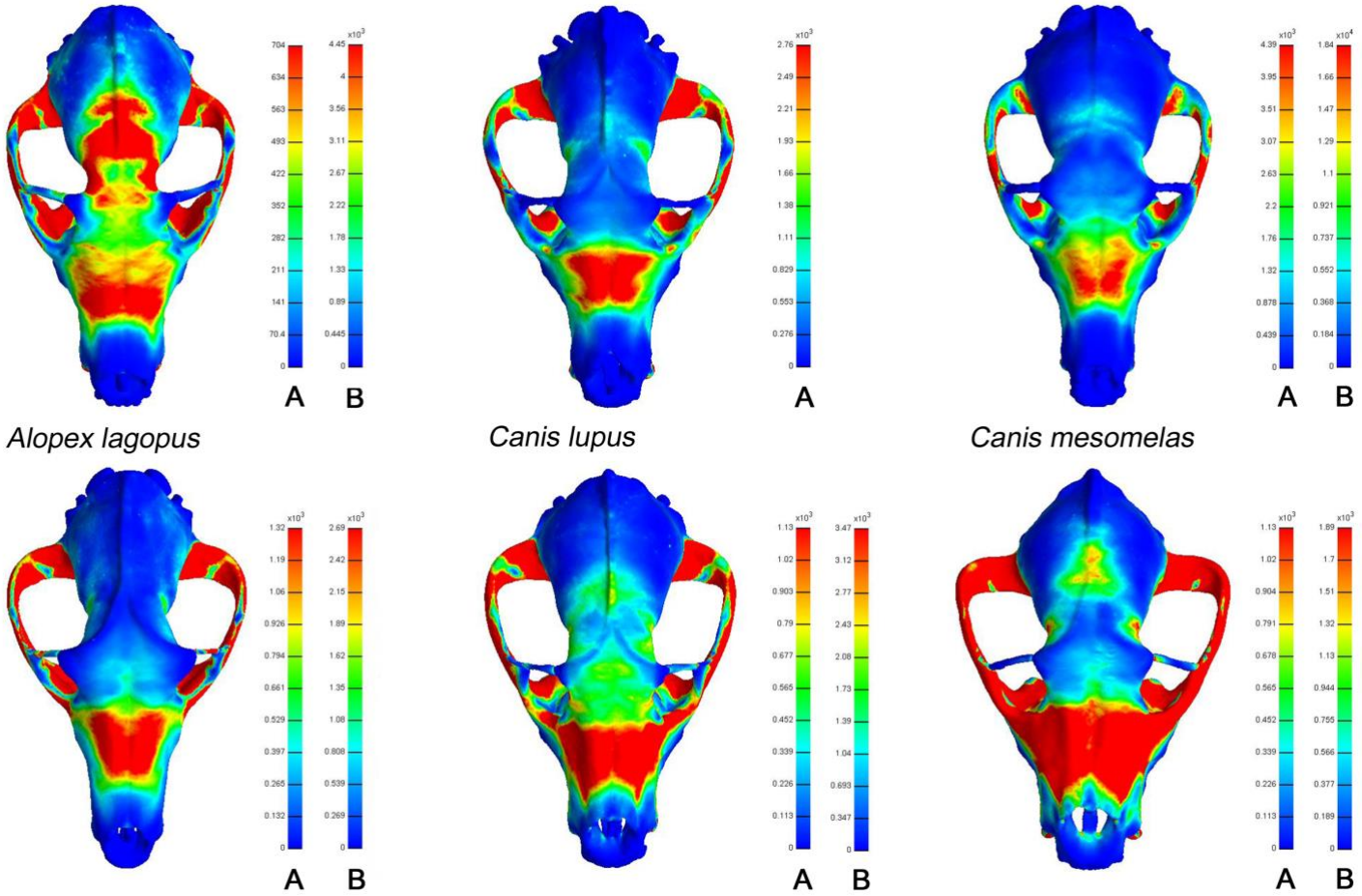

Figure 4.11 SED values in all species at canine closed bite, dorsal aspect. The top value of scale A represents the highest recorded value at sample site two. Scale B indicates the highest value at sample site two if the species were scaled to be the same volume as *Canis lupus.*

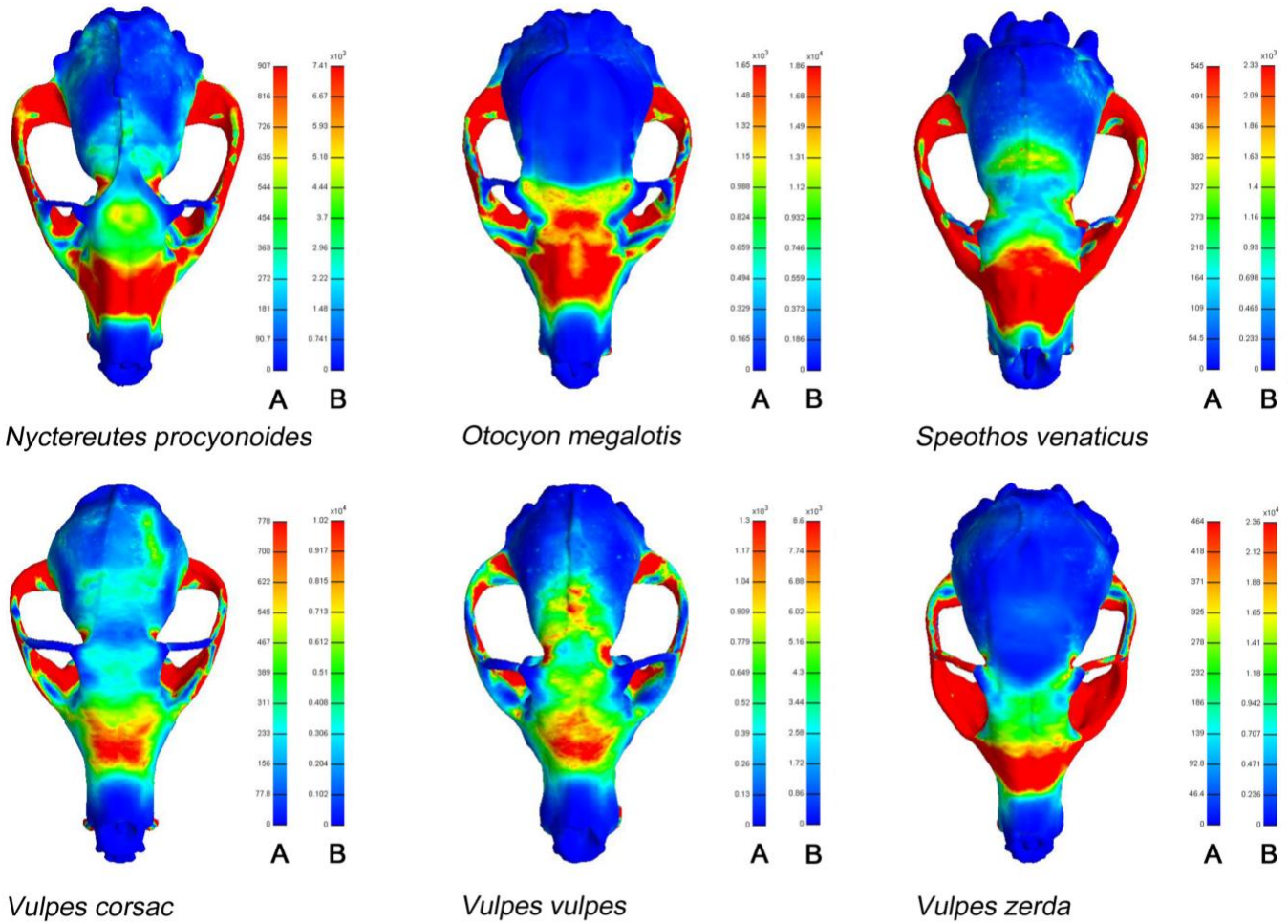

Figure 4.11 SED values in all species at canine closed bite, dorsal aspect. The top value of scale A represents the highest recorded value at sample site two. Scale B indicates the highest value at sample site two if the species were scaled to be the same volume as *Canis lupus.*

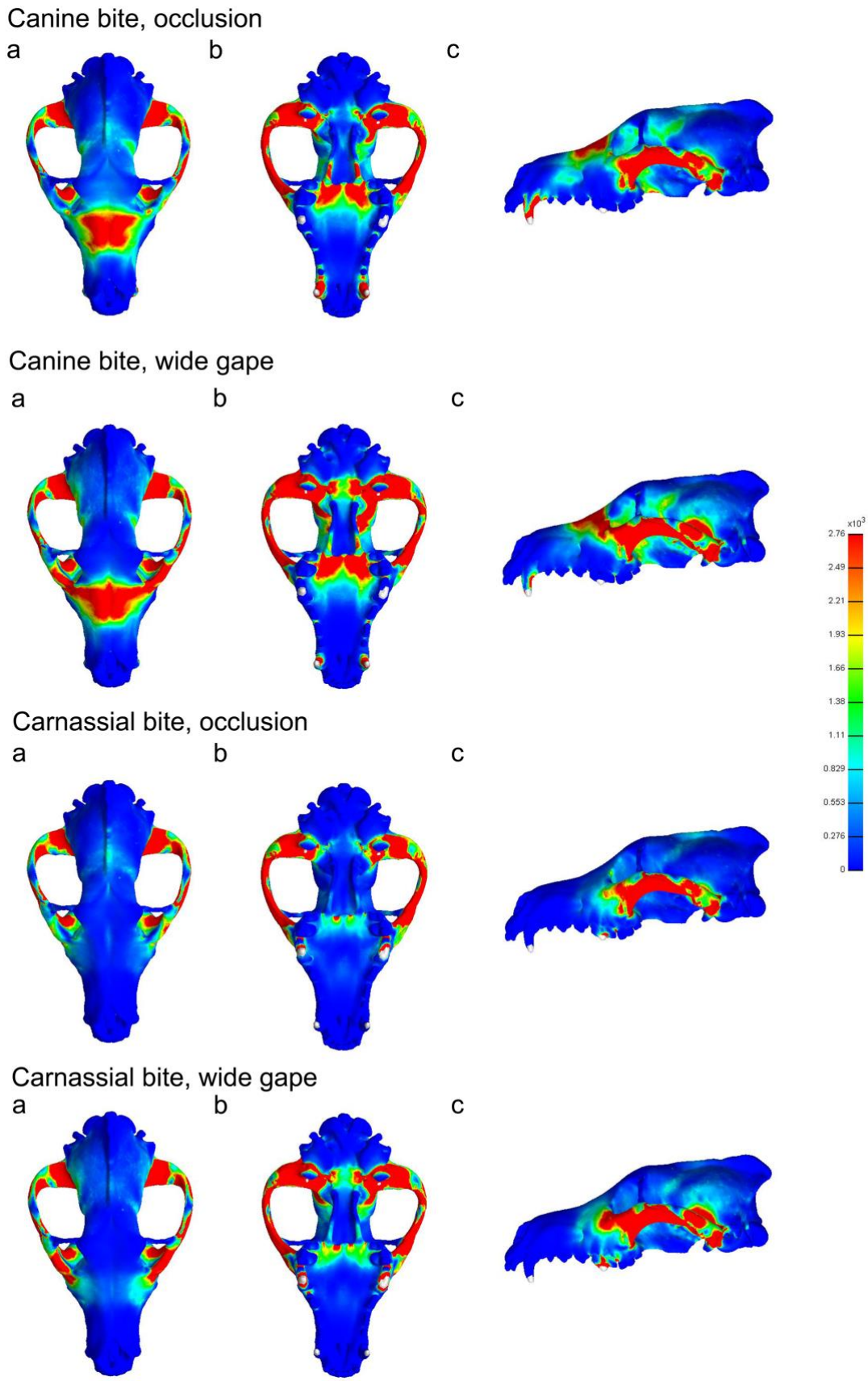

Figure 4.12 SED colour maps of dorsal (A), ventral (B) and lateral (C) aspects of the FE models of *Canis lupus*, in all four loading conditions. Scaled to the maximum value of sample site two.

4.3.7. Mechanical advantage

Values for MA are shown in Table 4.7. Both temporalis and masseter muscles showed dietary group differences in their MA at different bite points. MA of the temporalis at canine bite was between 0.20 and 0.30. All of the hypercarnivore species were grouped at the top end of the range, the small prey specialists in the middle, and the generalists at the low end. Kruskal-Wallis test results (H = 9.395, p = 0.008) showed that there were differences between the dietary groups, and the post hoc Dunn's analysis revealed that the generalists were significantly different from the hypercarnivores. MA of the masseter at canine bite was between 0.143 and 0.406. The hypercarnivores grouped together near the top end of the range and the small prey specialists grouped together near the bottom end of the range. However, the generalists were split, with two species, *Otocyon megalotis* and *Nyctereutes procyonoides*, having the highest MA of the masseter at canine bite, and one species, *Vulpes zerda*, having the lowest. Kruskal-Wallis test results (H = 4.145, p = 0.13) showed that there were no statistically significant differences between the groups. MA of the temporalis at carnassial bite was between 0.344 and 0.596 with all of the hypercarnivore species at the top end of the range, the small prey specialists in the middle, and the generalists at the low end. Kruskal-Wallis results (H = 8.862, p = 0.01) showed that there were statistically significant differences between the dietary groups, and the post hoc Dunn's analysis revealed that both the small prey specialists and generalists were significantly different from the hypercarnivores. MA of the masseter at carnassial bite was between 0.253 and 0.680 with all of the hypercarnivore species grouped toward the top end of the range, the small prey specialists grouped together near the bottom of the range. Again, the generalist group showed a wide range of MA, with *Otocyon megalotis* and *Nyctereutes procyonoides* having the highest values of all species, and *Vulpes corsac* one of the lowest. Kruskal-Wallis test results (H = 4.81, p = 0.08) showed that there were no statistically significant differences between the groups. The high MA values for the masseter exhibited by *Otocyon megalotis*

and *Nyctereutes procyonoides* were due to the large in-lever values, which in turn were due to the large pre-angular processes. The phylogenetically adjusted ANOVAs showed one difference from those using the raw data, that the MA of temporalis at carnassial bite was not significantly different between the small prey specialists and hypercarnivores.

Table 4.7 Mechanical advantage in all loading conditions

DIETARY GROUP	SPECIES	MA temporalis canine bite	MA masseter canine bite	MA temporalis carnassial bite	MA masseter carnassial bite
HYPERCARNIVORE	*Canis lupus signtaus*	0.26	0.22	0.52	0.45
	Cuon alpinus	0.28	0.21	0.55	0.40
	Lycaon pictus	0.26	0.23	0.50	0.44
	Speothos venaticus	0.30	0.24	0.60	0.47
SMALL PREY SPECIALIST	*Alopex lagopus*	0.24	0.15	0.39	0.25
	Canis mesomelas	0.24	0.19	0.46	0.37
	Chrysocyon brachyurus	0.21	0.18	0.41	0.35
	Vulpes corsac	0.23	0.15	0.49	0.31
	Vulpes vulpes	0.25	0.16	0.49	0.31
GENERALIST	*Nyctereutes procyonoides*	0.21	0.41	0.36	0.68
	Otocyon megalotis	0.20	0.37	0.34	0.62
	Vulpes zerda	0.20	0.14	0.41	0.29

4.3.8. Temporalis muscle angles relative to the occlusal plane

Results are reported in Table 4.8 and illustrated in Figure 4.13. The superficial temporalis had a mean line of action of 142.6° relative to the occlusal plane, and there were no significant differences between the dietary groups, Kruskal-Wallis H = 1.93, p = 0.38. The deep temporalis had a mean line of action of 119.9° relative to the occlusal plane. All hypercarnivore species values were below the mean and all generalist values were greater than the mean, indicating that the hypercarnivore species have more vertically aligned deep temporalis muscle fascicles, and the generalists have more horizontally aligned deep temporalis muscle fascicles. The Kruskal-Wallis results showed significant differences between the groups H = 9.118, p = 0.001) and the Dunn's post hoc test revealed that that the hypercarnivore angles were significantly different to the generalists. The suprazygomatic

temporalis had a mean line of action of 142.3°. All the generalist species values were above the mean and Kruskal-Wallis results showed significant differences between the groups (H = 6.779 p = .003). The Dunn's post hoc test reported that the generalists were significantly different to the hypercarnivores. Both the deep and suprazygomatic angles had significant phylogenetic signal (deep: K = 1.29, P = 0.0, suprazygomatic: K = 1.07, P = 0.02). The phylogenetically adjusted ANOVAs revealed no differences from those using the raw data.

Table 4.8 Temporalis lines of action

	Superficial temporalis	Deep temporalis	Suprazygomatic temporalis
Alopex lagopus	145.69	120.90	138.90
Canis lupus signtaus	141.50	109.50	138.49
Canis mesomelas	149.53	118.19	135.74
Chrysocyon brachyurus	136.44	123.63	148.50
Cuon alpinus	146.68	115.65	135.49
Lycaon pictus	138.51	117.91	142.47
Nyctereutes procyonoides	158.17	133.63	154.28
Otocyon megalotis	146.87	130.61	149.66
Speothos venaticus	119.11	107.42	132.87
Vulpes corsac	149.43	117.97	140.47
Vulpes vulpes	142.07	120.98	142.52
Vulpes zerda	137.66	122.45	148.10

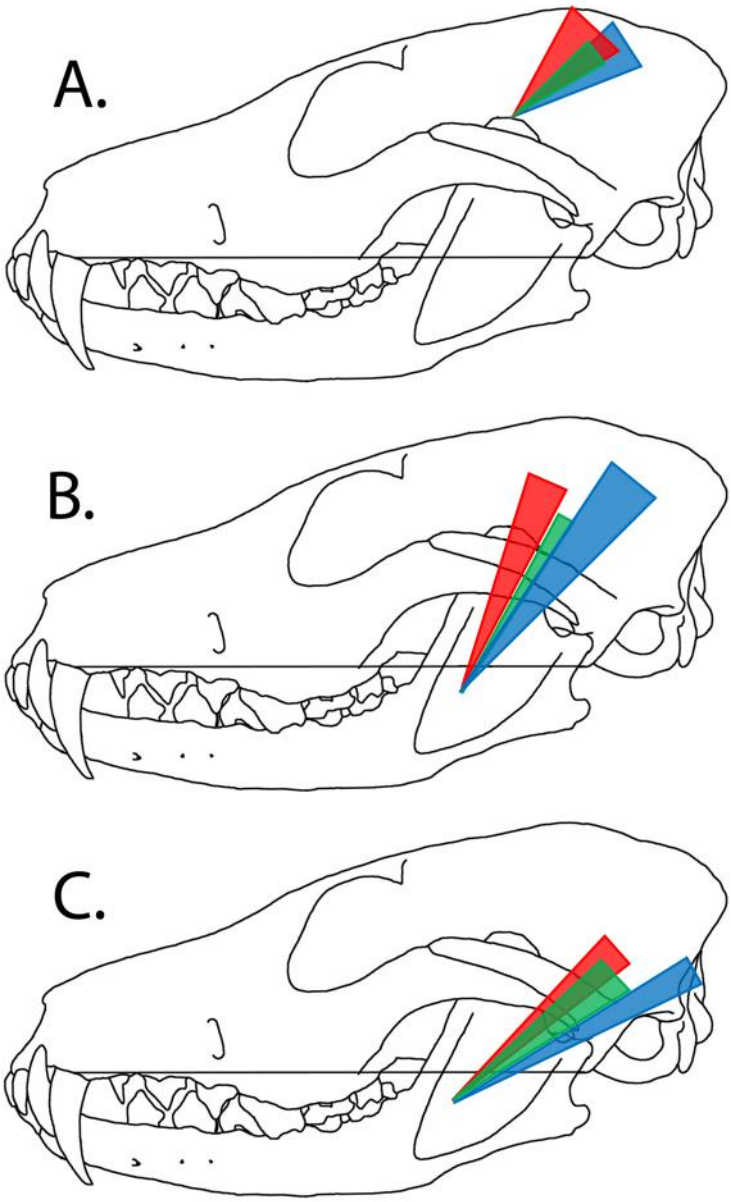

Figure 4.13 Lines of action for the temporalis muscle. The black horizontal line indicates the occlusal plane. For illustrative purposes, all species lines of action are shown on one skull, *Vulpes vulpes*. (A) superficial temporalis, (B) deep temporalis, (C) suprazygomatic temporalis. Hypercarnivore species lines of action are red, small prey species are green and generalist species are blue.

4.4. Discussion

Canid jaw adductor muscles and their relationships to the bony morphology of the head were explored to reveal differences in masticatory function. Two hypotheses were considered:

Hypothesis 1. There are significant relative, as well as absolute, differences of muscle force and bite force that reflect canid dietary niches.

This hypothesis was not strongly supported. Species tend to follow the same generalised size scaling trends, which appear to be predominantly isometric, though weak patterns of allometry may be hidden within the sample noise. A possible exception to isometry was temporalis muscle force vs occlusal bite forces. Regression confidence intervals indicate that as absolute temporalis muscle force increased, occlusal carnassial and canine bite forces increased at a greater rate. This suggests that although temporalis force production is relatively lower in larger species due to the muscle architecture, as evidenced by the absolutely and relatively longer muscle fascicles, the geometry of the skull and mandible compensate for this. This results in isometric or positively scaling bite forces. This finding was similar to that of Wroe et al (Wroe 2004), who used a bite force quotient calculation to evaluate scaling differences between species. In their work they used predicted bite forces from dry skull models which were then regressed against body mass, and the residuals used to normalise for differences in body mass. Although their work concluded that the hypercarnivorous canid species had a higher bite force quotient than the small prey hunting species, their dataset did not include *Speothos venaticus*, the small hypercarnivore, or Chrysocyon brachyurus, the small prey hunter with a large body mass. and so they may simply be reporting on body mass correlation with bite force. In my work in this chapter the *t*-tests of the residuals from the regression slopes showed no statistically significant dietary specialism trends.

As expected, muscle architecture has a clear influence on muscle force production and I found that individual muscle force contributions to overall muscle force do not reflect muscle mass contribution. The temporalis 'underperforms', that is, it contributes a mean 62% of mass but only a mean 52% of force production, whereas the masseter and pterygoid both 'over perform', i.e. they both contribute a greater percentage of force production than their percentage contribution toward the overall muscle mass. This disparity is attributable to the longer fascicle lengths of the larger temporalis affecting force production. In the RPCSA calculation, muscle mass is divided by fascicle length, meaning that the RPCSA value is inversely proportional to the fascicle length, and muscles with absolutely longer fascicles are proportionally weaker than those with short fascicles. Some previous FE studies (Slater *et al*. 2009; Tseng and Wang, 2010) have applied muscle forces to skulls in proportion to their mass which may lead to the incorrect weighting of muscle force application. The temporalis does, however, still contribute the greatest share of both muscle mass and force. Despite the force production relative inefficiency of the temporalis, the more caudal and dorsal siting of both its origin and insertion, when compared to those of the masseter, mean that it has less of a limiting effect on the gape of the jaw, and consequently the longer fascicles are advantageous in species requiring a wide gape. The influence of taking the muscle architecture into account can also be seen when comparing the interspecific muscle forces that were derived from the RPCSA method, to those I calculated using the dry skull method. As the dry skull method calculates cross-sectional area values only, it simply scales up force in direct proportion to area. As it does not consider architectural differences it cannot discriminate the functional differences between large and small muscles and also, between large and small species. I found that within our dataset the dry skull method calculated higher muscle forces in large species, and lower muscle forces in small species, when compared to those calculated by the RPCSA method (Figure 4.9). This led to the dry skull method indicating that temporalis force scales with positive allometry in regression tests,

whilst the RPCSA method indicates it scales with no marked allometric trend. Loading the FEA models with higher muscle input forces would result in higher output forces, i.e. increased bite forces. Absolutely higher temporalis forces for large species were predicted by Christiansen and Adolfssen (Christiansen and Adolfssen, 2005) using the dry skull method, than those predicted using the RPCSA method. They, and Damasceno *et al*., using the dry skull method, predicted higher bite forces in most of the larger species (Christiansen and Adolfssen, 2005; Damasceno *et al*., 2013). Whilst the above comparison remains speculative, due to small data sets and lack of comparative information, it illustrates that the detail of the architecture of the muscles can have a notable impact on predicting muscle forces. However, as the *t*-tests between the two differently derived muscle force values showed no statistically significant differences between the two groups, the differences in absolute values are small, and dry skull derived values are a good approximation of RPCSA values where dissection derived data is unobtainable. It should be noted that as the differences become more marked at either end of the body mass spectrum within this data set (dry skull muscle force calculations slightly underestimated forces in all species below 14kg and slightly overestimated forces in all species above 25 kg), this may not hold true for samples outside of this body mass range. Phylogenetic signal, that is, the statistical non-independence of trait values due to species relatedness (Felsenstein, 1985; Harvey & Pagel, 1991; Revell et al. 2008), was present amongst several of the datasets including bite force. This indicates that the mechanisms of bite force may be phylogenetically conserved. Canids may therefore be constrained in adaptability and have remained as functional generalists, never exploring the highly specialized niches that, for instance, the felids have exploited. Divergence of canids into hypercarnivory may rely more on behavioral rather than functional adaptations, as the ability to tackle large prey relies on working in packs, rather than radically changing morphology to increase relative bite force.

Hypothesis 2. The efficacy of muscle force production and its conversion into bite force, is indicative of different dietary niches.

There were demonstrable differences in efficiency between all four bite conditions. Carnassial bite at occlusion produced the highest bite force and is the most mechanically efficient. The greatest midline SED values were found at both closed and wide canine gape, revealing that canine biting is the most biomechanically testing and the least energetically efficient loading condition. Areas under greatest burden during canine biting were identified as the zygomatic arches and caudal rostrum, both dorsally and ventrally. It is difficult to know how functionally important this is, as all species can clearly accommodate the energy expenditure required, and Kruskal-Wallis tests revealed no statistically significant differences between the SED values between the dietary groups. However, when small species were scaled to the size of the largest canid species, their skull shapes exhibited much higher values of SED than were seen in any unscaled models, demonstrating up to a fifty-fold increase in their original SED values (Table 4.6), which may indicate that they would be structurally untenable if 'scaled up'. As SED is proportional to stress this may lead to ductile failure as well as being an energetic constraint. Kruskal-Wallis tests of the scaled SED values revealed significantly higher values for the generalists than the hypercarnivores at both canine bite conditions, and that the generalists had significantly higher values than both the small specialists and hypercarnivores at both carnassial bite conditions. These findings imply a limitation on the size of particular features, which suggests some evidence of specialist function of shape. The work in Chapter Three also highlighted the scaling component to shape adaptation. These findings suggest that the ability to withstand generated forces, and the ability to house isometrically scaling muscles on negatively scaling crania, are both factors in adaptive shape changes seen in different species of canid.

Mechanical advantage calculations, unlike the mechanical efficiency calculations, were able to distinguish between the dietary specialisms. This may be attributable to the MA methods

more accurately describing the morphology of the different skulls rather than a simple force input/force output calculation. MA calculations revealed that the temporalis had greater MA in the hypercarnivores than the other two trophic groups, indicating that the mandibular morphology of the jaw in these species is advantageous to force transmission. The increased MA may go some way to offsetting the disadvantage of longer temporalis fascicles in the large species. *Speothos venaticus*, the only small hypercarnivore, exhibits a mechanically advantageous skull shape combined with a small body mass and in turn has the greatest positive residuals in all body mass vs bite force regressions. The masseter MA did not have any trophic group differentiation, although the specific morphology of the two species with a pronounced preangular process (*Otocyon* and *Nyctereutes*), had a very marked influence on MA for this muscle in these species. Again, this did not result in any clear advantage of bite force, but it may be used to offset the disadvantage of having an extra-long tooth row, in *Otocyon megalotis* at least. It was also noticeable that although these two species had the highest MA values for the masseter, they had amongst the lowest for the temporalis, so perhaps the masseter compensates and provides a higher proportion of muscle force toward bite force in these species. This muscle arrangement may also align with the more pronounced grinding function associated with the caudal teeth in these species. Possible future studies could consider running models with muscles sequentially removed, following Cox *et al*., (Cox *et al*., 2013; Cox, 2017) to establish how individual muscles contribute to bite force outputs.

The line of action of temporalis revealed trophic group differentiation in two of the three muscle subdivisions. As well as potentially increasing bite force this may also have other functional outcomes. Sophisticated dynamic modelling, using multibody dynamic analyses for example, has not yet been explored in canids, but theoretically the species with horizontally aligned temporalis fascicles, the small prey hunters and generalists, should be able to pull the coronoid process of the jaw caudally, which aids quick snapping shut of the

mandible. In contrast, species with more vertically aligned fascicles, the hypercarnivores, may have a slower but more sustained bite. These contrasting dynamic strategies are reflected in their observed hunting behaviours: the pack hunting hypercarnivores kill by many sustained bites, whereas species taking small prey utilise their fast closing jaws for relatively short periods of time. Future work could consider histological analysis of muscle fascicles from the three trophic groups to determine if their fibres contain a similar distribution of muscle fibre types.

This work demonstrates that inclusion of muscle architectural details, however simplified, has an effect of muscle force calculation, and that the siting of muscles on the skull may also influence bite speed. The mechanical responses of the skull were assessed using analysis of the FE models. In contrast to previous interspecific canid studies (Christiansen and Adolfssen, 2005; Wroe *et al*., 2005; Christiansen and Wroe, 2007; Slater *et al*., 2009) I created the models using empirically derived specimen-specific muscle forces. The skulls were modelled with six different biological materials each with distinct material properties. Although inevitably, some differentiation of materials within the models differed from the true condition, for example, the teeth were modelled as one material, and the trabecular bone within the diploe was not included, the models represent the most complex canid FE models reported to date. To date no work has been done in carnivoran species exploring how the inclusion of the different dental materials may influence performance, but work in rodents (Cox *et al*, 2011) suggests that changing the material properties of the teeth appears to have little effect on skull deformation. Inclusion of trabecular bone of the diploe may decrease the overall stiffness in the dorsal aspect of the models, and work on human crania suggest this may reduce the peak forces experienced at sites containing diploe (Andersson, 2016). Such refinements could improve the accuracy of future models but a sensitivity test with and without their inclusion should first establish the impact in overall model performance, as their inclusion requires manual segmentation which is very time consuming. The improved

accuracy of the loading conditions, in addition to validating our models against *ex vivo* laboratory data, allowed me to use a modelling method that considers both size and shape differences between species. The FE models indicated the highest SED at canine biting, particularly in the caudal rostrum. Given that canine biting appears to be the least efficient and most biomechanically demanding condition, it may represent the limiting factor on skull performance. As canine biting chiefly occurs during the capture, restraint and killing of prey, it is fundamental to predatory success, and limitations on canine bite performance must be an important factor in determining trophic niche.

I established that bite forces do not scale with a marked allometric trend, but that individual species have morphological compensatory techniques to achieve similar relative outputs. The link between mechanical performance and whole organism performance is poorly understood (Dumont *et al*. 2011) and by considering only two functional elements of bite performance, the skull and masticatory muscles, other potentially important factors were ignored. These include the role of the neck muscles, the effect of supporting the mass of the skull and mandible, anchorage of the tooth roots in the alveoli, and the uniting role of other soft tissue structures. Soft-tissue structures, such as tendon, connective tissue and muscle fascia may facilitate integration of separate elements during biting. During the dissection work I noted that the muscle fascia covering temporalis was particularly thick and was contiguous with the fascia and periosteum covering the zygomatic arch, and then ran down onto the masseter muscle, in effect unifying all of these functioning parts. I also noted that some temporalis and masseter muscle fascicles appeared to arise from their covering fascia, although this would need to be confirmed using histological techniques. Curtis *et al.* (Curtis *et al*., 2011) have explored the role of the fascia in macaques during biting, and concluded, using FE analysis, that the temporal facia has an impact on biomechanical function by opposing that pull of the masseter on the zygomatic arches, greatly reducing localised strains. If future FE work on canids could include data on these poorly reported structures,

this may resolve some of the disparity between the FE and *ex vivo* models and improve the accuracy of modelling techniques.

4.5 Conclusion

The inclusion of muscle architectural detail is shown to influence masticatory muscle force production capability calculations, indicating that muscles with longer fascicles were disadvantaged compared to muscles with shorter fascicles. However, compensatory morphological features allow bite forces to scale isometrically or with weak positive allometry. Dietary groups were differentiated by temporalis fascicle angles, which, when allied with the differentiation of rostral length reported in previous studies (Van Valkenburgh and Koepfli, 1993; Slater *et al*., 2009; Penrose *et al*., 2016) may further contribute to specialisations of fast jaw closing or forceful jaw closing species. The most biomechanically demanding masticatory function is canine biting, and the highest strain energy values were reported in these conditions, particularly in the zygomatic arches and caudal rostrum. Specific head shapes may be constrained by size, with scaled strain energy models predicting that some bony morphologies may only be viable in species with small body masses.

This chapter is the most comprehensive investigation of the biomechanics of canid biting to date. It provides important insights into morphological versus behavioral adaptive strategies to different dietary niches and will inform future comparative studies, in particular the building of computational models and estimations of bite force production.

Chapter Five. The biomechanical role of the orbital ligament in load transmission during canine biting in the Canidae.

5.1 Introduction

I would like to thank Dr Nathan Jeffery for advice on experimental design, for offering suggestions for manuscript improvement and for the critical revision of this chapter. I would also like to thank Professor Graham Kemp for his help in the concept development and critical revision of this chapter.

Biomechanical factors influence the evolution of head shape in carnivoran mammals (Radinsky, 1981; Van Valkenburgh, 1991, 2007; Christiansen and Wroe, 2007). Skulls must not only house sensory organs but also generate and withstand forces, particularly when tackling prey and processing food. Of particular interest in this chapter is the structure and function of post orbital ligament that makes up the lateral border of the orbit in the Canidae. The mammalian orbit is highly plastic resulting in a diverse range of morphological conditions (Cox, 2008; Jasarevic *et al.*, 2010). The primitive mammalian condition of this region demonstrates a postorbital ligament (POL). This is a collagenous structure running from the zygomatic process of the frontal bone to the frontal process of the zygomatic bone, covering the lateral aspect of the eye. The histological structure of the orbital ligament has been variously reported in different texts. This may be due to true differences between species, or the use of differing terminologies to describe the same structure or a combination of both. Whilst all sources report it as consisting of connective tissue, some sources report it as ligamentous (dense regular connective tissue) (Getty, 1975; Liebich *et al*., 2009; Evans and De Lahunta, 2013; Singh *et al.*, 2018), others describe it as a thickening of the temporal fascia, i.e. dense irregular connective tissue (Cartmill, 1970; Heesy, 2005; Herring *et al.*, 2011). In their work on rabbits Jasarevic *et al*. (Jasarevic *et al.*, 2010) report that the POL consists of elastic fibrocartilage. In domestic dogs it is most often decribed as ligamentous (Getty, 1975; Liebich *et al*., 2009; Evans and De Lahunta, 2013; Singh *et al.*, 2018). I am unaware of any histological analyses of the POL reported in the wild canid.

In some mammalian taxa, the POL has become ossified to form the postorbital bar (POB). This appears to have evolved independently in at least nine mammalian orders (Heesy, 2005). In most instances, the ventral process of the frontal bone and a dorsal process from the zygomatic bone unite to make up the bar. There is some variation to this pattern: in equid perissodactyls the ventral part of the bar originates from the squamous part of the temporal bone (Getty, 1975; Heesy, 2002), and in haplorrhine primates an even more derived condition, the post orbital septum, exists. This consists of an extension of the alisphenoid bone which unites with the POB to isolate the orbital contents from the temporal fossa (Cartmill, 1980; Ross and Hylander, 1996; Savakova, 2012; Smith *et al*., 2013). A wide range of post orbital conditions is exhibited within some mammalian families. In pteropodidae bats for example, several species have a well-defined POB, others have an orbital ligament and others have no lateral reinforcement to the orbit and the lateral eyeball is covered with only periorbital fascia, subcutaneous and cutaneous tissues (Noble *et al*., 2000; Ravosa *et al.*, 2000; Cox, 2008; Harvey *et al.*, 2016). Within the carnivoran order most species exhibit a POL, but some herpestids and felids demonstrate a post orbital bar (Noble *et al*., 2000; Heesy *et al*., 2007). All known extinct and extant canids demonstrate the ancestral condition and exhibit a POL. In domestic dogs the POL makes up around 20% of the circumference of the orbit (Evans and De Lahunta, 2013).

The wide variation in lateral orbit morphology demonstrates the great plasticity in this region and infers that the POB is an adaptive trait. However, the function of both the post orbital ligament or bar is unclear. It is difficult to find a common pattern to predict which mammals are likely to have a post orbital bar, and by inference, which are likely to have post orbital ligament or no lateral support to the orbit. This in turn makes it difficult to speculate on the functional significance of the POL or POB.

Several hypotheses regarding the role of the POL or POB have been put forward, and to some extent evaluated, by previous authors. Firstly, that the POB evolved to protect the eye from

injury (Prince, 1953; Simons, 1962). This is a largely discredited theory as the lateral aspect of the eyeball is only minimally covered by the bony strut of the POB (Cartmill, 1970; Greaves, 1985), and is clearly absent in many closely related species.

Secondly, that the POB counters masticatory stress, particularly in unilateral chewing. The bony strut resists torsional loading during at the balancing side during unilateral mastication (Greaves, 1985, 1995). In addition, a bony strut can transmit compressive as well as tensile forces generated through mastication. However, this theory has been largely rejected, in primates at least. POBs in anthropoid primates are incorrectly orientated to resist torsional strain (Hylander *et al.*, 1991; Ravosa, 1991a, 1991b; Ross and Hylander, 1996). In Strepsirrhine species where the POBs were aligned with strain orientations, the strain magnitudes generated during mastication were too low to warrant ossified reinforcement of the ligament (Ravosa *et al.*, 2000; Ross, 2001). However, Buckland -Wright proposed that the POL in cats acts to transmit tensile stress during biting (Buckland-Wright, 1978). This hypothesis is in alignment with Herring's work on pigs (Herring *et al.*, 2011). She found that the postorbital ligament elongates during masseter contraction and acts to resist distortion of the zygomatic arch, and therefore may have a role in tensile force transmission during chewing.

Cartmill proposed an alternative theory (Cartmill, 1970). He suggested that the POB evolved from the POL to provide rigidity to the lateral margin of the orbit to enhance visual acuity. Reinforcement is required in animals with large forward-facing eyes and a small temporal fossa. He argued that the reorienting of the visual plane of the eye to face forward (convergence) effectively also repositioned the temporalis muscle laterally rather than caudally relative to the eyeball. Contraction of temporalis causes tension on the ligament and via extraocular ligaments and smooth muscle attachments, distorts the eye and disrupts visual acuity (Cartmill, 1970, 1980). However, this does not explain the evolution of POBs in the large ungulates, i.e. the artiodactyls and perissodactyls, with laterally facing eyes.

Heesy (2005) expanded on Cartmill's work to include these taxa. He collected data from 1329 mammalian skulls from 324 taxa and 16 orders of mammalian skulls and found a correlation with the orientation of the orbit relative to the temporal fossa. Species with a smaller angle between the orbital and temporal planes were more likely to exhibit a POB. Possible reasons for having a smaller angle are multitudinous. They include having relatively greater orbital convergence, greater vertical orbit orientation, greater absolute eye size, greater eye size relative to body mass, and difference in brain size relative to temporalis size. Heesy (2005) argued that it is the spatial constraint in the postorbital region that impinges on eye function and drives the evolution of the ossification of the post orbital ligament. However, there appear to be many exceptions. In their 2016 paper Harvey *et al*. (Harvey *et al.*, 2016) described that the lack of either post orbital bar or ligament in three species of *Pteropodidae* bats did not preclude them from having large forward-facing eyes, despite closely related species exhibiting POBs. Similarly, most extant felids and all canids have large forward-facing eyes and have no POB. It is clear from these studies the function of the POL or POB is not fully resolved. Work on this region is dominated by primate, and to a lesser extent chiropteran and artiodactylan studies, and very little specific work has been done with other orders. No work has been published on the functional role of the POL in carnivorans. This may partly reflect the difficulty in obtaining specimens with intact soft tissue structures, when compared with purely osseous samples. Even in his major work on bone structure and stress in felid skulls, Buckland-Wright did not include intact POLs on the skulls he used , and did not place strain gauges in the region likely to undergo strain during masseteric contraction (Buckland-Wright, 1978).

As generalities cannot be ascribed to the functional role of the postorbital region, this experimental study applies a specific focus and uses finite element (FE) modelling to assess the biomechanical role of the postorbital ligament in load transmission during masseteric contraction in canids. When used in comparative morphological studies finite element

analysis (FEA) provides the researcher with a powerful tool to investigate form and function. A virtual model of the specimen is created consisting of many small elements connected by nodes (Chapter Four, part 4.2.4). The model is given material properties, limited by constraints and loaded with forces. Nodal displacements are determined and are used to calculate strain and stress. The composite calculation of all elements gives the mechanical behaviour of the entire structure (Richmond *et al.*, 2005; Rayfield, 2011). It is relatively straightforward, by altering any of the variables e.g. geometric shape or force values, to explore how they influence form and function, and to run alternative models. Running multiple iterations of models can aid in identifying functional adaptations and constraints. In this way FE modelling has been used in many biological studies. For example: to identify bony changes in short term adaptations (Vickerton *et al.*, 2013; Brunt *et al.*, 2015), identify ecological adaptations in related species (Slater and Van Valkenburgh, 2009; Slater *et al.*, 2009; Attard *et al.*, 2011; Cox *et al.*, 2011) discover how individual specimens behave under different conditions (Bourke *et al.*, 2008; Pierce *et al.*, 2009) (Chapter Four), or to give insight into evolutionary pathways (Dumont *et al.*, 2005; McHenry *et al.*, 2006; Slater and Van Valkenburgh, 2009; Tseng and Wang, 2010; Dumont *et al.*, 2011; Cox *et al.*, 2012).

However, all models are simplifications. The true detail of the biological condition is too complex to fully replicate. Questions of the minimal level of geometric information and the values attributed to material properties and applied forces must be addressed to ensure that the model behaves in a biologically realistic manner (Richmond *et al.*, 2005; Rayfield, 2007; Kupczik, 2008; Burkhart *et al.*, 2013; Godinho *et al.*, 2017). Validation studies endeavour to test the reliability of virtual models against empirically derived experimental data. Sensitivity analyses test the robustness of the experimental setup by exploring the relationship between the input variables and output values. Validation and sensitivity studies are increasing in the FEA literature (Kupczik *et al.*, 2007; Gröning *et al.*, 2009; Bright and Rayfield, 2011a, 2011b; Rayfield, 2011; Godinho *et al.*, 2017; Zander *et al.*, 2017), but to date, little

has been done regarding canid species. This study compares the FE derived outputs with *ex vivo* experimentally derived data in order to validate the current FE models and inform future work, addressing in particular if it is necessary to include the POL in carnivoran FE models concerned with masticatory analyses.

The aims of this study are:

- **to explore the biomechanical role of the postorbital ligament (POL) in transmitting load during canine biting using FE analysis,**
- **to validate the FE findings using empirically derived data from *ex vivo* laboratory experiments,**
- **to conduct a sensitivity analysis to explore the influence of differing the material properties of bone to determine which is most suitable to reflect *ex vivo* findings.**

Specifically, I test two hypotheses:

1. That the post orbital ligament plays a significant functional role in transmitting stress from the zygomatic arch to the frontal bone generated during masseteric contraction at canine biting.

2. That finite element models constructed to replicate laboratory conditions can suitably reflect the biomechanical behaviours of ex-vivo specimens.

5.2 Materials and Method.

5.2.1 Specimens

One species, *Vulpes vulpes* was chosen as the representative model canid. This was selected as it was the most accessible wild canid species to acquire for the *ex vivo* experiments, due to it being indigenous to the UK. It is considered by many to be vermin and is often culled for pest control reasons. One specimen was scanned and used to create the FE model, a

further 16 specimens were used for the laboratory work. Two of these were used only in preliminary exploratory dissections and a further five were discounted from the final laboratory analysis due to structural failure upon loading. Details of the samples are given in Chapter Two.

5.2.2 Experimental condition

In this study, canine biting during contraction of the masseter muscle was modelled. Canine biting is the most biomechanically demanding condition of the canid skull and is frequently experienced when tackling prey (Chapter Four). The masseter was chosen as it arises from the ventral aspect of the zygomatic arch, and during contraction would exert forces to pull the arch, and thus the POL, ventrally. Although the masseter is only the second largest jaw adductor muscle in canids, both in terms of its mass (mean 29% of total jaw adductor mass) (Chapter Three) and force production capabilities (mean 36% of total jaw adductor force)(Chapter Four), it originates from a relatively small area (19% of the total jaw adductor area of origin)(Chapter Three). This results in a greater force per area on the masseter area of origin than that of either of the other two jaw adductor muscles. In other words, as previous authors have pointed out, the masseter has a greater influence on cranial strain than the temporalis or the pterygoids (Buckland-Wright, 1978; Herring *et al.*, 2001). Strain is a dimensionless measure of the change in length of an object relative to its original length. It is measured in microstrain ($\mu\varepsilon$). Tensile strain is an elongation and is recorded as a positive value. Compressive strain is shortening and is recorded as a negative value. In this chapter strain values in the frontal bone were measured in loaded FE models with and without POLs, and validated with laboratory experiments using *ex-vivo* specimens before and after cutting the POL.

5.2.3 Finite Element models

FE models were created following the workflow described in Chapter Four, part 4.2.4.1, and illustrated in Figure 4.4. In brief, a *Vulpes vulpes* head was scanned using CT, and the skeletal components of the head, were reconstructed using Avizo Lite 9.0.1 software (FEI Systems, OR). This was then discretised into a mesh which was imported into FEBio Preview software (Maas *et al.*, 2012) in order to build FE models. To enable sensitivity analyses three pairs of models were created. Each of the three pairs had differing material properties for both cortical and trabecular bone: 3.5GPa/3Gpa, 7GPa/6Gpa and 14GPa/12GPa respectively. Although no currently available studies appear to model the Young's modulus of fresh mammalian bone at such a low value as 3.5GPa, it was included to explore the properties of a more flexible skull, as previous studies have established that stiffer models underestimate strain (Bright and Rayfield, 2011a; Rayfield, 2011). Each pair consisted of two skulls with the same material properties as each other but one had the left postorbital ligament intact, and the other had no left postorbital ligament. All other material properties i.e. for orbital ligaments, zygomatic sutures teeth and nasal septum are as described in Chapter Four, part 4.2.4.2. No sutures, other than the zygomaticotemporal suture, were included in the model. The zygomaticotemporal suture was included as it remains patent throughout the canid lifespan and is in an area closely associated with the masseter muscle and postorbital ligaments, which are the focus of this study. The distinction of the zygomatic arch into two separate bones has been shown to result in differing strain distributions in the two regions. In felidae and suidae the squamous temporal bone is subject to higher strain than the zygomatic bone, whilst the reverse is true in macaques (Buckland-Wright, 1978; Hylander and Johnson, 1997; Rafferty *et al.*, 2000; Herring *et al.*, 2001; Kupczik *et al.*, 2007). In addition, Kupczik *et al.* found that FE models that include a zygomaticotemporal suture produce strains more similar to those derived from empirical experiments than those with a fused arch (Kupczik *et al.*, 2007). To reflect the laboratory experiments, only the left

masseter muscle was loaded. Nodal points on the ventral aspect of the zygomatic arch were loaded directly, rather than via modelled muscle as direct nodal loading was shown to give a more realistic outcome than simulated muscle loading (Kupczik *et al.*, 2007). To reflect the *ex vivo* set up, the skull was fully constrained at both canine tips, both tympanic bullae and the right ventral zygomatic arch.

In addition to the FE models loaded to reflect the laboratory conditions, two further FE models were constructed. These were loaded in a more biologically meaningful way, that is they were constrained at both temporomandibular joints, and bilaterally loaded via both of the masseter muscles. Values used for cortical bone and trabecular bone were 7GPa and 6GPa respectively. All other material values were as in the other FE models in this chapter and Chapter 4. The aim of this part of the study was to ascertain if the laboratory set up and FE studies constructed to reflect them, deviated substantively from the more realistic loaded condition.

To be able to make direct comparisons with the output data of the similarly positioned strain gauges in the *ex vivo* specimens, analyses of these FE models focused on the tensile and compressive strains and vectors of ten topographically associated nodes on the dorsal aspect of the frontal bone (Figure 5.1). In FEBio tensile strain is reported as 1st principal strain, and compressive strain is reported as 3rd Principal strain. Strain magnitudes and vectors were calculated in FEBio Postview (Maas *et al.*, 2012).

As well as the magnitude and orientation of the principal strains, the strain data was also used to calculate strain ratio using the equation ($\varepsilon_{max}/|\varepsilon_{min}|$). Strain ratios indicate the overall strain condition at the sample point, that is, whether the bone is undergoing tensile or compressive force. Values less than 1 indicate tension is greater than compression and values less than 1 indicate compression is greater than tension force (Rayfield, 2011).

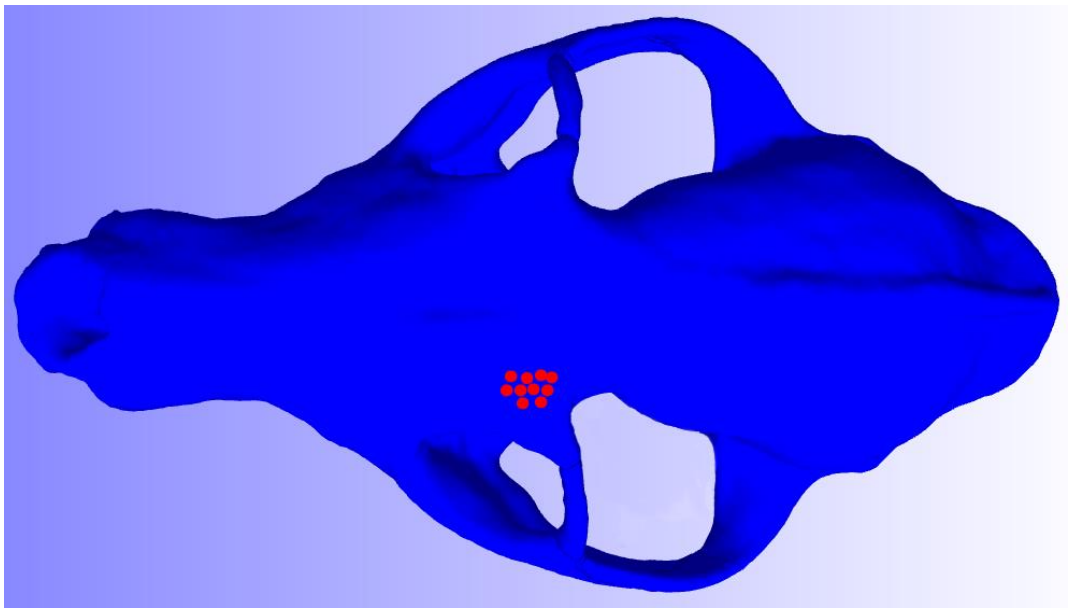

Figure 5.1. FE model of *Vulpes vulpes*, with orbital ligaments intact. The red dots indicate the position of the nodes that were sampled for strain data.

5.2.4 Laboratory experiments

Two *Vulpes vulpes* heads were used in a preliminary exploratory investigation to determine the optimum preparation protocol and to identify the best site to attach the strain gauges. The remaining fourteen *Vulpes vulpes* heads were then prepared following the identified protocol: firstly, the heads were skinned to the level of the muzzle, and the mandibles removed. The frontal, parietal and occipital bones were then further cleaned to remove the temporalis muscle and any overlying soft tissue structures. Only the left and right masseter muscles and orbital ligaments were left intact (Figure 5.2). An area of frontal bone dorsal and medial to the orbit was elected to attach the strain gauge. This was selected as it was relatively flat, close to the insertion of the orbital ligament and readily identifiable in all specimens (Figure 5.2). The flatness of the area is key to ensuring that there is a good contact between the bone and strain gauge. The attachment area was degreased with alcohol and abraded with fine gauge wet and dry sandpaper. When not being worked upon the heads were covered with damp cloths to prevent them from drying out.

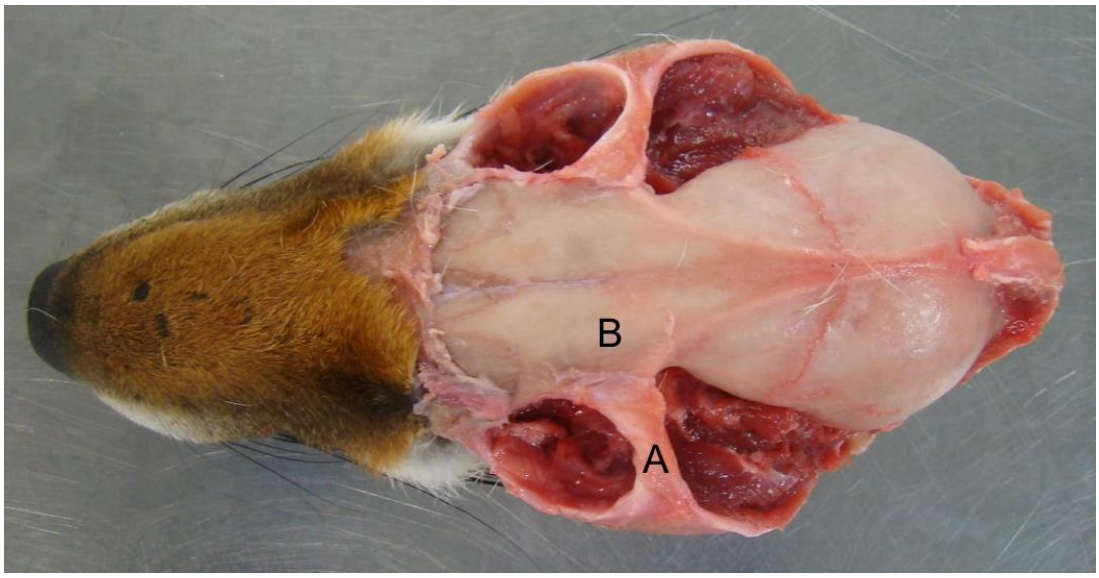

Figure 5.2. Prepared *Vulpes vulpes* head demonstrating the postorbital ligament (A), and the region of the frontal bone that the strain gauge was attached to (B).

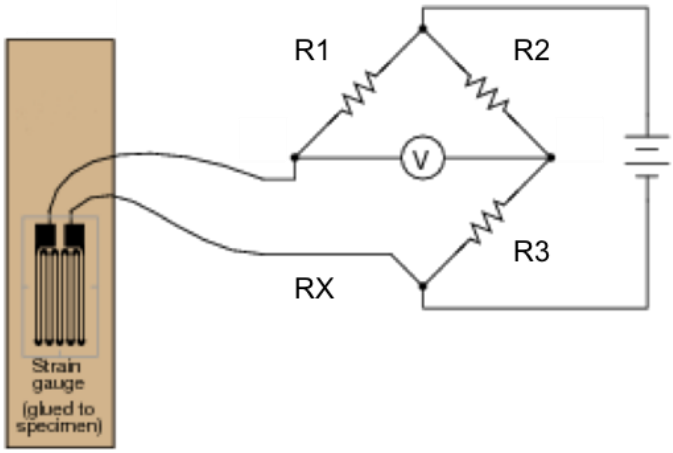

Figure 5.3. Strain gauge and Wheatstone bridge electronic circuit. If the value of the resistance in R1, R2 and R3 is known, the fourth resistor, 'RX' can be calculated using the equation R1/R2 = R3/RX. Figure adapted from allaboutcircuits.com.

Strain gauges are electronic sensors that consist of a grid of fine wires, protected by a film covering and attached to a Wheatstone bridge. A Wheatstone bridge is an electrical circuit

that balances two legs of a circuit to determine an unknown resistance (Figure 5.3). When the gauge is attached to a surface, distortion in surface shape results in changes in grid length which is converted into changes in electric resistance. If the grid lengthens this increases resistance and if it shortens this decreases resistance. In this way, tensile (positive) and compressive (negative) strains are recorded. To obtain information about strain on an irregular shaped surface such as the skull, more than one orientation of grid is required. For this study, a planar rosette grid was used as it consists of three grids orientated at 45 degrees to one other. In *in vivo* experiments the planar configuration is usually avoided in preference to a less invasive stacked grid arrangement. However, in *ex vivo* experiments where a greater exposure is possible, planar gauges are favoured as they sample a greater surface area and avoid local irregularities. The planar arrangement also avoids overlaying, and potential overheating, of the grids (Bright and Rayfield, 2011a). A 121.2 Ω ± 0.35 % s plane rosette strain gauge (Omega KFH-1.5-120-D17-11L3M3S) was attached to the cleaned area using cyanoacrylate gel (Loctite 2064940). In all specimens, strain gauges were aligned in the same orientation relative to the sagittal midline suture (Figure 5.4).

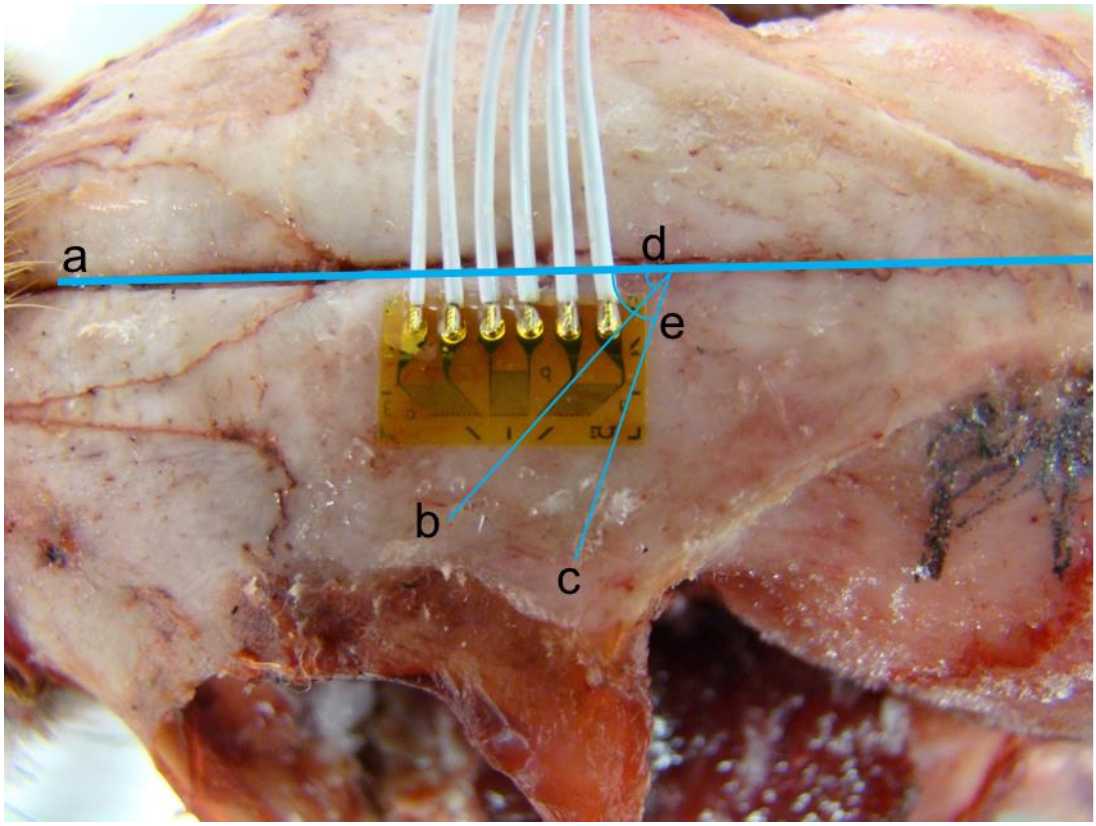

Figure 5.4. Close up view of frontal region of *Vulpes vulpes* skull with strain gauge attached. Line a- midline, line b - angle of grid 'a', line c angle of principal strain vector, angle d - the angle from midline to line b, angle e - the angle from midline to principal strain vector.

After positioning, gauges were covered with clear waterproof silicon to improve thermal stability. Each head was positioned close to the free edge of a wooden board, and held in position using metal bars and screws secured through the right masseter muscle. The only teeth in contact with the board were the tips of the canine teeth, which simulated canine biting. The left masseter was positioned over the free edge of the board and a bar affixed to enable a weight to be suspended from the muscle. The strain gauges were connected to an integrated amplifier and signal conditioner (Omega, OMB-NET6000). Each grid was recorded via one channel and measurements taken with Encore v1.1 (Omega). Gauges were left activated in situ for ten minutes prior to each experiment to account for drift. After this time, the left masseter was loaded with an 11kg hanging weight to replicate masseter muscle adduction force (Figure 5.5). The 11kg weight represented 110N force which is close to the

value calculated for masseter force in similar sized canids. The principal strain magnitudes and vectors were measured for the preload condition and post-load conditions. The role of the orbital ligament in dissipation of masticatory forces was examined by cutting the left orbital ligament after the 11kg weight had been suspended for a period of 10 seconds. Five specimens were discarded from the dataset as the caudal end of the masseter began to tear away from the zygomatic arch after loading. This may have been due to several factors; post mortem tissue degradation, lack of support from adjacent tissues such as the connective tissue and the muscles that would normally border the masseter, or the artificial directional loading (i.e. ventral) that did not precisely mimic the condition found in life (i.e. medioventral). A total of nine specimens were therefore included in the analysis. Strain magnitudes for the pre-cut and post-cut conditions for each channel were determined by calculating the mean strain shortly before and after cutting. However, the time point values immediately before and after the cut point were not used as they may have been affected by the manual cutting action (Figure 5.6). Maximum principal strain orientations were calculated by measuring the strain gauge angles of grid 'a' relative to midline on photographs using ImageJ (Schneider *et al.*, 2012) and converting these into orientations using the calculation tool on the Vishay website (vishaypg.com) (Figure 5.4). The orientation of the minimum principal strain (compression) was perpendicular to this (Figure 5.8). The strain gauge data was also used to calculate strain ratio.

Figure 5.5. Loading of *Vulpes vulpes* head to simulate masseteric biting.

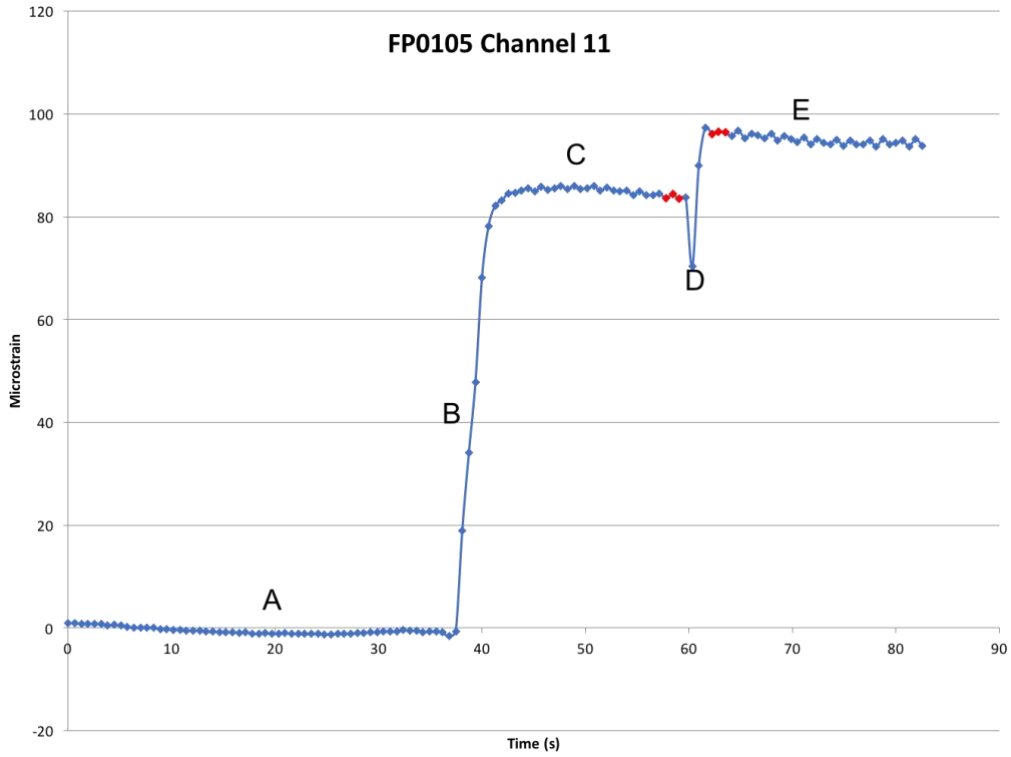

Figure 5.6. Output from strain gauge grid 'a', Specimen FP0105. A - pre-loaded specimen, B - load applied, C - pre-cut loaded condition, D - left postorbital ligament cut, E - post cut loaded condition. The red squares indicate the time point values used to calculate the pre-cut and post-cut mean values. Positive microstrain values indicate tensile loading.

5. 3 Results

The FE strain and *ex vivo* strain gauge magnitude and ratio values are reported in Table 5.1. The magnitude of the strain was generally lower in the FE models compared to that observed in the cadaveric models. As might be predicted, in the FE models that more closely reflected the laboratory conditions the assigned stiffness of the bone in the FE models had a clear effect on the derived strain values, with the most rigid bone material models reporting the lowest strain values, and those with the most flexible material properties reporting the highest strain values. Reported strain values in the the FE models that more closely reflected realistic loading conditions were lower in magnitude than their nearest FE laboratory condition counterpart. In the FE models that more closely reflected the laboratory

conditions strain ratios were also generally lower than the laboratory models and were also influenced by the stiffness of the bone in the FE models. Reported strain ratios in the the FE models that more closely reflected the realistic loading conditions were higher in magnitude the the FE models reflecting the laboratory conditions, and more closely aligned to those found in the cadavers. The mean of the pre-cut strain ratios in the cadavers was 0.88με (0.53-1.77 με) and in the FE models 0.63 με (0.59 to 0.69 με). The mean of the post cut strain ratios in the cadavers was 0.87 με (0.54- 1.64 με) and in the FE models 0.53 με (0.53-0.53 με). Outliers were identified by establishing the interquartile range to determine the upper and lower fence values. FP0111 was identified to be an outlier. With this specimen removed the mean strain ratio in the pre-cut cadavers was 0.77 με and in the post-cut 0.78 με. In both the FE loading model types (to reflect the laboratory conditions and with a more realistic loading regime) and cadaver models this indicates that the compressive strains were greater than the tensile ones at this sampling site. In both the FE and cadaver experiments tensile strain orientation ran mediocaudal to rostrolateral, and the compressive vectors ran perpendicular to these, i.e. caudolateral to rostromedial (Figure 5.8). The strain orientations were very consistent in all scenarios and changing the stiffness of the bone or the loading conditions in the FE models appeared to make minimal difference to the strain orientations (Figure 5.8 and Table 5.1).

In the *ex-vivo* specimens both first and third principal mean strain values showed only very small differences in pre-and post cut ligament values, less than 10 microstrain in both cases. The mean strain ratios also remained very similar in the pre-and post cut conditions, indicating that the post orbital ligament has a very limited role in transmitting load during masseter bite loading. All of the FE models, whilst underestimating the magnitude of the strain values, all showed similar trends, that the post cut values were slightly less or the same as the pre-cut values, with the most compliant bone model revealing the largest change in value, and the most rigid model showing the least. This is illustrated in Figure 5.7 where both

Vulpes vulpes 4p and 4q models are calibrated to the same scale and show little variation between the pre-cut and post-cut condition.

Table 5.1. FE model and *ex vivo* experimental pre-cut and post-cut values.

				Pre-cut					Post-cut				
	specimen	Cortical bone GPa	Trabecular bone GPa	1st principal	Angle from midline	3rd principal	Angle from midline	Strain ratio	1st principal	Angle from midline	3rd principal	Angle form midline	Strain ratio
FE models after laboratory conditions	FE redfox4r/4s	3.5	3	107	80	-154	173	0.69	74	74	-140	167	0.53
	FE redfox4p/4q	7	6	48	82	-77	171	0.61	39	81	-74	167	0.53
	FE redfox4t/4u	14	12	23	79	-40	166	0.58	21	79	-40	165	0.53
FE models after realistic conditions	FE redfox4v/4w	7	6	19	81	-24	170	0.79	14	80	-22	168	0.63
Cadavers	FP0101			223	71	-270	159	0.83	225	70	-272	150	0.83
	FP0105			192	81	-239	172	0.80	198	79	-250	166	0.80
	FP0106			122	68	-131	164	0.93	135	59	-145	154	0.93
	FP0107			126	77	-188	177	0.67	125	64	-183	168	0.68
	FP0108			118	89	-155	177	0.76	119	80	-155	162	0.77
	FP0109			213	85	-399	169	0.53	235	73	-433	159	0.54
	FP0111			230	67	-130	178	1.77	216	60	-132	170	1.64
	FP0112			309	85	-397	180	0.78	309	74	-396	164	0.78
	FP0113			213	88	-243	185	0.88	219	72	-248	176	0.88
	FP MEAN			194	79	-239	173	0.88	197	70	-246	163	0.87
	FP MEAN after outlier removed			190	81	-252	173	0.77	196	71	-260	162	0.78

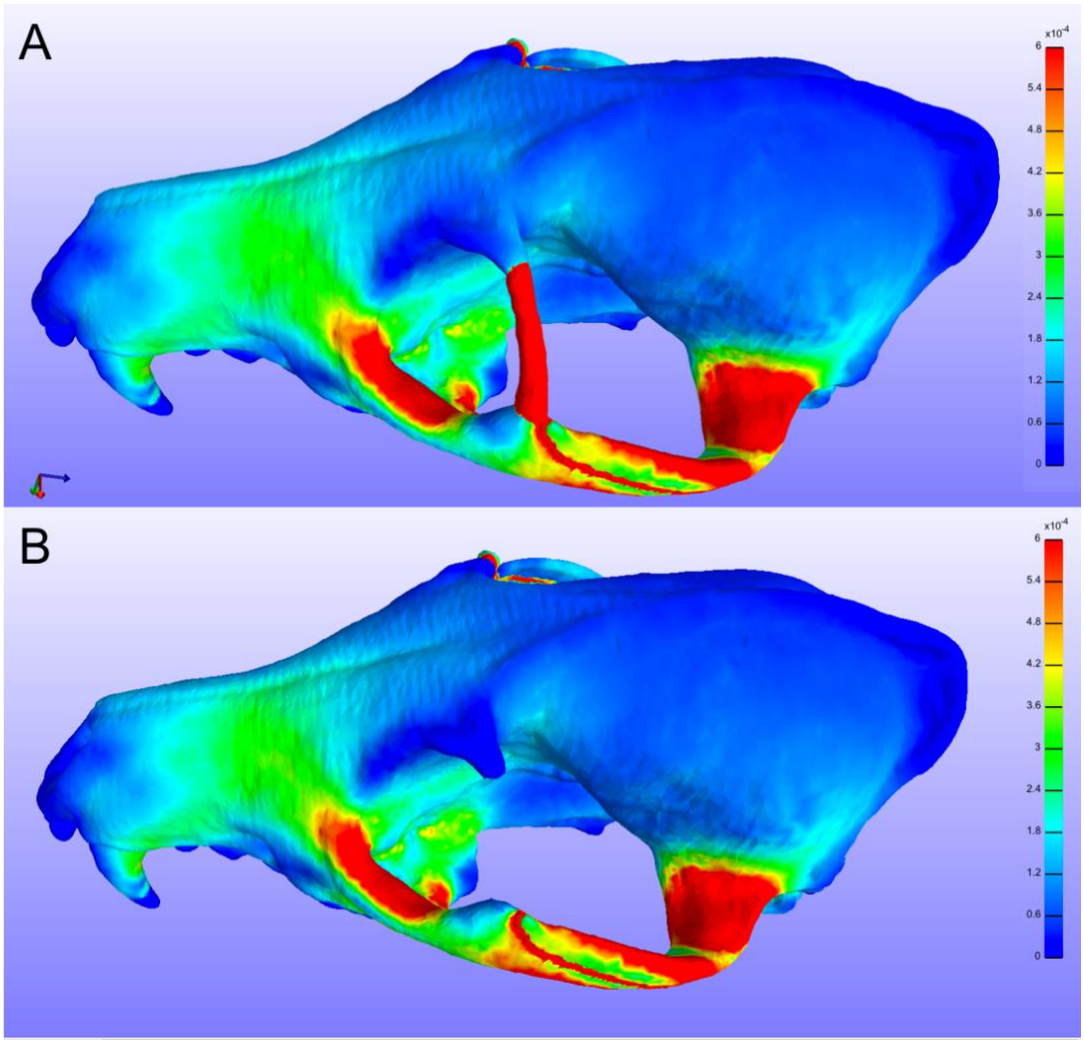

Figure 5.7. FE models of *Vulpes vulpes* skull loaded with left masseter force. Scaled to 600 microstrain. A - model ‘ 4p’ with post orbital ligament, B - model ‘4q’without post orbital ligament.

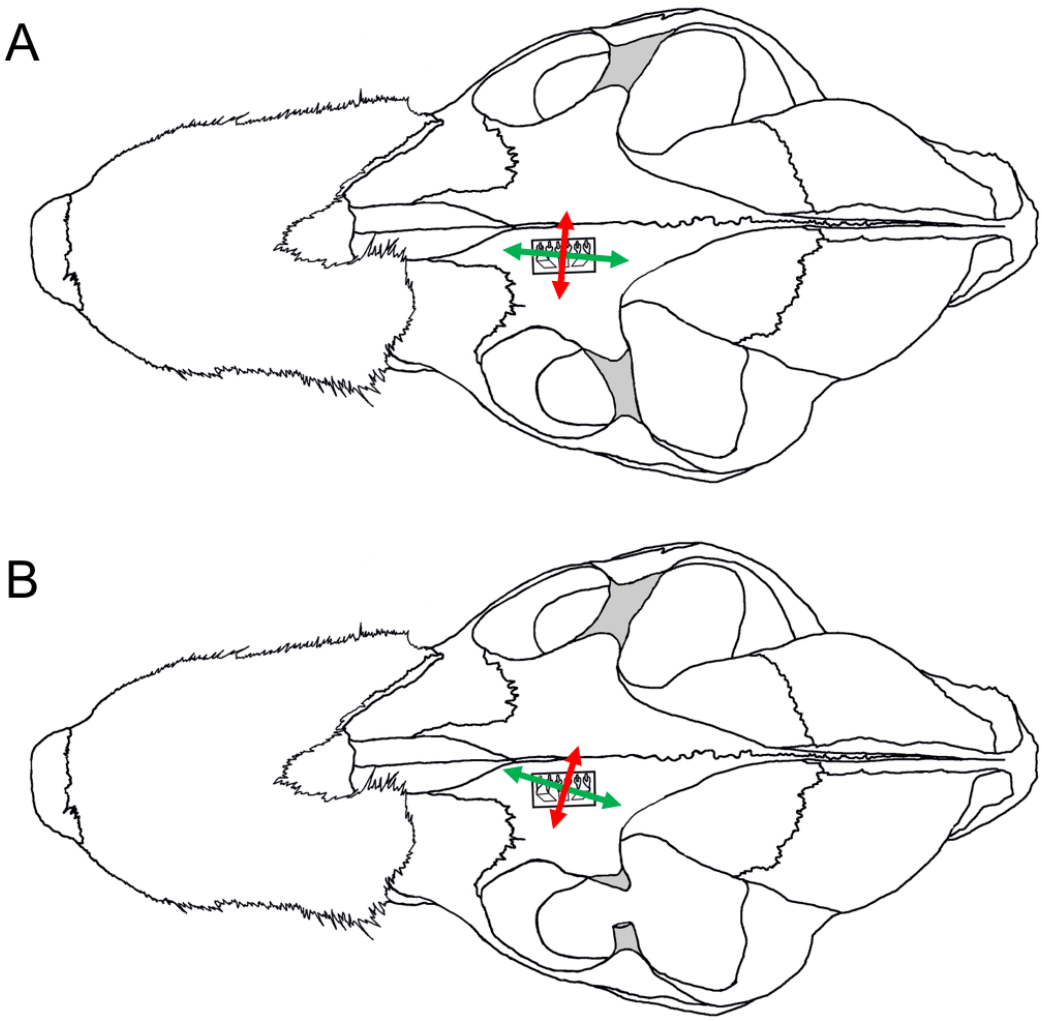

Figure 5.8. Drawings of dorsal aspect of dissected *Vulpes vulpes* with precut (A) and postcut (B) strain gauge magnitudes and vectors. The green double headed arrows indicate the orientation and relative magnitude of the compressive strain vectors, and the red double headed arrows the tensile strain vectors. The orbital ligaments are shaded grey.

5.4 Discussion

The role of the post orbital ligament during masseteric biting, was explored in one species of canid, *Vulpes vulpes*. Findings from *ex vivo* laboratory experiments were compared with a range of different finite element models to determine which, if any, loading conditions best reflect the laboratory findings.

Hypothesis 1. The primary aim of this chapter was to determine if the post orbital ligament played a significant functional role in transmitting stress from the zygomatic arch to the frontal bone generated during masseteric contraction at canine biting.

This hypothesis was not supported. Measuring strain values in the frontal bone of loaded skulls both with and without POLs determined that the POL in canids appears to play only a very small role in transmission of load during masseteric contraction. When compared to the *ex vivo* experiments, the FE models appeared to underestimate the magnitude of the strain, although they were broadly similar to those seen in other studies using mammalian species (Ravosa *et al.*, 2000; Thomason *et al.*, 2001; Kupczik *et al.*, 2007; Bright and Rayfield, 2011a). In their work on galagos, Ravosa *et al*. concluded that the low shear strain values (1^{st} principal strain – 3^{rd} principal strain) recorded at an interorbital strain gauge (mean 420 $\mu\varepsilon$) meant that the POB in these species did not play a meaningful role in transmitting force during biting. Although the strain gauges were slightly differently placed in this study, their position on the frontal bone would also be pertinent to detecting masseter force transmission. Not only do the shear strains in this study have similar or lower values than those in the galago, they also show very little difference between the FE models with and without a POL and the pre and post cut conditions in the *ex vivo* experiments (Table 5.1). This is further evidence to support the theory that the POL does not act to disperse load during biting.

The most compliant models, those with a cortical bone modulus of 3.5GPa, better reflected the values obtained in the *ex vivo* experiments. However, they also underwent the greatest

change in value in the with ligament/without ligament conditions, which was not reflected in the mean values of the pre-cut/post-cut *ex vivo* conditions. That is, the more flexible FE models may overestimate the role of the orbital ligament in load transmission. The strain magnitudes in the realistically loaded FE models were the lowest values of all scenarios, despite having the intermediate values for the bone material properties. In all of the FE models and all of the *ex vivo* models the orientation of strain was very similar. The orientation of the first principal strain ran rostro-laterally from midline and indicates tensile strain from midline toward the orbit during masseteric contraction. However, the orientation was not directed toward the lateral orbit, i.e. toward the POL, but somewhat more rostrally, and may be influenced instead by forces being transmitted by the bones constituting the rostral and medial orbit. In addition, in the loaded FE models, areas of high strain can be seen on the ventral orbits and are contiguous with strain running onto the rostrum and frontal bone. This finding is further borne out by the tensile strain orientation changing little in the FE models where the orbital ligament was removed, or in the experiments where the POL was cut. The orientation of the third principal strain (compression) is perpendicular to the tensile stress and indicates dorsoventral flexion of the skull. This occurs as the skull is constrained rostrally at the canines and caudally at either the tympanic bullae in the FE models constructed to reflect the laboratory conditions, or the temporomandibular joint in the FE models constructed to reflect a more life like loading scenario. Strain ratio describes the overall loading condition at the sample site. This was consistent in all models and *ex-vivo* specimens; that is, that compressive forces are greater than tensile force in this region of frontal bone. Strain ratios varied most between models with POL and without POL in the most compliant variant and also in the realistically loaded models, and least in the most rigid model.

Hypothesis 2. That finite element models constructed to replicate laboratory conditions can suitably reflect the biomechanical behaviours of ex-vivo specimens.

This study compared eight laboratory specimens to six iterations of one FE model designed to closely reflect the laboratory loading scenario, and two FE models with more realistic constraints. Previous studies have used lower numbers of real specimens, typically one or two, to validate *in silico* findings (Marinescu *et al.*, 2005; Kupczik *et al.*, 2007; Bright and Rayfield, 2011a; Rayfield, 2011; Cuff *et al.*, 2015; Toro-Ibacache *et al.*, 2016; Godinho *et al.*, 2017). One study on primates used four *in vivo* subjects to validate their work, but these subjects did not have normal lateral orbit anatomy due to previous experimental work (Ross, 2001). Many of these studies used the same subject to build the FE model and conduct the experimental work (Marinescu *et al.*, 2005; Kupczik *et al.*, 2007; Bright and Rayfield, 2011a; Cuff *et al.*, 2015; Toro-Ibacache *et al.*, 2016; Godinho *et al.*, 2017). Although this subject specific approach has much merit by ensuring accuracy particular to one sample, it does not address intraspecific variation, or allow for the detection of outliers. This work focuses on one species, *Vulpes vulpes*, and uses multiple individuals as *ex vivo* validation subjects. The use of fresh, rather than dried or preserved material also increases the likely fidelity of the experimentally derived data. In this instance, fourteen individuals were selected for the laboratory experiments, but five individuals were discarded due to poor laboratory performance and one outlier was detected. Analysis of the experimental results from the remaining eight specimens allowed for a greater confidence in the findings. The main disparity between the FE models and the real specimens was the magnitude of the strain found. This finding was also evidenced in previous studies (Marinescu *et al.*, 2005; Kupczik *et al.*, 2007; Bright and Rayfield, 2011; Cuff *et al.* , 2015; Toro-Ibacache *et al.*, 2016; Godinho *et al.*, 2017) The finding that the least similar strain magnitudes to the laboratory cadavers was the most realistically loaded FE model implies that the laboratory conditions may not truly reflect the true-life condition and perhaps more realistic ways of loading cadavers could be

explored in future studies. It can be concluded that there is still some aspect lacking in the FE modelling of skulls that means *in silico* models perform in a different way to *ex vivo* models. However, as both the strain ratio and orientation in all FE models appeared to match that found in the *ex vivo* models it may be assumed that the geometry of the model is sufficiently accurate to replicate real life, and that other factors such as material properties or constraints or loading regimes may have more bearing on strain magnitude outputs.

5.5 Conclusions

The role of the POL in canids is yet to be determined. It appears that it does not play a significant part in load dispersal during biting, at least not in the adult. Future FE studies on canid mastication need not include this aspect of anatomy to accurately model skull biomechanics. All FE models underestimated the magnitude of the strain at the location on the frontal bone, the stiffer model to a greater degree than the compliant models. However, strain orientation and to a lesser extent, strain ratio were well predicted in all models. The difference between the pre-cut and post-cut *ex vivo* conditions was not as marked as that suggested by the most compliant model. It was concluded that models with 7GPa Young's modulus for cortical bone and 6GPa for trabecular bone most closely followed the behaviours of the laboratory models and were best suited to replicate the true condition.

Chapter Six. Discussion.

6.1 Introduction

The overarching aim of this thesis was to examine the how the morphology of the jaw adductor muscles and postorbital ligament are related to the form and masticatory biomechanical function of the canid skull. Differences in canid head shape are reasonably straightforward to identify and have long been utilised by biologists to distinguish between species and infer phylogenetic relationships. In the early days of comparative anatomy, the recording of dentition and simple linear measurements of skulls were used to identify species, and over the course of evolutionary biological research, workers have used increasingly sophisticated means of quantifying head shape to understand canid relationships and lineages.

What is less well understood is the relatedness of form and function, and the selective biomechanical pressures and constraints that are associated with variation in canid head shape. It may be assumed that differences between species represent adaptive traits, and yet their functional role can be difficult to determine. Hunting behaviors and dietary preferences can be established by observing the behaviors and ecological interactions of extant species. Head shapes may be correlated with behavior, for example, canids with long snouts hunt prey smaller than themselves. However, this does not address the biomechanical basis for morphological variance.

6.2 Aims of the study

The purpose of the thesis was to add to the sum of knowledge regarding mammalian masticatory anatomy, specifically with a view to enabling more accurate predictions of biomechanical function. Firstly, I recorded and described the morphology of the skull and jaw adductor muscles of twelve species of wild canid. A key concept in this study was to describe both the bony and soft tissue structures for each individual specimen to enable subject specific analyses. To my knowledge this is the largest comparative jaw adductor

muscle dissection for any mammalian species. Having such a wide data set also allows for identification of factors that are common within the canid clade. Common or unchanging factors across multiple species can identify phylogenetic or functional constraints. The second aim was to use the empirically derived data to analyse head shape with respect to the accommodation of jaw adductor muscles, to determine if jaw muscles scale isometrically or allometrically. The implications of these findings then allowed for identification of cranial shape changes to allow for muscle accommodation. The third aim was to build *in silico* models to determine bite force and biomechanical loading in the canid skull under different conditions. This in turn allowed for the quantification of the impact of skull shape on bite performance. Finally, the biomechanical role of a previously under reported soft tissue structure, the postorbital ligament, was considered.

6.3 Generating and managing force

Early researchers interested in masticatory biomechanics used simplified models and beam theory to determine bite forces and identify regions of the skull undergoing high stress or strain (Greaves, 1985; Greaves, 2000; Therrien, 2005; Damasceno *et al.,* 2013). Computational programmes based on engineering software have revolutionized this field of work and increasingly complex models are being used to predict how the skull generates and withstands forces during mastication. The fidelity of models and the validity of their outputs depends upon the accuracy with which they are built. Osteological material, even of rare species, is reasonably easy to obtain via museum collections, and CT scanners are available to many researchers. Therefore, the bony components of models are usually empirically sourced, and depending on the level of detail included, faithful to the specimen. However, the soft tissues associated with mastication, in this case the jaw adductor muscles and orbital ligament, are more difficult to access, and empirically sourced numerical values for representing muscle force are correspondingly scarce.

Previous computer reconstructions of canid species have tackled this lack of directly observed data in a number of ways. Wroe *et al*. used the dry skull method after Thomason (Thomason, 1991) to determine jaw adductor force values from the single canid specimen (*Canis lupus dingo*) used in their reconstructive study of a dingo (Wroe *et al.,* 2007). Slater *et al*. (Slater *et al*., 2009) similarly calculated the jaw adductor cross sectional area using the dry skull method for one of the specimens used in their study (*Canis simensis*), and scaled the derived value to that of the larger (*Lycaon pictus*) and smaller specimens (*Canis mesomelas*) within the study. Tseng and Wang based the values used to load the fossil specimens in their study on maximum bite forces recorded in anaesthetized domestic dogs after Ellis (Ellis *et al*., 2008; Tseng and Wang, 2010). Both of these methods have limitations. The dry skull method fails to take the muscle architecture into account and may over or underestimate muscle force production values (Chapter Four) (Taylor and Vinyard, 2013). Bite force values derived from *in vivo* laboratory recordings are difficult to validate with real function, and domestic dogs exhibit neither the same body mass nor cranial morphology as extinct or extant wild species (Ellis *et al.*, 2008).

This thesis set out to provide detail of muscle architecture to inform the accuracy of models in future work. Very descriptive anatomical texts have fallen out of favour, and yet computer generated modelling techniques, such as finite element analysis and multibody dynamics depend upon quality input data to yield meaningful outcomes. In particular it is easy to overlook the effect of muscle architecture on muscle force capability. Both Taylor and Vinyard (Taylor and Vinyard, 2013) and Bates and Falkingham (Bates and Falkingham, 2018) note that the numerical value attributed to muscle fibre (fascicle) length in particular has a great impact on potential muscle force. However, muscle fascicle length is reported in only a limited number of studies, even in extant species (for example Herrel *et al.*, 2008; Eng *et al.*, 2009; Taylor and Vinyard, 2009; Hartstone-Rose *et al.,* 2012; Dickinson *et al.,* 2018; Hartstone-rose *et al.*, 2018). In this work, the fresh jaw adductor muscles were removed

from the cadavers and further analysed to describe their internal architecture and determine their muscle force production capabilities. Previous computer models attempting to recreate canid bite forces have attributed muscle force relative to muscle mass (Wroe *et al*., 2007; Slater *et al*., 2009), or distributed it evenly across total surface area (Tseng and Wang, 2010). However, as seen in Chapter Four, when muscle architecture is taken into account, this distribution is found to be erroneous. Temporalis contributes lower overall percentage to the muscle force than it does to muscle mass, whilst the opposite trend is seen in both the masseter and pterygoid muscles. Findings from this study recommend that when building FE models muscle force values are assigned to the regions of the skull relative to their force production capabilities on the skull, not their mass**.**

The role of the orbital ligament during biting was also explored. Little evidence was found to suggest that the postorbital ligament plays a role in dissipating masticatory forces. This finding suggests that there is no requirement to model the postorbital ligament in canine masticatory models. These outcomes may be of particular interest to those exploring function in extinct taxa, or other situations where analysis of soft tissue data is not possible. Witmer's inverted pyramid of inference demonstrates that assumptions made the early stages of reconstructive studies, e. g. in loading and constraining *in silico* models, may result in erroneous assumptions being made at higher levels of evolutionary and ecological understanding (Witmer, 1995; Bates and Falkingham, 2018).

6.4 Adapting to allometry

The common canid ancestor, *Hesperocyon*, was a small fox sized generalist, and following Cope's rule, evolutionary adaptations tended toward increasing body mass, firstly for the Hesperocyonids, then the Borophaginae, and finally the Caninae. Increase in body mass evidently results in changes in skull morphology. Some of these adaptations are directly

attributable to issues of scaling. Firstly, that the shape of the cranial module of the skull must adapt to accommodate the isometrically scaling temporalis on the negatively scaling cranium. This results in a disparity between the accommodation requirements of the brain and the temporalis. Shape analysis found that skull shape changes, such as widening of the zygomatic arches and enlargement of the sagittal crests are seen in species with higher body masses and allow the skull to accommodate the jaw adductor muscles on the negatively scaling cranial cavity. This finding may be of particular interest when considering specimens from the fossil record. That is, larger crests and other bony protuberances may not indicate relatively larger muscles but may be a product of scaling, particularly if the species concerned have evolved from a smaller ancestor. The second finding is that canids must offset the disadvantage of scaling a conserved muscle plan. Larger muscles are capable of generating relatively less muscle force than smaller muscles, due to having absolutely longer fascicles, which affects the efficiency of muscle force production abilities. This level of insight can only be considered using techniques that allow for details of the muscle architecture to be captured. The more frequently used, and more accessible method of calculating muscle force from dry skulls, Thomason's dry skull method (Thomason 1991), may only be reliable in canid specimens with a body mass of around 7-10kg. In the data set used in this thesis it was shown that below this mass the dry skull method underestimates force production capability and above this body mass, it overestimates it. The dry skull method effectively treats each muscle as a homogenous mass and does not consider the influence of the internal architecture on force production capability. The canid strategy to offset this disadvantage to muscle force production as species body mass increases, is to shorten the muzzle. Finally, the ability of head shape to withstand and attenuate forces generated during mastication was explored and finite element analyses found that the skull shapes found in small canids would risk ductile failure if scaled to greater volumes. The most demanding bite condition was canine bite at wide gape. In all species the zygomatic arches and caudal rostrum, both

dorsally and ventrally, experienced the highest levels of stress, strain and strain energy density during canine wide biting. This is the condition found when individuals are attacking and killing prey, a key behaviour in carnivorans. Morphological constraints during canine wide gape biting represent a limit in functional ability, namely, the size of prey that can be successfully tackled. There were no statistical differences between species of the strain energy density forces generated in any condition. However, when small species head shapes were scaled to the size of large species, the strain energy density exhibited up to a fifty-fold increase, indicating that the head shapes seen in small species are constrained by size, and that larger species demonstrate adaptations of shape to maintain function. Future work could investigate the structural limitations of the key areas of the skull in greater detail.

6.5 Is head shape a consequence of diet or is diet a consequence of head shape?

The common ancestor for all Caninae species, *Leptocyon*, was small and fox like. Small species have more efficient muscle force production capabilities and are self-sufficient and able to hunt and tackle prey alone. Their fast closing jaws allow for the hunting of small quick moving prey. All other canid morphotypes evolved from this ancestral condition and exhibit adaptations in diet and behaviour. Following Cope's rule, many species evolved to have a greater body mass. It has previously been reported that increase in body mass is concomitant with hypercarnivory as energetic demands of greater body mass make low risk foraging and predation of small prey untenable. Instead, large prey must be tackled to sustain the nutritional requirements of the derived condition (Carbone *et al.*, 1999; Van Valkenburgh *et al*., 2004). An important finding of this study is that large species cannot maintain the head shape of the smaller species. The changes in head morphology that are allied to increased body mass necessarily result in changes of diet and hunting strategy. In other words, there may be a morphological as well as a physiological driver pushing large canids toward hypercarnivory.

A key trait seen in larger canids is a comparatively short rostral component of the skull and a shortened mandible. The resultant short muzzle of the large species compensates for the loss in muscle efficiency seen in larger species, as, in energetic terms, short out levers are more efficient than long out levers. The negative consequence of reducing muzzle length is the reduction in speed with which the canine teeth can be brought together during biting, e.g. during prey capture. In addition, analyses of the positioning and orientation of the temporalis relative to the occlusal plane indicate a clear distinction between dietary groups. Small prey and generalist species revealed more horizontally orientated temporalis muscles, and the large prey hunters displayed more vertically aligned temporalis muscles. The basic geometries of this finding infer that this arrangement should advantage fast jaw closure in the small prey and generalist species, whilst the large prey specialists would be able to sustain a strong bite. This is evidenced by the hunting strategy where species with short rostra inflict sustained bites on their prey. However, only moderate shortening of the facial component can occur in canids as their dentition appears to be conserved, and rostral length must be maintained to accommodate the teeth (Tseng and Wang, 2011). Canids may also be phylogenetically, morphologically and functionally constrained by their olfactory apparatus. Canids have around 1.5 - 2 times the volume of nasal turbinates than similarly sized felids (Van Valkenburgh *et al.*, 2004; 2014). This reflects one of the different hunting strategies of the two families. Canids rely on olfaction to a greater degree than felids, who have a greater reliance on vision. (Werdelin, 1989; Van Valkenburgh *et al.*, 2004; Van Valkenburgh *et al.*, 2014). Again, a reasonably long rostral length must be maintained to house the olfactory apparatus. These potential constraints limit the range of possible phenotypic variants available to canids (Figueirido *et al.*, 2011), which in turn limits masticatory performance. The overall limitation on bite force production capabilities of the individual necessitates the collaborative pursuit pack hunting behaviour that is seen in the hypercarnivorous canids. Large prey, typically ungulates, are pursued, often over great

distances, until exhausted. They are then restrained by multiple individuals and killed by abdominal evisceration and blood loss. The results of this study suggest that morphological as well as physiological pressures had a role in the evolution of pack hunting as canid body mass increased. The work reported here linking head shape to functional limitations and hence to specific dietary specialisms sets the foundations for a greater understanding of selective pressures relating to body mass, hunting strategy and diet in the Caninae. Future investigations into other large carnivoran families may consider how skull size and shape changes impact jaw adductor muscle force production and bite force capabilities.

6.6 Head shape in the domestic canid breeds.

Future work could also consider the findings from this thesis when investigating implications of head shape in the domestic dog (*Canis lupus familiaris*). The skull differs more in size and shape in domestic dogs than in any other domestic species (Wayne, 1986, 2001; Evans and De Lahunta, 2013; Packer *et al.*, 2015). Although the exact dating of canid domestication remains controversial most recent sources concur it was around 30,000 years ago (Sablin and Khlopachev, 2002; Germonpré *et al.*, 2009; Pitulko and Kasparov, 2017). Early breed specialisations existed to select for hunting, fighting or running type dogs, and have been evidenced in the archaeological record as dating from at least 9000 years ago (Clutton-Brock, 1995; Lee *et al.*, 2015; Pitulko and Kasparov, 2017). However, extreme specialisation for both behavioural and physical traits occurred much more recently, particularly within the last two hundred years (Clutton-Brock, 1995; Schoenebeck and Ostrander, 2013). Although human intervention replaces evolutionary selection pressures, a remarkably wide range of domestic breed morphologies exist. Notably, body mass range reflects that seen in wild species, from the 1.5kg Chihuahua to the 90kg Neapolitan mastiff or Saint Bernard. The form and function of domestic dog breed head shapes also exhibits some superficial similarities with those seen in the wild species. Breeds with dolichocephalic head shapes such as greyhounds and salukis

have been bred to catch small prey at high speed with their slender fast snapping jaws. Brachycephalic breeds such as bulldogs and mastiffs on the other hand, were originally bred to attack and maintain a grip on large prey. These morphotypes mirror those seen in wild canids and, up to a point, they are functionally successful. However, all domestic dog breeds are a subspecies of just one species, *Canis lupus*. Of particular clinical interest is the functionality of brachycephalic and extreme toy breed head shapes. The chief modification of selective breeding is the radical shortening of the bones of the facial component of the skull. Lesser changes are also seen in other bones of the skull, for example the tympanic bullae are also reduced, and the zygomatic arches widened. Such changes are brought about by a number of genetic mechanisms including the early fusion of cranial sutures and synchondroses, and dysplasias promoting abnormal bone growth (Schoenebeck and Ostrander, 2013; Geiger and Haussman, 2016). The extreme form seen in brachycephalic dog heads is testament to the potential range of phenotypic variation that this *Canis lupus* subspecies is capable of. The fact that such extreme forms can be attained through selective breeding in domesticated animals implies that head shape in canids is not limited by the bony constituents of the skull, i.e. they are potentially highly labile, but that species occupying these morphospaces are not functionally viable in natural settings. This may be due to several factors including potential structural failure under normal hunting conditions, inability to generate or maintain the functional bite force required to tackle prey, or the lack of concomitant reduction in the soft tissues. Although the bony tissues of the head are clearly very plastic, the soft tissues appear to be less so. This can be seen in the surplus amounts of skin, overly large tongue, elongated soft palate, enlarged tonsils, exophthalmia and occluded nasal cavities that are typical of brachycephalic breeds. The excessive amount of soft tissue can cause debilitating conditions. Brachycephalic dogs are particularly prone to diseases of the upper airways, eyes, hard palate, skin and dentition. In addition, they are reported to have high incidences of diseases associated with the central nervous system such

as gliomas, astrocytomas and syringomyelia (Hayes *et al.,* 1975; Nafe, 1990; LeCouteur, 1999; Snyder *et al.*, 2006; LeCouteur and Withrow, 2007).

Some studies have attempted to geometrically categorise brachycephalic skulls with a view to identifying animals at risk from such conditions (Stockard and James, 1941; Regodón *et al.*, 1993; Hussein *et al*., 2012; Evans and De Lahunta, 2013), although the particular metrics used are somewhat disputed. I am unaware of any published work quantifying soft tissue ratios to skull shapes in domestic dogs. Findings in this study describe the wide range of conditions found in naturally evolved wild species. This work may help inform acceptable parameters for normal morphology and function in domestic breeds. A deeper understanding of the soft tissue relationship to the skull could aid in the understanding of the anatomical basis of disease and begin to identify and quantify risk factors. With an increased emphasis on companion animal welfare there is abundant potential for further studies regarding the biomechanical function of head shape in domestic dog breeds. For example, the breeds selected for extreme brachycephalic modification tend to be small breeds such as pugs and Pekingese. In the wild species, it is those with greater body mass that exhibit moderate shortening of the face. Therefore, is the problem of accommodation of jaw adductor muscles compounded by the small body mass of brachycephalic breeds? Are breeds with extreme morphologies at risk of structural failure due to having abnormal head shapes? Is the bite force of brachycephalic breeds compromised? With increased concern in brachycephalic dog welfare it would be of interest to both clinicians and dog breeders to identify the limits of normal function in head morphology.

6.7 Summary

The empirical and experimental findings from this study document the anatomy of canid jaw adductor muscles and allowed insight into their functional ability and relationships to head morphology. The form of the skull is associated with the form of the jaw adductor muscles,

which appear to be less labile than the skeletal components of the head. Canids may therefore be constrained in adaptability and have remained as functional generalists, never exploring the highly specialized niches that, for instance, the felids have exploited. Constraints on morphology lead to changes in diet and behavior. For example, the divergence of canids into hypercarnivory may rely more on behavioral rather than functional adaptations, as the ability to tackle large prey relies on working in packs, rather than radically changing morphology to increase relative bite force.

This work provides both original data and methodological recommendations for future projects. It is hoped that these findings can help to inform future studies on masticatory function in extant and extinct wild canids and domesticated canids.

Bibliography.

Abe, S., Hiroki, E., Iwanuma, O., Sakiyama, K., Shirakura, K.,Hirose, D., Shimoo, Y., Suzuki, M., Ikari, Y., Kikuchi, R., Ide, Y., Yoshimari, M., (2008). Relationship between function of masticatory muscle in mouse and properties of muscle fibers. The Bulletin of Tokyo Dental College, 49(2), pp. 53–58.

Abouheif, E. and Fairbairn, D. J., (1997). A Comparative Analysis of Allometry for Sexual Size Dimorphism: Assessing Rensch's Rule. The American Naturalist, 149(3), pp. 540–562.

Adams, D., Rohlf, J. L. and Slice, D., (2013). A field comes of age: geometric morphometrics in the 21 st century. Hystrix, the Italian Journal of Mammalogy, 24(1), pp. 7–14.

Agnarsson, I., Kuntner, M. and May-Collado, L. J., (2010). Dogs, cats, and kin: A molecular species-level phylogeny of Carnivora. Molecular Phylogenetics and Evolution, 54(3), pp. 726–745.

Al Dayeh, A. A., and Herring, S. W., (2014). Compressive and tensile mechanical properties of the porcine nasal septum. Journal of Biomechanics, 47(1), 154–161.

Altmann, J., Schoeller, D., Altmann, S. A., Muruthi, P. and Sapolsky, R. M., (1993). Body size and fatness of free-living baboons reflect food availability and activity levels. American Journal of Primatology. Wiley Online Library, 30(2), pp. 149–161.

Anapol, F. and Barry, K., (1996). Fiber architecture of the extensors of the hindlimb in semiterrestrial and arboreal guenons. American Journal of Physical Anthropology, 99(3), pp. 429–447.

Anapol, F., Shahnoor N, Ross CF., (2008). Scaling of reduced physiological cross-sectional area in primate muscles of mastication. In: Vinyard C; Ravosa MJ; Wall C, editors. Primate craniofacial function and biology. New York: Springer. pp. 201–216.

Andersson, F. (2016). Finite Element Modeling of Skull Fractures: Material model improvements of the skull bone in the KTH FE head model. Masters thesis. KTH Royal Institute of Technology.

Andersson, K., (2004). Elbow-joint morphology as a guide to forearm function and foraging behaviour in mammalian carnivores. Zoological Journal of the Linnean Society, 142(1), pp. 91–104.

Andersson, K., (2005). Were there pack-hunting canids in the Tertiary, and how can we know? Paleobiology, 31(1), pp. 56–72.

Andersson, K. and Werdelin, L.,(2003). The evolution of cursorial carnivores in the Tertiary: implications of elbow-joint morphology. Proceedings of the Royal Society B: Biological Sciences, 270(Suppl_2), pp. S163–S165.

Ange, K., Crissey, S. D., Doyle, C., Lance, K. and Hintz, H., (2001). A survey of African and Asian elephant diets and measured body dimensions compared to their estimated nutrient requirements. Proceedings of the Nutrifion Advisory Group (NAG), 4, pp. 5–14.

Angerbjorn, A., (2004). Arctic fox (*Alopex lagopus*). Status Survey and Conservation Action Plan, Canids : Foxes, Wolves, Jackals and Dogs, pp. 117–123.

Angerbjörn, A., Hersteinsson, P., Tannerfeldt, M., (2004). Arctic foxes: Consequences of resource predictability in the Arctic fox—two life history strategies. In The Biology and Conservation of Wild Canids. Oxford: Oxford University Press.

Ankel-Simons, F., (2007). Skull. In: Primate anatomy: an introduction. Third ed. London: Elsevier. pp. 161–197.

Anyonge, W., Baker, A., (2006). Craniofacial morphology and feeding behavior in *Canis dirus*, the extinct Pleistocene dire wolf. Journal of Zoology, 269(3), 309–316.

Armfield, B. A., Zheng, Z., Bajpai, S., Vinyard, C.J., Thewissen.J.G.M., (2013). Development

and evolution of the unique cetacean dentition. PeerJ, 1, p. e24.

Aryal, A., Panthi, S., Barraclough, R. K., Bencini, R., Adhikari, B., Ji, W., Raubenheimer, D., (2015). Habitat selection and feeding ecology of dhole (*Cuon alpinus*) in the Himalayas. Journal of Mammalogy, 96(1), 47–53.

Asa, C., Valdespino, C., Cuzin, F., (2004). Fennec fox (*Vulpes zerda*). Canids: Foxes, Wolves, Jackals, and Dogs. Status Survey and Conservation Action Plan, pp. 205–209.

Asahara, M., Takai, M., (2017). Estimation of diet in extinct raccoon dog species by the molar ratio method. Acta Zoologica, 98(3), pp. 292–299.

Ashman, R. B., Jae Young Rho., (1988). Elastic modulus of trabecular bone material. Journal of Biomechanics, 21(3), 177–181.

Attard, M. R. G., Chamoli, U., Ferrara, T. L., Rogers, T. L., Wroe, S., (2011). Skull mechanics and implications for feeding behaviour in a large marsupial carnivore guild: The thylacine, Tasmanian devil and spotted-tailed quoll. Journal of Zoology, 285(4), 292–300.

Audet, A. M., Robbins, C. B., Larivière, S., (2002). Alopex lagopus. Mammalian Species, 1410(713), pp. 1–10.

Auperrin, A., Delille, R., Lesueur, D., Bruyère, K., Masson, C., Drazétic, P., (2014). Geometrical and material parameters to assess the macroscopic mechanical behaviour of fresh cranial bone samples. Journal of Biomechanics, 47(5), 1180–1185.

Ausiello, P., Apicella, A., Davidson, C. L., (2002). Effect of adhesive layer properties on stress distribution in composite restorations--a 3D finite element analysis. Dental Materials : Official Publication of the Academy of Dental Materials, 18(4), 295–303.

Baker, P. J., Harris, S., (2004). Red foxes: The behavioural ecology of red foxes in urban Bristol. In The Biology and Conservation of Wild Canids. Oxford: Oxford University Press.

Balius, R., Alomar, X., Rodas, G., Miguel-Pérez, M., Pedret, C., Dobado, M. C., Blasi, J. and Koulouris, G., (2013). The soleus muscle: MRI, anatomic and histologic findings in cadavers with clinical correlation of strain injury distribution. Skeletal Radiology, 42(4), pp. 521–530.

Barbeito-Andrés, J., Anzelmo, M., Ventrice, F. and Sardi, M. L., (2012). Measurement error of 3D cranial landmarks of an ontogenetic sample using Computed Tomography. Journal of Oral Biology and Craniofacial Research, 2(2), pp. 77–82.

Bardeleben, C., Moore, R. L. and Wayne, R. K., (2005). A molecular phylogeny of the Canidae based on six nuclear loci. Molecular Phylogenetics and Evolution, 37(3), pp. 815-831.

Bartolini Lucenti, S. and Rook, L., (2016). A review on the Late Villafranchian medium-sized canid Canis arnensis based on the evidence from Poggio Rosso (Tuscany, Italy). Quaternary Science Reviews. Elsevier Ltd, 151, pp. 58–71.

Bateman, P. W. and Fleming, P. A., (2012). Big city life: Carnivores in urban environments. Journal of Zoology, 287(1), pp. 1–23.

Bates, K. T. and Falkingham, P. L. (2018). The importance of muscle architecture in biomechanical reconstructions of extinct animals: a case study using Tyrannosaurus rex. Journal of Anatomy, In Press.

Baverstock, H., Jeffery, N.S., Cobb, S.N., (2013). The morphology of the mouse masticatory musculature. Journal of Anatomy, 223, pp. 43-60.

Bauchot, R., (1978). Encephalization in vertebrates. Brain, Behaviour and Evolution, 15(1), pp. 1–18.

Begonia, M., Dallas, M., Johnson, M. L. and Thiagarajan, G., (2017). Comparison of strain measurement in the mouse forearm using subject-specific finite element models, strain gaging , and digital image correlation. Biomechanics and Modeling in Mechanobiology. Springer Berlin Heidelberg, 16(4), pp. 1243–1253.

Berta, A., (1987). Origin, diversification, and zoogeography of the South American Canidae. Fieldiana: Zoology, New Series, 39, pp. 455–471.

Biknevicius, A. R. and Ruff, C. B., (1992). The structure of the mandibular corpus and its relationship to feeding behaviours in extant carnivorans. Journal of Zoology, 228(3), pp. 479–507.

Binder, W. J. and Van Valkenburgh, B., (2000). Development of bite strength and feeding behaviour in juvenile spotted hyenas (Crocuta crocuta) Journal of Zoology, 252(3), pp. 273–283.

Boillat, C. S., Gaschen, F. P., Hosgood, G. L., (2000). Assessment of the relationship between body weight and gastrointestinal transit times measured by use of a wireless motility capsule system in dogs. American Journal of Veterinary Research, 71(8), pp.898-902.

Bolker, J. A., (2000). Modularity in Development and Why It Matters to Evo-Devo1. American Zoologist, 40(5), pp. 770–776.

Bookstein, F. L., (1986). Size and Shape Spaces for Landmark Data in Two Dimensions. Statistical Science, 1 (2), pp. 181-222.

Bookstein, F. L., (1997). Morphometric tools for landmark data: geometry and biology. Cambridge University Press.

Bookstein, F., Schafer, K., Prossinger, H., Seidler, H., Fieder, M., Stringer, C., Weber, G.W., Arsuaga, J-L., Slice, D., Rohlf, J.,Recheis, W., Mariam, A.J., Marcus, L.F., (1999). Comparing frontal cranial profiles in archaic and modern homo by morphometric analysis. *Anatomical Record*, 257(6), pp. 217–224.

Boruah, S., Subit, D. L., Paskoff, G. R., Shender, B. S., Crandall, J. R., Salzar, R. S. (2016). Influence of bone microstructure on the mechanical properties of skull cortical bone – A combined experimental and computational approach. Journal of the Mechanical

Behavior of Biomedical Materials, 65, 688–704.

Bourke, J., Wroe, S., Moreno, K., McHenry, C. and Clausen, P., (2008). Effects of gape and tooth position on bite force and skull stress in the dingo (*Canis lupus dingo*) using a 3-dimensional finite element approach. PLoS ONE, 3(5), pp. 1–5.

Bousdras, V. A., Cunningham, J. L., Ferguson-Pell, M., Bamber, M. A., Sindet-Pedersen, S., Blunn, G. and Goodship, A. E., (2006). A novel approach to bite force measurements in a porcine model in vivo. International Journal of Oral and Maxillofacial Surgery, 35(7), pp. 663–667.

Brenner, E.,(2014). Human body preservation - old and new techniques. Journal of Anatomy, 224(3), pp. 316–344.

Bright, J. A. and Gröning, F., (2011). Strain accommodation in the zygomatic arch of the pig: A validation study using digital speckle pattern interferometry and finite element analysis. Journal of Morphology, 272 (11), pp.1388-1398.

Bright, J. A. and Rayfield, E. J., (2011a). Sensitivity and ex vivo validation of finite element models of the domestic pig cranium. Journal of Anatomy, 219(4), pp. 456–471.

Bright, J. A., Rayfield, E. J., (2011b). The Response of Cranial Biomechanical Finite Element Models to Variations in Mesh Density. Anatomical Record, 294(4), pp.610–620.

Bruce, S. J. Guilford, W.G., Hedderley, D.I., McCauley, M., (1999). Development of reference intervals for the large intestinal transit of radiopaque markers in dogs. Veterinary Radiology and Ultrasound, 40(5), pp. 472–476.

Brunner, S., Bryden, M. M. and Shaughnessy, P. D., (2004). Cranial ontogeny of otariid seals. Systematics and Biodiversity, 2(1), pp. 83–110.

Brunt, L. H., Norton, J. L., Bright, J. A., Rayfield, E. J. and Hammond, C. L., (2015). Finite element modelling predicts changes in joint shape and cell behaviour due to loss of muscle strain in jaw development. Journal of Biomechanics, 48(12), pp. 3112–3122.

Brzeski, K. E., DeBiasse, M.B., Rabon Jr, D.R., Chamberlain, M.J, Taylor, S.S., (2016). Mitochondrial DNA variation in southeastern pre-columbian canids. Journal of Heredity, 107(3), pp. 287–293.

Buckland-Wright, J. C., (1978). Bone structure and the patterns of force transmission in the cat skull (Felis catus). Journal of Morphology. Wiley Online Library, 155(1), pp. 35–61.

Budras, K. D., McCarthy, P. H., Fricke, W., Richter, R., Horowitz, A., Berg, R., (2007). *Anatomy of the dog: an illustrated text*. Schlütersche.

Buezas, G., Becerra, F. and Vassallo, A., (2017). Cranial suture complexity in caviomorph rodents (Rodentia; Ctenohystrica). Journal of Morphology, 278(8), pp. 1125–1136.

Burkhart, T. A., Andrews, D. M. and Dunning, C. E., (2013). Finite element modeling mesh quality, energy balance and validation methods: A review with recommendations associated with the modeling of bone tissue. Journal of Biomechanics. Elsevier, 46(9), pp. 1477–1488.

Burn, A.K., Herring, S.W., Hubbard, R., Zink, K., Rafferty, K., Lieberman, D.E., (2010). Dietary consistency and the midline sutures in growing pigs. Orthodontics and Craniofacial Research, 13(2), pp. 106–113.

Burrows, A. M., (2018). Functional Morphology of Mimetic Musculature in Primates : How Social Variables and Body Size Stack up to Phylogeny. Anatomical Record, 301 (2) pp. 202–215.

Butler, D. L., Guan, Y., Kay, M. D., Cummings, J. F., Feder, S. M., Levy, M. S., (1992). Location-dependent variations in the material properties of the anterior cruciate ligament. Journal of Biomechanics, 25(5), pp. 511–518.

Button, K. S., Ioannidis, J. P. A., Mokrysz, C., Nosek, B. A., Flint, J., Robinson, E. S. J. and Munafò, M. R., (2013). Power failure: Why small sample size undermines the reliability of neuroscience. Nature Reviews Neuroscience. Nature Publishing Group, 14(5), pp. 365–376.

Buzug, T. M., (2008). Computed tomography. From photon statistics to modern cone-beam CT. Berlin : Springer.

Byrd, B. F., Cornellas, A., Eerkens, J.W., Rosenthal, J.S., Carpenter,T.R., Leventhal, A., Leonard, A.J., (2013). The role of canids in ritual and domestic contexts: New ancient DNA insights from complex hunter-gatherer sites in prehistoric Central California. Journal of Archaeological Science. Elsevier Ltd, 40(4), pp. 2176–2189.

Byron, C. D., (2009). Cranial Suture Morphology and its Relationship to Diet in Cebus. Journal of Human Evolution. Elsevier Ltd, 57, pp. 649–655.

Byron, C., Segreti, M., Hawkinson, K., Herman, K., Patel, S., (2018). Dietary material properties shape cranial suture morphology in the mouse calvarium. Journal of Anatomy.

Cachel, S.S., (1984). Growth and allometry in primate masticatory muscles. Archives of Oral Biology, 29(4), pp. 287–293.

Carbone, C., Mace, G. M., Roberts, S. C. and Macdonald, D. W., (1999). Energetic constraints on the diet of terrestrial carnivores. *Nature*. Nature Publishing Group, 402(6759), p. 286.

Carbone, C., Toit, J. T. Du and Gordon, I. J., (1997). Feeding Success in African Wild Dogs: Does Kleptoparasitism by Spotted Hyenas Influence Hunting Group Size? The Journal of Animal Ecology, 66(3), p. 318.

Cartmill, M., (1970). The orbits of arboreal mammals: a reassessment of the arboreal theory of primate evolution. Ph.D. Thesis, The University of Chicago.

Cartmill, M., (1980). Morphology, function, and evolution of the anthropoid postorbital

septum, in Evolutionary biology of the New World monkeys and continental drift. Springer, pp. 243–274.

Carver, E. and Carver, B., (2012). Medical Imaging - E-Book: Techniques, Reflection and Evaluation. Churchill Livingstone.

Cheung, J. T. M., Zhang, M., Leung, A. K. L., Fan, Y. B., (2005). Three-dimensional finite element analysis of the foot during standing - A material sensitivity study. Journal of Biomechanics, 38(5), pp. 1045–1054.

Cheverud, J. M. (1996). Developmental Integration and the Evolution of Pleiotropy. Integrative and Comparative Biology, 36(1), pp. 44–50.

Choi, K., Kuhn, J. L., Ciarelli, M. J., Goldstein, S. A., (1990). The elastic moduli of human subchondral, trabecular, and cortical bone tissue and the size-dependency of cortical bone modulus. Journal of Biomechanics, 23(11), pp. 1103–1113.

Christiansen, P., (2008). Evolution of skull and mandible shape in cats (Carnivora: Felidae). PLoS ONE, 3(7).

Christiansen, P., Adolfssen, J.S., (2005). Bite forces, canine strength and skull allometry in carnivores (Mammalia, Carnivora). Journal of Zoology, 266(2), pp. 133–151.

Christiansen, P., Wroe, S., (2007). Bite forces and evolutionary adaptations to feeding ecology in carnivores. Ecology, 88(2), pp. 347–358.

CIBC., (2016). Seg3D: Volumetric Image Segmentation and Visualization.

Clair, E. M. S. T. and Reback, N., (2018). Craniomandibular Variation in Phalangeriform Marsupials : Functional Comparisons with Primates. *Anatomical Record*, 301 (2),pp. 227–255.

Clark, H. O., (2005). *Otocyon megalotis.* Mammalian Species, 766(766), pp. 1–5.

Clark, H. O. J., Murdoch, J. D., Newman, D. P., Sillero-Zubiri, C., (2009). *Vulpes corsac*

(Carnivora: Canidae). Mammalian Species, pp. 832, 1–8.

Clausen, P., Wroe, S., Mchenry, C., Moreno, K. and Bourke, J., (2008). The vector of jaw muscle force as determined by computer-generated three dimensional simulation : A test of Greaves ' model. Journal of Biomechanics, 41 (15), pp. 3184–3188.

Clauss, M. and Hatt, J. M., (2006). The feeding of rhinoceros in captivity. International Zoo Yearbook, 40(1), pp. 197–209.

Clauss, M., Hofmann, R.R., Streich, W.J., Fickel, J., Hummel, J., (2008). Higher masseter muscle mass in grazing than in browsing ruminants. Oecologia, 157(3), pp. 377–385.

Close, R. I., (1972). Dynamic properties of mammalian skeletal muscles. Physiological reviews. Am Physiological Soc, 52(1), pp. 129–197.

Clutton-Brock, J., (1995). Origins of the dog: domestication and early history. The domestic dog: Its evolution, behaviour and interactions with people. Cambridge University Press Cambridge, pp. 7–20.

Conith, A. J., Meagher, M. A. and Dumont, E. R., (2018). The Influence of Climatic Variability on Morphological Integration, Evolutionary Rates, and Disparity in the Carnivora. The American Naturalist. The University of Chicago Press, 191(6), pp. 704–715.

Coogan, J. S., Kim, D.-G., Bredbenner, T. L. and Nicolella, D. P., (2018). Determination of sex differences of human cadaveric mandibular condyles using statistical shape and trait modeling. Bone, 106, pp. 35–41.

Cooke, S. B. and Terhune, C. E., (2015). Form, Function, and Geometric Morphometrics. Anatomical Record, 298(1), pp. 5–28.

Copes, L. E., Kimbel, W. H., (2016). Cranial vault thickness in primates: Homo erectus does not have uniquely thick vault bones. Journal of Human Evolution, *90*, 120–134.

Correro-Shahgaldian, M. R., Introvigne, J., Ghayor, C., Weber, F. E., Gallo, L. M., Colombo, V., (2016). Properties and Mechanobiological Behavior of Bovine Nasal Septum Cartilage. Annals of Biomedical Engineering, 44(5), pp. 1821–1831.

Courant, R., (1943). Variational methods for the solution of problems of equilibrium and vibrations. Bulletin of the American mathematical Society, 49(1), pp. 1–23.

Cox, P. G., (2008). A quantitative analysis of the Eutherian orbit: Correlations with masticatory apparatus. Biological Reviews, 83(1), pp. 35–69.

Cox, P. G., (2017). The jaw is a second-class lever in Pedetes capensis (Rodentia : Pedetidae). PeerJ, Vol 5, p e3741.

Cox, P. G. and Baverstock, H., (2016). Masticatory Muscle Anatomy and Feeding Efficiency of the American Beaver, Castor canadensis (Rodentia, Castoridae). Journal of Mammalian Evolution. Journal of Mammalian Evolution, 23(2), pp. 191–200.

Cox, P. G., Fagan, M. J., Rayfield, E. J. and Jeffery, N., (2011). Finite element modelling of squirrel, guinea pig and rat skulls: Using geometric morphometrics to assess sensitivity. Journal of Anatomy, 219(6), pp. 696–709.

Cox, P. G., Kirkham, J., Herrel, A., (2013). Masticatory biomechanics of the Laotian rock rat, *Laonastes aenigmamus* , and the function of the zygomaticomandibularis muscle. PeerJ, 1, e160.

Cox, P. G., Rayfield, E. J., Fagan, M. J., Herrel, A., Pataky, T. C. and Jeffery, N., (2012). Functional evolution of the feeding system in rodents. *PLoS ONE*, 7(4). doi: 10.1371/journal.pone.0036299.

Creel, S. and Creel, N. M., (1995). Communal hunting and pack size in African wild dogs, Lycaon pictus. Animal Behaviour, 50(5), pp. 1325–1339.

Creel, S. and Creel, N. M., (2002). The African wild dog : behavior, ecology, and conservation. New Jersey, USA: Princeton University Press (Monographs in behavior and

ecology).

Cuff, A. R., Bright, J. A. and Rayfield, E. J., (2015). Validation experiments on finite element models of an ostrich (*Struthio camelus*) cranium. PeerJ, 3, p. e1294. doi: 10.7717/peerj.1294.

Curth, S., Fischer, M. S. and Kupczik, K., (2017). Patterns of integration in the canine skull: an inside view into the relationship of the skull modules of domestic dogs and wolves. Zoology, 125, pp. 1-9.

Curtis, A. A. and Van Valkenburgh, B., (2014). Beyond the sniffer: Frontal sinuses in carnivora. Anatomical Record, 297(11), pp. 2047–2064.

Curtis, N., Kupczik, K., Higgins, P. O., Moazen, M., Fagan, M. and Al, C. E. T., (2008). Predicting Skull Loading : Applying Multibody Dynamics Analysis to a Macaque Skull. The Anatomical Record: Advances in Integrative Anatomy and Evolutionary Biology, 291(5), 491–501.

Curtis, N., Jones, M. E. H., Evans, S. E., Higgins, P. O. and Fagan, M. J. (2013). Cranial sutures work collectively to distribute strain throughout the reptile skull. Journal of the Royal Society Interface, 10 (86) p20130442.

Curtis, N., Witzel, U., Fitton, L., O'Higgins, P. and Fagan, M., (2011). The mechanical significance of the temporal fasciae in macaca fascicularis: An investigation using finite element analysis. Anatomical Record, 294(7), pp. 1178–1190.

Cypher, B. L. and Spencer, K. A., (1998). Competitive Interactions Between Coyotes. Journal of Mammalogy, 79(1), pp. 204–214.

Dale, B. M., Brown, M. A. and Semelka, R. C., (2015) MRI : basic principles and applications. Chichester, West Sussex : Wiley Blackwell.

Damasceno, E. M., Hingst-Zaher, E. and Astua, D., (2013). Bite force and encephalization in the Canidae (Mammalia: Carnivora). Journal of Zoology, 290(4), pp. 246–254.

Davis, D.D., (1955). Masticatory apparatus in the spectacled bear, *Tremarctos ornatus*. Chicago Natural History Museum.

Davis, D.D., (1964). The giant panda : a morphological study of evolutionary mechanisms. Chicago Natural History Museum.

Davis, J. L., Santana, S. E., Dumont, E. R. and Grosse, I. R., (2010). Predicting bite force in mammals: two-dimensional versus three-dimensional lever models. Journal of Experimental Biology, 213(11), pp. 1844–1851.

Davis, J. S., (2014). Functional morphology of mastication in musteloid carnivorans. Ohio University.

Davis, W. E., Templer, J. and Parsons, D. S., (1996). Anatomy of the paranasal sinuses. Otolaryngologic clinics of North America, 29(1), p. 57—74.

de Mello Beisiegel, B. and Zuercher, G., (2005). Speothos venaticus. American Society of Mammalogists, (783), pp. 1–6.

De Souza Lima, E., Pinto Jorge, R. S., Dalponte, J. C., (2009). Habitat use and diet of bush dogs, *Speothos venaticus*, in the Northern Pantanal, Mato Grosso, Brazil. Mammalia, 73(1), pp. 13–19.

Dechow, P. C. and Carlson, D. S., (1983). A method of bite force measurement in primates. Journal of biomechanics, 16(10), pp. 797–802.

Delisle, I. and Strobeck, C., (2005). A phylogeny of the Caniformia (order Carnivora) based on 12 complete protein-coding mitochondrial genes. Molecular Phylogenetics and Evolution, 37(1), pp. 192-201.

Dessem, D., (1989). Interactions between jaw-muscle recruitment and jaw-joint forces in Canis familiaris. Journal of anatomy, 164, pp. 101–121.

Dessem, D. and Druzinsky, R. E., (1992). Jaw muscle activity in ferrets, *Mustela putorius furo*. Journal of Morphology, 213(2), pp. 275–286.

Dickinson, E., Stark, H. and Kupczik, K., (2018). Non-destructive determination of muscle architectural variables through the use of diceCT. The Anatomical Record, 301(2), pp. 363–377.

Doncaster, A. C. P., Dickman,C.R., Macdonald D.W., (1990). Feeding Ecology of Red Foxes (Vulpes vulpes) in the City of Oxford, England. Journal of Mammalogy 71(2), pp. 188–194.

Douglass, J. K., Wcislo, W. T. (2010). An inexpensive and portable microvolumeter for rapid evaluation of biological samples. BioTechniques, 49(2), pp. 566–572.

Drake, A. G., Coquerelle, M. and Colombeau, G., (2015). 3D morphometric analysis of fossil canid skulls contradicts the suggested domestication of dogs during the late Paleolithic. Scientific Reports, 5, p. 8299.

Drake, A. G., Coquerelle, M., Kosintsev, P. A., Bachura, O. P., Sablin, M., Gusev, A. V., Fleming, L. S. and Losey, R. J., (2017). Three-Dimensional Geometric Morphometric Analysis of Fossil Canid Mandibles and Skulls. Scientific Reports. 7(1), pp. 1–8.

Drake, A. G. and Klingenberg, C. P., (2008). The pace of morphological change: historical transformation of skull shape in St Bernard dogs. Proceedings of the Royal Society B: Biological Sciences, 275(1630), pp. 71–76.

Drake, A. G. and Klingenberg, C. P., (2010). Large-Scale Diversification of Skull Shape in Domestic Dogs: Disparity and Modularity. The American Naturalist, 175(3), pp. 289–301.

Druzhkova, A. S., Thalmann, O., Trifonov, V. A., Leonard, J. A., Vorobieva, N. V., Ovodov, N. D., Graphodatsky, A. S., Wayne, R.K., (2013). Ancient DNA Analysis Affirms the Canid from Altai as a Primitive Dog. PLoS ONE, 8(3).

Druzinsky, R. E., (2010). Functional Anatomy of Incisal Biting in Aplodontia rufa and

Sciuromorph Rodents – Part 1: Masticatory Muscles, Skull Shape and Digging. Cells Tissues Organs, 191(6), pp. 510–522.

Druzinsky, R. E., Doherty, A. H. and De Vree, F. L., (2011). Mammalian masticatory muscles: Homology, nomenclature, and diversification. Integrative and Comparative Biology, 51(2), pp. 224–234.

Dryden, I. L. and Mardia, K. V., (1998). Statistical shape analysis. Wiley.

Drygala, F., Zoller, H., (2014). Diet composition of the invasive raccoon dog (*Nyctereutes procyonoides)* and the native red fox (*Vulpes vulpes*) in north-east Germany. Hystrix, the Italian Journal of Mammalogy, 24(2), pp. 190–194.

Dumont, E. R., Davis, J. L., Grosse, I. R. and Burrows, A. M., (2011). Finite element analysis of performance in the skulls of marmosets and tamarins. *Journal of Anatomy*, 218(1), pp. 151–162.

Dumont, E. R., Grosse, I. R., Slater, G. J., (2009). Requirements for comparing the performance of finite element models of biological structures. Journal of Theoretical Biology, 256(1), pp. 96–103.

Dumont, E. R. and Herrel, A., (2003). The effects of gape angle and bite point on bite force in bats. The Journal of experimental biology, 206(Pt 13), pp. 2117–2123.

Dumont, E. R., Piccirillo, J. and Grosse, I. R.. (2005). Finite-element analysis of biting behavior and bone stress in the facial skeletons of bats. Anatomical Record - Part A Discoveries in Molecular, Cellular, and Evolutionary Biology, 283(2), pp. 319–330.

Durbin, L. S., Venkataraman, A., Hedges, S., Duckworth, W. (2004). Dhole (*Cuon alpinus*). Canids: Foxes, Wolves, Jackals and Dogs. Status Survey and Conservation Action Plan, IUCN/SSC Canid Specialist Group, Gland, Switzerland, 210–219.

Dutel, H., Sharp, A. C., Jones, M. E. H., Evans, S. E., Fagan, M. J. and Gröning, F., (2017). Comparative skull biomechanics in Varanus and Salvator “Tupinambis” PeerJ PrePrints.

Dyce, K. M., Sack, W. O. and Wensing, C. J. G., (2009). Textbook of veterinary anatomy. Elsevier Health Sciences.

Echarri, S. and Prevosti, F. J., (2015). Differences in mandibular disparity between extant and extinct species of metatherian and placental carnivore clades. Lethaia, 48(2), pp. 196–204.

Ellis, J.L., Thomason, J.J., Kebreab, E. and France, J., (2008). Calibration of estimated biting forces in domestic canids: comparison of post-mortem and in vivo measurements. Journal of Anatomy, 212(6), pp.769-780.

Ellis, J. L., Thomason, J., Kebreab, E., Zubair, K. and France, J. (2009). Cranial dimensions and forces of biting in the domestic dog. Journal of Anatomy, 214 (3), pp.362-373.

Elmhagen, B., Tannerfeldt, M., Angerbjorn, A., (2002). Food niche overlap between arctic and red foxes. Canadian Journal of Zoology, 80(7), pp. 1274–1285.

Elmhagen, B., Tannerfeldt, M., Verucci, P., Angerbjorn, A. (2000). The arctic fox (*Alopex lagopus*): an opportunistic specialist. Journal of Zoology, 251(2000), pp. 139–149.

Emerson, S.B., Bramble, D.M., (1993). Scaling, Allometry and Skull Design. In: Hanken J; Hall B, editors. The Skull. Volume 3: functional and evolutonary mechanisms. Chicago: University of Chicago Press. pp. 384–421.

Emerson, S. B. and Hastings, P. A., (1998). Morphological Correlations in Evolution: Consequences for Phylogenetic Analysis. The Quarterly Review of Biology, 73(2), p. 141.

Endo, H., Taru, H., Yamamoto, M., Arishima, K., Sasaki, M., (2003). Comparative morphology of the muscles of mastication in the giant panda and the Asiatic black bear. Annals of Anatomy, 185(3), pp. 287–292.

Eng, C. M., Ward, S. R., Vinyard, C. J. and Taylor, A B., (2009). The morphology of the masticatory apparatus facilitates muscle force production at wide jaw gapes in tree-

gouging common marmosets (Callithrix jacchus). The Journal of experimental biology, 212, pp. 4040–4055.

Evans, H. E. and De Lahunta, A. (2013). Miller's Anatomy of the Dog. Elsevier Health Sciences.

Evans, H. E., & De Lahunta, A. (2016). Guide to the Dissection of the Dog-E-Book. Elsevier Health Sciences.

Evans, H. E. and Sack, W. O.. (1973). Prenatal Development of Domestic and Laboratory Mammals: Growth Curves, External Features and Selected References. Anatomia, Histologia, Embryologia, 2(1), pp. 11–45.

Ewer, R. F., (1973). The carnivores. Ithaca NY: Cornell University Press.

Fabre, A.-C., Perry, J., Hartstone-Rose, A., Lowie, A. and Dumont, M., (2017). Do muscles constrain skull shape evolution in Strepsirrhines? The Anatomical Record, 301 (2), pp. 291–310.

Fabre, P. H., Herrel, A., Fitriana, Y., Meslin, L., Hautier, L., (2017). Masticatory muscle architecture in a water-rat from Australasia (Murinae, Hydromys) and its implication for the evolution of carnivory in rodents', Journal of Anatomy, (June), pp. 380–397.

Falland-Cheung, L., Waddell, J. N., Chun Li, K., Tong, D., Brunton, P., (2017). Investigation of the elastic modulus, tensile and flexural strength of five skull simulant materials for impact testing of a forensic skin/skull/brain model. Journal of the Mechanical Behavior of Biomedical Materials, 68, pp. 303–307.

Fanshawe, J. H. and Fitzgibbon, C. D., (1993). Factors influencing the hunting success of an African wild dog pack', Animal Behaviour, 45(3), pp. 479–490.

Farncombe, T. and Iniewski, K. (2013) Medical imaging: technology and applications. Boca Raton, Florida : CRC Press, 2013.

Farke, A. A., (2008). Frontal sinuses and head-butting in goats: a finite element analysis. Journal of Experimental Biology, 211(19), pp. 3085–3094.

Fay, D. S., (2013). A biologist's guide to statistical thinking and analysis. WormBook, pp. 1–54. doi: 10.1895/wormbook.1.159.1.

Fearnhead, R. W., Shute, C. C. D., Bellairs, A. D., (1955). The temporo-mandibular joint of shrews. Proceedings of the Zoological Society of London, 125(3–4), pp. 795–806.

Fedorov, A., Beichel, R., Kalpathy-Cramer, J., Finet, J., Fillion-Robin, J-C., Pujol, S., Bauer, C., Jennings, D., Fennessy, F., Sonka, M., (2012). 3D Slicer as an image computing platform for the Quantitative Imaging Network. Magnetic Resonance Imaging, 30(9), pp. 1323–1341.

Felsenstein, J., (1985). Phylogenies and the Comparative Method. The American Naturalist, 125(1), pp. 1–15.

Ferguson, W. W., (1981). The systematic position of Canis aureus lupaster (Carnivora: Canidae) and the occurrence of Canis lupus in North Africa, Egypt and Sinai. Mammalia, 45(4), pp. 459–466.

Fernández-Jalvo, Y. and Andrews, P., (2016). Atlas of taphonomic identifications. Vertebrate Paleobiology and Paleoanthropology, Springer, pp. 1–359.

Figueirido, B., MacLeod, N., Krieger, J., De Renzi, M., Pérez-Claros, J. A., Palmqvist, P., (2011). Constraint and adaptation in the evolution of carnivoran skull shape. Paleobiology, 37(3), 490–518.

Figueirido, B., Martin-Serra, A., Tseng, Z.J., Janis, C.M., (2015). Habitat changes and changing predatory habits in North American fossil canids. Nature Communications, 6., p.7676.

Figueirido, B., Serrano-Alarcon, F. J., Slater, G. J. and Palmqvist, P. (2010). Shape at the

cross-roads: Homoplasy and history in the evolution of the carnivoran skull towards herbivory. Journal of Evolutionary Biology, 23(12), pp. 2579–2594.

Fillios, M. A. and Taçon, P. S. C., (2016). Who let the dogs in? A review of the recent genetic evidence for the introduction of the dingo to Australia and implications for the movement of people', Journal of Archaeological Science: Reports, 7, pp. 782–792.

Finarelli, J. A., (2006). Estimation of Endocranial Volume Through the Use of External Skull Measures in the Carnivora (Mammalia). Journal of Mammalogy, 87(5), pp. 1027–1036.

Finarelli, J. A., (2007). Mechanisms Behind Active Trends in Body Size Evolution of the Canidae (Carnivora: Mammalia). The American Naturalist, 170 (6), pp. 876-885.

Finarelli, J. A. and Goswami, A., (2013). Potential Pitfalls Of Reconstructing Deep Time Evolutionary History With Only Extant Data, A Case Study Using The Canidae (Mammalia, Carnivora). Evolution, 67(12), pp. 3678–3685.

Floyd, T., Mech, L., and Jordan, P., (1978). Relating wolf scat content to prey consumed. The Journal of Wildlife Management, 42(3), pp. 528–532.

Forbes-Harper, J. L., Crawford, H.M., Dundas, S.J., Warburton, N. M., Adams, P. J., Bateman, P.W.,Calver, M.C., Fleming, P.A., (2017). Diet and bite force in red foxes: ontogenetic and sex differences in an invasive carnivore. Journal of Zoology, 303(1), pp.54-63.

Fox, C. H., Johnson, F. B., Whiting, J. and Roller, P. P., (1985). Formaldehyde fixation. The journal of histochemistry and cytochemistry, pp. 845–853.

Frafjord, K., (1993). Food habits of Arctic foxes (*Alopex lagopus*) on the western coast of Svalbard. Arctic, 46(1), pp. 49–54.

Frankino, W. A., Zwaan, B. J., Stern, D. L. and Brakefield, P. M., (2007) Natural Selection and Developmental Constraints in the Evolution of Allometries. Science, 307 (5710) pp. 718–720.

Freeman, S. and Herron, J. C., (2014). Evolutionary Analysis. Pearson, Prentice, Hall.

Frontier, S. (1976). Decrease of eigenvalues in principal component analysis-comparison with broken stick model. Journal of Experimental Marine Biology and Ecology, 25(1), pp. 67–75.

Frost, S.R., Marcus, L.F., Bookstein, F.L., Reddy, D.P., Delson, E., (2003). Cranial allometry, phylogeography, and systematics of large-bodied papionins (primates: Cercopithecinae) inferred from geometric morphometric analysis of landmark data. Anatomical Record, Part A: Discoveries in Molecular, Cellular, and Evolutionary Biology: An Official Publication of the American Association of Anatomists, 275(2), pp. 1048–1072.

Fujiwara, S. and Suwa, F., (1991). On the Facial Artery of the Raccoon Dog (Nyctereutes Procyonoides Viverrinus Temminck)', Okajimas Folia Anatomica Japonica, 68(2–3), pp. 81–93.

Gandiwa, E., (2016). Rainfall variability and its impact on large mammal populations in a complex of semi-arid African savanna protected areas. Tropical Ecology, 57(2), pp. 163–180.

Gans, C., (1961). The feeding mechanism of snakes and its possible evolution', *American Zoologist*, 1(2), pp. 217–227.

Gans, C., (1982). Fiber Architecture and Muscle Function. Exercise and Sport Sciences Reviews, 10(1), pp. 160–207.

Gans, C. and Gaunt, A. S., (1991). Muscle architecture in relation to function. Journal of Biomechanics, 24, pp. 53–65.

Garland, T., (1983). The relation between maximal running speed and body mass in terrestrial mammals. Journal of Zoology, 199(2), pp. 157–170.

Garland, T., (2005). Phylogenetic approaches in comparative physiology Journal of

Experimental Biology, 208(16), pp. 3015–3035.

Garland, T., Midford, P. E. and Ives, A. R., (1999). An introduction to phylogenetically based statistical methods, with a new method for confidence intervals on ancestral value. Integrative and Comparative Biology, 39(2), pp. 374–388.

Gefen, A. and Seliktar, R., (2002). Dominant trabecular patterns of the calcaneus are aligned with the principal stress flow during standing. Proceedings of the Second Joint 24th Annual Conference and the Annual Fall Meeting of the Biomedical Engineering Society.

Geffen, E., Mercure, A., Girman, D. J., Macdonald, D.W., Wayne, R.K., (1992). Phylogenetic relationships of the fox-like canids: mitochondrial DNA restriction fragment , site and cytochrome b sequence analyses. Journal of Zoology, 228, pp. 27–39.

Geiger, M. and Haussman, S., (2016). Cranial Suture Closure in Domestic Dog Breeds and Its Relationships to Skull Morphology. Anatomical Record, 299(4), pp. 412–420.

Germonpré, M., Sablin, M. V., Stevens, R. E., Hedges, R. E. M., Hofreiter, M., Stiller, M. and Després, V. R., (2009). Fossil dogs and wolves from Palaeolithic sites in Belgium, the Ukraine and Russia: osteometry, ancient DNA and stable isotopes. Journal of Archaeological Science, 36(2), pp. 473–490.

Getty, R. (1975). Sisson and Grossman's the Anatomy of the Domestic Animals. Philadelphia: Saunders.

Gibbs, C. H., Mahan,P.E., Wilkinson, T.M., Mauderli, A., (1984). EMG activity of the superior belly of the lateral pterygoid muscle in relation to other jaw muscles. Journal of Prosthetic Dentistry, 51(5), pp. 691–702.

Gidaszewski, N.A., Baylac, M., Klingenberg, C., (2009). Evolution of sexual dimorphism of wing shape in the Drosophila melanogaster subgroup. BMC Evolutionary Biology, 9(1), p.110

Gioso, M. A. and Carvalho, V. G. G., (2005). Oral anatomy of the dog and cat in veterinary dentistry practice. Veterinary Clinics of North America - Small Animal Practice, 35(4), pp. 763–780.

Gittleman, J.L., (1985). Carnivore body size: Ecological and taxonomic correlates. Oecologia, 67(4), pp.540-554.

Gittleman, J. L., (1986). Carnivore brain size, behavioral ecology, and phylogeny. Journal of Mammalogy. American Society of Mammalogists, 67(1), pp. 23–36.

Gittleman, J. L., (1989). Carnivore Group Living: Comparative Trends. In Carnivore Behavior, Ecology, and Evolution, pp. 183–207.

Gittleman, J. L., (1991). Carnivore olfactory bulb size: allometry, phylogeny and ecology. Journal of Zoology, 225(2), pp. 253–272.

Gittleman, J. L., and Valkenburgh, B. Van.,(1997). Sexual dimorphism in the canines and skulls of carnivores: effects of size, phylogency, and behavioural ecology. Journal of Zoology, 242(1), pp. 97–117.

Godinho, R. M., Toro-Ibacache, V., Fitton, L. C. and O'Higgins, P., (2017). Finite element analysis of the cranium: Validity, sensitivity and future directions. Comptes Rendus Palevol, 16(5–6), pp. 600–612.

Gorrel, C., (2004). Veterinary Dentistry for the General Practitioner. Elsevier.

Goswami, A., (2006a). Cranial Modularity Shifts during Mammalian Evolution. The American Naturalist, 168(2), pp. 270–280.

Goswami, A., (2006b). Morphological Integration in the Carnivoran Skull. Evolution, 60(1), pp. 169–183.

Goswami, A., Foley, L. and Weisbecker, V., (2013). Patterns and implications of extensive

heterochrony in carnivoran cranial suture closure. Journal of Evolutionary Biology, 26(6), pp. 1294–1306.

Goswami, A., Milne, N., Wroe, S., (2011). Biting through constraints: cranial morphology, disparity and convergence across living and fossil carnivorous mammals. Proceedings of the Royal Society B: Biological Sciences, p. rspb 20102031.

Gould, S.J., (1966). Allometry and size in ontogeny and phylogeny. Biological Reviews, 41(4), pp.587-638.

Gould, S. J. and Lewontin, R. C., (1979). The Spandrels of San Marco and the Panglossian Paradigm: A Critique of the Adaptationist Programme. Proceedings of the Royal Society B: Biological Sciences, 205(1161), pp. 581–598.

Grant, P. G., (1973). Lateral pterygoid: two muscles? Developmental Dynamics, 138(1), pp. 1–9.

Greaves, W. S., (1982). A mechanical limitation on the position of the jaw muscles of mammals: the one-third rule. Journal of Mammalogy, 63(2), pp. 261–266.

Greaves, W. S., (1983). A Functional-Analysis of Carnassial Biting. Biological Journal of the Linnean Society, 20(4), pp. 353–363.

Greaves, W. S., (1985). The generalized carnivore jaw. Zoological Journal of the Linnean Society. Oxford University Press, 85(3), pp. 267–274.

Greaves, W. S., (1985). The mammalian postorbital bar as a torsion-resisting helical strut. Journal of Zoology, 207(1), pp. 125–136.

Greaves, W. S., (1995). Functional predictions from theoretical models of the skull and jaws in reptiles and mammals. Functional morphology in vertebrate paleontology. Cambridge University Press, Cambridge, pp. 99–115.

Greaves, W. S., (2000). Location of the vector of jaw muscle force mammals. Journal of

Morphology, 243(3), pp. 293–299.

Greaves, W. S., (2012). The Mammalian Jaw. Cambridge University Press.

Grellmann, W., Berghaus, A., Haberland, E.-J., Jamali, Y., Holweg, K., Reincke, K., Bierögel, C., (2006). Determination of strength and deformation behavior of human cartilage for the definition of significant parameters. Journal of Biomedical Materials Research Part A, 78A(1), pp. 168–174.

Gröning, F., Fagan, M. J. and O'Higgins, P., (2011). The effects of the periodontal ligament on mandibular stiffness: A study combining finite element analysis and geometric morphometrics. Journal of Biomechanics, 44(7), pp. 1304–1312.

Gröning, F., Jones, M. E. H., Curtis, N., Herrel, A., O'Higgins, P., Evans, S. E. and Fagan, M. J., (2013). The importance of accurate muscle modelling for biomechanical analyses: a case study with a lizard skull', Journal of the Royal Society Interface. The Royal Society, 10(84), p. 20130216.

Gröning, F., Liu, J., Fagan, M. J. and O'Higgins, P., (2009). Validating a voxel-based finite element model of a human mandible using digital speckle pattern interferometry. Journal of Biomechanics, 42(9), pp. 1224–1229. .

Hall, B. K., (2005). Bones and Cartilage: Developmental and Evolutionary Skeletal Biology, Elsevier.

Hammer, Ø., Harper, D., Ryan, P.D., (2001). PAST: Paleontological statistics software package for education and data analysis. Palaeontología Electrónica 4:9.

Hand, M. S. and Lewis, L. D. (2000) Small animal clinical nutrition. 4th ed. Mark Morris Institute.

Hannam, A. G., Wood, W.W., De Cou, R.E., Scott, J.D., (1981). The effects of working-side occlusal interferences on muscle activity and associated jaw movements in man. Archives of Oral Biology, 26(5), pp. 387–392.

Harano, T. and Kutsukake, N., (2018). The evolution of male infanticide in relation to sexual selection in mammalian carnivores. Evolutionary Ecology, 32(1), pp. 1–8.

Hartstone-Rose, A., Deutsch, A. R., Leischner, C. L., Pastor, F., (2018). Dietary Correlates of Primate Masticatory Muscle Fiber Architecture. Anatomical Record, 301 (2) pp. 311–324.

Hartstone-Rose, A., Perry, J.M.G., Morrow, C.J., (2012). Bite force estimation and the fiber architecture of felid masticatory muscles. Anatomical Record 295 (8), pp. 1336–1351.

Hartstone-Rose, A., Werdelin, L., De Ruiter, D.J., Berger, L.R., Churchill, S.E., (2010). The Plio-Pleistocene ancestor of wild dogs, Lycaon sekowei n. sp. Journal of Paleontology, 84(02), pp. 299–308.

Harvey, B. M., Bhatnagar, K. P., Schenck, R. J., Rosenberger, A. L., Rehorek, S. J., Burrows, A. M., Deleon, V. B. and Smith, T. D., (2016). Membranous Support for Eyes of Strepsirrhine Primates and Fruit Bats. The Anatomical Record, 299 (12), pp. 1690-1703.

Harvey, P. H., (1982). On rethinking allometry. Journal of Theoretical Biology, 95(1), pp. 37–41.

Harvey, P. H. and Pagel, M. D., (1991). The comparative method in evolutionary biology. Trends in Ecology and Evolution. Oxford University Press.

Hashemi, R. H., Bradley, W. G. and Lisanti, C. J., (2010). MRI : the basics. Philadelphia, PA : Lippincott Williams and Wilkins.

Hautier, L. and Saksiri, S., (2009). Masticatory muscle architecture in the Laotian rock rat Laonastes aenigmamus (Mammalia, Rodentia): New insights into the evolution of hystricognathy. Journal of Anatomy, 215(4), pp. 401–410.

Haxton, H. A., (1944). Absolute muscle force in the ankle flexors of man. The Journal of

physiology, 103(3), pp. 267–273.

Hayashi, S., Naito, M., Kawata, S., Qu, N., Hatayama, N., Hirai, S. and Itoh, M., (2016). History and future of human cadaver preservation for surgical training: from formalin to saturated salt solution method. Anatomical Science International, 91(1), pp. 1–7.

Hayes Jr, H. M., Priester, W. A. and Pendergrass, T. W., (1975). Occurrence of nervous-tissue tumors in cattle, horses, cats and dogs. International Journal of Cancer, 15(1), pp. 39–47.

Heesy, C. P., (2002). The evolution of orbit orientation in mammals and the function of the primate postorbital bar. PhD Thesis. Stony Brook University.

Heesy, C. P., (2005). Function of the mammalian postorbital bar. Journal of Morphology, 264(3), pp. 363–380.

Heesy, C. P., Ross, C. F. and Demes, B., (2007). Oculomotor stability and the functions of the postorbital bar and septum, in Primate origins: Adaptations and evolution. Springer, pp. 257–283.

Hernot, D. C., Biourge, V.C., Martin, L.J., Dumon, H.J., Nguyen, P.G., (2005). Relationship between total transit time and faecal quality in adult dogs differing in body size. Journal of Animal Physiology and Animal Nutrition, 89(3–6), pp. 189–193.

Herrel, A. and O'Reilly, J. C., (2006). Ontogenetic Scaling of Bite Force in Lizards and Turtles. Physiological and Biochemical Zoology, 79(1), pp. 31–42.

Herrel, A., De Smet, A., Aguirre, LF., Aerts, P., (2008). Morphological and mechanical determinants of bite force in bats: do muscles matter? The Journal of Experimental Biology 211 (1), pp. 86–91.

Herring, S. W., (2005). Ontogeny of bone strain: the zygomatic arch in pigs. Journal of Experimental Biology, 208(23), pp. 4509–4521.

Herring, S.W., (2007). Masticatory muscles and the skull: a comparative perspective. Archives of oral biology, 52(4), pp.296-299.

Herring, S. W., Anapol, F. C. and Wineski, L. E., (1991). Motor-unit territories in the masseter muscle of infant pigs. Archives of Oral Biology, 36(12), pp. 867–873.

Herring, S. W., Mucci, R. J., (1991). In vivo strain in cranial sutures: The zygomatic arch. Journal of Morphology, *207*(3), 225–239.

Herring, S. W. and Ochareon, P., (2005). Bone-special problems of the craniofacial region. Orthodontics and Craniofacial Research, 8(3), pp. 174–182.

Herring, S. W., Rafferty, K. L., Liu, Z. J., Lemme, M., (2011). Mastication and the postorbital ligament: Dynamic strain in soft tissues. Integrative and Comparative Biology, 51(2), pp. 297–306.

Herring, S. W., Rafferty, K. L., Liu, Z. J. and Marshall, C. D., (2001). Jaw muscles and the skull in mammals: The biomechanics of mastication. Comparative Biochemistry and Physiology - A Molecular and Integrative Physiology, 131(1), pp. 207–219.

Herring S.W., Teng, S., (2010). Strain in the Braincase and Its Sutures During Function. American Journal of Physics, 112(4).

Hildebrand, M., (1952). An analysis of body proportions in the Canidae. American Journal of Anatomy, 90, pp. 217–256.

Hildebrand, M., Goslow,G.E., Hildebrand, V., (1995). Analysis of Vertebrate Structure, Wiley.

Hobson, P., (2005). Normal occlusion in the dog. J Vet Dent, 22(3), pp. 196–198.

Horsburgh, K. A., (2008). Wild or domesticated? An ancient DNA approach to canid species identification in South Africa's Western Cape Province. Journal of Archaeological Science, 35(6), pp. 1474–1480.

Hsieh, J., (2009). Computed tomography: principles, design, artifacts, and recent advances. Bellingham : SPIE.

Huber, D. R., (2005). Analysis of the bite force and mechanical design of the feeding mechanism of the durophagous horn shark *Heterodontus francisci*. Journal of Experimental Biology, 208(18), pp. 3553–3571.

Hunt, R. M. (1974). The auditory bulla in Carnivora: an anatomical basis for reappraisal of carnivore evolution. Journal of Morphology, 143(1848), pp. 21–76.

Hunt Jr., R. M., (1996). Biogeography of the Order Carnivora. Carnivore behavior, ecology, and evolution, 2, pp. 485–541.

Hunt Jr, R.M. and Tedford, R.H., (1993). Phylogenetic relationships within the aeluroid Carnivora and implications of their temporal and geographic distribution. Mammal Phylogeny (Placentals), pp. 53–73.

Huq, E., Wall, C. E. and Taylor, A. B., (2015). Epaxial muscle fiber architecture favors enhanced excursion and power in the leaper Galago senegalensis. Journal of Anatomy, 227(4), pp. 524–540.

Hussein, A. K., Sullivan, M. and Penderis, J., (2012). Effect of brachycephalic, mesaticephalic and dolichocephalic head conformations on olfactory bulb angle and orientation in dogs as determined by use of in vivo magnetic resonance imaging. American Journal of Veterinary Research. 73(7), pp 946-951.

Huxley, T. H., (1880). On the Cranial and Dental Characters of the Canidae. Proceedings of the Zoological Society of London, XVI, pp. 238–288.

Hylander, W. L. and Johnson, K. R., (1994). Jaw muscle function and wishboning of the mandible during mastication in macaques and baboons. American Journal of Physical Anthropology, 94(4), pp. 523–547.

Hylander, W. L. and Johnson, K. R., (1997). In vivo bone strain patterns in the zygomatic arch of macaques and the significance of these patterns for functional interpretations of craniofacial form. American Journal of Physical Anthropology, 102(2), pp. 203–232.

Hylander, W. L., Johnson, K. R. and Picq, P. G., (1991). Masticatory-stress hypotheses and the supraorbital region of primates. American Journal of Physical Anthropology. Wiley Online Library, 86(1), pp. 1–36.

Iwanaga, Y., Wen, J., Thollander, M. S., Kost, L. J., Thomforde, G. M., Allen, R. G., Phillips, S. F., (1998). Scintigraphic measurement of regional gastrointestinal transit in the dog. The American journal of physiology, 275(5 Pt 1), pp. 904-10.

Jackson, D.A., (1993). Stopping rules in prinicipal components analysis: a comparison of heuristical and statistical approaches. Ecology, 74(8), pp. 2204-2214.

Janis, C. M., (1993). Tertiary Mammal Evolution in the Context of Changing Climates, Vegetation, and Tectonic Events. Annual Review of Ecology and Systematics, 24(1), pp. 467–500.

Janis, C. M., Damuth, J. and Theodor, J. M., (2004). The species richness of Miocene browsers, and implications for habitat type and primary productivity in the North American grassland biome. Palaeogeography, Palaeoclimatology, Palaeoecology, 207(3–4), pp. 371–398.

Janis, C. M. and Figueirido, B., (2014). Forelimb anatomy and the discrimination of the predatory behavior of carnivorous mammals: The thylacine as a case study. Journal of Morphology, 275(12), pp. 1321–1338.

Jasinski, S. E. and Wallace, S. C., (2015). A Borophagine canid (Carnivora: Canidae: Borophaginae) from the middle Miocene Chesapeake Group of eastern North America. Journal of Paleontology, 89(06), pp. 1082–1088.

Jasarevic, E., Ning, J., Daniel, A. N., Menegaz, R. A., Johnson, J. J., Stack, M. S. and Ravosa, M. J., (2010). Masticatory loading, function, and plasticity: A microanatomical analysis of

mammalian circumorbital soft-tissue structures. Anatomical Record, 293(4), pp. 642–650.

Jaslow, C. R., (1990). Mechanical properties of cranial sutures. Journal of Biomechanics, 23(4), pp. 313–321.

Jensen, R. H., Davy, D. T., (1975). An investigation of muscle lines of action about the hip: A centroid line approach vs the straight line approach. Journal of Biomechanics, 8(2), pp.105–110.

Jerison, H.J., (1955). Brain to body ratios and the evolution of intelligence. Science, 121(3144), pp.447-449.

Jones, D. G., (1997). Reassessing the importance of dissection: a critique and elaboration. Clinical Anatomy: The Official Journal of the American Association of Clinical Anatomists and the British Association of Clinical Anatomists, *10*(2), 123–127.

Juniper, R. P., (1984). Temporomandibular joint dysfunction: A theory based upon electromyographic studies of the lateral pterygoid muscle. British Journal of Oral and Maxillofacial Surgery, 22(1), pp. 1–8.

Karanth, K. U., Sunquist, M. E., (1995). Prey Selection by Tiger, Leopard and Dhole in Tropical Forests. The Journal of Animal Ecology, 64(4), pp. 439.

Kardong, K. V., (2015). Vertebrates : comparative anatomy, function, evolution. New York, McGraw-Hill Education.

Kauhala, K., (1993). Growth, size, and fat reserves of the raccoon dog in Finland. Acta Theriologica, 38, pp. 139–150.

Kauhala, K., Helle, E., Taskinen, K., (1993). Home range of the raccoon dog (*Nyctereutes procyonoides*) in southern Finland. Journal of Zoology, 231(1), pp. 95–106.

Kauhala, K., Laukkanen, P., Von Rege, I. (1998). Summer food composition and food niche overlap of the raccoon dog, red fox and badger in Finland. Ecography, 21(5), pp. 457–463.

Kauhala, K. and Saeki, M., (2004). Raccoon dogs: Finnish and Japanese raccoon dogs—on the road to speciation? in The Biology and Conservation of Wild Canids. Oxford: Oxford University Press.

Kawamura, Y., Kato, I., Miyoshi, K., (1968). Functional anatomy of the lateral pterygoid muscle in the cat. Journal of Dental Research. 47 (6), pp. 1142 - 1148.

Kawarizadeh, A., Bourauel, C. and Jäger, A., (2003). Experimental and numerical determination of initial tooth mobility and material properties of the periodontal ligament in rat molar specimens. European Journal of Orthodontics, 25(6), pp. 569–578.

Kieser, J. A. (1995). Gnathomandibular morphology and character displacement in the bat-eared fox. Journal of Mammalogy, 76, 542–550.

Kieser, J. A and Groeneveld, H. T., (1992). Comparative morphology of the mandibulodental complex in wild and domestic canids. Journal of anatomy, 180 (3), pp. 419–24.

Kiltie, R. A. (1984). Size ratios among sympatric neotropical cats. Oecologia. Springer, 61(3), pp. 411–416.

Kim, D.-G., Haghighi, A., Kwon, H.-J., Coogan, J. S., Nicolella, D. P., Johnson, T. B., Kim, H. D., Kim, N. and Agnew, A. M., (2017). Sex dependent mechanical properties of the human mandibular condyle. Journal of the mechanical behavior of biomedical materials, 71, pp. 184–191.

Kim, S.-I., Suzuki, S., Oh, J., Koyabu, D., Oshida, T., Lee, H., Kimura, J. (2012). Sexual Dimorphism of Craniodental Morphology in the Raccoon Dog *Nyctereutes procyonoides* from South Korea. Journal of Veterinary Medical Science, 74(12), pp. 1609–1616.

King, J. R. and Jackson, D. A. (1999). Variable selection in large environmental data sets using principal components analysis. Environmetrics, 10 (1), pp. 67–77.

Kinney, J. H., Marshall, S. J., Marshall, G. W., (2003). The mechanical properties of human dentin: a critical review and re-evaluation of the dental literature. Critical Reviews in Oral Biology and Medicine, 14(1), pp. 13–29.

Kitao, N., Fukui, D., Hashimoto, M., Osborne, P.G., (2009). Overwintering strategy of wild free-ranging and enclosure-housed Japanese raccoon dogs (Nyctereutes procyonoides albus). International Journal of Biometeorology, 53(2), pp. 159–165.

Kitchener, A. C., Merryweather, J. and Allchurch, T., (1998). The effect of captivity on the flight musculo-skeletal system of fruit bats (*Pteropus* spp.). EEP Yearbook, 99, pp. 553–555.

Klare, U., Kamler, J. F. and Macdonald, D. W., (2011). The bat-eared fox: A dietary specialist? Mammalian Biology, 76(5), pp. 646–650.

Klingenberg, C. P., (2008). Morphological Integration and Developmental Modularity. Annual Review of Ecology, Evolution, and Systematics, 39(1), pp. 115–132.

Klingenberg, C.P., (2009). Morphometric integration and modularity in configurations of landmarks: tools for evaluating a priori hypotheses. Evolution and development, 11(4), pp.405-421.

Klingenberg, C.P., (2011). MorphoJ: an integrated software package for geometric morphometrics. Molecular ecology resources, 11(2), pp.353-357.

Klingenberg, C. P., (2016). Size, shape, and form: concepts of allometry in geometric morphometrics. Development Genes and Evolution. Development Genes and Evolution, 226(3), pp. 113–137.

Klingenberg, C.P. and Gidaszewski, N.A., (2010). Testing and quantifying phylogenetic signals and homoplasy in morphometric data. Systematic biology, 59(3), pp.245-261.

Klingenberg, C. P. and Marugán-Lobón, J., (2013). Evolutionary covariation in geometric morphometric data: Analyzing integration, modularity, and allometry in a phylogenetic context. Systematic Biology, 62(4), pp. 591–610.

Knupp, P. M., (2001). Algebraic mesh quality metrics. SIAM journal on scientific computing. SIAM, 23(1), pp. 193–218.

Knupp, P. M., (2007). Remarks on Mesh Quality. 45th AIAA Aerospace Sciences Meeting and Exhibit, (January), pp. 2 - 5.

Koepfli, K. P., Pollinger, J., Godinho, R., Robinson, J., Lea, A., Hendricks, S., Schweizer, R.M., Thalmann, O., Silva, P., Fan, Z., Yurchenko, A.A., Dobrynin, P., Makunin, A., Cahill, J.A., Shapiro, B., Alvares, F., Brito, J.C., Geffen, E., Leonard, J.A., Helgen, K.M., Johnson, W.E., O'Brien, S.J., Van Valkenburgh, B., Wayne, R.K., (2015). Genome-wide evidence reveals that African and Eurasian golden jackals are distinct species. Current Biology, 25(16), pp. 2158–2165.

Kolpakova-Hart, E., McBratney-Owen, B., Hou, B., Fukai, N., Nicolae, C., Zhou, J., Olsen, B. R., (2008). Growth of cranial synchondroses and sutures requires polycystin-1. Developmental Biology, *321*(2), 407–419.

König, H.E., Hans-Georg, H.G. and Bragulla, H., (2009). Veterinary anatomy of domestic mammals: textbook and colour atlas. Schattauer Verlag

Koolstra, J. H., Van Eijden, T. M. Weijs, W.A., Naeije, M., (1988). A three-dimensional mathematical model of the human masticatory system predicting maximum possible bite forces. Journal of Biomechanics, 21(7), pp. 563–576.

Korf, H., Wicht, H., Snipes, R. L., Timmermans, J., Paulsen, F., Rune, G., Baumgart-vogt, E. (2008). The dissection course – necessary and indispensable for teaching anatomy to medical students, Annals of Anatomy, *190*, 16–22.

Kozlowski, A. J., Gese, E. M. and Arjo, W. M., (2008). Niche Overlap and Resource

Partitioning Between Sympatric Kit Foxes and Coyotes in the Great Basin Desert of Western Utah. *Am. Midl. Nat.*, 160(1), pp. 191–208.

Kreeger, T. J., DelGiudice, G. D. and Mech, L. D., (1997). Effects of fasting and refeeding on body composition of captive gray wolves (Canis lupus). Canadian Journal of Zoology, 75, pp. 1549–1552.

Kuhn, J. L., Goldstein, S. A., Ciarelli, M. J., Matthews, L. S., (1989). The limitations of canine trabecular bone as a model for human: A biomechanical study. Journal of Biomechanics, 22(2), pp. 95–107.

Kumaresan, S., Yoganandan, N., Pintar, F. A., Voo, L. M., Cusick, J. F., Larson, S. J., (1997). Finite element modeling of cervical laminectomy with graded facetectomy. Clinical Spine Surgery, 10(1), pp. 40–46.

Kuntzsch, V., Nel, J. A. J., (1992). Diet of bat-eared foxes *Otocyon megalotis* in the Karoo. Koedoe, 35 (2), pp.37-48.

Kupczik, K., (2008). Virtual biomechanics : basic concepts and technical aspects of finite element analysis in vertebrate morphology. Journal of Anthropological Sciences, 86 (4), pp. 193-198.

Kupczik, K., Dobson, C. A., Fagan, M. J., Crompton, R. H., Oxnard, C. E., O'higgins, P., (2007). Assessing mechanical function of the zygomatic region in macaques: Validation and sensitivity testing of finite element models. Journal of Anatomy, 210(1), pp. 41–53.

Kupczik, K., Stark, H., Mundry, R., Neininger, F. T., Heidlauf, T. and Röhrle, O., (2015). Reconstruction of muscle fascicle architecture from iodine-enhanced microCT images: A combined texture mapping and streamline approach. Journal of Theoretical Biology, 382, pp. 34–43.

Kutschera, V. E., Lecomte, N., Janke, A., Selva, N., Sokolov, A.A., Haun, T., Steyer, K., Nowak, C., Hailer, F., (2013). A range-wide synthesis and timeline for phylogeographic events in the red fox (*Vulpes vulpes*). BMC Evolutionary Biology, 13(1), p. 114.

Kyle, C. J., Johnson, A.R., Patterson, B.R., Wilson, P.J., Shami, K., Grewal, S.K., White, B.N., (2006). Genetic nature of eastern wolves: Past, present and future. *Conservation Genetics*, 7(2), pp. 273–287.

LaBarbera, M., (1989). Analyzing body size as a factor in ecology and evolution. Annual review of ecology and systematics, 20(1), pp. 97–117.

Landon, D. B., Waite, CA., Peterson, R.O., Mech, l.D., (1998). Evaluation of Age Determination Techniques for Gray Wolves. The Journal of Wildlife Management, 62(2), p. 674.

Langenbach, G. E. J. and van Eijden, T. M. G. J., (2001). Mammalian feeding motor patterns. American Zoologist, 41(6), pp. 1338–1351.

Lappin, A. K., Hamilton, P. S. and Sullivan, B. K., (2006). Bite-force performance and head shape in a sexually dimorphic crevice-dwelling lizard, the common chuckwalla [Sauromalus ater (= obesus)]. Biological Journal of the Linnean Society, 88(2), pp. 215–222.

Larivière, S. (2002). *Vulpes zerda*. Mammalian Species, 714(714), 1–5.

Larivière, S., Pasitschniak-Arts, M. (2018). *Vulpes vulpes*. Mammalian Species, (537), 1–11.

Leary, R. P., Manuel, C. T., Shamouelian, D., Protsenko, D. E., Wong, B. J. F., (2015). Finite element model analysis of cephalic trim on nasal tip stability. JAMA Facial Plastic Surgery, 17(6), pp. 413–420.

LeCouteur, R. A. (1999) 'Current concepts in the diagnosis and treatment of brain tumours in dogs and cats', Journal of small animal practice. 40(9), pp. 411–416.

LeCouteur, R. A. and Withrow, S. J. (2007). Tumors of the nervous system, in Withrow and MacEwen's Small Animal Clinical Oncology. Elsevier.

Lee, E. J., Merriwether, D.A., Kasparov, A.K., Nikolskiy, P.A., Sotnikova, M.V., Pavlova, E.Y. Pitulko, V., (2015). Ancient DNA analysis of the oldest Canid species from the Siberian Arctic and genetic contribution to the domestic dog. PLoS ONE, 10(5), pp. 1–14.

Lefebvre, H. P., Ferre J-P., Watson, A.D., Brown, C.A., Serthelon, J-P., LaRoute, V., Concordet, D., Toutain, P-L., (2001). Small bowel motility and colonic transit are altered in dogs with moderate renal failure. American journal of physiology. Regulatory, integrative and comparative physiology, 281(1), pp. 230–238.

Lida, X., Yikun, W., Eric, S., Jianping, Z., Zhiming, D., Michael E, B. and Philip J, C., (2015). Model-Based Identification of Mechanical Characteristics of Sinosaurus (Theropoda) Crests. Acta Geologica Sinica-English Edition, 89(1), pp. 1–11.

Lieber, R. L. and Friden, J., (2000). Functional and clinical significance of skeletal muscle architecture', Muscle and Nerve, 23, pp. 1647–1666.

Liebich, H. G., König, H. E. and Maierl, J., (2009). Veterinary anatomy of domestic mammals, Schattauer Verlag.

Lindblad-Toh, K., Wade, C. M., Mikkelsen, T. S., Karlsson, E. K., Jaffe, D. B., Kamal, M., Clamp, M., Chang, J. L., Kulbokas, E. J., Zody, M. C., Mauceli, E., Xie, X., Breen, M., Wayne, R. K., Ostrander, E. A., Ponting, C. P., Galibert, F., Smith, D. R., deJong, P. J., Kirkness, E., Alvarez, P., Biagi, T., Brockman, W., Butler, J., Chin, C.-W., Cook, A., Cuff, J., Daly, M. J., DeCaprio, D., Gnerre, S., Grabherr, M., Kellis, M., Kleber, M., Bardeleben, C., Goodstadt, L., Heger, A., Hitte, C., Kim, L., Koepfli, K.-P., Parker, H. G., Pollinger, J. P., Searle, S. M. J., Sutter, N. B., Thomas, R., Webber, C., Baldwin, J., Abebe, A., Abouelleil, A., Aftuck, L., Ait-zahra, M., Aldredge, T., Allen, N., An, P., Anderson, S., Antoine, C., Arachchi, H., Aslam, A., Ayotte, L., Bachantsang, P., Barry, A., Bayul, T., Benamara, M., Berlin, A., Bessette, D., Blitshteyn, B., Bloom, T., Blye, J., Boguslavskiy, L., Bonnet, C., Boukhgalter, B., Brown, A., Cahill, P., Calixte, N., Camarata, J., Cheshatsang, Y., Chu, J., Citroen, M., Collymore, A., Cooke, P., Dawoe, T., Daza, R., Decktor, K., DeGray, S., Dhargay, N., Dooley, K., Dooley, K., Dorje, P., Dorjee, K., Dorris, L., Duffey, N., Dupes, A., Egbiremolen, O., Elong, R., Falk, J., Farina, A., Faro, S., Ferguson, D., Ferreira, P., Fisher, S., FitzGerald, M., Foley, K., Foley,

C., Franke, A., Friedrich, D., Gage, D., Garber, M., Gearin, G., Giannoukos, G., Goode, T., Goyette, A., Graham, J., Grandbois, E., Gyaltsen, K., Hafez, N., Hagopian, D., Hagos, B., Hall, J., Healy, C., Hegarty, R., Honan, T., Horn, A., Houde, N., Hughes, L., Hunnicutt, L., Husby, M., Jester, B., Jones, C., Kamat, A., Kanga, B., Kells, C., Khazanovich, D., Kieu, A. C., Kisner, P., Kumar, M., Lance, K., Landers, T., Lara, M., Lee, W., Leger, J.-P., Lennon, N., Leuper, L., LeVine, S., Liu, J., Liu, X., Lokyitsang, Y., Lokyitsang, T., Lui, A., Macdonald, J., Major, J., Marabella, R., Maru, K., Matthews, C., McDonough, S., Mehta, T., Meldrim, J., Melnikov, A., Meneus, L., Mihalev, A., Mihova, T., Miller, K., Mittelman, R., Mlenga, V., Mulrain, L., Munson, G., Navidi, A., Naylor, J., Nguyen, T., Nguyen, N., Nguyen, C., Nguyen, T., Nicol, R., Norbu, N., Norbu, C., Novod, N., Nyima, T., Olandt, P., O'Neill, B., O'Neill, K., Osman, S., Oyono, L., Patti, C., Perrin, D., Phunkhang, P., Pierre, F., Priest, M., Rachupka, A., Raghuraman, S., Rameau, R., Ray, V., Raymond, C., Rege, F., Rise, C., Rogers, J., Rogov, P., Sahalie, J., Settipalli, S., Sharpe, T., Shea, T., Sheehan, M., Sherpa, N., Shi, J., Shih, D., Sloan, J., Smith, C., Sparrow, T., Stalker, J., Stange-Thomann, N., Stavropoulos, S., Stone, C., Stone, S., Sykes, S., Tchuinga, P., Tenzing, P., Tesfaye, S., Thoulutsang, D., Thoulutsang, Y., Topham, K., Topping, I., Tsamla, T., Vassiliev, H., Venkataraman, V., Vo, A., Wangchuk, T., Wangdi, T., Weiand, M., Wilkinson, J., Wilson, A., Yadav, S., Yang, S., Yang, X., Young, G., Yu, Q., Zainoun, J., Zembek, L., Zimmer, A. and Lander, E. S., (2005). Genome sequence, comparative analysis and haplotype structure of the domestic dog', Nature, 438(7069), pp. 803–819.

Legendre and Legendre., (1998). Ordination in reduced space. Developments in environmental modelling, 20, pp.387-480.

Lindner, D. L., Marretta, S. M., Pijanowski, G. J., Johnson, A. L. and Smith, C. W., (1995). Measurement of bite force in dogs: a pilot study. Journal of veterinary dentistry, 12(2), pp. 49–52.

Liu, S., Wang, M., Ai, T., Wang, Q., Wang, R., Chen, W., Pan, C. and Zhu, W., (2016). In vivo morphological and functional evaluation of the lateral pterygoid muscle: a Diffusion tensor imaging study. The British journal of radiology, 89 (1064) p. 20160041.

Lovegrove, B. G. and Mowoe, M. O., (2013). The evolution of mammal body sizes: Responses to Cenozoic climate change in North American mammals. Journal of

Evolutionary Biology, 26(6), pp. 1317–1329.

Loveridge, A., Nel, J. A. J., (2004). Black-backed jackal. Canids: Foxes, Wolves, Jackals and Dogs. Status Survey and Conservation Action Plan. Gland and Cambridge: IUCN/SSC Canid Specialist Group, pp. 161 - 166.

Lund, J. P., (1991). Mastication and its Control by the Brain Stem. Critical Reviews in Oral Biology and Medicine, 2(1), pp. 33–64.

Lundberg, J. O. N., Rinder, J., Weitzberg, E., Lundberg, J.M., Alving, K., (1994) 'Nasally exhaled nitric oxide in humans originates mainly in the paranasal sinuses', Acta Physiologica Scandinavica, 152(4), pp. 431–432.

Lynnerup, N., Astrup, J. G. and Sejrsen, B., (2005). Thickness of the human cranial diploe in relation to age, sex and general body build. Head and Face Medicine, 1(1), p. 13.

Maas, B., (1993). Bat-eared fox behavioural ecology and the incidence of rabies in the Serengeti National Park. The Onderstepoort journal of veterinary research, 60(4), pp. 389–93.

Maas, S. A., Ellis, B. J., Ateshian, G. A. and Weiss, J. A., (2012). FEBio: Finite Elements for Biomechanics. Journal of Biomechanical Engineering, 134(1), pp. 11005.

Maas, S., Rawlins, D., Weiss, J. and Ateshian, G., (2014). FEBio Theory Manual Version 2.0.

MacDonald, D. W., (1977). On food preference in the Red fox. Mammal Review, 7(1), pp. 7–23.

MacDonald, D. W., (2009). The encyclopedia of mammals. Oxford University Press.

MacDonald, D. W., (1992). The Velvet Claw. Bristol: BBC Books.

MacDonald, D. W., Doncaster, P., Newdick, M., Hofer, H., Mathews, F., Johnson, P. J.,

(2015). Foxes in the landscape: ecology and sociality. In Wildlife Conservation on Farmland Volume 2. Oxford: Oxford University Press.

MacDonald, D. W., Reynolds, J. C., (2004). Red fox, *Vulpes vulpes*, Linnaeus, 1758. In Sillero-Zubiri C. Canids: Foxes, Volves, Jackals and Dogs. Status Survey and Conservation Action Plan. IUCN/SSC Canid Specialist Group. Gland, Switzerland and Cambridge, UK, 129–136.

MacDonald, D. W. and Sillero-Zubiri, C., (2004). The biology and conservation of wild canids; Ed. by DW Macdonald, C. Sillero-Zubiri. Oxford University Press

Machado, F. A., Zahn, T. M. G., Marroig, G., (2018). Evolution of morphological integration in the skull of Carnivora (Mammalia): Changes in Canidae lead to increased evolutionary potential of facial traits. Evolution, 72 (7), pp.1399-1419.

Madeira, M. C. and de Oliveira, J. A., (1979). Anatomical aspects of the masticatory muscles of the tufted capuchin (Cebus apella). *Okajimas folia anatomica Japonica*, 56(1), pp. 35–44.

Maddison, W. P. and Maddison, D. R., (1989). Interactive analysis of phylogeny and character evolution using the computer program MacClade. Folia primatologica, 53(1–4), pp. 190–202.

Maddison, W.P. and Maddison, D.R., 2016. Mesquite: a modular system for evolutionary analysis. Version 3.04. 2015.

Malcom, J. R., (1986). Socio-ecology of Bat-eared foxes (*Otocyon megalotis*). Journal of Zoology, 208(3),pp. 457–469.

Mann, S. A., Van Valkenburgh, B. and Hayward, M. W., (2017). Tooth fracture within the African carnivore guild: the influence of intraguild competition and resource availability. Journal of Zoology, 303(4), pp. 261–269.

Mansour, R. M. and Reynik, R. J. (1975). In vivo occlusal forces and moments: I. Forces measured in terminal hinge position and associated moments. Journal of Dental Research, 54(1), pp. 114–120.

Marcus, L. F. and Corti, M., (1996). Overview of the new, or geometric morphometrics, in Advances in morphometrics. Springer, pp. 1–13.

Margulies, S. S., Thibault, K. L., (2000). Infant skull and suture properties: measurements and implications for mechanisms of pediatric brain injury. Journal of Biomechanical Engineering, 122(4), pp. 364–371.

Marinescu, R., Daegling, D. J. and Rapoff, A. J., (2005). Finite-element modeling of the anthropoid mandible: The effects of altered boundary conditions. Anatomical Record - Part A Discoveries in Molecular, Cellular, and Evolutionary Biology, 283(2), pp. 300–309.

Márquez, S., (2008). The paranasal sinuses: The last frontier in craniofacial biology. Anatomical Record, 291(11), pp. 1350–1361.

Marshall, A. J., Boyko, C. M., Feilen, K. L., Boyko, R. H. and Leighton, M., (2009). Defining fallback foods and assessing their importance in primate ecology and evolution. American Journal of Physical Anthropology, 140(4), pp. 603–614.

Marshall, A. J. and Wrangham, R. W., (2007). Evolutionary consequences of fallback foods. International Journal of Primatology, 28(6), pp. 1219–1235.

Martín-Serra, A., Figueirido, B. and Palmqvist, P., (2016). In the Pursuit of the Predatory Behavior of Borophagines (Mammalia, Carnivora, Canidae): Inferences from Forelimb Morphology. Journal of Mammalian Evolution. Journal of Mammalian Evolution, 23(3), pp. 237–249.

Martin, R. B., Burr, D. B. and Sharkey, N. A. (2004). Skeletal Tissue Mechanics. New York: Springer.

Mason, G. J., (2010). Species differences in responses to captivity: Stress, welfare and the

comparative method. Trends in Ecology and Evolution, 25(12), pp. 713–721.

Mason, G. J. and Veasey, J. S., (2010). What do population-level welfare indices suggest about the well-being of zoo elephants? Zoo Biology, 29(2), pp. 256–273.

Maynard-Smith, J. and Savage, R., (1959). The mechanics of mammalian jaws. School Science Review, 40, pp. 289–301.

Mazel, F., Wüest, R. O., Lessard, J., Renaud, J., Ficetola, G. F., Lavergne, S., Thuiller, W., (2017). Global patterns of β-diversity along the phylogenetic time-scale: The role of climate and plate tectonics. Global Ecology and Biogeography, 26(10), pp. 1211–1221.

Maurel, N., Lavaste, F., Skalli, W., (1997). A three-dimensional parameterized finite element model of the lower cervical spine. Study of the influence of the posterior articular facets. Journal of Biomechanics, 30(9), pp. 921–931.

Mazonakis, M. and Damilakis, J., (2016). Computed tomography: What and how does it measure? European Journal of Radiology, 85(8), pp. 1499–1504.

Mazzolli, M. (2009). Mountain Lion, *Puma concolor*, attacks on a maned wolf, *Chrysocyon brachyurus*, and a domestic dog in a forestry system. Mastozoología Neotropical, 16(2), 465–470.

McBrayer, L. D. and White, T. D., (2002). Bite Force, Behavior, and Electromyography in the Teiid Lizard, Tupinambis teguixin. Copeia, 1, pp. 111–119.

McCreery, E. K., (2000). Spatial relationships as an indicator of successful pack formation in free-ranging african wild dogs. Behaviour, 137, pp. 579–590.

McElhaney, J., Melvin, J. W., Haynes, R. R., Roberts, V. L., Alemt, N. M., (1970). Mechanical properties of cranial bone. Journal of Biomechanics, 3(5), pp. 497–511.

McHenry, C. R., Clausen, P. D., Daniel, W. J. T., Meers, M. B., Pendharkar, A., (2006). Biomechanics of the rostrum in crocodilians: a comparative analysis using finite-element

modeling. The Anatomical Record. Part A, Discoveries in Molecular, Cellular, and Evolutionary Biology, 288(8), pp. 827–849.

McHenry, C. R., Wroe, S., Clausen, P. D., Moreno, K. and Cunningham, E., (2007). Supermodeled sabercat, predatory behavior in *Smilodon fatalis* revealed by high-resolution 3D computer simulation. Proceedings of the National Academy of Sciences of the United States of America, 104(41), pp. 16010–16015.

McIntosh, A. F. and Cox, P. G., (2016). Functional implications of craniomandibular morphology in African mole-rats (*Rodentia: Bathyergidae*). Biological Journal of the Linnean Society, 117(3), pp. 447–462.

McKenna, M. C. and Bell, S. K., (1997). Classification of Mammals Above the Species Level. Columbia University Press.

McNamara, J. A., (1973). The independent functions of the two heads of the lateral pterygoid muscle. Developmental Dynamics, 138(2), pp. 197–205.

McNitt-Gray, M., (2006). Tradeoffs in Image Quality and Radiation Dose for CT. Medical Physics, 33(14), pp. 2154–2155.

Meachen-Samuels, J., Van Valkenburgh, B., (2009). Craniodental indicators of prey size preference in the Felidae. Biological Journal of the Linnean Society, 96(4), pp. 784–799.

Mech, L. D., (1970). The wolf: the ecology and behavior of an endangered species. Natural History Press.

Mech, L. D. and Boitani, L., (2003). Wolves : behavior, ecology, and conservation. University of Chicago Press.

Mech, L. D. and Frenzel, L. D. J., (1971). Ecological studies of the timber wolf in northeastern Minnesota. Research Paper NC-52. St. Paul, MN: US Dept. of Agriculture, Forest Service, North Central Forest Experiment Station, 52.

Mech, L. D. and Nelson, M., (1990). Evidence of prey-caused mortality in three wolves. American Midland Naturalist, 123(1), pp. 207–208.

Mech, L. and Peterson, R., (2003a). 'Wolf-prey relations, in Wolves: Behavior, Ecology, and Conservation, 1, pp. 131–157. University of Chicago Press.

Melke, G. S. de F., Costa, A. L. F., Lopes, S. L. P. de C., Fuziy, A. and Ferreira-Santos, R. I., (2016). Three-dimensional lateral pterygoid muscle volume: MRI analyses with insertion patterns correlation. Annals of Anatomy, 208, pp. 9–18.

Meloro, C., Hudson, A. and Rook, L., (2015). Feeding habits of extant and fossil canids as determined by their skull geometry. Journal of Zoology, 295(3), pp. 178–188.

Meloro, C., Hunter, J., Tomsett, L., Portela Miguez, R., Prevosti, F. J. and Brown, R. P., (2017). Evolutionary ecomorphology of the Falkland Islands wolf *Dusicyon australis*. Mammal Review, 47(2), pp. 159–163.

Meloro, C., Raia, P., Piras, P., Barbera, C. and O'Higgins, P., (2008). The shape of the mandibular corpus in large fissiped carnivores: Allometry, function and phylogeny. Zoological Journal of the Linnean Society, 154(4), pp. 832–845.

Mhamdi, M. A. and Devaux, J. (1994). Phosphorus exchanges between sediment and water in trophically different reservoirs. Water Research, 28(9), pp. 1971–1980.

Michaud, M., Veron, G., Peignè, S., Blin, A. and Fabre, A.-C., (2018). Are phenotypic disparity and rate of morphological evolution correlated with ecological diversity in Carnivora? Biological Journal of the Linnean Society, 124(3), pp. 294-307.

Midford, P.E., Garland Jr, T. and Maddison, W.P., 2006. PDAP package of Mesquite. Version 1.07.

Milella, M., Zollikofer, C. P. E. and Ponce de León, M. S., (2015). Virtual reconstruction and geometric morphometrics as tools for paleopathology: A new approach to study rare developmental disorders of the skeleton. Anatomical Record, 298(2), pp. 335–345.

Miller, R. E. and Fowler, M. E., (2014). Fowler's zoo and wild animal medicine. Elsevier,Saunders.

Miller, W., (2015). MR bone imaging. Journal of Therapeutic Ultrasound, 3(Suppl 1), p. 37.

Mitchell, B. S. and Peel, S., (2009). Histology : an illustrated colour text. Edinburgh : Churchill Livingstone.

Mitsiopoulos, N., Baumgartner, R. N., Heymsfield, S. B., Lyons, W., Gallagher, D., Ross, R., Maddocks, M., Shrikrishna, D., Vitoriano, S., Natanek, S. A., Rebecca, J., Hart, N., Kemp, P. R., Moxham, J., Polkey, M. I., Nicholas, S., Al-gindan, Y. Y., Hankey, C., Govan, L., Gallagher, D., Steven, B., Sheean, P. M., Peterson, S. J., Perez, S. G., Troy, K. L., Patel, A., Joy, S., Ajanaku, F. C. and Braunschweig, C. A., (1998). Cadaver validation of skeletal muscle measurement by magnetic resonance imaging and computerized tomography Cadaver validation of skeletal muscle measurement by magnetic resonance imaging and computerized tomography. American Physiological Society, 85(1), pp. 115–122.

Mitteroecker, P. and Bookstein, F., (2008). The evolutionary role of modularity and integration in the hominoid cranium. Evolution, 62(4), pp. 943–958.

Mitteroecker, P. and Gunz, P., (2009). Advances in Geometric morphometrics. Evolutionary Biology, 36(2), pp. 235–247.

Moazen, M., Curtis, N., Evans, S. E., Higgins, P. O., Fagan, M. J. and York, H., (2008). Combined finite element and multibody dynamics analysis of biting in a Uromastyx hardwickii lizard skull. Journal of Anatomy, 21 (5), pp.499-508.

Moazen, M., Curtis, N., O'Higgins, P., Jones, M. E. ., Evans, S. E. and Fagan, M. J., (2009). Assessment of the role of sutures in a lizard skull: a computer modelling study. Proceedings of the Royal Society B: Biological Sciences, 276(1654), pp. 39–46.

Mohamed, A. N. A., Brown, M. A., Shabana, A. A., (2010). Study of the ligament tension

and cross-section deformation using nonlinear finite element/multibody system algorithms. Multibody System Dynamics, 23(3), pp. 227–248.

Monteiro, L. R. and Lessa, L. G., (2000). Comparative Analysis of Cranial Suture Complexity in the Genus Caiman (Crocodylia, Alligatoridae). Revista Brasileira De Biologia, Programa De Apoio A Publicacoes Cientificas, (4), p. 689.

Monteiro, L. R. and Nogueira, M. R., (2010). Adaptive radiations, ecological specialization, and the evolutionary integration of complex morphological structures. Evolution, 64(3), pp. 724–744.

Motherway, J. A., Verschueren, P., Van der Perre, G., Vander Sloten, J., Gilchrist, M. D., (2009). The mechanical properties of cranial bone: The effect of loading rate and cranial sampling position. Journal of Biomechanics, 42(13), pp. 2129–2135.

MottaJunior, J., Talamoni, S., Lombardi, J. and Simokomaki, K., (1996). Diet of the maned wolf, Chrysocyon brachyurus, in central Brazil', Journal Of Zoology, 240, pp. 277–284.

Müller, D. W. H., Gaillard, J.-M., Lackey, L. B., Hatt, J.-M. and Clauss, M., (2010). Comparing life expectancy of three deer species between captive and wild populations. European Journal of Wildlife Research, 56(2), pp. 205–208.

Murdoch, J. D., Munkhzul, T., Buyandelger, S., Reading, R. P. and Sillero-Zubiri, C., (2010). Seasonal food habits of corsac and red foxes in Mongolia and the potential for competition. Mammalian Biology. Elsevier, 75(1), pp. 36–44.

Murphy, R. A., Beardsley, A. C., (1974). Mechanical properties of the cat soleus muscle in situ. The American Journal of Physiology, 227(5), pp. 1008–13.

Murray, G. M., (2012). The Lateral Pterygoid Muscle: Function and Dysfunction. Seminars in Orthodontics, 18(1), pp. 44–50.

Nafe, L. A., (1990). The clinical presentation and diagnosis of intracranial neoplasia, in Seminars in veterinary medicine and surgery (small animal), pp. 223–231.

Nanova, O., Pröa, M., Fitton, L. C., Evteev, A. and O'Higgins, P., (2017). Comparison of cranial performance between mainland and two island subspecies of the Arctic fox Vulpes lagopus (Carnivora: Canidae) during simulated biting. Biological Journal of the Linnean Society, 121(4), pp. 923-935.

Nel, J. A. J., (1978). Notes on the food and foraging behavior of the bat-eared fox, *Otocyon megalotis*. Bulletin of the Carnegie Museum of Natural History, 1, pp. 132–137.

Nickel, R., Schummer, A., Seiferle, E., (1981). The circulatory system, the skin, and the cutaneous organs of the domestic mammals. Verlag Paul Parry.

Nickel, R., Schummer, A., S. and E., (1979). The Viscera of the Domestic Mammals. New York: Springer-Verlag.

Noble, V. E., Kowalski, E. M. and Ravosa, M. J., (2000). Orbit orientation and the function of the mammalian postorbital bar. Journal of Zoology, 250(3), pp. 405–418.

Nowak, R. M., (2005). Walker's Carnivores of the World. John Hopkins University Press.

Nyakatura, K. *et al.* Nyakatura, K., Bininda-Emonds, O. R., Bininda-Emonds, O., Gittleman, J., Purvis, A., Purvis, A., Gittleman, J., Cowlishaw, G., Mace, G., Brashares, J., Diniz-Filho, J., Meloro, C., O'Higgins, P., Clubb, R., Mason, G., Bush, E., Allman, J., Lindenfors, P., Tullberg, B., Biuw, M., Nunn, C., Gittleman, J., Antonovics, J., Torres, J., Miquel, J., Casanova, J., Ribas, A., Feliu, C., Morand, S., Sanderson, M., Purvis, A., Henze, C., Wyss, A., Flynn, J., Wozencraft, W., Wozencraft, W., Bininda-Emonds, O., Dragoo, J., Bradley, R., Honeycutt, R., Templeton, J., Dragoo, J., Honeycutt, R., Flynn, J., Finarelli, J., Zehr, S., Hsu, J., Nedbal, M., Gaubert, P., Veron, G., Yoder, A., Burns, M., Zehr, S., Delefosse, T., Veron, G., Goodman, S., Flynn, J., Hunt, R., Wiig, Ø., Flynn, J., Neff, N., Tedford, R., Arnason, U., Widegren, B., Wayne, R., Benveniste, R., Janczewski, D., O'Brien, S., Vrana, P., Milinkovitch, M., Powell, J., Wheeler, W., Veron, G., Mishler, B., Gatesy, J., Matthee, C., DeSalle, R., Hayashi, C., Bininda-Emonds, O., Wilkinson, M., Pisani, D., Cotton, J., Corfe, I., Meredith, R., Janecka, J., Gatesy, J., Ryder, O., Fisher, C., Teeling, E., Goodbla, A., Eizirik, E., Simao, T., Stadler, T., Rabosky, D., Honeycutt, R., Flynn, J., Ingram, C.,

Steiner, C., Williams, T., Robinson, T., Burk-Herrick, A., Westerman, M., Ayoub, N., Springer, M., Murphy, W., Springer, M., Murphy, W., Eizirik, E., O'Brien, S., Bininda-Emonds, O., Cardillo, M., Jones, K., MacPhee, R., Beck, R., Grenyer, R., Price, S., Vos, R., Gittleman, J., Purvis, A., Eizirik, E., Murphy, W., Koepfli, K., Johnson, W., Dragoo, J., Wayne, R., O'Brien, S., Beck, R., Bininda-Emonds, O., Cardillo, M., Liu, F.-G., Purvis, A., Bininda-Emonds, O., Cardillo, M., Jones, K., MacPhee, R., Beck, R., Grenyer, R., Price, S., Vos, R., Gittleman, J., Purvis, A., Kitchener, A., Wang, X., Tedford, R., Valkenburgh, B. Van, Wayne, R., Werdelin, L., Solounias, N., Deméré, T., Tedford, R., Taylor, B., Wang, X., Wayne, R., Geffen, E., Girman, D., Koepfli, K., Lau, L., Marshall, C., Zrzavy, J., Ricankova, V., Lindblad-Toh, K., Wade, C., Mikkelsen, T., Karlsson, E., Jaffe, D., Kamal, M., Clamp, M., Chang, J., Kulbokas, E., Zody, M., Mauceli, E., Xie, X., Breen, M., Wayne, R., Ostrander, E., Ponting, C., Galibert, F., Smith, D., DeJong, P., Kirkness, E., Alvarez, P., Biagi, T., Brockman, W., Butler, J., Chin, C., Cook, A., Cuff, J., Daly, M., DeCaprio, D., Gnerre, S., Graphodatsky, A., Perelman, P., Sokolovskaya, N., Beklemisheva, V., Serdukova, N., Dobigny, G., O'Brien, S., Ferguson-Smith, M., Yang, F., Agnarsson, I., Kuntner, M., May-Collado, L., Clutton-Brock, J., Corbet, G., Hills, M., Fulton, T., Strobeck, C., Higdon, J., Bininda-Emonds, O., Beck, R., Ferguson, S., Fulton, T., Strobeck, C., Arnason, U., Gullberg, A., Janke, A., Kullberg, M., Lehman, N., Petrov, E., Väinolä, R., Palo, J., Väinolä, R., Chapskii, K., Muizon, C. de, Wyss, A., Burns, J., Fay, F., King, J., Higdon, J., Bininda-Emonds, O., Beck, R., Ferguson, S., Bininda-Emonds, O., Russell, A., Berta, A., Wyss, A., Repenning, C., Peterson, R., Hubbs, C., Wynen, L., Goldsworthy, S., Insley, S., Adams, M., Bickham, J., Francis, J., Gallo, J., Hoelzel, A., Majluf, P., White, R., Slade, R., Fulton, T., Strobeck, C., Brunner, S., Koepfli, K., Wayne, R., Koepfli, K., Deere, K., Slater, G., Begg, C., Begg, K., Grassman, L., Lucherini, M., Veron, G., Wayne, R., Pagès, M., Calvignac, S., Klein, C., Paris, M., Hughes, S., Hänni, C., Yu, L., Li, Q., Ryder, O., Zhang, Y., Koepfli, K., Jenks, S., Eizirik, E., Zahirpour, T., Valkenburgh, B. Van, Wayne, R., Barycka, E., Gaubert, P., Wozencraft, W., Cordeiro-Estrela, P., Veron, G., Veron, G., Colyn, M., Dunham, A., Taylor, P., Gaubert, P., Patou, M., Mclenachan, P., Morley, C., Couloux, A., Jennings, A., Veron, G., Patou, M., Debruyne, R., Jennings, A., Zubaid, A., Rovie-Ryan, J., Veron, G., Gaubert, P., Cordeiro-Estrela, P., O'Brien, S., Martenson, J., Miththapala, S., Janczewski, D., Pecon-Slattery, J., Johnson, W., Gilbert, D., Roelke, M., Packer, C., Bush, M., Wildt, D., Johnson, W., Eizirik, E., Pecon-Slattery, J., Murphy, W., Antunes, A., Teeling, E., O'Brien, S., Robinson, D., Foulds, L., Steel, M., Penny, D., Bininda-Emonds, O., Salamin, N., Hodkinson, T., Savolainen, V., Bininda-Emonds, O., Sanderson, M., Hone, D., Benton, M., Lewis, P., Tuffley, C., Steel, M.,

Purvis, A., Mace, G., Gittleman, J., Purvis, A., Orme, C., Toomey, N., Pearson, P., Phillimore, A., Price, T., Chan, K., Moore, B., Slowinski, J., Guyer, C., Slowinski, J., Guyer, C., Faith, D., Isaac, N., Turvey, S., Collen, B., Waterman, C., Baillie, J., Maddison, D., Swofford, D., Maddison, W., Maddison, W., Maddison, D., Maddison, W., Maddison, D., Bininda-Emonds, O., Jones, K., Price, S., Cardillo, M., Grenyer, R., Purvis, A., Ahmed, A., Jahan, M., Braunitzer, G., Anderson, E., Gelder, R. Van, Slade, R., Moritz, C., Heideman, A., Graphodatsky, A., Sharshov, A., Ternovsky, D., Ternovskaya, Y., Zhang, Y.-P., Ryder, O., Bininda-Emonds, O., Jones, K., Price, S., Grenyer, R., Cardillo, M., Habib, M., Purvis, A., Gittleman, J., Bidartondo, M., Bruns, T., Blackwell, M., Edwards, I., Taylor, A., Horton, T., Zhang, N., Koljalg, U., May, G., Kuyper, T., Bever, J., Gilbert, G., Taylor, J., DeSantis, T., Pringle, A., Borneman, J., Thorn, G., Berbee, M., Mueller, G., Anderson, G., Vellinga, E., Branco, S., Anderson, I., Dickie, I., Avis, P., Timonen, S., Kjøller, R., Lodge, D., Bateman, R., Larkin, M., Blackshields, G., Brown, N., Chenna, R., McGettigan, P., McWilliam, H., Valentin, F., Wallace, I., Wilm, A., Lopez, R., Thompson, J., Gibson, T., Higgins, D., Bininda-Emonds, O., Edgar, R., Stamatakis, A., Stamatakis, A., Hoover, P., Rougemont, J., Baum, B., Ragan, M., Bininda-Emonds, O., Beck, R., Purvis, A., Kupczok, A., Schmidt, H., Haeseler, A. von, Bininda-Emonds, O., Bryant, H., Nixon, K., Swofford, D., Price, S., Bininda-Emonds, O., Gittleman, J., Purvis, A., Posada, D., Crandall, K., Holm, S., Guindon, S., Gascuel, O., Guindon, S., Dufayard, J., Lefort, V., Anisimova, M., Hordijk, W., Gascuel, O., Nee, S., Mooers, A., Harvey, P., Pybus, O., Harvey, P. and Stadler, T., (2012). Updating the evolutionary history of Carnivora (Mammalia): a new species-level supertree complete with divergence time estimates. BMC Biology, 10 (1) pp. 12.

O'Higgins, P., (2000). The study of morphological variation in the hominid fossil record; biology, landmark and geometry. Journal of Anatomy, 197(1), pp. 103–120.
Check in right place alphabetically.

O'Regan, H. J. and Kitchener, A. C., (2005). The effects of captivity on the morphology of captive, domesticated and feral mammals. Mammal Review, 35(3–4), pp. 215–230.
Check in right place alphabetically.

Ogle, R. C., Tholpady, S. S., McGlynn, K. A., Ogle, R. A. (2004). Regulation of Cranial Suture Morphogenesis. Cells Tissues Organs, *176*(1–3), 54–66.

Ogutu, J. O., Piepho, H. P., Dublin, H. T., Bhola, N. and Reid, R. S. (2008). Rainfall influences on ungulate population abundance in the Mara-Serengeti ecosystem. Journal of Animal Ecology, 77(4), pp. 814–829.

Oldfield, C. C., McHenry, C. R., Clausen, P. D., Chamoli, U., Parr, W. C. H., Stynder, D. D., Wroe, S., (2012). Finite element analysis of ursid cranial mechanics and the prediction of feeding behaviour in the extinct giant *Agriotherium africanum*. Journal of Zoology, 286(2), pp. 171-171.

Opperman, L. A. (2000). Cranial sutures as intramembranous bone growth sites. Developmental Dynamics, *219*(4), 472–485.

Owen-smith, N., (1990). Demography of a Large Herbivore, the Greater Kudu Tragelaphus strepsiceros, in Relation to Rainfall. Journal of Animal Ecology, (3), pp. 893-399.

Oxnard, C. E., (1968). The architecture of the shoulder in some mammals. Journal of Morphology, 126(3), pp. 249–290.

Palmqvist, P., Martínez-Navarro, B., Pérez-Claros, J. A., Torregrosa, V., Figueirido, B., Jiménez-Arenas, J. M., Patrocinio Espigares, M., Ros-Montoya, S. and De Renzi, M., (2011). The giant hyena *Pachycrocuta brevirostris*: Modelling the bone-cracking behavior of an extinct carnivore. Quaternary International, 243(1), pp. 61–79.

Penrose, F., Kemp, G. J., Jeffery, N., (2016). Scaling and Accommodation of Jaw Adductor Muscles in Canidae. Anatomical Record, 299(7), pp. 951–966.

Pereira, M. E. and Pond, C. M., (1995). Organization of white adipose tissue in Lemuridae. American Journal of Primatology, 35(1), pp. 1–13.

Perini, F. A., Russo, C. A. M. and Schrago, C. G., (2010). The evolution of South American endemic canids: A history of rapid diversification and morphological parallelism. Journal of Evolutionary Biology, 23(2), pp. 311–322.

Perry, J. M. G., Hartstone-Rose, A. and Wall, C. E., (2011). The Jaw Adductors of Strepsirrhines in Relation to Body Size, Diet, and Ingested Food Size. Anatomical Record, 294(4), pp. 712–728.

Perry, J. M. G., Macneill, K. E., Heckler, A. L., Rakotoarisoa, G. and Hartstone-Rose, A., (2014). Anatomy and adaptations of the chewing muscles in Daubentonia (Lemuriformes). Anatomical Record, 297(2), pp. 308–316.

Perry, J.M. and Wall, C.E., (2008). Scaling of the chewing muscles in prosimians. In Primate craniofacial function and biology (pp. 217-240). Springer, Boston, MA.

Peterson, J., Dechow, P. C., (2003). Material properties of the human cranial vault and zygoma. The Anatomical Record. Part A, Discoveries in Molecular, Cellular, and Evolutionary Biology, 274(1), pp. 785–797.

Peterson, R., Ciucci, P., (2003). The Wolf as a Carnivore in Wolves: Behavior, Ecology, and Conservation, pp. 104–130. University of Chicago Press.

Peterson, T. and Müller, G. B. (2018). Developmental finite element analysis of cichlid pharyngeal jaws: Quantifying the generation of a key innovation. PloS one, 13(1), p. e0189985.

Piancino, M. G., Isola, G., Cannavale, R., Cutroneo, G., Vermiglio, G., Bracco, P., Anastasi, G. P., (2017). From periodontal mechanoreceptors to chewing motor control: A systematic review. Archives of Oral Biology. Elsevier Ltd, 78, pp. 109–121.

Pierce, S. E., Angielczyk, K. D. and Rayfield, E. J., (2009). Shape and mechanics in thalattosuchian (Crocodylomorpha) skulls: Implications for feeding behaviour and niche partitioning. Journal of Anatomy, 215(5), pp. 555–576.

Pinares-Toledo, J., Marileo Zagal, R., Bruce Castillo, L. and Villanueva Conejeros, R., (2018). Is the buccal compartment a masticatory space extension or an anatomic space in itself? Evidence based on medical images and human cadaver dissection. Oral

Radiology, 34(1), pp. 49–55.

Pitulko, V. V and Kasparov, A. K., (2017). Journal of Archaeological Science : Reports Archaeological dogs from the Early Holocene Zhokhov site in the Eastern Siberian Arctic. Journal of Archaeological Science: 13, pp. 491–515.

Pocock, R. I. (1935). The races of *Canis lupus*. In Proceedings of the Zoological Society of London,105, pp. 647–686

Powell, P. L., Roy, R. R., Kanim, P., Bello, M. a and Edgerton, V. R., (1984). Predictability of skeletal muscle tension from architectural determinations in guinea pig hindlimbs. Journal of applied physiology, 57(6), pp. 1715–1721.

Poyarkov, A., Ovsyanikov, N., (2004). Corsac Fox, *Vulpes corsac*. In Canids: Foxes, Wolves, Jackals, and Dogs. Status Survey and Conservation Action Plan. IUCN/SSC Canid Specialist Group. Gland, Switzerland and Cambridge, UK, 142–148.

Prestrud, P., (1991). Adaptations By the Arctic Fox (*Alopex-Lagopus*) To the Polar Winter. Arctic, 44(2), pp. 132–138.

Prestrud, P., (1992). Food habits and observations of the hunting behaviour of Arctic foxes, *Alopex lagopus*, in Svalbard. Canadian Field-Naturalist 106 (2), pp. 225-36.

Preuschoft, H., Witzel, U. (2005). Functional shape of the skull in vertebrates: Which forces determine skull morphology in lower primates and ancestral synapsids? Anatomical Record - Part A Discoveries in Molecular, Cellular, and Evolutionary Biology, 283(2), pp. 402–413.

Prevosti, F. J., (2010). Phylogeny of the large extinct South American Canids (Mammalia, Carnivora, Canidae) using a “total evidence” approach. Cladistics, 26(5), pp. 456–481.

Prevosti, F. J. and Forasiepi, A. M., (2018). South American Fossil Carnivorans (Order Carnivora), in Evolution of South American Mammalian Predators During the Cenozoic: Paleobiogeographic and Paleoenvironmental Contingencies, pp. 85–136, Springer.

Prevosti, F. J. and Rincón, A. D., (2007). A new fossil canid assemblage from the late Pleistocene of northern South America: the canids of the Inciarte Asphalt Pit (Zulia, Venezuela), fossil record and biogeography. Journal of Paleontology, 81(5), pp. 1053–1065.

Prevosti, F. J., Turazzini, G. F., Ercoli, M. D. and Hingst-Zaher, E., (2012). Mandible shape in marsupial and placental carnivorous mammals: A morphological comparative study using geometric morphometrics. Zoological Journal of the Linnean Society, 164(4), pp. 836–855.

Prince, J. H., (1953). Comparative anatomy of the orbit. The British Journal of Physiological Optics, 10(3), pp. 144–154.

Prossinger, H., Bookstein, F., Schäfer, K. and Seidler, H., (2000). Reemerging stress: Supraorbital torus morphology in the mid-sagittal plane? Anatomical Record, 261(5), pp. 170–172.

Qian, H., Chen, J. and Katona, T. R., (2001). The influence of PDL principal fibers in a 3-dimensional analysis of orthodontic tooth movement. American Journal of Orthodontics and Dentofacial Orthopedics, 120(3), pp. 272–279.

Radhakrishnan, P., Mao, J. J., (2004). Nanomechanical properties of facial sutures and sutural mineralization front. Journal of Dental Research, 83(6), pp. 470–475.

Radinsky, L. B., (1981). Evolution of skull shape in carnivores: 1. Representative modern carnivores. Biological Journal of the Linnean Society, 16(4), pp. 337–355.

Rae, T. C. and Koppe, T., (2008). Independence of biomechanical forces and craniofacial pneumatization in Cebus. Anatomical Record, 291(11), pp. 1414–1419.

Rafferty, K. L. and Herring, S. W., (1999). Craniofacial sutures: Morphology, Growth, and In Vivo Masticatory Strains. J. Morphol, 242(2), pp. 167–179.

Rafferty, K. L., Herring, S. W. and Artese, F., (2000). Three-dimensional loading and growth of the zygomatic arch. Journal of Experimental Biology, 203 (14), pp. 2093–2104.

Rager, L., Hautier, L., Forasiepi, A., Goswami, A. and Sánchez-Villagra, M. R., (2014). Timing of cranial suture closure in placental mammals: Phylogenetic patterns, intraspecific variation, and comparison with marsupials. Journal of Morphology, 275(2), pp. 125–140.

Rahmoun, J., Auperrin, A., Delille, R., Naceur, H., Drazetic, P., (2014). Characterization and micromechanical modeling of the human cranial bone elastic properties. Mechanics Research Communications, *60*, 7–14.

Ramos, A. and Simões, J. A., (2006). Tetrahedral versus hexahedral finite elements in numerical modelling of the proximal femur. Medical Engineering and Physics, 28(9), pp. 916–924.

Ravosa, M. J., (1991a). Interspecific perspective on mechanical and nonmechanical modeis of primate circumorbital morphology. American Journal of Physical Anthropology, 86 (3), pp.369-396.

Ravosa, M. J., (1991b). Ontogenetic perspective on mechanical and nonmechanical models of primate circumorbital morphology. American Journal of Physical Anthropology. 85(1), pp. 95–112.

Ravosa, M. J., Johnson, K. R., Hylander, W. L., Carolina, N., (2000). Strain in the Galago Facial Skull. Journal of Morphology, 245 (1), pp.51-66.

Rayfield, E. J., (2007). Finite Element Analysis and Understanding the Biomechanics and Evolution of Living and Fossil Organisms. Annu. Rev. Earth Planet. Sci, 35, pp. 541–76.

Rayfield, E. J., (2011). Strain in the ostrich mandible during simulated pecking and validation of specimen-specific finite element models. Journal of Anatomy, 218(1), pp. 47–58.

Rayfield, E. J., Norman, D. B., Horner, C. C., Horner, J. R., Smith, P. M., Thomason, J. J., Upchurch, P., (2001). Cranial design and function in a large theropod dinosaur. Nature, 409(6823), pp. 1033–1037.

Reduker, D. W., (1983). Functional analysis of the masticatory apparatus in two species of Myotis. Journal of Mammalogy, 64(2), pp. 277–286.

Regodón, S., Vivo, J. M., Franco, A., Guillen, M. T. and Robina, A., (1993). Craniofacial angle in dolicho-, meso-and brachycephalic dogs: radiological determination and application. Annals of anatomy, Anatomischer Anzeiger: official organ of the Anatomische Gesellschaft, 175(4), pp. 361–363.

Reynolds, S. C., (2012). Nyctereutes terblanchei: The raccoon dog that never was. South African Journal of Science, 108(1–2), pp. 1–10.

Rho, J. Y., Tsui, T. Y., Pharr, G. M., (1997). Elastic properties of human cortical and trabecular lamellar bone measured by nanoindentation. Biomaterials, 18(20), pp. 1325–1330.

Richardson, L. F., (1911). The approximate arithmetical solution by finite differences of physical problems involving differential equations, with an application to the stresses in a masonry dam. Phil. Trans. R. Soc. Lond. A. The Royal Society, 210(459–470), pp. 307–357.

Richmond, B. G., Wright, B. W., Grosse, I., Dechow, P. C., Ross, C. F., Spencer, M. A. and Strait, D. S., (2005). Finite element analysis in functional morphology. The Anatomical Record Part A: Discoveries in Molecular, Cellular, and Evolutionary Biology, 283A(2), pp. 259–274.

Ricklefs, R. E., Road, N. B. and Louis, S., (2016). Nordic Society Oikos Applications of Phylogenetically Independent Contrasts : A Mixed Progress Report. Nordic Society Oikos 77(1), pp. 167–172.

Rilling, J.K., (2006). Human and nonhuman primate brains: are they allometrically scaled versions of the same design? Evolutionary Anthropology: Issues, News, and Reviews, 15(2), pp.65-77.

Rizzuto, M., Carbone, C. and Pawar, S., (2018). Foraging constraints reverse the scaling of activity time in carnivores. Nature Ecology and Evolution, 2(2), pp. 247–253.

Rodden, M., Rodrigues, F. and Bestelmeyer, S., (2004). Maned wolf (*Chrysocyon brachyurus*), Canids: Foxes, Wolves, Jackals and Dogs, Status Survey and Conservation Action Plan. Cambridge: IUCN/SSC Canid Specialist Group, pp. 38–43.

Rohlf, F. J. and Marcus, L. F., (1993). A revolution in morphometrics. Trends in ecology and evolution, 8, p. 129.

Rolfe, V. E., Adams, C. a, Butterwick, R. F. and Batt, R. M., (2002). Relationship between faecal character and intestinal transit time in normal dogs and diet-sensitive dogs. The Journal of small animal practice, 43(7), pp. 290–294.

Röhrle, O. and Pullan, A. J., (2007). Three-dimensional finite element modelling of muscle forces during mastication. Journal of Biomechanics, 40(15), pp. 3363–3372.

Rolland, J., Condamine, F. L., Jiguet, F., Morlon, H., (2014). Faster speciation and reduced extinction in the tropics contribute to the mammalian latitudinal diversity gradient. PLoS Biology. Public Library of Science, 12(1), p. e1001775.

Ross, C. F., (2001). In vivo function of the craniofacial haft: The interorbital “pillar”. American Journal of Physical Anthropology, 116(2), pp. 108–139.

Ross, C. F. and Hylander, W. L., (1996). In vivo and in vitro bone strain in the owl monkey circumorbital region and the function of the postorbital septum. American Journal of Physical Anthropology, 101(2), pp. 183–215.

Rueness, E. K., Asmyhr, M. G., Sillero-Zubiri, C., Macdonald, D. W., Bekele, A., Atickem,

A., Stenseth, N. C., (2011). The cryptic African wolf: Canis aureus lupaster is not a golden jackal and is not endemic to Egypt. PLoS ONE,6(1).doi:10.1371/journal.pone.0016385.

Rueness, E. K., Trosvik, P., Atickem, A., Sillero-Zubiri, C. and Trucchi, E., (2015). The African wolf is a missing link in the wolf-like canid phylogeny. BioRxiv, p. 17996.

Ryan, S. D., Williams, J. L., (1989). Tensile testing of rodlike trabeculae excised from bovine femoral bone. Journal of Biomechanics, 22(4), 351–355.

Sablin, M. and Khlopachev, G., (2002). The earliest Ice Age dogs: evidence from Eliseevichi. Current Anthropology, 43(5), pp. 795–799.

Sacco, T., Van Valkenburgh, B., (2004). Ecomorphological indicators of feeding behaviour in the bears (Carnivora: Ursidae). Journal of Zoology, 263(1), pp. 41–54.

Sacks, R. D. and Roy, R. R., (1982). Architecture of the hind limb muscles of cats: Functional significance. Journal of Morphology, 173(2), pp. 185–195.

Sakamoto, M., Lloyd, G. T. and Benton, M. J. (2010). Phylogenetically structured variance in felid bite force: The role of phylogeny in the evolution of biting performance. Journal of Evolutionary Biology, 23(3), pp. 463–478.

Sanal, H. T., Chen, L., Negrao, P., Haghighi, P., Trudell, D. J. and Resnick, D. L., (2009). Distal attachment of the brachialis muscle: Anatomic and MRI study in cadavers. American Journal of Roentgenology, 192(2), pp. 468–472.

Santana, S. E., (2016). Quantifying the effect of gape and morphology on bite force: Biomechanical modelling and in vivo measurements in bats. Functional Ecology, 30(4), pp. 557–565.

Santana, S. E., (2018). Comparative Anatomy of Bat Jaw Musculature via Diffusible Computed Tomography. Anatomical Record, 301(2),, pp. 267–278.

Satoh, K. and Iwaku, F., (2006). Jaw muscle functional anatomy in northern grasshopper

mouse, *Onychomys leucogaster*, a carnivorous murid. Journal of Morphology, 267(8), pp. 987–999.

Satoh, K. and Iwaku, F., (2009). Structure and direction of jaw adductor muscles as herbivorous adaptations in Neotoma mexicana (Muridae, Rodentia). Zoomorphology, 128(4), pp. 339–348.

Savakova, D. G., (2012). The Influence of Orbit Size on Cranial Morphology in Tarsius. PhD Thesis. Northwestern University.

Scapino, R., (1981). Morphological investigation into functions of the jaw symphysis in carnivorans. Journal of Morphology. Wiley Online Library, 167(3), pp. 339–375.

Scapino, R., (1965). The third joint of the canine jaw. Journal of Morphology, 116(1), pp. 23–50.

Schneider, C.A., Rasband, W.S. and Eliceiri, K.W., (2012). NIH Image to ImageJ: 25 years of image analysis. Nature methods, 9(7), p.671.

Schoenebeck, J. J. and Ostrander, E. A., (2013). The Genetics of Canine Skull Shape Variation. Genetics, 193(2), pp. 317–325.

Schumacher, G.-H., (1961). Funktionelle morphologie der kaumuskulatur. Fischer.

Schwitzer, C. and Kaumanns, W., (2001). Body weights of ruffed lemurs (*Varecia variegata*) in European zoos with reference to the problem of obesity. Zoo Biology, 20(4), pp. 261–269.

Seeram, E., (2009). Computed tomography : physical principles, clinical applications, and quality control. St. Louis, Mo. : Saunders/Elsevier.

Segura, V. and Prevosti, F., (2012). A quantitative approach to the cranial ontogeny of Lycalopex culpaeus (Carnivora: Canidae). Zoomorphology, 131(1), pp. 79–92.

Selvan, K. M., Veeraswami, G. G., Hussain, S. A., (2013). Dietary preference of the Asiatic

wild dog (*Cuon alpinus*). Mammalian Biology, 78(6), pp. 486–489.

Sharp, A. C. and Rich, T. H., (2016). Cranial biomechanics, bite force and function of the endocranial sinuses in Diprotodon optatum, the largest known marsupial. Journal of Anatomy, *228*(6), 984–995.

Sharp, A. C. and Trusler, P. W., (2015). Morphology of the jaw-closing musculature in the common wombat (*Vombatus ursinus*) using digital dissection and magnetic resonance imaging. PLoS ONE, 10(2), pp. 1–20.

Sicuro, F. L., Oliveira, L. F. B., (2011). Skull morphology and functionality of extant Felidae (Mammalia: Carnivora): a phylogenetic and evolutionary perspective. Zoological Journal of the Linnean Society, 161(2), pp. 414–462.

Sidorovich, V. E., Solovej, I. A, Sidorovich, A., Dyman, A. A., (2008). Seasonal and annual variation in the diet of the raccoon dog *Nyctereutes procyonoides* in northern Belarus: The role of habitat type and family group. Acta Theriologica, 53(1), pp. 27–38.

Sillero-Zubiri, C., Hoffmann, M., MacDonald, D. W., (2004). Canids: foxes, wolves, jackals, and dogs: status survey and conservation action plan. IUCN Gland, Switzerland.

Simons, E. L., (1962). Fossil evidence relating to the early evolution of primate behavior. Annals of the New York Academy of Sciences, 102(2), pp. 282–294.

Singh, B., Klimek, J., Dyce, K. M., Sack, W. O. and Wensing, C. J. G., (2018) Dyce, Sack, and Wensing's textbook of veterinary anatomy. Elsevier.

Sjaastad, O. V, Hove, K. and Sand, O., (2010). Physiology of domestic animals. Scan. Vet. Press.

Slater, G. J., (2015). Iterative adaptive radiations of fossil canids show no evidence for diversity-dependent trait evolution. Proceedings of the National Academy of Sciences, 112(16), pp. 4897–4902.

Slater, G. J., Dumont, E. R. and Van Valkenburgh, B., (2009). Implications of predatory specialization for cranial form and function in canids', Journal of Zoology, 278(3), pp. 181–188.

Slater, G.J. and Van Valkenburgh, B., (2008). Long in the tooth: evolution of sabertooth cat cranial shape. Paleobiology, 34(3), pp.403-419.

Slater, G. J., Figueirido, B., Louis, L., Yang, P. and Valkenburgh, B. Van, (2010) Biomechanical Consequences of Rapid Evolution in the Polar Bear Lineage. 5(11), pp. 1–7.

Slater, G.J. and Van Valkenburgh, B., (2009). Allometry and performance: the evolution of skull form and function in felids. Journal of evolutionary biology, 22(11), pp.2278-2287.

Smith, K. K., (1993). The form of the feeding apparaus in terrestrial vertebrates, in The Skull, Volume 3, pp. 150–195. University of Chicago Press.

Smith, T. D., Deleon, V. B. and Rosenberger, A. L., (2013). At Birth, Tarsiers Lack a Postorbital Bar or Septum. Anatomical Record, 296(3), pp. 365–377.

Smith, T. G., (1976). Predation of ringed seal pups (*Phoca hispida*) by the arctic fox (*Alopex lagopus*). Canadian Journal of Zoology, 54(10), pp. 1610–1616.

Snyder, J. M., Shofer, F. S., Winkle, T. J. Van and Massicotte, C., (2006). Canine Intracranial Primary Neoplasia: 173 Cases (1986–2003). Journal of Veterinary Internal medicine 20 (3) 78, pp. 669–675.

Soibelzon, L. H., Grinspan, G. A., Bocherens, H., Acosta, W. G., Jones, W., Blanco, E. R. Prevosti, F., (2014). South American giant short-faced bear (*Arctotherium angustidens*) diet: evidence from pathology, morphology, stable isotopes, and biomechanics. Journal of Paleontology, 88(06), pp. 1240–1250.

Sotnikova, M., (2006). A new canid Nurocyon chonokhariensis gen. et sp. nov. (Canini,

Canidae, Mammalia) from the Pliocene of Mongolia. Courier Forschungsinstitut Senckenberg, 256, pp. 11–21.

Spencer, M. A., (1998). Force production in the primate masticatory system: electromyographic tests of biomechanical hypotheses. Journal of Human Evolution, 34(1), pp.25-54.

Spector, S. A., Gardiner, P. F., Zernicke, R. F., Roy, R. R. and Edgerton, V. R., (1980). Muscle architecture and force-velocity characteristics of cat soleus and medial gastrocnemius: implications for motor control. Journal of Neurophysiology. Am Physiological Soc, 44(5), pp. 951–960.

Stevens-Sparks, C. and Strain, G. M., (2014). The canine jaw-ear connection: The malleomandibular and tympanomandibular ligaments. Anatomical Record, 297(5), pp. 876–891.

Stockard, C. R. and James, W. T., (1941). The genetic and endocrinic basis for differences in form and behavior: as elucidated by studies of contrasted pure-line dog breeds and their hybrids (19). The Wistar Institute of Anatomy and Biology.

Storey, R. N., Meikle, G. R., Stringer, M. D. and Woodley, S. J., (2016). Proximal hamstring morphology and morphometry in men: an anatomic and MRI investigation. Scandinavian Journal of Medicine and Science in Sports, 26(12), pp. 1480–1489.

Ström, D., Holm, S., Clemensson, E., Haraldson, T. and Carlsson, G.E., (1988). Gross anatomy of the craniomandibular joint and masticatory muscles of the dog. Archives of oral biology, 33(8), pp.597-604.

Ström, D. and Holm, S., (1992). Bite-force development, metabolic and circulatory response to electrical stimulation in the canine and porcine masseter muscles. Archives of Oral Biology, 37(12), pp. 997–1006.

Sutor, A., Kauhala, K., Ansorge, H., (2010). Diet of the raccoon dog *Nyctereutes procyonoides* — a canid with an opportunistic foraging strategy. Acta Theriologica, 55(2),

pp. 165–176.

Tanner, J. B., Dumont, E. R., Sakai, S. T., Lundrigan, B. L. and Holekamp, K. E. (2008). Of arcs and vaults: The biomechanics of bone-cracking in spotted hyenas (Crocuta crocuta). Biological Journal of the Linnean Society, 95(2), pp. 246–255.

Tanner, J. B., Zelditch, M. L., Lundrigan, B. L. and Holekamp, K. E., (2010). Ontogenetic change in skull morphology and mechanical advantage in the spotted hyena (*Crocuta crocuta*). Journal of Morphology, 271(3), pp. 353–365.

Tarnawski, B. A., Flores, D., Cassini, G. and Cappozzo, H. L., (2015). A comparative analysis on cranial ontogeny of South American fur seals (*Otariidae: Arctocephalus*). Zoological Journal of the Linnean Society, 173(1), pp. 249–269.

Taylor, A. B., Jones, K. E., Kunwar, R. and Ravosa, M. J., (2006). Dietary consistency and plasticity of masseter fiber architecture in postweaning rabbits. Anatomical Record - Part A Discoveries in Molecular, Cellular, and Evolutionary Biology, 288(10), pp. 1105–1111.

Taylor, A. B., Terhune, C. E., Toler, M., Holmes, M., Ross, C. F. and Vinyard, C. J., (2018). Jaw-Muscle Fiber Architecture and Leverage in the Hard-Object Feeding Sooty Mangabey are not Structured to Facilitate Relatively Large Bite Forces Compared to Other Papionins. Anatomical Record, 342(August 2017), pp. 325–342.

Taylor, A. B. and Vinyard, C. J., (2009). Jaw-muscle fiber architecture in tufted capuchins favors generating relatively large muscle forces without compromising jaw gape. Journal of human evolution. 57(6), pp. 710–720.

Taylor, A. B., Vinyard, C. J., (2013). The relationships among jaw-muscle fiber architecture, jaw morphology, and feeding behavior in extant apes and modern humans. American Journal of Physical Anthropology, 151(1), pp. 120–134.

Taylor, A. B., Yuan, T., Ross, C. F. and Vinyard, C. J. (2015). Jaw-muscle force and excursion scale with negative allometry in platyrrhine primates. American Journal of Physical Anthropology, 158(2), pp. 242–256.

Tchaicka, L., de Freitas, T. R. O., Bager, A., Vidal, S. L., Lucherini, M., Iriarte, A., Novaro, A., Geffen, E., Garcez, F. S., Johnson, W. E., Wayne, R. K. and Eizirik, E., (2016). Molecular assessment of the phylogeny and biogeography of a recently diversified endemic group of South American canids (Mammalia: Carnivora: Canidae). Genetics and Molecular Biology, 39(3), pp. 442-451.

Tedford, R. H., Taylor, B. E. and Wang, X., (1995). Phylogeny of the Caninae (Carnivora: Canidae): the living taxa', American Museum Novitates, 3146(3146), pp. 1–37.

Tedford, R. H., Wang, X. and Taylor, B. E., (2009). Phylogenetic Systematics of the North American Fossil Caninae (Carnivora: Canidae). Bulletin of the American Museum of Natural History, 325(325), pp. 1–218.

Terhune, C. E., Hylander, W. L., Vinyard, C. J. and Taylor, A. B., (2015). Jaw-muscle architecture and mandibular morphology influence relative maximum jaw gapes in the sexually dimorphic *Macaca fascicularis*. Journal of Human Evolution, 82, pp. 145–158.

Therrien, F., (2005). Feeding behaviour and bite force of sabretoothed predators. Zoological Journal of the Linnean Society, 145 (3), pp. 393–426.

Thomason, J. J., (1991). Cranial strength in relation to estimated biting forces in some mammals. Canadian Journal of Zoology, 69(9), pp. 2326–2333.

Thomason, J. J., Grovum, L. E., Deswysen, A. G. and Bignell, W. W., (2001). In Vivo Surface Strain and Stereology of the Frontal and Maxillary Bones of Sheep : Implications for the Structural Design of the Mammalian Skull. The Anatomical Record, 264 (4), pp. 325–338.

Thompson, E. N., (2003). Ontogeny of feeding function in the gray short-tailed opossum *Monodelphis domestica*: empirical support for the constrained model of jaw biomechanics. Journal of Experimental Biology, 206(5), pp. 923–932.

Thrall, D.E. and Robertson, I.D., (2015). Atlas of normal radiographic anatomy and anatomic variants in the dog and cat. Elsevier Health Sciences.

Tolhurst, D. E. and Hart, J., (1990). Cadaver preservation and dissection. European Journal of Plastic Surgery, 13(2), pp. 75–78.

Tomo, S., Nakajima, K., Tomo, I., Nodai, E. and Kobayashi, S., (1995). The morphology and innervation of the lateral pterygoid muscle of the dog. Journal of anatomy, 186 (2), pp. 435–9.

Tonndorf, M. L., Sasaki, K. and Hannam, A. G., (1989). Single-wire recording of regional activity in the human masseter muscle. Brain Research Bulletin, 23(1–2), pp. 155–159.

Toro-Ibacache, V., Fitton, L. C., Fagan, M. J. and O'Higgins, P., (2016). Validity and sensitivity of a human cranial finite element model: Implications for comparative studies of biting performance', Journal of Anatomy, 228(1), pp. 70–84.

Tseng, Z. J., (2011). Variation and implications of intra-dentition Hunter-Schreger band pattern in fossil hyaenids and canids (Carnivora, Mammalia). Journal of Vertebrate Paleontology, 31(5), pp. 1163–1167.

Tseng, Z. J., Antón, M., Salesa, M. J., (2011). The evolution of the bone-cracking model in carnivorans: cranial functional morphology of the Plio-Pleistocene cursorial hyaenid *Chasmaporthetes lunensis* (Mammalia: Carnivora). Paleobiology, 37(1), pp. 140–156.

Tseng, Z. J. and Wang, X., (2010). Cranial functional morphology of fossil dogs and adaptation for durophagy in Borophagus and Epicyon (Carnivora, Mammalia). Journal of Morphology, 271(11), pp. 1386–1398.

Turnbull, W. D., (1970). Mammalian masticatory apparatus. Fieldiana Geology, 18, pp. 147–356.

Turner, M. J., (1956). Stiffness and deflection analysis of complex structures. Journal of the Aeronautical Sciences, 23(9), pp. 805–823.

Turner, T. R., Cramer, J. D., Nisbett, A. and Gray, J. P., (2016). A comparison of adult body

size between captive and wild vervet monkeys (*Chlorocebus aethiops sabaeus*) on the island of St. Kitts. Primates, 57(2), pp. 211–220.

Tutt, C., Crossley, D. A. and Deeprose, J., (2006). The BSAVA manual of canine and feline dentistry. British Small Animal Veterinary Association.

Ungar, P. S., Scott, R. S., Scott, J. R. and Teaford, M., (2008). Dental microwear analysis: historical perspectives and new approaches. Technique and application in dental anthropology, 53, p. 389.

Ulrich, D., Van Rietbergen, B., Weinans, H. and Rüegsegger, P., (1998). Finite element analysis of trabecular bone structure: A comparison of image-based meshing techniques. Journal of Biomechanics, 31(12), pp. 1187–1192.

Van Eijden, T., Korfage, J. A. M. and Brugman, P., (1997). Architecture of the human jaw-closing and jaw-opening muscles. The anatomical record. Wiley Online Library, 248(3), pp. 464–474.

Van Rietbergen, B., Weinans, H., Huiskes, R., Odgaard, A., (1995). A new method to determine trabecular bone elastic properties and loading using micromechanical finite-element models. Journal of Biomechanics, 28(1), pp. 69–81.

Van Valkenburgh, B., (1985). Locomotor Diversity Within Past and Present Guilds of Large Predatory Mammals Locomotor diversity within past and present guilds of large predatory mammals. Paleobiology, 11(2), pp. 406–428.

Van Valkenburgh, B., (1987). Skeletal indicators of locomotor behavior in living and extinct carnivores. Journal of Vertebrate Paleontology, 7(2), pp. 162–182.

Van Valkenburgh, B., (1991). Iterative evolution of hypercarnivory in canids (Mammalia: Carnivora): Evolutionary interactions among sympatric predators. Paleobiology, 17(4), pp. 340–362.

Van Valkenburgh, B., (1996). Feeding Behavior in Free-Ranging , Large African Carnivores.

American society of mammalogists, 77(1), pp. 240–254.

Van Valkenburgh, B., (1999). Major Patterns in the History of Carnivorous Mammals. Annual Review of Earth and Planetary Sciences, 27, pp. 463–493.

Van Valkenburgh, B., (2007). Deja vu: The evolution of feeding morphologies in the Carnivora', Integrative and Comparative Biology, 47(1), pp. 147–163.

Van Valkenburgh, B. and Koepfli, K.-P., (1993). Cranial and dental adaptations to predation in canids. Symposia of the Zoological Society London, 65, pp. 15–37.

Van Valkenburgh, B., Pang, B., Bird, D., Curtis, A., Yee, K., Wysocki, C., Craven, B. A., (2014). Respiratory and olfactory turbinals in feliform and caniform carnivorans: The influence of snout length. Anatomical Record, 297(11), pp. 2065–2079.

Van Valkenburgh, B., Ruff, C. B., (1987). Canine tooth strength and killing behaviour in large carnivores. Journal of Zoology, 212(3), pp. 379–397.

Van Valkenburgh, B., Sacco, T. and Wang, X. M., (2003). Pack hunting in Miocene borophagine dogs: Evidence from craniodental morphology and body size. Bulletin of the American Museum of Natural History, 279(279), pp. 147–162.

Van Valkenburgh, B. and Slater, G., (2009). Craniofacial form and performance of the canid skull during prey killing. Journal of Veterinary Behavior: Clinical Applications and Research, 4(2), pp. 60–61.

Van Valkenburgh, B., Theodor, J., Friscia, A., Pollack, A. and Rowe, T., (2004). Respiratory turbinates of canids and felids: A quantitative comparison. Journal of Zoology, 264(3), pp. 281–293.

Van Valkenburgh, B., Wang, X. and Damuth, J., (2004). Cope's rule, hypercarnivory, and extinction in North American canids. Science, 306(5693), pp. 101–104.

Vaughan, T. A., Ryan, J. M. and Czaplewski, N. J., (2013). Mammalogy. Jones and Bartlett.

Veron, S., Davies, T. J., Cadotte, M. W., Clergeau, P., Pavoine, S., (2017). Predicting loss of evolutionary history: Where are we? Biological Reviews, 92(1), pp. 271–291.

Verwaijen, D., Van Damme, R. and Herrel, A., (2002). Relationships between head size, bite force, prey handling efficiency and diet in two sympatric lacertid lizards. Functional Ecology, 16(6), pp. 842–850.

Vickerton, P., Jarvis, J. and Jeffery, N., (2013). Concentration-dependent specimen shrinkage in iodine-enhanced microCT. Journal of Anatomy, 223(2), pp. 185–193.

Vinyard, C. J., Wall, C. E., Williams, S. H. and Hylander, W. L., (2003). Comparative functional analysis of skull morphology of tree-gouging primates. American Journal of Physical Anthropology, 120(2), pp. 153–170.

Vinyard, C. J., Williams, S. H., Wall, C. E., Doherty, A. H., Crompton, A. W. and Hylander, W. L., (2011). A preliminary analysis of correlations between chewing motor patterns and mandibular morphology across mammals. Integrative and Comparative Biology, 51(2), pp. 260–270.

Vucetich, J. A., Vucetich, L. M. and Peterson, R. O., (2012). The causes and consequences of partial prey consumption by wolves preying on moose. Behavioral Ecology and Sociobiology, 66(2), pp. 295–303.

Vuorisalo, T., Talvitie, K., Kauhala, K., Bläuer, A. and Lahtinen, R., (2014). Urban red foxes (Vulpes vulpes L.) in Finland: A historical perspective. *Landscape and Urban Planning*, 124, pp. 109–117.

Wainwright, P. C., and Richard, B. A., (1995). Predicting patterns of prey use from morphology of fishes. Environmental Biology of Fishes, 44(1–3), pp. 97–113.

Walmsley, A., Elton, S., Louys, J., Bishop, L. C. and Meloro, C., (2012). Humeral epiphyseal shape in the felidae: The influence of phylogeny, allometry, and locomotion. Journal of Morphology, 273(12), pp. 1424–1438.

Walton, B. L. R., (2018). *Canis mesomelas*. Mammalian Species, (715), pp. 1–9.

Wang, Q., Smith, A. L., Strait, D. S., Wright, B. W., Richmond, B. G., Grosse, I. R., Byron, C. D. and Zapata, U., (2010). The global impact of sutures assessed in a finite element model of a macaque cranium. Anatomical Record, 293(9), pp. 1477–1491.

Wang, Q., Wood, S. A., Grosse, I. A. N. R., Ross, C. F., Zapata, U., Byron, C. D. and Wright, B. W., (2012). The Role of the Sutures in Biomechanical Dynamic Simulation of a Macaque Cranial Finite Element Model : Implications for the Evolution of Craniofacial Form. The Anatomical Record: Advances in Integrative Anatomy and Evolutionary Biology, 295(2), pp.278-288.

Wang, S. W., Macdonald, D. W., (2009). Feeding habits and niche partitioning in a predator guild composed of tigers, leopards and dholes in a temperate ecosystem in central Bhutan. Journal of Zoology, 277(4), pp. 275–283.

Wang, X., (1993). Transformation from plantigrady to digitigrady: functional morphology of locomotion in Hesperocyon (Canidae: Carnivora). American Museum Novitates, (3069), pp. 1–23.

Wang, X., Tedford, R., Van Valkenburgh, B., Wayne, R.K., (2004). Phylogeny , Classification , and Evolutionary Ecology of the Canidae, in Canids: Foxes, Wolves, Jackals and Dogs. Status survey and conservation action plan, pp. 8–20.

Wang, X., Li, Q. and Xie, G., (2015). Earliest record of Sinicuon in Zanda Basin, southern Tibet and implications for hypercarnivores in cold environments. Quaternary International, 355, pp. 3–10.

Wang, X. and Tedford, R. H., (2010). Dogs: their fossil relatives and evolutionary history. Columbia University Press.

Wang, X., Tedford, R. H. and Taylor, B. E., (1999. Phylogenetic systematics of the Borophaginae (Carnivora, Canidae). Bulletin of the American Museum of Natural History,

243, pp. 1–391.

Warburton, N.M., (2009). Comparative jaw muscle anatomy in kangaroos, wallabies, and rat-kangaroos (marsupialia: macropodoidea). The Anatomical Record: Advances in Integrative Anatomy and Evolutionary Biology, 292(6), pp.875-884.

Ward, O. G., Wurster-Hill, D. H., (1990). *Nyctereutes procyonoides.* Mammalian Species, (358), pp. 1–5.

Wayne, R.K., (1986). Cranial morphology of domestic and wild canids: the influence of development on morphological change. Evolution, 40(2), pp.243-261.

Wayne, R. K., (1986). Limb morphology of domestic and wild canids: the influence of development on morphologic change. Journal of morphology. 187(3), pp. 301–319.

Wayne, R. K. (1993). Molecular evolution of the dog family. Trends in Genetics, 9 (6), pp.218-224.

Wayne, R. K., (2001). Consequences of domestication: morphological diversity of the dog. The genetics of the dog. CABI, pp. 43–60.

Wayne, R. K., Geffen, E. L. I., Girman, D. J., Koepfli, K. P., Lau, L. M., Marshall, C. R. and Brien, O., (1997). Molecular Systematics of the Canidae. Syst. Biol, 46(4), pp. 622–653.

Wayne, R.K., Van Valkenburgh, B., Kat, P.W., Fuller, T.K., Johnson, W.E. and O'Brien, S.J., (1989). Genetic and morphological divergence among sympatric canids. Journal of Heredity, 80(6), pp.447-454.

Weaver, J. L., Arvidson, C. and Wood, P., (1992). 2 Wolves, Canis-Lupus, Killed by a Moose, Alces-Alces, in Jasper National-Park, Alberta. Canadian Field-Naturalist, 106(1), pp. 126–127.

Werdelin, L., (1989). Constraint and adaptation in the bone-cracking canid Osteoborus (Mammalia: Canidae). Paleobiology. 15(4), pp. 387–401.

Widmer, C. G., Carrasco, D. I. and English, A. W., (2003). Differential activation of neuromuscular compartments in the rabbit masseter muscle during different oral behaviors. Experimental Brain Research, 150(3), pp. 297–307.

Weber, E. F., (1851). Ueber die Langenverhaltnisse der Fleischfasern der Muskeln im allgemeinen. Berichte uber die Verhandlungen der Koniglich Sachsischen Akademie der Wissenschaften zu Leipsig, Mathematisch-physische Classe. Leipzig: Weidmannsche Buchhandlung.

Webster, M. and Sheets, H. D., (2010). A practical introduction to landmark-based geometric morphometrics. The Paleontological Society Papers, 16, pp. 163–188.

Weed, D., Maqueda, L. G., Brown, M. A., Hussein, B. A., Shabana, A. A. (2010). A new nonlinear multibody/finite element formulation for knee joint ligaments. Nonlinear Dynamics, 60(3), 357–367.

Weijs, W. A., (1994). Evolutionary Approach of Masticatory Motor Patterns, in Biomechanics of feeding in vertebrates, Springer. pp. 281-320.

Weijs, W. A., Hillen, B., (1985). Cross-sectional areas and estimated intrinsic strength of the human jaw muscles. Acta Morphologica Neerlando-Scandinavica, 23(3), pp. 267.

Widmer, C. G., Carrasco, D. I., English, A. W., (2003). Differential activation of neuromuscular compartments in the rabbit masseter muscle during different oral behaviors. Experimental Brain Research, 150(3), pp. 297–307.

Williams, R. C. and Evans, H. E., (1978). Prenatal Dental Development in the Dog, Canis familiaris: Chronology of Tooth Germ Formation and Calcification of Deciduous Teeth. Anatomia, Histologia, Embryologia, 7(2), pp. 152–163.

Williams, S. B., Wilson, A. M., Rhodes, L., Andrews, J. and Payne, R. C., (2008). Functional anatomy and muscle moment arms of the pelvic limb of an elite sprinting athlete: The racing greyhound (Canis familiaris). Journal of Anatomy, 213(4), pp. 361–372.

Williams, S. H., Peiffer, E., Ford, S., (2009). Gape and bite force in the Rodents Onychomys leucogaster and Peromyscus maniculatus: Does Jaw-Muscle anatomy predict performance? Journal of Morphology, 270(11), pp. 1338–1347.

Wilson, D. E. and Reeder, D. M., (1993). Mammal species of the world: A taxonomic and geographic reference, Second edition. John Hopkins University Press.

Wilson, D. E. and Reeder, D. M. (2005) Mammal Species of the World. A Taxonomic and Geographic Reference, Third edition. John Hopkins University Press.

Wilson, L. A. B. and Sánchez-Villagra, M. R., (2009). Heterochrony and patterns of cranial suture closure in hystricognath rodents. Journal of Anatomy, 214(3), pp. 339–354.

Witmer, L. M., (1995). The extant phylogenetic bracket and the importance of reconstructing soft tissues in fossils. Functional morphology in vertebrate paleontology, 1, pp. 19–33.

Wolbarst, A. B., Capasso, P. and Wyant, A. R., (2013). Medical imaging: essentials for physicians. Wiley/Blackwell, 2013.

Woodroffe, R., McNutt, J. W., Mills, M. G. L., (2004). African wild dog, *Lycaon pictus* (Temminck, 1820). Canids: Foxes, Wolves, Jackals and Dogs. Status Survey and Conservation Action Plan. IUCN/SSC Canid Specialist Group, Gland, Switzerland and Cambridge, UK, 174–183.

Wozencraft, W. C., (1993). Order Carnivora, in Mammal species of the world: a taxonomic and geographic reference. Second edition. John Hopkins University Press, pp. 279–348.

Wozencraft, W. C., (2005). Order Carnivora, Mammal species of the world: a taxonomic and geographic reference. Third Edition. John Hopkins University Press, pp. 532–628.

Wroe, S., (2010). Cranial mechanics of mammalian carnivores: recent advances using a

finite element approach, in Carnivoran evolution: new views on phylogeny, form, and function (eds Goswami, A., Friscia, A.). Cambridge University Press. pp. 466–485.

Wroe, S., Clausen, P., McHenry, C., Moreno, K. and Cunningham, E., (2007). Computer simulation of feeding behaviour in the thylacine and dingo as a novel test for convergence and niche overlap. Proceedings. Biological sciences / The Royal Society, 274 (1627), pp. 2819–2828.

Wroe, S., McHenry, C. and Thomason, J., (2005). Bite club: comparative bite force in big biting mammals and the prediction of predatory behaviour in fossil taxa. Proceedings of the Royal Society of London B: Biological Sciences, 272(1563), pp.619-625.

Wroe, S. and Milne, N., (2007). Convergence and remarkably consistent constraint in the evolution of carnivore skull shape. Evolution: International Journal of Organic Evolution, 61(5), pp.1251-1260.

Wu, Y., Wang, H., Wang, H. and Feng, J., (2018). Arms race of temporal partitioning between carnivorous and herbivorous mammals. Scientific Reports, 8(1), p. 1713.

Yang, Z. and Rannala, B., (2012). Molecular phylogenetics: principles and practice. Nature Reviews Genetics, 13(5), pp. 303–314.

Yarnell, R. W., Phipps, W. L., Burgess, L. P., Ellis, J. A., Harrison, S. W. R., Dell, S., MacTavish, D., MacTavish, L. M. and Scott, D. M., (2013). The influence of large predators on the feeding ecology of two African mesocarnivores: the black-backed jackal and the brown hyaena. South African Journal of Wildlife Research, 43(2), pp. 155–166.

Young, B., O'Dowd, G. and Woodford, P., (2014). Wheater's functional histology : a text and colour atlas. Philadelphia, PA : Churchill Livingston/Elsevier.

Yushkevich, P.A., Piven, J., Hazlett, H.C., Smith, R.G., Ho, S., Gee, J.C. and Gerig, G., (2006). User-guided 3D active contour segmentation of anatomical structures: significantly improved efficiency and reliability. Neuroimage, 31(3), pp.1116-1128.

Zander, T., Dreischarf, M., Timm, A., Baumann, W. W. and Schmidt, H., (2017). Impact of material and morphological parameters on the mechanical response of the lumbar spine – A finite element sensitivity study. Journal of Biomechanics, 53, pp. 185–190.

Zelditch, M. L., Swiderski, D. L. and Sheets, H. D., (2012). Geometric morphometrics for biologists: a primer. Academic Press.

Zollikofer, C. P. E. and Weissmann, J. D., (2008). A morphogenetic model of cranial pneumatization based on the invasive tissue hypothesis. Anatomical Record, 291(11), pp. 1446–1454.

Zrzavý, J. and Řičánkova, V., (2004). Phylogeny of Recent Canidae (Mammalia, Carnivora): relative reliability and utility of morphological and molecular datasets. Zoologica Scripta, 33(4), pp. 311–333.

Zuercher, G. L., Gipson, P. S., Carrillo, O., (2005). Diet and habitat associations of bush dogs *Speothos venaticus* in the Interior Atlantic Forest of eastern Paraguay. Oryx, 39(1), pp. 86–89.

Zuercher, G. L., Swarner, M., Silveira, L. and Carrillo, O., (2004). Bush dog, *Speothos venaticus* (Lund, 1842), in Canids: foxes, wolves, jackals and dogs. Status survey and conservation action plan. IUCN Gland, Switzerland, p. 430.

Zysset, P. K., Edward Guo, X., Edward Hoffler, C., Moore, K. E., Goldstein, S. A., (1999). Elastic modulus and hardness of cortical and trabecular bone lamellae measured by nanoindentation in the human femur. Journal of Biomechanics, 32(10), pp. 1005–1012.

Appendices

Appendix 1. Species details.

***Alopex lagopus*, Arctic fox.**

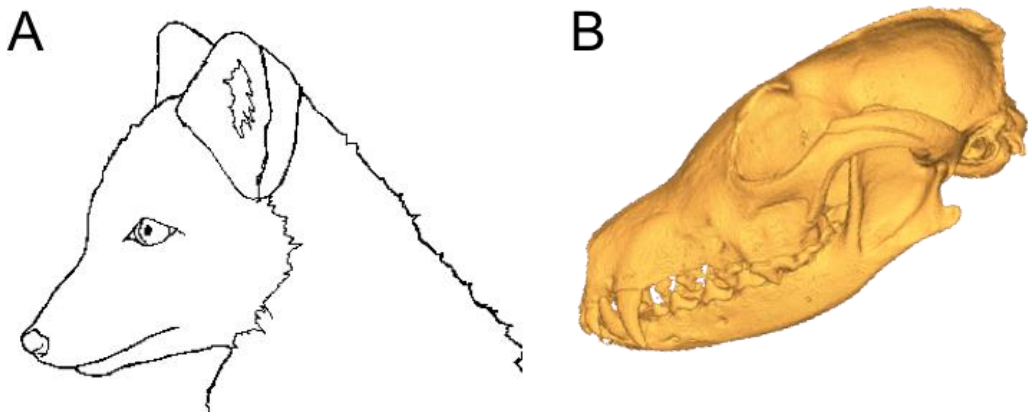

Appendix Figure 1.1 *Alopex lagopus*, A, outline of head, B, reconstruction of skull from CT.

Taxonomy

A fox like canid. In some taxonomic categorisations, this is also called *Vulpes lagopus* as it is grouped with the vulpes. Closely related to *Vulpes velox* and *Vulpes macrotis* (Angerbjorn, 2004).

Physical characteristics

1.4 – 9kg, putting on up to 50% body mass in the autumn to survive the winter. Very insulative fur, short muzzle, short ears, short legs and a rounded appearance to the body (Macdonald and Sillero-Zubiri, 2004; Nowak, 2005).

Dentition

The dental formula is 3/3-1/1-4/4-2/3=42 (Angerbjorn, 2004).

Geographical distribution

Circumpolar arctic and alpine areas. The northern limit of the red fox, *Vulpes vulpes*, is determined by resource availability, then artic fox takes over the territory. Can cover great distances to find food (Elmhagen *et al*., 2002).

Social behaviour

Live in social groups, monogamous, possibly pair for life. 2 to 25 pups born usually 6-12. Largest known litter size in Carnivora (Angerbjörn *et al*., 2004).

Diet – small prey specialist

Mainly small rodents and seabirds (Elmhagen *et al*., 2002; Angerbjorn and Hersteinsson, 2004). Will also scavenge from larger carcasses such as reindeer (Prestrud, 1992) and seals (Frafjord, 1993) and their pups (Smith, 1976).

Hunting strategy – pounce/pursuit predator

Lone hunters, often pounce on small rodents (MacDonald, 2009).

***Canis lupus*, Grey wolf.**

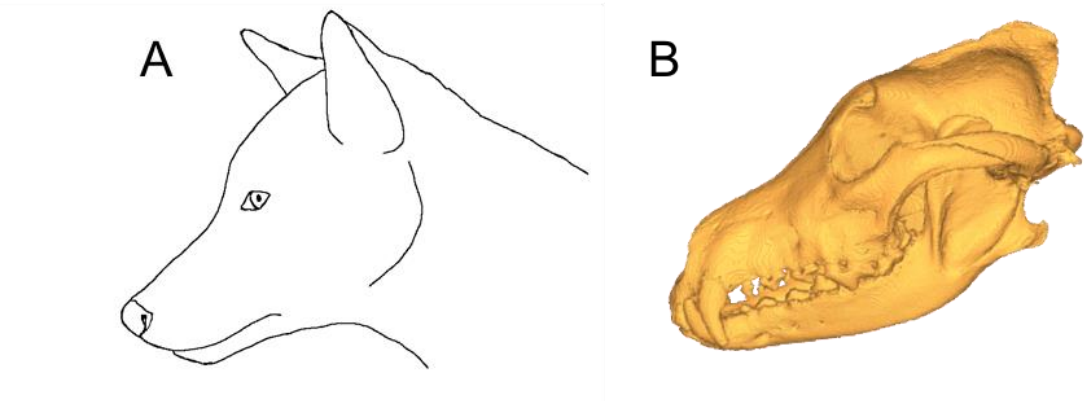

Appendix Figure 1.2 *Canis lupus*, A, outline of head, B, reconstruction of skull from CT.

Taxonomy

Wolf like canid. Up to 37 reported subspecies, including the red wolf (*Canis rufus*), domestic dog (*Canis lupus familiaris*) and dingo (*Canis dingo*) (Wilson and Reeder, 2005).

Physical characteristics

Body mass up to 80kg, with northern subspecies tending to be larger(Nowak, 2005).

Dentition

The dental formula is 3/3-1/1-4/4-2/3=42

Geographical distribution

Occurs throughout the northern hemisphere (Macdonald and Sillero-Zubiri, 2004; Mech and Boitani, 2003). Can cover great distances in search of food. Packs have large territories (Nowak, 2005).

Social behaviour

Live in groups of up to 36 individuals but less is more common with a mean size of 5-12 individuals. Usually a large family group with one alpha male and female pair (Nowak, 2005). Mean litter size is 6, sexually mature at 22 months.

Diet – hypercarnivore

Large ungulates such as moose reindeer, musk ox, bison and white-tailed deer. Daily consume up 10 kg animal protein. More diverse diet in summer. Smaller prey such as beaver and voles plus some berries eaten seasonally. (Peterson and Ciucci, 2003; MacDonald and Sillero-Zubiri, 2004; Mech and Botani, 2003; Mech, 1970; Sillero-Zubiri *et al*., 2004).

Hunting strategy – pursuit predator

Pack hunters especially in winter, may hunt in pairs or singly for small prey in the summer. Can cover 20-40km looking for prey per day but the hunts themselves rarely last more than 2km (Mech, 1970; Peterson and Ciucci, 2003).

***Canis mesomelas*, Black backed jackal.**

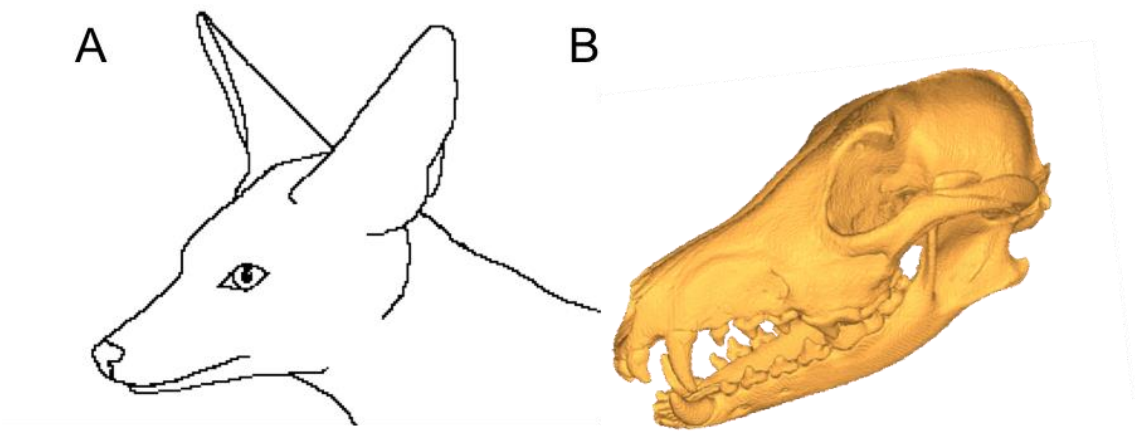

Appendix Figure 1.3 *Canis mesomelas* A, outline of head, B, reconstruction of skull from CT.

Taxonomy

Wolf like canid.

Physical characteristics

5.9 – 12kg (Loveridge and Nel, 2004) males average 1kg heavier than females (Nowak, 2005).

Dentition

The dental formula is 3/3-1/1-4/4-2/3=42. They have a well-developed carnassial shear with a longer premolar cutting blade than other jackal species, an indication of a greater tendency towards carnivory (Van Valkenburgh and Koepfli, 1993; Van Valkenburgh, 1991).

Geographical distribution

Two separate populations in east and south Africa (Loveridge and Nel, 2004; Nowak, 2005)

Social behaviour

Live as monogamous pairs with their offspring. 1-6 pups (Loveridge and Nel, 2004).

Diet – small prey specialist

Unspecialised diet, will readily take small to medium mammals, reptiles, birds, eggs, carrion, fruit and refuse. Can cope with low water levels. Good hunters will take up to large lagomorph size or newborn antelope when hunting alone, or larger antelope and seals, when hunting in packs (Loveridge and Nel, 2004).

Hunting strategy – pounce/pursuit predator

Mainly crepuscular and diurnal, but nocturnal in areas populated by humans. Listen for prey in long grass leap in air. Pounce with forefeet before killing bite. Hunt larger prey in pairs or even small groups (Loveridge and Nel, 2004; MacDonald, 2009).

***Chrysocyon brachyurus,* Maned wolf.**

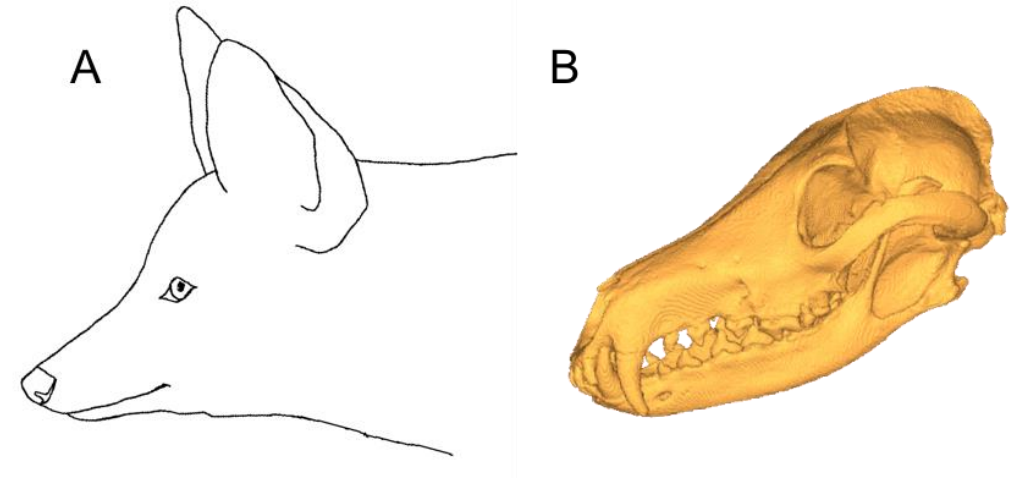

Appendix Figure 1.4 *Chrysocyon brachyurus*, A, outline of head, B, reconstruction of skull from CT.

Taxonomy

South American canid. Alone in its own genus, *Chrysocyon*.

Physical characteristics

Very long legs, large ears, reddish coat, 20.5kg – 30 kg (Macdonald and Sillero-Zubiri, 2004; Nowak, 2005; Rodden *et al*., 2004).

Dentition

The dental formula is 3/3-1/1-4/4-2/3=42 (Rodden *et al*., 2004).

Geographical distribution

Currently found throughout large parts of south America Lives in grasslands, savannahs, swampy areas and scrubby forest (Nowak, 2005).

Social behaviour

Solitary or in pairs (Rodden *et al*., 2004) Shares territories in pairs, but mainly lives alone outside of breeding season (Nowak, 2005).

Diet – small prey specialist

Up to 64% of the diet may be plant based. Will hunt small mammals fish, insects and reptiles (MacDonald, 2009; MottaJunior *et al*., 1996; Rodden *et al*., 2004).

Hunting strategy – pounce/pursuit predator

Nocturnal and crepuscular habits. Hunts alone. Long legs allow it to see above long grasses. Stalking with pounce, digging after burrowing prey, leaping in to the air to catch birds and sprinting after deer have all been observed (Rodden *et al*., 2004). Does not pursue prey for any great distance (Nowak, 2005).

***Cuon alpinus,* Dhole.**

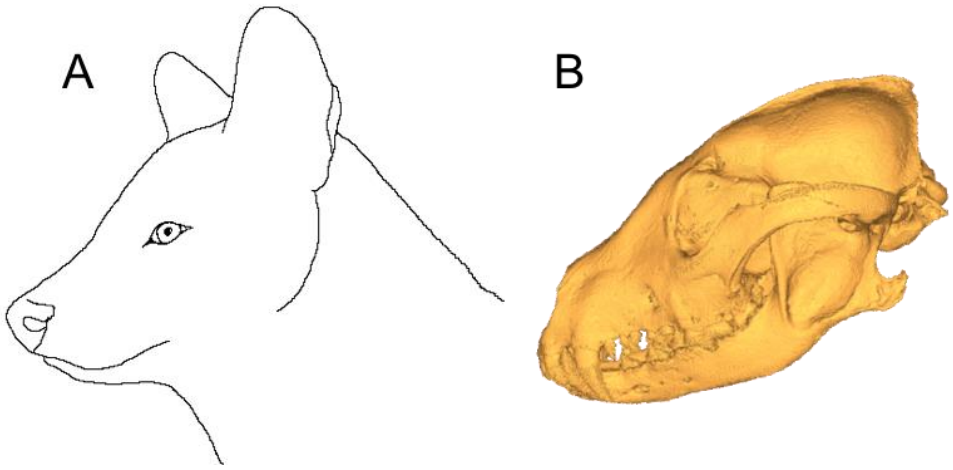

Appendix Figure 1.5 *Cuon alpinus*, A, outline of head, B, reconstruction of skull from CT.

Taxonomy

Physical characteristics 10 – 20 kg reddish brown (Durbin *et al*., 2004; Macdonald and Sillero-Zubiri, 2004).

Dentition

The dental formula is 3/3-1/1-4/4-2/2=42, with one less lower molar. Also, the form of LM1 is has only one cusp, all other canids have two. Hypercarnivorous adaptation to enhance shearing ability (Durbin *et al*., 2004).

Geographical distribution

Historically its range covered much of east south Asia including Mongolia, China. Tibet and Russia, now confined to central and eastern Asia, India, Tibet, Bangladesh and much of Indochina (Durbin *et al*., 2004).

Social behaviour

Live in packs of up to 25, but 5-10 individuals more common. Usually only the dominant female breeds, 5- 10 pups (Durbin *et al*., 2004; MacDonald and Sillero-Zubiri, 2004).

Diet – hypercarnivore

Hunts large ungulates such as spotted deer and wild pigs. Will take prey up to 175kg.
(Durbin *et al*., 2004; Karanth and Sunquist, 1995; Selvan *et al*., 2013).

Hunting strategy – pursuit predator

Dhole hunt in a variety of habitats, during day or by moonlight. Communal hunters. Detect prey by scent, and may jump up to see it. When hunting in thick cover they form a line to flush prey, whilst others in the pack wait to catch it. They employ a nosehold to subdue large prey then others attach rump and flank to eviscerate it. Small prey seized and shaken. (Aryal *et al*., 2015; Selvan *et al*., 2013; Wang and Macdonald, 2009).

***Lycaon pictus,* African hunting dog.**

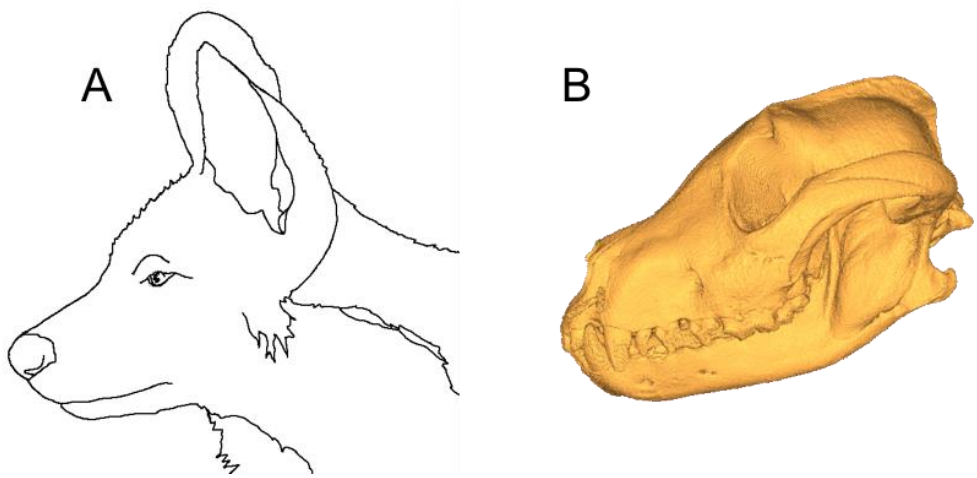

Appendix Figure 1.6 *Lycaon pictus*, A, outline of head, B, reconstruction of skull from CT.

Taxonomy

Physical characteristics

Large but lightly built, 17 – 36 kg, males and females similar size ranges. Long legs, only four toes per foot, no dew claws (first digit) (MacDonald and Sillero-Zubiri, 2004; Nowak, 2005; Woodroffe *et al*., 2004).

Dentition

The dental formula is 3/3-1/1-4/4-2/3=42. Usual number of canid teeth but the caudal part of LM1 has blade like form, rather than basin like, indicative of hypercarnivory (MacDonald, 2009; Woodroffe *et al*., 2004).

Geographical distribution

Historically occurred in most of Africa, but now occurs in two populations west and central Africa. Lives in grassland, savannah, open woodlands (MacDonald and Sillero-Zubiri, 2004; Nowak, 2005; Woodroffe *et al.,* 2004).

Social behaviour

Live in social groups of up to 30 individuals. Dominant pair only will reproduce, all pack members contribute to raising the large litters of up to 21 pups (Macdonald and Sillero-Zubiri, 2004; Woodroffe *et al*., 2004).

Diet – hypercarnivore

Impala, gazelle and wildebeest make up most of the prey, but will also take zebra, warthogs or ostriches. Up to 9kg stomach capacity (Creel and Creel, 1995; Fanshawe and Fitzgibbon, 1993; MacDonald and Sillero-Zubiri, 2004).

Hunting strategy – pursuit predator

Can maintain a gentle trot for hours when searching for quarry. Hunts mainly by sight, in the early morning or evening (Nowak, 2005). After initial visual contact with prey the pack will stalk and chase quarry for up to one hour (Nowak, 2005). Packs consist of up to 30 individuals. Increasing pack numbers means better overall success rate. Average prey is around 50 kg but packs may take individuals up to 200kg. Pursue prey until exhausted. One or two dogs grab the prey by the nose whilst others grab the hind quarters and flank and pull it to the ground, and disembowel it. Prey must then be defended from scavengers, chiefly hyenas and lions. Individuals may take small prey (Creel and Creel, 1995; Mccreery, 2000; Woodroffe *et al*., 2004).

***Nyctereutes procyonoides*, Raccoon dog.**

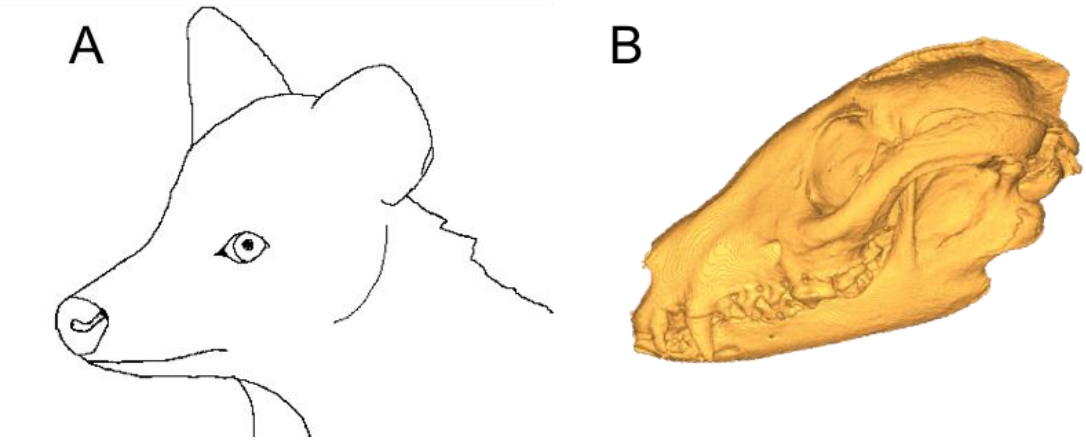

Appendix Figure 1.7 *Nyctereutes procyonoides*, A, outline of head, B, reconstruction of skull from CT.

Taxonomy

Diverged from other canids 7-10 Ma (Macdonald and Sillero-Zubiri, 2004; Wayne, 1993). Most closely related to *Cerdocyon* species, with whom they had a common ancestor (Berta, 1987).

Physical characteristics

4-6kg in summer, 6-10 kg early winter. Increase bodyweight by nearly 50% (MacDonald and Sillero-Zubiri, 2004; Nowak, 2005). Caudal mandible has an additional bony projection, the preangular process, for masticatory muscle insertion (Asahara and Takai, 2017; Ewer, 1973; Fujiwara and Suwa, 1991; Reynolds, 2012; Tedford *et al*., 1995).

Dentition

The dental formula is 3/3-1/1-4/4-2/3=42

Geographical distribution

Occurs in dense forests and thick vegetation (Nowak, 2005). Native range is the far eastern Asia, but introduced to the US, Russia and Europe as fur species in early 20th C. Now widespread in northern Europe (Kauhala *et al.,* 1993; Macdonald and Sillero-Zubiri, 2004).

Social behaviour

In cold areas individuals may hibernate from November to March, with occasional days awake and foraging. In warmer areas, the species does not hibernate. Ranges shared by monogamous pairs, but hunting and foraging occurs alone. (Nowak, 2005; Macdonald and Sillero-Zubiri, 2004).

Diet - generalist

Omnivourous. Small rodents, reptiles, amphibians, fish and vegetable material. A high proportion of the autumnal diet is made up of nuts and berries to sustain the raccoon dog through periods of hibernation in cold winters (Kauhala, 1993; Kauhala *et al*., 1998; Sidorovich *et al*., 2008; Sutor *et al*., 2010).

Hunting strategy – pounce/pursuit predator

Lone nocturnal foragers (Drygala and Zoller, 2014; Kauhala *et al.,* 1993; MacDonald, 2009; Nowak, 2005).

***Otocyon megalotis*, Bat eared fox.**

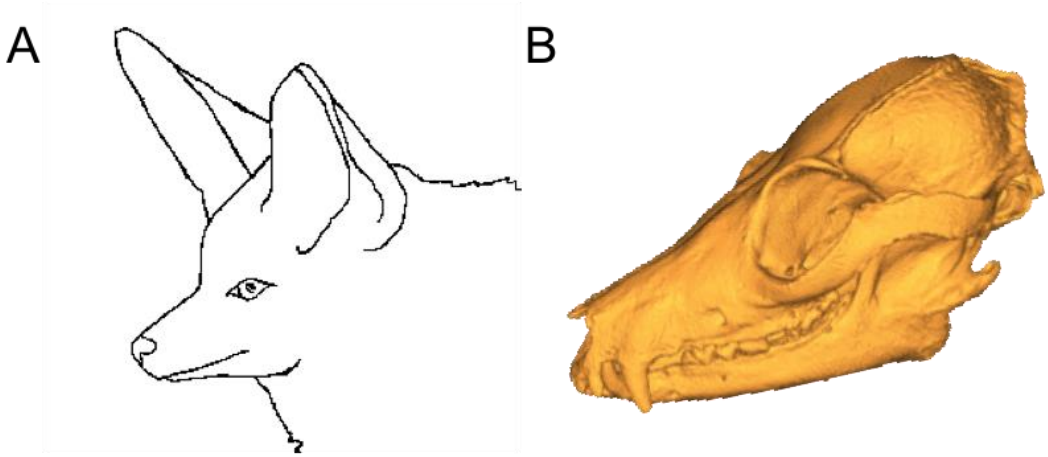

Appendix Figure 1.8 *Otocyon megalotis*, A, outline of head, B, reconstruction of skull from CT.

Taxonomy

Unresolved position in many phylogenetic analyses (Zrzavy and Ricankova, 2004).

Physical characteristics

Small and slight, 3.9 – 5.3kg (Gittleman, 1989; Maas, 1993; Macdonald and Sillero-Zubiri, 2004). Very large ears. Caudal mandible has an additional bony projection, the preangular process, for masticatory muscle insertion (Ewer, 1973; Tedford *et al*., 1995).

Dentition

The dental formula is 3/3-1/1-4/4-3-4/4-5= total dentition is variable but is up to 50 teeth. The highest number of any eutherian mammal outside of odontocetes, the toothed whale species. The deciduous dentition demonstrates unreduced carnassial teeth, however the adult dentition has lost the carnassial sheer and has almost uniform bunodont dentition in the premolars and molars (Kieser, 1995).

Geographical distribution

Two distinct ranges in eastern and Southern Africa, in short grass and scrubland environments (Macdonald and Sillero-Zubiri, 2004; Nowak, 2005).

Social behaviour

Live communally in dens, but forage in groups of 2-3 individuals (Malcolm, 1986; Macdonald and Sillero-Zubiri, 2004).

Diet - generalist

Predominantly insectivorous. Preferentially eats the adults and larvae of dung beetles and termites, but will also take small mammals, scorpions, birds and fruit. Although they do not eat large ungulates they rely on dung beetles that utilise ungulate dung, and on the termites that thrive on grasslands where ungulates roam, so are closely associated with large ungulate populations (Malcom, 1986; Kuntzsch and Nel, 1992; Maas, 1993; Klare *et al*., 2011).

Hunting strategy – pounce/pursuit predator

Often but not always nocturnal. Listens for insect activity and may dig out subterranean prey (notably termites) (Malcom, 1986; Kuntzsch and Nel, 1992; Maas, 1993; Klare *et al*., 2011).

***Speothos venaticus*, Bush dog.**

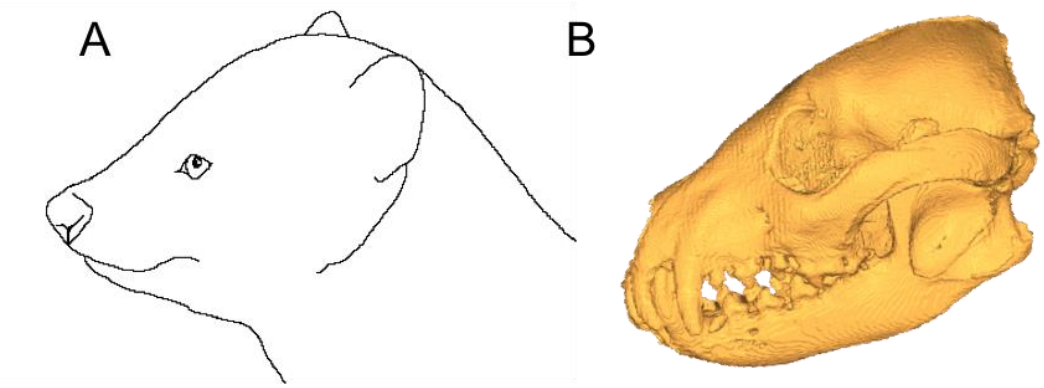

Appendix Figure 1.9 *Speothos venaticus*, A, outline of head, B, reconstruction of skull from CT.

Taxonomy

Sole extant member of genus. Possibly a monophyletic group with *Chrysocyon brachyurus* (Wayne *et al*., 1997; Lindblad-Toh *et al*., 2005), although this is unresolved, and other authors group *Speothos* with the canis group (Nyakatura *et al.,* 2012).

Physical characteristics

A small compact dog with, short legs and tail, 5-8kg. Has webbed feet and is semi-aquatic (Macdonald and Sillero-Zubiri, 2004; Nowak, 2005).

Dentition

The dental formula is 3/3-1/1-4/4-2/2=40. Lacking LM3 and having a distinctive cutting blade to LM1 (Zuercher *et al*., 2004).

Geographical distribution Much of South America as far south as the southern extent of Brazil. Live in forests and wet savannahs, usually near water (Nowak, 2005; Zuercher *et al*., 2004).

Social behaviour Very social. Lives and hunts in packs of up to 12 (Nowak, 2005; Zuercher *et al*., 2004).

Diet – hypercarnivore

Primarily carnivorous hunts large rodents such as paca and capybara. Will also take armadillo, and mammals as large as tapir (de Mello Beisiegel and Zuercher, 2005; De Souza Lima *et al*., 2009; Zuercher *et al*., 2004; Zuercher *et al*., 2005).

Hunting strategy – pursuit predator

Usually diurnal. Primarily carnivorous hunts large rodents such as paca, capybara and armadillo, even taking mammals as large as tapir. May chase and capture prey in water (de Mello Beisiegel and Zuercher, 2005; De Souza Lima *et al*., 2009; Nowak, 2005; Zuercher *et al*., 2004; Zuercher *et al*., 2005).

***Vulpes corsac*, Corsac fox.**

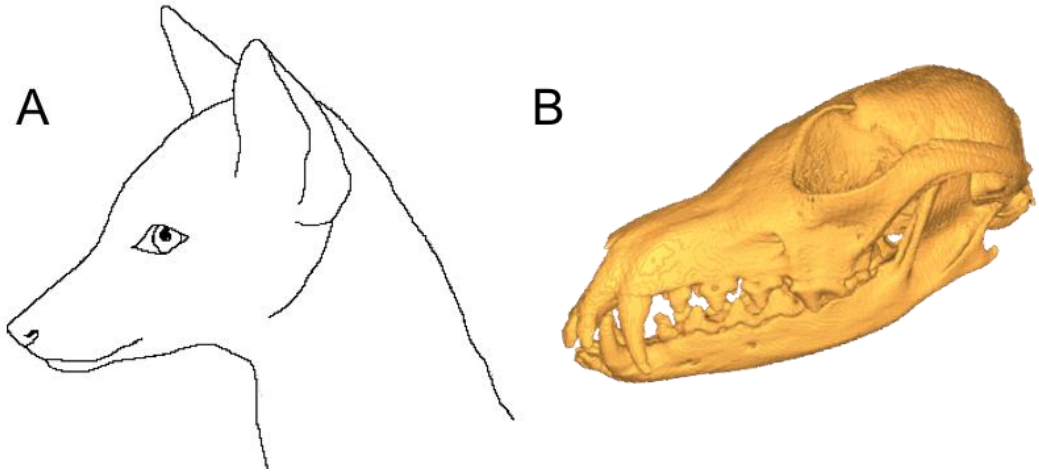

Appendix Figure 1.10 *Vulpes corsac,* A, outline of head, B, reconstruction of skull from CT.

Taxonomy

Physical characteristics.

Small vulpine, 2.1 – 3.2kg (Macdonald and Sillero-Zubiri, 2004; Nowak, 2005; Poyarkov and Ovsyanikov, 2004).

Dentition

The dental formula is 3/3-1/1-4/4-2/3=42 (Macdonald and Sillero-Zubiri, 2004; Poyarkov and Ovsyanikov, 2004).

Geographical distribution

Extensive range throughout middle Asia and southern Russia. As far east as Mongolia and China, and as far west as the Ukraine. Lives on the Steppes or semi desert. (Nowak, 2005; Poyarkov and Ovsyanikov, 2004).

Social behaviour.

The social unit is the breeding pair, with offspring which disperse at the end of the summer (Poyarkov and Ovsyanikov, 2004).

Diet – small prey specialist

Corsac – small and medium rodents and lagomorphs typically ground squirrels, marmots and hares. Will scavenge large ungulate carcasses after larger predator kills (Clark *et al*., 2009; Murdoch *et al*., 2010; Poyarkov and Ovsyanikov, 2004).

Hunting strategy – pounce/pursuit predator

Solitary crepuscular and nocturnal hunters. Often detect prey through sound and scent. Stalk and then fast lunge at prey (Clark *et al*., 2009; Murdoch *et al*., 2010; Poyarkov and Ovsyanikov, 2004).

***Vulpes vulpes*, Red fox.**

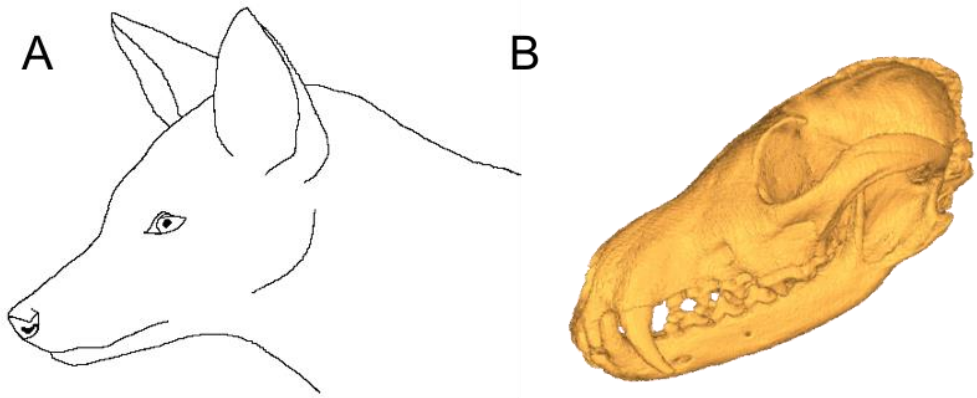

Appendix Figure 1.11 *Vulpes vulpes*, A, outline of head, B, reconstruction of skull from CT.

Taxonomy

Physical characteristics

Wide variation on body size and mass, 3-14kg. *Vulpes vulpes* is the largest species of *vulpes* (Macdonald and Sillero-Zubiri, 2004; Nowak, 2005).

Dentition

The dental formula is 3/3-1/1-4/4-2/3=42 (MacDonald, 2009).

Geographical distribution

Widest geographical range of any extant Carnivoran. Can be found in almost all parts of the Northern hemisphere, with the exception of the extreme arctic and extreme desert conditions. Diverse habitats, from arctic tundra to cities, forests, desert (Macdonald and Reynolds, 2004; Macdonald and Sillero-Zubiri, 2004; Nowak, 2005).

Social behaviour

The usual social unit is a pair, but may also live with other related females in groups of up to 6 (Macdonald and Reynolds, 2004).

Diet – small prey specialist

Very varied diet, dependent on geographical location and opportunities. Will take small mammals, invertebrates including earthworms, birds, eggs, carrion vegetable matter and refuse (Baker and Harris, 2004; Macdonald, 1977).

Hunting strategy – pounce/pursuit predator

Hunts alone, usually nocturnal and crepuscular. Will kill small mammals with a jump high into air, land on quarry with forepaws, kill with shake and or bite. May forage in groups for small invertebrates. Creep up on earthworms and gently pull them from their burrows. Will ambush small rodents and chase larger quarry, such as lagomorphs for a short time (Doncaster *et al*., 1990; Macdonald *et al*., 2015; Macdonald and Reynolds, 2004; Nowak, 2005).

***Vulpes zerda*, Fennec fox.**

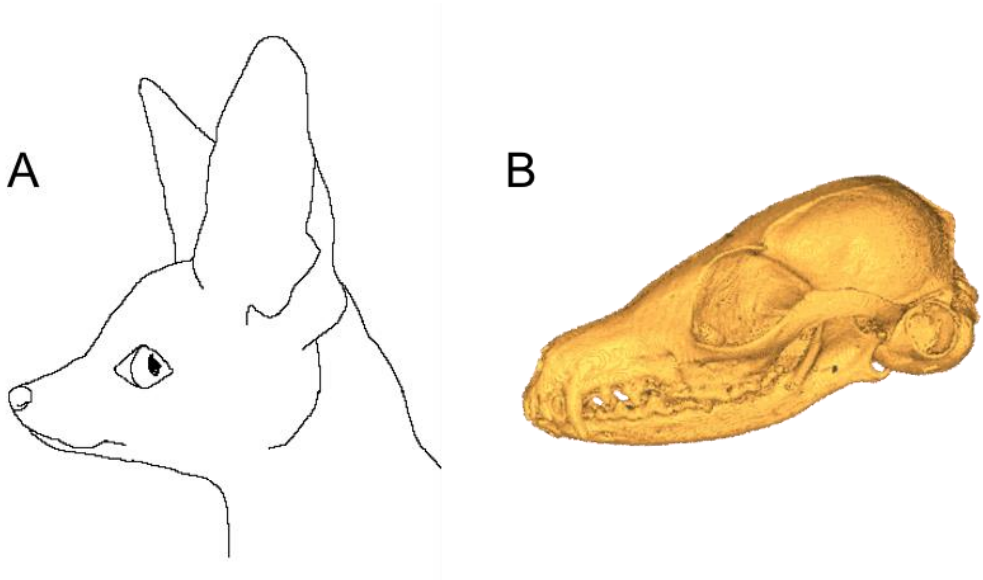

Appendix Figure 1.12 *Vulpes zerda*, A, outline of head, B, reconstruction of skull from CT.

Taxonomy

Sometimes considered in own separate genus, *Fennecus,* but more usually grouped with *Vulpes* (Asa *et al*., 2004; MacDonald and Sillero-Zubiri, 2004; Nowak, 2005; Wozencraft, 2005).

Physical characteristics

The smallest canid, usually around 1kg. Very large ears and corresponding tympanic bullae. Slender muzzle and legs, with fur on underside of feet to help protect against hot sand (Asa *et al.,* 2004; Nowak, 2005).

Dentition

The dental formula is 3/3-1/1-4/4-2/3=42 (Asa *et al*., 2004; MacDonald, 2009).

Geographical distribution.

Widespread across Northern Africa, in arid desert and sand dunes (Asa *et al*., 2004; Macdonald and Sillero-Zubiri, 2004).

Social behaviour.

Social unit is usually a mated pair and their offspring, often including the offspring from the previous year (Asa *et al*., 2004).

Diet - generalist

Mainly insects and small invertebrates. Also takes small rodents and reptiles, vegetable matter and readily take refuse. Can live without direct water source (Asa *et al*., 2004; Larivière, 2002; MacDonald and Sillero-Zubiri, 2004; Nowak, 2005).

Hunting strategy – pounce/pursuit predator

Lone nocturnal hunters. No evidence of pouncing behaviour but are likely to dig to find their mainly invertebrate prey (Asa *et al*., 2004; Larivière, 2002; Macdonald and Sillero-Zubiri, 2004; Nowak, 2005).

Appendix 2. Dhole body mass in captivity details

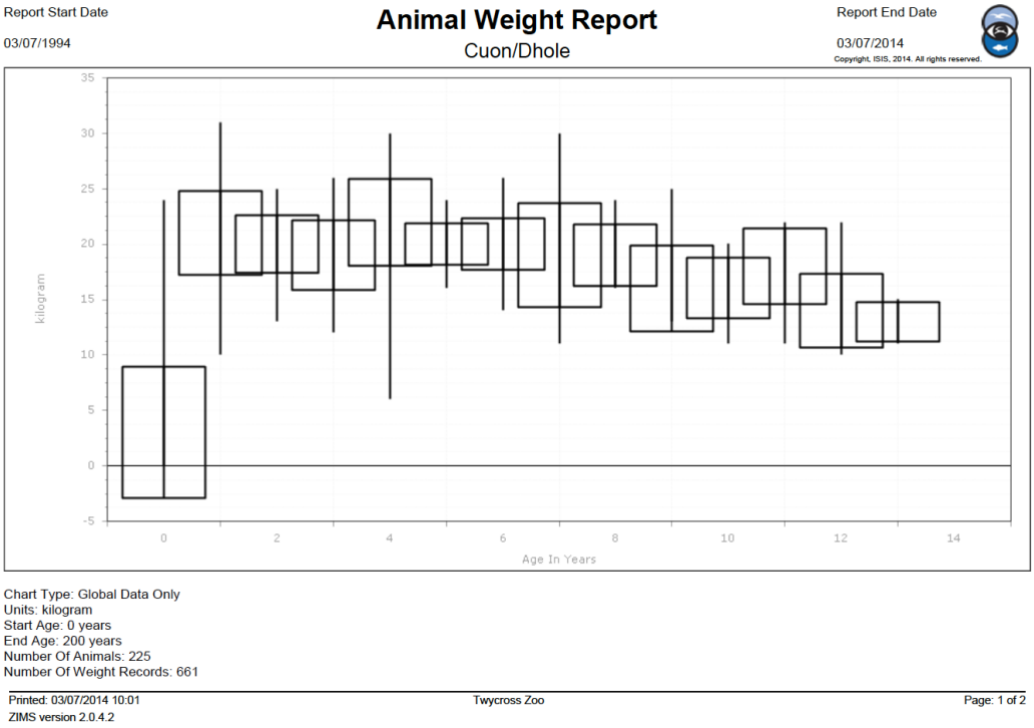

Appendix Figure 2.1. Animal weight report from ISIS documenting body mass range in 225 captive individuals from 1994 - 2014.

Appendix 3. Soft tissue landmarks.

Landmark number		Descriptor
LEFT	RIGHT	
1	5	Ventral most extent of temporalis inserting onto mandible
2	6	Medial extent of temporalis (at mid brain level)
3	7	Lateral extent of temporalis (opposite both caudal coronoid and foramen in cranial wall)
4	8	Dorsal extent of temporalis (where it attaching to cranium).
9	14	Dorsal medial pterygoid on cranium
10	15	Dorsal lateral pterygoid on cranium
11	16	Ventral medial pterygoid on cranium
12	17	Ventral lateral pterygoid on cranium
13	18	Lateral extent of masseter (opposite upper tooth).
19	26	Dorsal temporalis (above coronoid process)
20	27	Ventral temporalis attaching to cranium
21	28	Ventral temporalis attaching to medial rostral mandible
22	29	Ventral medial pterygoid on mandible
23	30	Ventral lateral pterygoid on mandible
24	31	Lateral masseter (just below mid zygomatic arch)
25	32	Ventral extent of masseter
33	37	Cranial ventral extent of (suprazygomatic) temporalis
34	38	Dorsal extent of temporalis (above coronoid process)
35	39	Extent of temporalis caudal to horizon of eye (i.e landmark immediately behind eye)
36	40	Caudal extent of temporalis (opposite horizon of eye and caudal coronoid
41	50	Rostroventral attachment of temporalis to cranium
42	51	Rostral extent of temporalis below eye
43	52	Rostral extent of temporalis above eye
44	53	Dorsal extent of temporalis
45	54	Caudal extent of temporalis (level of base of cranium, above tympanic bulla)
46	55	Caudal ventral pterygoid
47	56	Cranial ventral pterygoid
48	57	Craniodorsal pterygoid
49	58	Caudodorsal pterygoid
59	66	Lateral masseter level with TMJ
60	67	Lateral masseter level with rostral mandible
61	68	Rostral lateral masseter
62	69	Caudal masseter
63	70	Rostral medial temporalis (medial to mandible)
64	71	Rostrolateral attachment of pterygoids
65	72	Caudal extent of temporalis medial to mandible
73	74	Lateral extent of temporalis opposite midway point

Appendix 4. Pruned tree after Nyakatura (Nyakatura *et al*., 2012) to only include species in this study.